Physical Aspects of Group V Halide Systems.

A thesis submitted by

CHRISTOPHER ROBERT CORNELL DEAN

in candidature for the degree of Doctor of Philosophy

of the University of London.

May 1972.

Royal Holloway College,
Englefield Green,
Surrey.

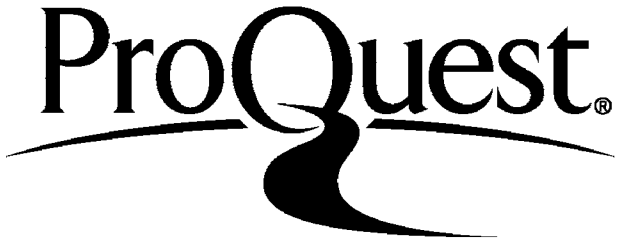

ABSTRACT

An apparatus has been designed and constructed to measure solubilities of the order of 10^{-6} to 10^{-5} mole fraction of non-reactive gases in liquid phases. The solubilities of NF_3 and N_2F_4 are reported, and the estimated enthalpies and entropies of solution are compared with values predicted by semi-empirical relationships.

The reaction of N_2F_4 with aqueous ferrous ions buffered at pH 0.4 has been studied. The results supported the predicted equation for the reaction:

$$10\ Fe^{2+} + 8H^+ + N_2F_4 \longrightarrow 10\ Fe^{3+} + 2NH_4^+ + 4F^-$$

Under the conditions used, the reaction was controlled by the rate of solution of N_2F_4 into the aqueous phase, and it appeared likely that the rate of the reaction was not affected by ferrous ion concentration.

Methemoglobin formation by NF_3 and N_2F_4 is discussed with regard to the solubilities and reactivities of these gases.

Raman and infrared spectra (20-1200 cm^{-1}) of PF_2I have been recorded. Vibrational assignments have been made on the basis of these spectra and of approximate normal coordinate calculations, and statistical thermodynamic functions have been calculated. Statistical thermodynamic functions of PF_3 have been calculated using revised structural data and confirmed vibrational frequencies. The thermal decomposition of PF_2I is discussed.

Raman (100 - 1100 cm^{-1}) and infrared (380-4000 cm^{-1}) spectra of P_2F_4 have been recorded, and the analysis of the nuclear magnetic resonance spectrum of P_2F_4 has been reinvestigated. The results strongly favour a trans configuration for P_2F_4, and tentative vibrational assignments are made for four infrared-active and six Raman-active fundamental frequencies.

The ultraviolet spectrum (2000Å-7000Å) of P_2F_4 has been recorded. $\lambda_{max.}$ was divergent from that predicted by the previously proposed relationship between $\lambda_{max.}$ and substituent electronegativity. The decomposition of P_2F_4 was followed, and the order of the decomposition reaction was estimated as 2.59 ($\pm$ 0.08).

Electron-impact appearance potentials for the parent and PF_2^+ fragment ions from P_2F_4, PF_3, PF_2I and PF_2H have been measured. The ionization potentials are reported and $D(F_2P-PF_2)$ has been estimated as 58 ($\pm$ 9) $kcal.mole^{-1}$.

ACKNOWLEDGEMENTS

The author sincerely thanks Dr. A. Finch for his advice and encouragement throughout the supervision of this work, and Drs. P.J. Gardner and P.N. Gates for their advice and helpful discussions.

The author also wishes to thank Dr. D. Payling for his help during the measurement of appearance potentials at A.W.R.E. Aldermaston.

Finally, the author gratefully acknowledges the financial support of the Medical Research Council.

DEDICATION

To my wife and my parents.

CONTENTS

DIAGRAMS

TABLES

NOMENCLATURE

The nomenclature of nitrogen fluorine compounds has been developed by the many chemists involved, and it is not, therefore, surprising that in some cases a particular compound or class of compounds has acquired two or more chemical names. Frequently non-systematic names have been used to denote the preparative route or some novel characteristic of the compound. Thus a completely consistent nomenclature compatible with the names commonly in use is not possible at present, and in this thesis the names most commonly used in the literature have been used. Similar problems have arisen with phosphorus-fluorine compounds and also with the hemoglobin derivatives and again the most common names have been used.

	Usual nomenclature	Others
NF_3	Nitrogen trifluoride	Trifluoramine
N_2F_4	Tetrafluorohydrazine	Dinitrogen tetrafluoride
$ClNF_2$	Chlorodifluoramine	
HNF_2	Difluoramine	
PF_3	Phosphorus trifluoride	Trifluorophosphine
P_2F_4	Tetrafluorodiphosphine	Diphosphorus tetrafluoride
PF_2I	Difluoroiodophosphine	Phosphorus difluoride iodide
PF_2H	Difluorophosphine	

Hemoglobin	Fe in +2 state	Fe in +3 state
	Hemoglobin	Methemoglobin
	(Ferrohemoglobin)	(Ferrihemoglobin)
	(Haemoglobin)	(Haemiglobin)

Although the Enzyme Commission of the International Union of Biochemistry (Amsterdam, 1965) has recommended the use of the prefixes ferro- and ferri- to denote the valence state of iron in hemoproteins, the older terms using the prefix met- to denote the trivalent state are still more commonly used, and will be used through this thesis.

PART 1. NITROGEN-FLUORINE COMPOUNDS

INTRODUCTION

Interest in compounds containing nitrogen-fluorine bonds has been continuous since the beginning of this century when Moissan[1] fluorinated several organic amines.

Only four binary compounds between nitrogen and fluorine can be envisaged[2]: nitrogen trifluoride, NF_3; tetrafluorohydrazine, N_2F_4; difluorodiazine, N_2F_2 and azine fluoride, N_3F. Although there are a few examples of organic molecules with chains of more than two nitrogen atoms, most of these compounds are unstable and it seems unlikely that a stable binary fluoride of this type will be prepared.

The search for methods to synthesize these binary fluorides has received spasmodic attention since Ruff and Geisel[3] first attempted a preparation in 1903, but it was not until 1928 that Ruff and co-workers[4] reported the preparation of nitrogen trifluoride by the electrolysis of anhydrous ammonium bifluoride. In subsequent studies the preparations of several related materials such as NHF_2, H_2NF and NF_2 were claimed, but these claims were later shown to be in error.

It was not until fourteen years later that two other binary nitrogen fluorides were prepared. Haller[5] isolated fluorine azide from the interaction of fluorine and hydrazoic acid in 1942, and obtained difluorodiazine from its decomposition.

The field of nitrogen-fluorine chemistry received little attention in the years following 1942, with only scattered reports such as a

structural determination of N_2F_2 [6] and some studies by Bigelow[7] of the action of fluorine on organic nitrogen compounds. However, the study of liquid and solid rocket propellants has again stimulated widespread interest in compounds containing nitrogen-fluorine bonds. This third phase of the study of these compounds is a direct result of the search for high-energy inorganic oxidisers[8] for use in rocket propulsion systems. Consideration of bond energies dictates that this search must be centred on the fluorine and oxygen atoms with nitrogen, oxygen and chlorine as carrier atoms. Although a liquid hydrogen-liquid fluorine combination gives a very good theoretical performance, the difficulties associated with storage and controlled combustion make this combination impracticable.

For liquid propellant systems, oxidisers are usually compared theoretically on the basis of combustion with N_2H_4 or B_5H_9. Calculations on nitrogen-fluorine compounds by Niederhauser and Wilde[3] and also on oxygen-fluorine compounds have shown that the performance of these oxidisers is excellent when compared with the more conventional oxidisers such as nitrogen tetroxide, nitric acid, hydrogen peroxide, liquid oxygen, ammonium nitrate and ammonium perchlorate. Performance figures for these had been calculated previously by Barrere[9].

The search for high energy oxidisers based upon nitrogen-fluorine and oxygen-fluorine bonding is considered to be the area in which the most significant advances can be made, since the oxidiser comprises

70-80% of the fuel combination. A small improvement in the oxidiser is therefore of greater value than a similar improvement in the fuel itself.

The search for better oxidisers began in the 1950's, and the last of the envisaged binary nitrogen-fluorine compounds, tetrafluorohydrazine, was prepared in 1957[10,11]. Since then there has been a rapid growth in the interest and effort in this area of chemistry. Tetrafluorohydrazine was found to be an important intermediate in the preparation of other compounds containing N-F bonds. Calculations of its performance as an oxidiser in combination with either B_5H_9 or N_2H_4 have shown that there is considerable promise in fuels based on N_2F_4 and its derivatives, especially if it proves possible to form derivative molecules of higher molecular weight.

The preparation of N_2F_4 has led the way to the preparations of several other inorganic N-F compounds. Difluoramine was first prepared in 1931[12] as one product from the electrolysis of ammonium difluoride, but Kennedy and Colburn[13] were unable to repeat this work. It was not until 1960 that a reproducible preparation[14] from the reaction between N_2F_4 and arsine, or better thiophenol, was found. Chlorodifluoramine ($ClNF_2$) was first prepared and characterised in 1959[15]. Although not itself a useful propellant oxidiser, it received extensive studies in the hope that it would prove a valuable intermediate in the synthesis of high energy NF_2 compounds. This hope has so far not been fulfilled. Bromodifluoramine has also been prepared[16,17]

but iododifluoramine was not prepared by an analogous reaction using aqueous iodine.

Much research has been concluded on better preparations of these N-F compounds and NF_3[18,19] and N_2F_4[20,21,22,23] are now available commercially and their physical and chemical properties have been well reviewed[11,24,25,26,27]. Both NF_3 and N_2F_4 are colourless gases at room temperature, NF_3 melting at about -208.5°C and boiling at about -129°C[28,29,30] while N_2F_4 melts at about -165°C and boils at -73°C[31,32].

As with most industrial chemicals, it was necessary to investigate the possibility of toxic hazards arising from accidental release of these compounds in manufacture, transport, storage and handling at the site of use. This is all the more important where chemicals could be produced in large quantities, as would be the case for rocket propellant systems where very large quantities are used and failure of the rocket would result in widespread contamination by the fuel and oxidiser. Several toxicological studies of the effects of NF_3 and N_2F_4 inhalation by mammals have been carried out and have shown that both gases are relatively toxic.

In 1931, Ruff[33] reported that, although the mono- and difluorides of nitrogen (H_2NF and HNF_2) were quite toxic, nitrogen trifluoride was rather low in acute toxicity when inhaled, and that it produced methemoglobinemia (oxidation of the iron atoms in the hemoglobin molecule from the +2 to the +3 state). Preliminary studies on the toxicology of nitrogen trifluoride[34] by intraperitoneal injection of the gas into rats

and rabbits showed that rabbits were less affected than rats, which developed severe cyanotic appearance (chocolate-brown). Methemoglobin levels produced by single sublethal doses of nitrogen trifluoride gas were up to 5.5 g/100 cm^3 of blood as compared with control animals where the level was not more than 0.02 g/100 cm^3. Pathological changes including the enlargement of the spleen, the heart and the liver were observed, and increased fluorine content of the blood, bones and teeth showed that nitrogen trifluoride was at least in part metabolised.

Similar results were observed for inhalation by rats of single doses of nitrogen trifluoride at concentrations from 1,000 to 2,000 parts per million for durations from 12 minutes to 7 hours. Deaths at all but the lowest concentration were ascribed to excessive methemoglobinemia. Repeated doses of inhaled nitrogen trifluoride at 100 ppm for 7 hours daily, 5 days a week for 4.5 months indicated no significant changes in the blood hemoglobin content, but total fluorine content of the urine was increased and definite injury was observed microscopically to the livers and kidneys of exposed animals.

The authors[34] recommended further research before a level without any adverse effect could be defined, but that human exposures should be limited to well below 100 ppm. Olfactory tests showed that concentrations of 500 ppm of nitrogen trifluoride could not be detected, and thus monitoring instruments should be used to prevent excessive exposure.

Although of moderate to high toxicity, the mode of toxic action

of nitrogen trifluoride during repeated inhalation could not be understood. The lack of gross accumulation of fluorine found in the bones and teeth indicated that little fluoride ion was released by the molecule, and hence it was concluded that the pathological changes and high methemoglobin levels could have been caused by the intact nitrogen trifluoride molecule.

Similar preliminary studies on tetrafluorohydrazine, N_2F_4, have estimated the 4-hour 50% lethal concentration for rats to be 50 ppm[35]. Further experiments with rats, guinea pigs and dogs showed that the toxic signs of N_2F_4 exposure included nasal and eye irritation, cyanosis, body weight suppression and death. Pathological changes to the lungs, livers, kidneys and spleens were observed for near lethal concentrations, while at low level exposures, methemoglobin levels show that methemoglobinemia is a real danger. Significantly, dogs were found to be more sensitive than rats to methemoglobin formation by N_2F_4. Lester[37] has shown that for two antipyretics the descending order of methemoglobin formation in various species is cat, man, dog and rat. If this order is also significant for methemoglobin formation by N_2F_4, the greatest hazard expected from short exposures of man to N_2F_4 is methemoglobinemia. The authors[36] noted that N_2F_4 was unstable in the presence of air, and detected nitrite ion on absorbing room air, from around a leaking N_2F_4 cylinder, in an NO_2 absorbing reagent.

This toxicity of NF_3 and N_2F_4 is somewhat surprising considering the investigations by Hurst and Khayat[33] on the hydrolysis of these nitrogen fluorides. NF_3 was found to be inert at 133°C to pure H_2O and dilute acids (HNO_3, H_2SO_4 and $HClO_4$), but to react with aqueous ionic nucleophiles such as aqueous base and halide ions. The rate of reaction under similar conditions was increased monotonically with the accepted value[114] of the nucleophilicity of the anion. Reaction was also observed with electrophiles such as $AlCl_3$ and acidic and neutral ferrous sulphate solutions were readily oxidised by NF_3 to give ammonium, fluoride and ferric ions. Aqueous ferric chloride acted as a hydrolysis catalyst yielding nitric oxide and nitrate, but this was not found to be a general property of transition metal ions as shown by the total inertness of solutions of other transition metal salts tested.

Tetrafluorohydrazine was found to react more readily than NF_3 with aqueous solutions. Hydrolysis at 133°C was rapid, giving significant quantities of nitrogen gas and nitrate in addition to nitric oxide, but at lower temperatures nitric oxide formation was nearly quantitative. Kinetic studies showed that long induction periods were followed by exponential increases in reaction rate, indicating a complex mechanism. The marked acceleration with time was shown to result from nitric oxide formation catalysing the reaction, and from a similar but smaller catalysis by hydrofluoric acid formation. Oxygen was shown to be at least ten times as effective as nitric oxide in promoting the reaction.

While studies of the toxicology had covered the results of inhalation of various concentrations of NF_3 and N_2F_4 over various periods of time, the mode of intoxication had received little attention. In particular, the question of whether methemoglobin formation was caused by the unreacted molecule, or by a reaction product was not answered. The study of the hydrolysis of these gases[38] showed that both were extremely resistant to chemical attack by pure water. NF_3 reacted with aqueous base at elevated temperatures yielding nitrite and fluoride ions. N_2F_4 reacted with acidic, basic and neutral solutions to give mainly nitric oxide and fluoride ions, further reaction of nitric oxide with the aqueous system giving rise to nitrite ions and nitrous oxide.

This formation of nitrite ions from the hydrolysis of both NF_3 and N_2F_4 has caused speculation about the possibility that the methemoglobin formation in intoxicated animals might result from a nitrite intermediate. Nitrite ion is a well known cause of methemoglobinemia[39,40,41]. The reduction of nitrate ions to nitrite in the intestine[42,43] and by bacterial action on spinach[44,45,46] is well known as a cause of the cyanosis resulting from methemoglobinemia. Very recently the dietary committee of the United Nations Food and Agriculture Organisation and of the World Health Organisation (Bonn, 1972) recommended that spinach be eaten immediately after being cooked and urged that babies aged under three months should be banned from eating fresh or frozen spinach. Other sources of nitrite poisoning have been reported, amongst which are

the adulteration of fish with sodium nitrite[47] and the use of meat-curing salt[48,49,50].

These dangers have caused the kinetics of methemoglobin formation by nitrite ions to be studied. In vitro peculiarities occur[51], and with low nitrite concentrations the reaction is very slow, but increasing the nitrite concentration promptly produces methemoglobin. This has been shown to result from an induction period[52] which, at pH 7, is inversely proportional to the square of nitrite concentration[53]. The reaction was found to be strongly affected by the nitrite and hydrogen ion concentrations[54,55] and on the degree of oxygen coordination on the hemoglobin,[53,56] and to be autocatalytic, but ferrihemoglobin concentration had no observable effect on the rate[57,58,55]. It has also been shown that the initial retardation of the reaction is not due to reduction of methemoglobin by nitrite[59]. Hydrogen peroxide is generated during the reaction[60] and nitric oxide hemoglobin is produced as well as methemoglobin, although the relative proportions of the products varies greatly with species[61].

Similar results have been observed in vivo for dogs and mice[62,63]. The degree of methemoglobin formation was not affected by changes in atmospheric pressure[64] and the action of nitrite in red cells appeared to be limited to methemoglobin formation although nitric oxide hemoglobin has been observed in a fatal case of human nitrite poisoning[65].

Dost et al have completed several further studies concerning the toxicology of NF_3 and N_2F_4. They have examined the decomposition of

tetrafluorohydrazine in the presence of oxygen and water[66] and showed that nitrosyl fluoride (NOF) was an intermediate in the formation of the products, NF_3, NO and NO_2. No reaction could be detected in the absence of either oxygen or water and under all conditions no NF_3 was observed as a reaction product. This was contrary to the findings of a previous study[67] in which N_2F_4 was reported to react with oxygen from laboratory air to produce NOF and NF_3. It is possible that the spectroscopic evidence for NF_3 as a product in this earlier work was due to an NF_3 impurity in the original N_2F_4, its presence being masked by the large infrared adsorption of N_2F_4 in the same region of the spectrum.

A study of the fluorine distribution in rats after acute intoxication with NF_3[68] showed that a general increase in fluoride throughout the tissues was produced during the inhalation, but disappeared mainly within the next 24 hours. The pattern of fluoride distribution following N_2F_4 treatment was similar; these effects were also similar, but on a smaller scale, to those observed following NaF administration. An important exception to the mobilization of fluoride accumulated in the tissues was observed in erythrocytes for both NF_3 and N_2F_4, but not for NaF. High fluoride concentrations in erythrocytes caused by intoxication persisted throughout the post-intoxication sampling period and appreciable amounts of fluoride which appeared in the spleens of some animals were taken as reflecting these high concentrations. Although this fluoride was shown to be associated with the hemoglobin and methemoglobin in the erythrocytes, it did not appear to be located on the heme iron.

Dost et al[69] have confirmed the degree of toxicity of inhaled NF_3 reported earlier[34], and observed that all animals tested recovered, if not dead by five minutes after the termination of exposure. Administration of NF_3 by intraperitoneal injection, however, caused death, usually two to three hours after methemoglobin had been dispelled, indicating that a second lethal mechanism might be operative.

A comparison of the rate of methemoglobin reduction following NF_3 inhalation with the rate following sodium nitrite intoxication showed that NF_3 induced methemoglobin was reduced approximately twice as fast as that produced from nitrite. While no major interference by NF_3 on the rate of methemoglobin reduction was observed, the level of methemoglobin, however, remained at 2 to 5% for several days, higher than similar results for control or sodium nitrite intoxication. This might be attributable to Heinz body formation caused by the NF_3 intoxication which has been observed by Vernot et al.[69].

The 60% to 70% oxidation of hemoglobin to methemoglobin in terminal stages of intoxication was thought to be the cause of death even though cats and dogs can tolerate methemoglobin levels up to 80%[70]. However, the delayed death following intraperitoneal injection of NF_3 indicates that other lesions may be caused. The differences between the effects of NF_3 and of its hydrolysis products, nitrite and fluoride ions, were felt to indicate that these ions were probably not involved in NF_3 intoxication.

Dost et al have also investigated the stoichiometry of the reaction of NF_3 with hemoglobin both in vitro and in vivo[71]. In vitro, the

disappearance of 1 mole of NF_3 was accompanied in each case by the oxidation of approximately 3 heme equivalents to methemoglobin regardless of pH or oxygen content of the hemoglobin solutions. Spectra indicated that the methemoglobin formed was identical to that formed by the action of nitrite and no evidence was found for the formation of methemoglobin fluoride[72]. No reaction could be detected in a control experiment between NF_3 and 0.1M ferrous sulphate solution under similar conditions. In in-vivo experiments on dogs the rate of reduction of methemoglobin by reductase activity had to be determined in order to correct the observed final methemoglobin concentration. Corrected results indicated that 1 mol of NF_3 was removed from the atmosphere in the oxidation of approximately 3 heme equivalents as was found for in vitro experiments. This agreement was taken as indicating that inhaled NF_3 reacted only with circulating hemoglobin.

Dost et al[142] have made similar toxicologic studies on N_2F_4 in an attempt to determine the toxicity of N_2F_4 itself rather than its degradation products[38,66]. Following lethal exposures to a confirmed N_2F_4 atmosphere, a high terminal methemoglobin concentration of between 60 and 70% of total hemoglobin was found in almost all animals. Rats exhibited rapid, sharp, gasping respiration during and after exposures. The cyanosis accompanying N_2F_4 intoxication did not appear identical to that caused by NF_3 or nitrite poisoning and the more pronounced gray-blue skin and mucous membrane colour indicated that methemoglobinemia might be accompanied by peripheral circulatory stasis. In earlier experiments in which the integrity of the

N_2F_4 atmospheres was not maintained, a similar overall lethality was observed, but with lower terminal methemoglobin levels of only 7 to 15%. These results were similar to those of Carson and Wilinski[36] and indicated that the manifestations of N_2F_4 intoxication depend on the extent and nature of the products of N_2F_4 decomposition in the air and respiratory gases. Intraperitoneal injection of N_2F_4 failed to cause high methemoglobin levels with only about 10% oxidation of hemoglobin from lethal doses.

In order to clarify the relation of N_2F_4 decomposition products to these results, rats were exposed to NO_2 and NO for qualitative observations. NO_2- induced methemoglobin failed to exceed 11% even with lethal doses, and methemoglobin formation appeared unrelated to lethal effect, NO_2 concentration or exposure time. The physical signs of intoxication were identical to those observed for N_2F_4 in early experiments when the integrity of the atmosphere was not maintained, indicating that N_2F_4 might well have been degraded to NO_2 and NF before inhalation in these experiments.

However, NO concentrations of 300 parts per million or greater caused very rapid and extensive methemoglobin formation which exceeded 85% of total hemoglobin in some animals before reflex activity was lost. Nitric oxide reacted rapidly with oxyhemoglobin in vitro to form methemoglobin and it seemed likely that NO might be a major contributor to the toxicity of N_2F_4 when the atmosphere was maintained prior to inhalation.

However, the lasting high fluoride concentrations in erythrocytes showed that a fluorine-bearing component, which was not derived from NaF or HF, was active in both NF_3 and N_2F_4 intoxication and therefore the toxicity of N_2F_4 cannot be entirely due to degradation to NO and HF.

The characteristics of NF_3 intoxication cannot be produced by administration of a combination of fluoride and nitrite ions[68,69] and it therefore appears that the mode of intoxication probably involves reaction of NF_3 itself with hemoglobin. However, results from intraperitoneal injection of NF_3 seem to indicate that the lethal effects are not confined to methemoglobin formation[69]. The studies on the stoichiometry of the reaction of NF_3 with hemoglobin[71], however, suggest that inhaled NF_3 can only react with circulating hemoglobin and that oxidation of hemoglobin by NF_3 is the only lethal pathway when the gas is inhaled.

With N_2F_4, the similarities to nitric oxide-induced methemoglobinemia indicate that degradation of N_2F_4 to NO may be a major factor in its mode of intoxication. However, administration of fluoride, or a combination of fluoride and nitrite, does not lead to retention of fluoride in the erythrocytes as was observed for N_2F_4. The degree of N_2F_4 degradation before inhalation caused little change in the overall lethality but caused large changes in the properties accompanying intoxication, most especially in methemoglobin concentrations. Using 'intact' N_2F_4 atmospheres, the large resulting methemoglobin concentration was apparently the cause of fatalities, but when the N_2F_4 atmosphere was not maintained, lethal doses

failed to cause extensive methemoglobin formation.

The retention of fluoride in erythrocytes indicates the possibility that the mode of intoxication by both NF_3 and N_2F_4 may be via direct reaction of these gases with hemoglobin, and not through intermediates. Since, in this case, the first stage of the intoxication must be the solution of the gas in a liquid phase, the solubilities of these gases are important factors (Part 1, Section 1).

Phosphorus has a valence shell structure of electrons formally similar to that of Nitrogen (both are Group V elements; second and first rows respectively). However, the absence of available d-orbitals in the nitrogen valence shell causes differences between the chemistries of the two elements. Thus nitrogen will form very strong $p\pi$-$p\pi$ bonds, but none of $p\pi$-$d\pi$ character, while for phosphorus, weak to moderate $d\pi$-$p\pi$ bonding is important, but no $p\pi$-$p\pi$ bonds are known. The availability of vacant d-orbitals in the valence shell of phosphorus allows valency expansion to occur with the formation of such entities as PX_5, PX_4^+, PX_6^-, etc., where X is a halide, alkoxy or phenyl group. However, the tendency towards ionic character with increasing atomic weight in the Group V elements is not sufficiently advanced in phosphorus, which is essentially covalent in its chemistry. In the case of the trivalent derivatives, however, there is a great similarity between the phosphorus and nitrogen compounds, the exception being in some of their reactions when valency expansion or π-bonding becomes possible.

Thus phosphorus trifluoride and tetrafluorodiphosphine may be considered as model compounds in the study of nitrogen trifluoride and tetrafluorohydrazine, and similarly difluoroiodophosphine may be considered as a model compound in the study of NF_2X (X = Cl or Br) (vide infra).

PART 1: SECTION 1

GAS SOLUBILITIES

INTRODUCTION

Although the solubilities of gases in liquids has received much attention, much of the earlier work was more qualitative than quantitative[77]. Gas solubilities have become increasingly more important both for the theoretical understanding of the liquid state and solutions, and for practical applications and a greater understanding of the solubility of gases in mammalian tissues and of the solubility of gases in molten salts and metals.

With the increase in work towards a theoretical understanding of gaseous solutions, there was a demand for practical determinations of solubilities both of a greater accuracy and also covering a larger range of solutes and solvents. The data available have been compiled and reviewed periodically[73,74,75,76,77]. The anomalous solubility properties of fluorine compounds[78] have proved to be of great importance in the investigation of solutions of non-electrolytes[75,76,79]. Although hydrocarbons show a regular behaviour in their solubilities in non-polar solvents[80,81], plots of partial molal entropy of solution against $-R \ln X_2$ (X_2 = mole fraction of gas) for fluorocarbon and other fluorinated gases and solvents show an anomalous behaviour[80,81,82,83]. Studies of the solubilities of these fluorine-containing gases have also proved useful in advancing the understanding of aqueous solutions[83,84]. Early work on CF_4 and SF_6 [83,85] showed that, at 25°C, these gases had the

lowest reported solubilities in water. The very low solubility of SF_6 was attributed to the unusually large entropy decrease on forming the solution[83]. However, since most workers had used equipment designed to measure considerably higher solubilities[83, 85], estimates of the changes in thermodynamic properties on solution of gases with such low solubilities were subject to great uncertainty.

Smith et al[84] used an apparatus specifically designed for the measurement of the solubilities of gases of the order of 10^{-6} mole fraction. They measured the solubilities of CF_4, SF_6 and NF_3 in water over a wide temperature range in order to compile accurate thermodynamic data. Previous reports of the change in entropy for the transfer of one mole of SF_6 gas at one atmosphere to a hypothetical solution of unit mole fraction had varied from -50 cal.mol.$^{-1}$deg.$^{-1}$ [83] to -36 cal.mol.$^{-1}$deg.$^{-1}$ [85] and such discrepancies hindered theoretical analysis of the dissolution process.

In this thesis the design and construction of an apparatus to measure the solubilities of gases in water are reported together with the solubilities of NF_3 and N_2F_4 obtained.

A variety of approaches has been used for the determination of solubilities of gases in liquids, and these may be broadly classified into two groups; chemical and physical. The first of these involves the quantitative measurement of dissolved gas by chemical means. However, although in specific cases this method can be highly precise

these methods are usually specific for a single gas and do not show general applicability. The most notable successful use has been in the measurement of the solubility of oxygen in water. Winkler[86] used the oxidation of freshly precipitated manganous hydroxide by dissolved oxygen at high pH values to form manganic hydroxide. At acidic pH the manganic hydroxide oxidised iodide ions to iodine which was then titrated against standard thiosulphate. However the lack of well documented quantitative reactions of N_2F_4 and NF_3 suitable for this type of estimation of these gases makes this approach inapplicable.

The second group involves the estimation of the dissolved gas by physical measurements, and can be subdivided into saturation and extraction methods. The saturation methods involve the equilibration of previously degassed solvent with a gas under conditions where appropriate pressure, volume and temperature measurements can be made. Extraction methods require the quantitative degassing of a previously saturated solvent, again under conditions where the appropriate parameters may be determined. The methods in the former subdivision have the disadvantage of requiring the measurement of the difference between two, usually large, quantities. This is the difference between the total amount of gas in the system and that remaining in the gas phase when saturation of the solvent has been achieved. However, the methods in the latter subdivision require not only the attainment of an equilibrium saturation of the solvent, but also the quantitative

degassing of this saturated liquid. This complete degassing incorporates many difficulties. Also, NF_3 has a vapour pressure at -196°C of 6.65×10^{-2} torr[87,27] (a printing error in Ref. 87, p 554, Eqn. 3 is repeated in Ref. 27, Appendix B), and therefore cannot be quantitatively trapped at liquid nitrogen temperatures, making this approach impracticable for this gas. The saturation methods have the further advantage of allowing several measurements for a range of temperatures and pressures to be made for a single charging of the apparatus and this also allows a test of saturation.

For these reasons, the apparatus described in this thesis was designed to measure solubilities by the saturation method. Further, since the solubility of NF_3 is small and the solubility of N_2F_4 was expected to be similar, the apparatus was designed to measure accurately gas solubilities of the order of 10^{-6} mole fraction. Measurements of the solubility of N_2F_4 in water were expected to be further complicated by its slow hydrolysis. Hurst and Khayat[38] have followed this reaction at 60°C and with partial pressures of N_2F_4 gas between one and two atmospheres. Long induction periods were observed of 5 to 9 days. This period was followed by an exponential increase in reaction rates.

Although the apparatus used by Smith *et al*[84] was specifically designed for the measurement of very low gas solubilities, the authors stated that 12 hours was usually sufficient for complete equilibration.

This long time for the equilibration between solute in the dissolved- and gas- phases would necessitate charging the apparatus several times should the solute hydrolyse slowly. The apparatus described by Dymond *et al*[80,88] was designed to reduce this equilibration time partly by using a considerably smaller solvent volume of about 250 cm^3 to 300 cm^3 as opposed to a volume of nearly 1200 cm^3 used by Smith *et al*. The central feature of Dymond's apparatus was a side arm containing a glass-encapsulated magnetically-activated pump which rapidly pumped solvent from a lower bulb containing the solvent into an upper bulb where the liquid flowed down the side of the bulb, continually exposing a fresh surface to the gas. By these means an equilibration time of one to three hours was found to be sufficient. However, although a series of measurements of the solubilities of various gases in cyclohexane and dimethylsulphoxide have been made using this apparatus[80,88,92], most of the solubilities recorded were greater than 10^{-4} mole fraction of gas and none less than 2.24×10^{-5} mole fraction (He in dimethylsulphoxide[80]). However, Dymond claimed that the values of the mole fractions for solutions of gases in cyclohexane were accurate to well within 1% (mole fractions ranging from 1.79×10^{-4} to 1760×10^{-4} [80]).

(a) The Main Solution Vessel

An attempt was made to construct a main solution vessel as designed by Dymond *et al*[88]. The main features of this design are shown in

Figure 1. The greatest problem in this construction was found to be its essential part, the side-arm P containing the magnetically operated pump. Numerous attempts by a professional manufacturer (Quartz Fused Products, Walton, Surrey) failed to produce a reliable pump. Precision bore tubing was used in order to obtain a sliding fit between the exterior of a glass encapsulated hollow cylindrical soft iron follower and the interior wall of the pyrex glass side arm. Too close a fit was found to cause too great a frictional resistance to allow the pump to be operated magnetically, and too loose a fit allowed too much back-flow of the solvent. The main cause of failure of pumps with reasonable fit appeared to be from excessive strain imposed by movement of the glass encapsulated follower. It was also found that the size of the soft iron follower was critical, too small a size not allowing the plunger to follow the magnetic field, and too large a size causing similar problems due to the increased weight of the plunger and greater restriction of flow through the decreased internal bore of the plunger.

In an attempt to overcome these problems, a soft iron core was imbedded in a solid block of P.T.F.E. (Crane Packing Ltd., Slough). The P.T.F.E. was then machined to give a sliding fit inside a length of precision bore tubing and then a hole was drilled centrally through the P.T.F.E. inside the soft iron core. While allowing an excellent fit

FIGURE 1.

Main Solubility Vessel as designed by Dymond et al.[88].

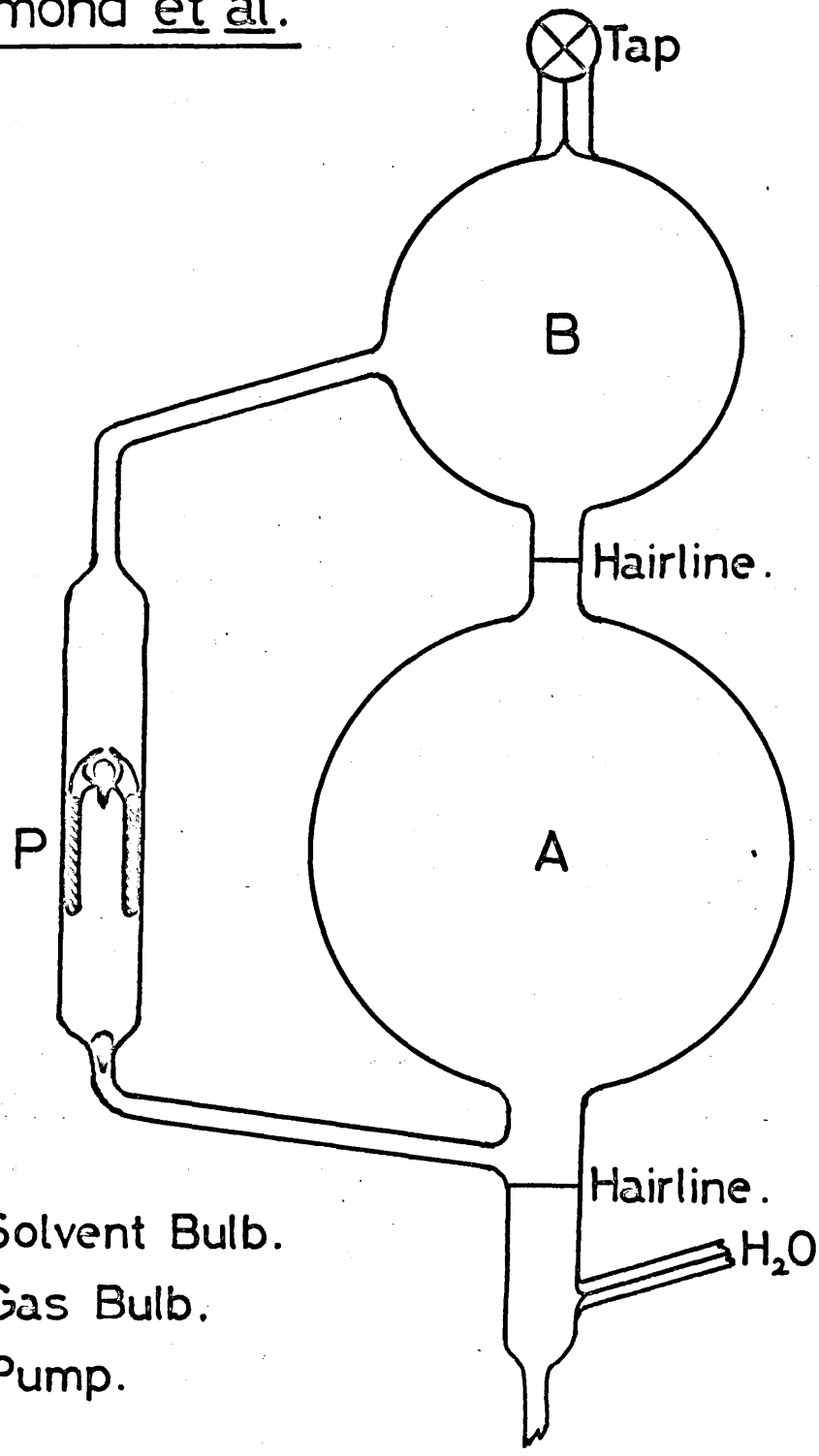

A. Solvent Bulb.
B. Gas Bulb.
P. Pump.

and almost frictionless sliding of the plunger within the side arm, the size of the plunger had to be kept larger than expected due to thermal cooling effects within the P.T.F.E. around the soft iron core. This had caused excessive cracking of the P.T.F.E. in the vicinity of the iron core due to impeded flow of the P.T.F.E. on cooling. In consequence the increased mass of the plunger over that expected caused considerable problems in its activation.

In the absence of a reliable pump for the circulation of the solvent, and with no suitable substitute for this part of the apparatus, the attempt to construct a main solubility vessel on the lines of that described by Dymond *et al* was eventually discontinued.

Two main methods of obtaining equilibrium between the gas and liquid phases, other than flowing a film of the liquid through the gas, have been used. The first of these involves the shaking of the apparatus containing the two phases as was described by Cook and Hanson[89] and Mader *et al*[90]. The basic apparatus was mounted on a steel plate which was vibrated horizontally at a frequency of about 170 min^{-1} and amplitude of about $\frac{3}{8}$ inch. An air thermostat controlled to at least $\pm 0.1^{\circ}$ was used. Using this system Cook *et al*[89,91] have measured the solubilities of hydrogen and deuterium in a variety of non-aqueous solvents. These ranged between a mole fraction solubility of 0.965×10^{-4} for H_2 in CS_2 at $-25^{\circ}C$. to 15.329×10^{-4} for D_2 in fluoroheptane at $35^{\circ}C$ and an accuracy of 0.1% was claimed.

The second method of equilibration involving bubbling the gas

through the liquid does not appear to have been widely used in conjunction with the saturation method. However, many methods have been used utilising internal stirring or agitation of the solvent. This increases the surface area of contact between the two phases and with fast stirring this area is often increased by gas from the bottom of the vortex bubbling through the solvent This type of equilibration has been often used[92] and was used by Smith[84] in the apperatus mentioned earlier.

This method was adopted, but involved considerable modification of the main solubility vessel. The design used is shown in Figure 2. The two bulbs used in Dymond's design have been replaced by one bulb B of approximately the same total volume. The side arm A was retained but with hair lines a and a' delineating fixed volumes. The base of the bulb was flattened but on a slope to allow drainage of the solvent into the vertical manometer arm C. The flattened base of the vessel allowed excellent stirring using a P.T.F.E. encapsulated magnetic follower about 23 mm long and about 8 mm diameter (F), ridged centrally to provide a pivot for rotation. This follower was driven by a fully submersible magnetic stirrer motor (Rank Brothers, Botisham, Cambridge). In operation at high stirring rates the liquid vortex reached the magnetic follower, spraying gas bubbles into the liquid thus increasing the surface area of contact between the two phases.

FIGURE 2.

Main Solubility Vessel.

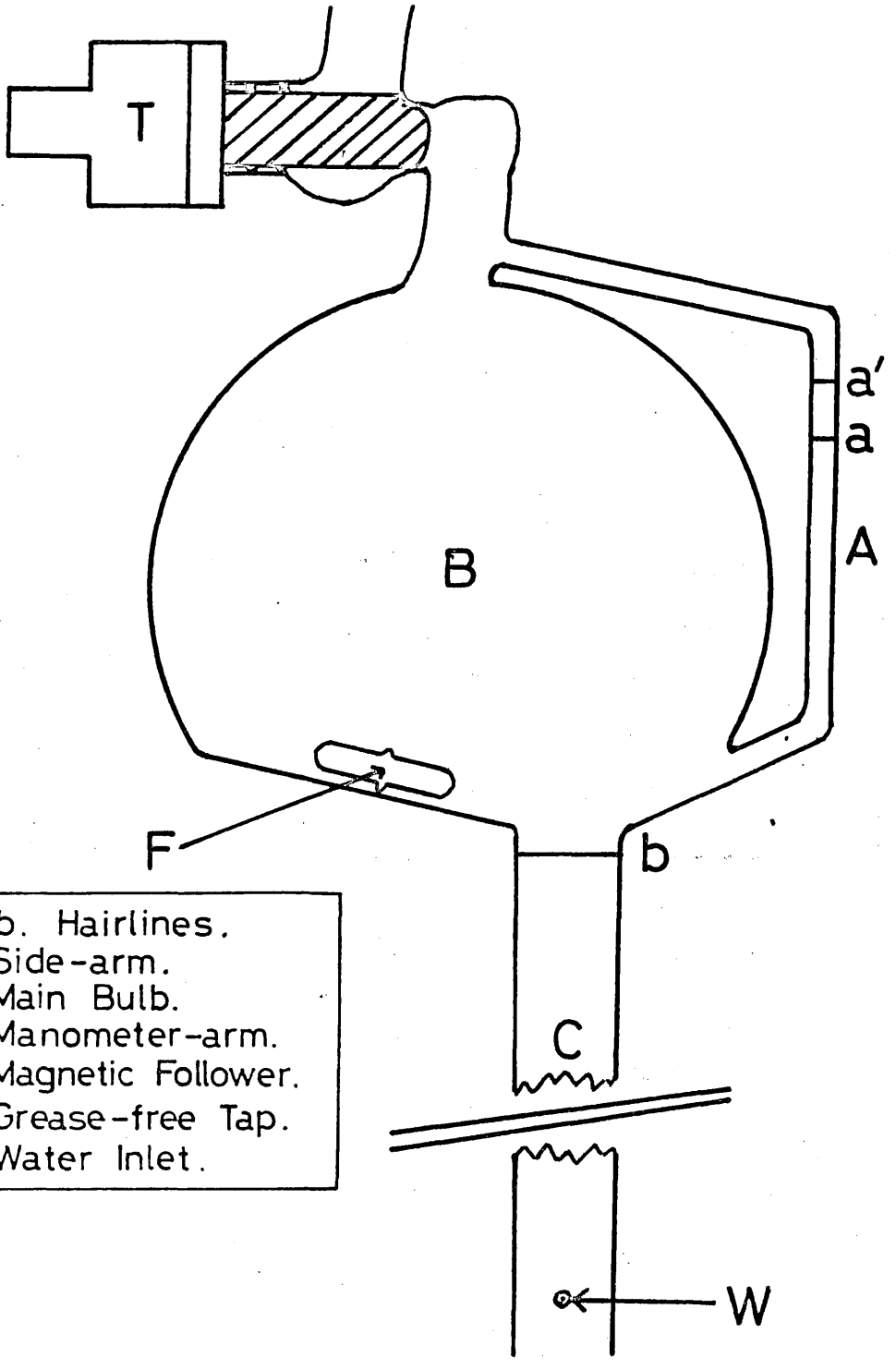

KEY

a,a',b. Hairlines.
A. Side-arm.
B. Main Bulb.
C. Manometer-arm.
F. Magnetic Follower.
T. Grease-free Tap.
W. Water Inlet.

This main solubility vessel was calibrated to give the volume between tap T and hairline b and also to give the volumes of water required to raise the meniscus from hairline b to hairline a and from hairline b to hairline a'. For this purpose the apparatus was cleaned thoroughly using a warmed solution of Quadralene Laboratory Detergent (Quadralene Chemical Products Ltd., Derby) followed by copious rinsing with greasfree distilled and deionised water. Measurements were made by additions of water from pipettes and burettes previously calibrated by weight of water delivered at 25°C. The laboratory distilled water supply was found to be contaminated by significant quantities of greasy material which was presumably carried by the steam supply. This could not be used for calibration as successive determinations of the volume between hairlines b and a' showed a steady increase which was attributed to deposition of grease on the vessel causing changes in surface tension. Water distilled in an all glass apparatus and deionised was found to give far better reproducibility. For all these measurements care was taken to maintain the arm C in a vertical position using a spirit level, as slight deviations caused inaccurate results especially in the measurement of the volumes delineated by the hairlines a and a'.

The vertical manometer arm C, fabricated from precision bore tubing, was calibrated to give the volume per unit length by the addition of known aliquots of water and measurement of the change in distance between the water meniscus and the hairline b using a cathetometer.

The tap T was a grease-free high vacuum stopcock (Glass Precision Engineering Ltd., Hemel Hempstead). These taps have a valve key fabricated from P.T.F.E. and therefore limit the solvent and solute to contact with Pyrex glass, P.T.F.E. and the mercury in the manometer.

The vertical manometer arm C was approximately 30 cm long, there being about 24 cm between the hairline b and the water inlet capillary W. This length allowed the solubilities of gases to be measured over a considerable range of pressures and temperatures using a single charging of the apparatus.

(b) The Manometer

In order to follow the change in pressure accompanying the dissolution of gas, the vertical tube C of the main solubility vessel (Figures 2 and 3) was used as the high pressure arm of a mercury manometer. This was connected through a high vacuum grease-free stopcock to a second vertical tube M (Figure 2) which was used as the low pressure arm of the manometer. This tube was about 140 cm long and allowed the measurement of pressure differences from zero to 130 cm Hg (1300 torr). In order to maintain the level of mercury in the solubility vessel within the tube C, a mercury reservoir arm R was incorporated, adjustment being achieved by varying the pressure through taps S and U of the air above the mercury in the reservoir. With high pressures in the main solubility vessel, pressures greater than one atmosphere were required in the reservoir arm and were obtained using a bicycle pump fitted with a football-blader adaptor/valve.

FIGURE 3.

The Manometer System.

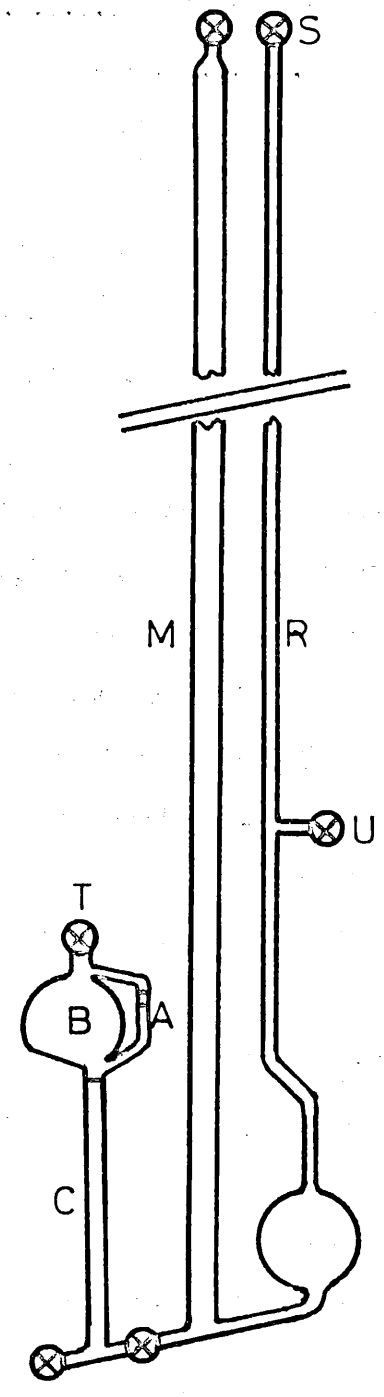

KEY

A. Side-arm.
B. Main Bulb.
C. Manometer-arm : high P.
M. Manometer-arm : low P.
R Reservoir-arm.
S,U. Stopcocks.

The reservoir bulb was approximately the same volume as the combined volumes of the manometer arms M and C to allow complete adjustment for all pressures up to 130cm Hg.

One of the greatest errors in the measurement of pressures using mercury columns is the capillary error[94] due to the surface tension of mercury at the meniscus. This error was partly compensated by using Pyrex glass tubing of the same internal diameter for both manometer arms, C and M. However, the magnitude of this effect is not only influenced by the bore of the tubing used, but also by the condition of the glass and mercury surfaces. Many precautions were taken in order to ensure clean glass surfaces and clean mercury. The glass was cleaned using warm Quadralene solutions followed by copious rinsing with grease-free water. The mercury used in the manometer was of triply-distilled quality, and was filtered through a pinhole and then redistilled under vacuum using grease-free glass apparatus fitted with P.T.F.E. sleeves on standard ground-glass joints. The manometer was filled with mercury while under high vacuum and with continuous pumping, the mercury being allowed to enter slowly to ensure that all dissolved gases were removed.

However, there was no way of avoiding one meniscus being 'wet' through contact with the water used as solvent, and the other being 'dry', and correction for this difference between the menisci could not be applied due to lack of data on the surface tension of mercury in contact with water. This error was therefore minimised by using a large

internal diameter of 16 mm for the manometer tubes C and M. A greater diameter was not used as this would have increased the volume and weight of mercury required excessively and also would decrease the sensitivity of the measurement of volume in terms of the length of tube C below hairline t. (Figure 1).

In order to maintain a reliable reference pressure in the low pressure arm of the manometer (M), this arm was pumped continuously during pressure measurements. The vapour pressure of mercury at the temperatures used is of the order of 10^{-3} torr and this continuous pumping thus ensured a reference pressure of less than 10^{-3} torr. The entire manometer was thermostated to the same temperature as the main solubility vessel (vide infra).

Both arms of the manometer were set vertical using a spirit level, and were positioned 8 cm apart, as close as possible. This facilitated accurate measurements of the positions of the mercury menisci using a cathetometer situated about 2250 cm away from the manometer. The 'sine error'[94] due to deviations from the vertical of the cathetometer, was thus limited by allowing both menisci to be observed with minimum rotation. This error was further reduced by careful levelling of the cathetometer. For this purpose the incorporated small circular spirit level was inadequate, and it was found to be far more precise to use the linear spirit level on the telescope itself. Levelling was achieved by altering both the main and the telescope adjustments until rotation of the telescope and scale through 180° caused no change in the position of

the spirit level bubble. This procedure was repeated at 90° to the former positions, before the former positions were checked.

It has long been recognised that a greater accuracy is achieved by placing a scale alongside the mercury tubes rather than by using the cathetometer scale (Morley, 1889.Ref.94,p.15). Where the cathetometer scale is used, large errors are introduced from slight deviations of the optical axis of the telescope from horizontal. With a manometer-to-cathetometer distance of 2250 cm a deviation from the horizontal of 1.5 minutes of arc would cause an error of 0.1 mm if the cathetometer scale was used[94]. Two steel rules (Rabone Chesterman Ltd., Birmingham), calibrated in mm and half-mm, were used to provide a scale between, and at approximately the same distance from the cathetometer as, the manometer arms (in practice, it was found necessary to place the steel rules 2 cm further away). The first of these was a matensitic stainless rule graduated over 60 cm and was used inside the water thermostating bath (vide infra). The second was a 1% carbon steel metre rule and was used outside the bath,above,but overlapping,the first rule. The rules were both clamped firmly at the top, but only sufficiently at the bottom to maintain a vertical position set by spirit level. The vertical position was checked before and after each run in order to limit the error caused by deviations ('cosine error'[94]). The light clamping at the bottom of each rule allowed thermal expansion to tube place without bending of the rule.

The combined use of the two steel rules permitted the accurate measurement of any level within the manometer system relative to these rules. To determine subdivisions of the rule scale divisions, the following method was used. The vertical cathetometer was focussed on the mercury meniscus and adjustments made to bring the sighting-cross coincident with the mercury meniscus. The cathetometer scale reading was recorded and the procedure repeated for two steel rule graduations, 1 mm apart, one above and one below the mercury meniscus. The position of the mercury meniscus relative to the rule was then obtained by interpolation. The same procedure was adopted for measuring the levels of hairline b (Figure 2) and of the solvent (water) meniscus and also for the relative positions of the two steel rules. In this way no correction was required for the thermal expansion of the cathetometer scale.

Good illumination was required for accurate sighting on the mercury meniscus and also on the other levels recorded. Frontal illumination was found to be adequate for sighting on the two steel rules, but inadequate for the other levels due to reflection of light from the glass and mercury surfaces. Green transmitted light has been recommended[94] and was found to silhouette the mercury menisci sharply and also greatly facilitate sighting on hairline b and on the solvent meniscus. Best results were obtained by blanking off the light just above the meniscus thus preventing any reflections from its surface.

This method gives illumination of the meniscus as seen through the cathetometer by nearly parallel light in the vertical direction thus simulating the conditions found necessary for greatest precision by other authors[95,96] without necessitating the use of lenses. The illumination however had to be repositioned for each reading. A 15 watt 'pearl' bulb in conjunction with a clear-green filter was blanked off for half its vertical illuminated length and used for the low pressure arm M of the manometer. The high pressure arm C was illuminated using an 11 inch fluorescent 8 watt tube. This was wrapped in a green filter and sealed inside a pyrex tube for use in the water bath (vide infra). A black plastic rider on the pyrex tube movable by a wire from outside the water bath allowed the light above the meniscus to be blanked off.

Using the above method, measurements of the positions of all the levels were poproducible to $\pm$ 0.002 cm. The calculation of the pressures from these readings together with the corrections that had to be applied, is discussed in a later section (h).

(c) The Gas Burette and Barometer

A gas burette was built to the normal design. The volumes used were slightly smaller than those used by Dymond et al[88], the fixed volumes being approximately 20 cm^3 and 30 cm^3 in combination with a 25 cm^3 graduated burette tube. These two volumes and the burette tube were calibrated by weighing the mercury displaced from each. The gas

burette was designed to be used outside the thermostating tank for the solubility apparatus (vide infra) in order to facilitate operation and was thermostated by rapid circulation of water through a jacket. A thermostating circulator with inbuilt chiller (Churchill Instrument Co. Ltd. Perivale, Middlesex) was used and was set at 25°C. The temperature of the circulating water was measured on exit from the gas-burette jacket. Grease-free, high vacuum, P.T.F.E. stopcocks were used throughout. The pressure reference tube, open to the atmosphere, was beside the graduated burette tube and of the same internal diameter.

The operation of this apparatus necessitated a knowledge of the atmospheric pressure at the time and place of use. Two barometers were tested using the gas solubility apparatus manometer, with the main vessel open to the atmosphere, as a standard. The first of these barometers (Chemistry Department) was found to give readings about 2.5 mm above those obtained using the manometer. The second (Physics Department) differed from the manometer readings by only about 0.1 mm, but this was considered to be within the limits of reproducibility for this barometer, since the mercury in the reservoir was covered with a scum. It also became apparent, from a series of readings using the first barometer compared with readings on the manometer, that this instrument was not capable of the precision required. The apparent reproducibility of the readings from the first barometer was $\pm$ 0.4 mm Hg, far worse than the estimated precision of $\pm$ 0.025 mm for this type of instrument under optimum conditions[94].

Due to this lack of an adequate existing instrument, a barometer was constructed and incorporated into the solubility apparatus. A reservoir of about 40 mm internal diameter was used in conjunction with a medium bore (approximately 8 mm external diameter) barometer tube which was connected to 16 mm internal bore tubing to cover the region 70 cm to 82 cm above the reservoir. The 'capillary error'[94] was therefore limited by the large areas of the menisci. The cathetometer was used for measuring the height of the mercury column using the same steel rules as for the manometer and the same type of illumination. Similar precautions were taken, but the barometer unavoidably had to be placed about 50 cm further from the cathetometer that the rules, necessitating very careful levelling of the cathetometer. Continuous pumping on the upper mercury surface ensured a good vacuum. The calculations and the corrections involved in these calculations of the atmospheric pressure from the height of the mercury column were the same as for the manometer and are discussed later.

To operate, the gas burette was evacuated and mercury from the reservoir admitted to fill the fixed volumes and graduated burrete tube. The gas was then introduced, displacing the mercury from the two fixed volumes and the graduated tube back into the reservoir. The mercury level in the two fixed volumes was adjusted to the bottom hairline and the stopcock to this arm closed. By adjustment of the height of the reservoir, the menisci in the graduated tube and in the pressure reference tube were brought to the same level using the cathetometer for comparison. The graduated burette tube reading was recorded. Gas

was then admitted to the solubility vessel and the levels of the mercury menisci in the gas burette readjusted. In most cases this involved filling both fixed volumes with mercury followed by adjustment of the levels in the graduated and reference tubes. A glass plunger fitted with P.T.F.E. 'O' rings was fitted in a side arm on the reservoir and coupled to a screw-thread to allow fine adjustment of the mercury level in the reservoir. The atmospheric pressure, using the barometer described in the previous section and the temperature of the thermostating water, were recorded, allowing the amount of gas added to the solubility vessel to be calculated from the difference between the volumes in the gas burette before and after the addition.

This method allowed the initial quantity of gas to be measured in a 'dry' state, i.e. free of solvent vapour. It has been suggested that the commonly used 'wet' method frequently gives rise to low values in the measurement of gas solubilities[77,84,97] especially if there is any uncertainty as to whether the gas is saturated with solvent vapour.

The main difficulty found during operation of the gas burette was caused by changes in atmospheric pressure. Changes of only 1 to 2 cm Hg in the gas pressure within the gas burette can cause adiabatic heating or cooling sufficient to require an additional half-hour in order to attain temperature equilibrium[77,91]. Thus after addition of gas to the solubility apparatus and rough adjustment of the gas burette back to atmospheric pressure, at least half an hour had to be allowed

before final adjustment and measurements could be made. This time was almost invariably sufficient for significant changes in atmospheric pressure to have occurred, and no method for the control of atmospheric pressure was available. These fluctuations made it essential for the barometer to be read as near to the time of reading the gas burette as possible. However, under some weather conditions, these fluctuations were so fast that, even during the interval between the measurements of the two mercury menisci of the barometer, there were significant changes in atmospheric pressure.

It was also found necessary to add the solvent to the solubility vessel after addition of the gas. In early experiments addition in the reverse order led to errors due to diffusion of water vapour from the solubility apparatus into the gas burette during the addition of gas. This caused low values for the amount of gas added, and consequently low values for gas solubilities.

(d) Solvent and Solute purifications

For gas solubilities, the purification of the solvent and solute are contributing factors to the accuracy, especially where low solubilities are involved. In particular, incomplete degassing has been considered to be a main source of error in the determination of gas solubilities[88]. The most frequently used method of degassing a liquid is to boil away a portion of it under vacuum. Usually 10% to 20% of the solvent has to be evaporated off and tests (vide infra) have to be used to ensure complete degassing. This pumping usually has to be continued for several hours.

An alternative method has been used in order to minimise the loss of solvent involving pumping on the frozen solvent followed by melting without pumping. This cycle has to be repeated several times and tests to ensure complete degassing are even more important than in the previous method[77].

In order to ensure complete degassing, Clever et al[98] used the first method to remove about 90% of the dissolved gas, and then sprayed the preliminary degassed liquid through a fine nozzle into an evacuated flask. Rapid and complete degassing by this method was claimed. A similar method had been employed for the degassing of oils[99].

From previous experience on the vacuum line, degassing by pumping on frozen or liquid solvents was found to be far less efficient than by trap-to-trap distillation. This method effectively combines the two operations used by Clever et al[98] into one operation. Since all the solvent is evaporated, degassing is almost complete after one distillation. However, even with continuous pumping, some gas is trapped in a matrix of condensed solvent and a second distillation is required to remove the last traces of gas from the solvent.

The apparatus used was completely grease-free. This was achieved by using grease-free, high-vacuum, stopcocks with P.T.F.E. valve keys in pyrex glass. Grease-free distilled water was obtained by distillation from acidic potassium permanganate solution. This was introduced into the vacuum line in a 500 cm^3 round-bottomed flask fitted with a grease-free joint (J. Young, Scientific Glassware, Acton). The traps used

were of a 'U' tube design, but built to accommodate the distillation of 250 cm^3 aliquots of solvent, the two arms being approximately 6.5 cm and 2.5 cm in diameter with the solvent being condensed in the larger arm. This diameter was found to be sufficient for condensing about 300 cm^3 of liquid solvent before blocking the tube. The two arms were joined by a horizontal 6.5 cm tube just over 9 cm long. This large volume below the two arms allowed the solvent to melt inside the 'U' tube without the liquid meniscus being in the arms. With volumes greater than about 275 cm^3, the solvent in the arms prevented water vapour passing through the trap and caused severe 'bumping' when the solvent was being distilled out of the trap.

Two traps of this design were used to allow two successive distillations. In order to ensure complete degassing the solvent was distilled a third time under high vacuum into a 500 cm^3 round-bottomed flask equipped with a capillary tube for siphoning the solvent out. By this method the solvent could be transferred to a 500 cm^3 storage vessel, the vapour pressure of the solvent being sufficient to initiate siphoning if the solvent was slightly warmed.

The most used criterion for complete degassing has been the reproducibility of the measurements or, its corollary, the agreement between several workers for the same measurement. This criterion has been criticised[77] in that it does not allow for the repetition of systematic errors and also perpetuates older measurements as standards when they may have been superseded by more reliable measurements.

Two additional criteria for complete degassing have been used[89]. The first involves the monitoring of the pressure of non-condensible (by liquid nitrogen) vapours during degassing. A vacuum gauge is situated between the pumping system and a liquid nitrogen trap protecting it from the solvent degassing system. In this way the pressure recorded drops during degassing until the base pressure of the pump is reached indicating that only negligible amounts of non-condensible gases are present. However, when the degassing procedure involves the simultaneous boiling and pumping on the solvent, it has been recommended that an additional quantity of solvent should be evaporated to be certain of complete degassing[77].

The second method requires the cushioning of the degassed solvent between mercury followed by inspection for gas bubbles. This method is quite sensitive since gas bubbles much smaller than 10^{-3} cm^3 can be detected, and since solution rates are slow, the bubbles will persist for several minutes.

The former of these two criteria was used to ensure the complete degassing of the solvent during trap-to-trap distillations. A liquid nitrogen trap situated between the water distillation assembly and the rest of the vacuum line and gas solubility apparatus prevented water vapour reaching the pumping system, the base pressure of which was between 10^{-6} and 10^{-5} torr. An ionisation-type pressure gauge was used to monitor the pressure of gases not condensed by the liquid-nitrogen trap.

Preliminary evacuation of the round-bottomed flask in which the solvent was introduced removed most of the gas above the water with only a little water being lost to the liquid-nitrogen trap. Following this, it was found beneficial to allow several hours for re-equilibration between the liquid and gas phases before distallation to the first 'U' tube was commenced. Crushed solid carbon dioxide in acetone was used throughout for the condensing of water vapour.

Following an initial pressure surge during the first distillation, the gauge-recorded pressure was maintained below 10^{-2} torr by adjustment of the interconnecting stopcock, which could be fully opened after a few minutes of distillation. By maintaining this low pressure, only small amounts of gas were trapped in the ice matrix. During the second distillation, the gauge-recorded pressure quickly fell from an initial pressure of under 10^{-3} torr to the base pressure of the pumping system. This base pressure was maintained throughout the third distillation, indicating that, within the limits of this criterion, complete degassing had been achieved by the first two distillations. A water bath roughly thermostated at temperatures up to 60°C was used to increase the rates of the second and third distillation and also for the first after the interconnecting stopcock was opened fully. The water was stored in a vessel sealed by high-vacuum stopcocks. The vacuum system between the siphon trap and the main solubility vessel inclusively was thoroughly cleaned with warm Quadralene Laboratory Detergent solutions followed by copious rinsing with grease-free distilled water and finally pumped for several days.

This guarded against contamination of the water after the final distillation.

NF_3 for use in the gas solubility apparatus was purified by trap-to-trap distillation within the main vacuum line (vide infra). Distillation through a trap refrigerated by an iso-pentane slush (-160°C) removed all likely impurities from the research grade NF_3 used (Air Products and Chemicals, Inc., Pennsylvania, U.S.A.). The NF_3 passing through this trap was mainly collected in a liquid nitrogen trap and any nitrogen or oxygen impurity was pumped off. Some NF_3 was unavoidably lost on passing through the liquid nitrogen trap. The purity of the NF_3 was confirmed by pressure measurements on the vapour above liquid NF_3 held at -126°C (Methyl-cyclohexane slush) before and after expansion of the vapour into an evacuated bulb. No significant change in the vapour pressure was observed ($\pm$ 1.5 mm Hg).

Research grade N_2F_4 (Air Products and Chemicals, Inc., Pennsylvania, U.S.A.) was used with a stated purity of 99.9%, the major contaminants being NOF and N_2O. N_2F_4 exhibited a pale purple coloration when condensed in the vacuum line straight from the cylinder. This purple coloration has been attributed to the thermally unstable compound NF_2NO[27,100,101], it being estimated that as little as 0.1% of NF_2NO caused a pronounced purple coloration. Pumping on the condensed gas held at -196°C also showed the presence of an impurity with a vapour pressure at this temperature of about 5×10^{-2} torr (probably NF_3) and this impurity was removed by repeated fractionation with pumping through

a trap held at -196°C. Although the presence of NF_2NO as an impurity in N_2F_4 samples is well documented, a survey of the literature revealed that most studies had apparently been carried out without further purification, and no method for the removal of this impurity could be found. However, the presence of an impurity even to the extent of less than 0.1% could cause serious errors in solubility determinations. The impure N_2F_4 was therefore fractionated through a trap at -160°C (Isopentane slush) to a trap at -196°C in an attempt at purification. The vapour pressure of N_2F_4 at -160°C has been variously estimated as 0.389 torr[102], 0.564 torr[103] and 1.638 torr[18] and thus this gas should pass slowly through a trap at -160°C. NF_2NO is known to dissociate in the gas phase to N_2F_4 and NO[27], and since the vapour pressure of the latter is greater than 100 torr at -160°C, NO should pass through this trap quickly. During this distillation, N_2F_4 passed only very slowly through the trap at -160°C, but comparison of the contents of the two traps after about one hour of fractionation revealed only a very slight difference in coloration, the contents of the -196°C trap being slightly darker. It was evident that either the NF_2NO had not decomposed extensively in the vapour phase during distillation, or that recombination of NF_2 radicals with NO had occurred during condensation of the N_2F_4 in the -160°C trap. No vapour pressure data for NF_2NO has been reported, but from this distillation it was apparent that at -160°C its vapour pressure must be approximately the same as that for N_2F_4.

Purification was eventually achieved by mixing the impure N_2F_4 with bromine in the vapour phase. Bromine should not react with N_2F_4 under these conditions, but should react with nitric oxide to form NOBr. A reaction time of approximately 1 hour was allowed before excess bromine was removed by fractionation through a trap at -30°C (solid CO_2/acetone). The fraction not retained by this trap was trapped at -196°C and on warming formed a clear liquid, in which a very faint mauve coloration could just be detected, above a brown solid. Fractionation of this through -160°C to -196°C at first produced a fraction passing through -160°C which on melting was a pale mauve liquid, the coloration being of about the same intensity as the liquid before purification. Continued fractionation through these traps produced fractions held at -196°C with steadily decreasing coloration, until after one hour no coloration could be detected. This fraction was collected for a further ten hours in order to obtain slightly less than 10 cm^3 of liquid sample.

The gas phase infra-red spectrum of this sample recorded over the range 4000 cm^{-1} to 625 cm^{-1} (Perkin-Elmer, Model 257) showed absorption maxima at 1029, 1013, 1009, 997, 959, 945, 932 and 735 cm^{-1}. These frequencies are in excellent agreement with literature values[10,104,105,106,107,108,109]. No other absorptions were detected even at high pressures and the absorption observed at 852 cm^{-1} [108] must be assigned

as an impurity in agreement with the assignment of Koster and Miller.[109] In particular, no absorption was found in the region of 645 cm^{-1}, the frequency assigned to the N-Br stretch for NF_2Br.[110,111] The purity of this sample was confirmed by the method used for NF_3 by vapour pressure measurements before and after expansion with the liquid N_2F_4 held at about -30°C. (Solid CO_2/acetone slush). No significant pressure change was observed. (± 1.5 mm Hg.).

NF_3 and N_2F_4 were stored in previously evacuated vessels at -196°C.

(c) Temperature Control.

A full analysis of the effect of temperature fluctuations on gas solubility measurements has been published by Cook.[112,77] Four main factors were given; the temperature coefficient of the solvent vapour pressure; the temperature coefficient of solubility or the change in the equilibrium partial pressure of the dissolved gas with temperature at approximately constant concentration; the temperature level of the experiment; and the pressure level of the experiment. The magnitude of these factors depends not only on the system studied, but also on the type of apparatus used. Cook found that temperature control to ± 0.1°C was adequate for an overall precision of ± 0.05% using his apparatus for the system H_2 - n-heptane in the range - 30°C to 50°C. A preliminary calculation, however, showed that considerably better thermostating was required for use with the present apparatus. This difference partly resulted from the lower solubilities to be measured, but also from the

design of the apparatus. Cook's apparatus [77] was [112] designed such that all but about 1 cm^3 of the solute gas was dissolved, limiting the range of pressures and temperatures that could be covered using one charging of the apparatus and also necessitating a good estimate of the solubility before starting to take measurements. In the present apparatus, the gas dissolved was calculated from the difference between the gas originally added (about 100 cm^3 at N.T.P.) and the gas remaining undissolved (90 cm^3 to 95 cm^3 approximately).

From calculations on NF_3 using the solubility data reported by Smith et al [84] this difference should be 5-10 cm^3. Analysis of the effect of temperature fluctuations on this basis showed that for an overall precision of 0.1%, temperature control to $\pm$ 0.01C would be necessary at 50°C, but only to $\pm$ 0.03C at 15°C.

A water bath was fabricated from a 30 gallon galvanised iron tank (2' x 1' 3" by 2' high). The front 2' x 2' face was removed and replaced by $\frac{1}{4}$" plate glass. A water tight seal between the glass and the metal was achieved using Cold-Cure Silastomer 9161 (Hopkin and Williams Ltd., Chadwell Heath, Essex). The glass was wedged to maintain a position about 3/16" from the frame and held in position by stays across the tank before the liquid Silastomer was poured between the frame and the glass and allowed to set under the influence of the catalyst. The stays were left permanently in position since Silastomer has poor adhesive properties when set. This method of sealing was found preferable to

the use of window or 'fish-tank' putty since both of these harden at temperatures above 25°C causing extensive leaking. This tank could be raised to surround completely the main solubility vessel to above tap T (Figure 2) and the manometer arm M and compensating arm R up to this level. A semi-submersible pump (Grant Instruments (Cambridge) Ltd., Barrington, Cambridge) was used to provide fast circulation of water from the bath through a jacket enclosing the part of the manometer arm M above the water bath. This ensured that the manometer and main solubility vessel were thermostated to the same temperature. The level of mercury in the compensating arm R was never outside the water bath and no further thermostating was required.

Temperature control was achieved using a mercury contact thermometer adjustable between 0° and 100°C (A. Gallenkamp and Co. Ltd., London.) in conjunction with a hot-wire control relay (Sunvic Controls Ltd., supplied by Griffin and George Ltd., Wembley). Four immersion heaters were used to allow heating rates between 250 watts and 2250 watts, and the rate was varied with the bath temperature required such that the heaters were operating 50% of the time. A neon indicator light fitted to the control relay facilitated this selection of heating rate. For temperatures just above and below ambient, an even, slow cooling rate was ensured by slow cold water flow through a cooling coil, made from 5 feet of 3/8" diameter copper tubing, which was submersed in the water bath. For temperatures well below ambient, two chiller circulators (Churchill Instruments Co. Ltd., Perivale, Middlesex)

were used in series to circulate refrigerated anti-freeze solution through the copper cooling coil. Thermostatic control could be maintained at temperatures down to about 10 degrees below the ambient temperature by this method.

A four inch, six-bladed stirrer was mounted on a 12" shaft and driven by an electric motor rated at 0.13 horsepower and 1400 revolutions per minute. This motor was originally mounted on the framework supporting the main solubility vessel and manometer, but was found to cause excessive vibration. A heavy-duty flexible drive was therefore used to allow the motor to be mounted remote from the main framework, considerably reducing the vibration. Further reduction was achieved using a P.T.F.E. bearing round the shaft near the stirring blade. This stirrer was positioned to give maximum circulation of water round the tank, with the shaft at an angle of about 45° to the horizontal. The immersion heaters and cooling coil were positioned such that water flowed past the heaters, down past the stirring blades and through the coil.

The temperature stability of this system was tested using a platinum-resistance wire coupled through a bridge to a chart recorder, giving a 3 cm per centigrade degree scale. Temperatures between 15°C and 45°C were tested, and each was maintained to $\pm$ 0.01°C, with slightly better stability than this at temperatures near ambient.

A constant-level device was incorporated into the design in order to compensate for changes of the water level in the water bath due to

evaporation or to a change of temperature. A siphon tube maintained the water in the water bath at the same level as in a tube outside the bath, and the level in this tube was maintained by constant flow of water into the tube and out of an overflow.

The vacuum stopcocks used on the main solubility vessel and at the bottom of the manometer system were immersed in the water bath during runs. Despite the temperature range of from -20°F to +400°F (-29°C to 204°C) quoted by the manufacturers, these P.T.F.E. keyed stopcocks failed to maintain a vacuum at 15°C. This necessitated a modification which is described in the section dealing with the vacuum line (vide infra).

(f) Calibrations.

The results of the volume calibrations of the main solubility vessel and of the gas burette, which have been described, are given in Table 1. The accuracies of these calibrations have been estimated and the limits are expressed either in terms of twice the standard deviation of the mean for the measurements made [120] (For n readings v_n with mean $\bar{V}$, Standard Deviation of the mean $= \sqrt{\frac{(\bar{V} - v_n)^2}{n(n-1)}}$), or as the spread of the readings from the mean.

Data of the accuracy and coefficients of linear thermal expansion of the two steel rules and of the coefficient of thermal expansion of 'Pyrex' glass are listed in Table 2.

TABLE 1. VOLUME CALIBRATIONS

Main Solubility Vessel at 25°C

Part	Volume(cm^3)	Estimated Accuracy(cm^3)
Tap T to hairline b.	378.0136	± 0.005 *
Hairline b to hairline a.	218.3	(see text)
Hairline b to hairline a'.	282.0	(see text)
Per cm length of tube below hairline b.	2.0006	± 0.012

Gas Burette at 25°C

Part	Volume (cm^3)	Estimated Accuracy(cm^3)
Large calibrated volume.	29.078	± 0.002 *
Small calibrated volume.	13.185	± 0.001 *

Graduated tube.

Scale Reading	Volume (cm^3)	Deviation from scale
0	0	0
2	1.998	-0.002
3	3.013	+0.013
5	5.023	+0.023
7	7.039	+0.039
10	10.051	+0.051
12	12.060	+0.060
15	15.073	+0.073
17	17.075	+0.075
20	20.073	+0.073
22	22.067	+0.067
25	25.069	+0.069

Estimated accuracy of volume between any two levels ±0.02cm^3

[Estimated limits are expressed in terms of twice the standard deviation of the mean[100] or (for limits marked by *) in terms of the spread of the readings taken.]

TABLE 2

Steel Rules

Rule	Accuracy	Coefficient of linear expansion
60 cm Matensitic Stainless.	± 0.02 cm at 20°C	10.9×10^{-6} C^{-1}
100 cm 1% Carbon Steel.	± 0.025 cm at 20°C	11.1×10^{-6} C^{-1}

'Pyrex' Glass

Coefficient of Linear Thermal Expansion = 0.033×10^{-4} C^{-1}

(for $20°C < T < 300°C$)

Coefficient of Cubical Thermal Expansion = 0.099×10^{-4} C^{-1}

TABLE 3

Thermometer 1. (for use with Gas Burette). Calibrated at 13 different temperatures between 24°C and 26.5°C. At all temperatures tested.

T = [(Reading of thermometer 1) + 0.08]°C.

Thermometer 2. (for use in Water Thermostat Bath)

T = [(Reading of thermometer 2) + Δ]°C.

Temperature(°C)	Δ(°C)
15	0.10
25	0.16
35	0.24
45	0.33

Thermometer 3. (for use to measure ambient temperature-temperature of 0.1% Carbon Steel rule).

Calibrated from 20°C to 30°C.

Temperature(°C)	Δ(°C)
20	0.15
25	0.13
30	0.13

Three mercury-in-glass thermometers, graduated from -5°C to 50°C, were calibrated by comparison with a therometer calibrated at the National Physical Laboratory, Teddington, Middlesex. The results of these calibrations are listed in Table 3.

During the calibrations of the volumes of solvent contained between hairlines b and a and hairlines b and a' of the main solubility vessel, great difficulty was experienced in filling the apparatus to place the meniscus exactly on the hairlines a and a'. The accuracy of these calibrations affects not only the accuracy of the measurement of the solvent volume, but also the accuracy of the measurement of the volume of residual gas after solution equilibration. Since only 5-10 cm^3 of gas at N.T.P. should dissolve, the accuracy of the measurement of this gas volume must be to about $\pm$ 0.05 cm^3 for an overall accuracy of 1% in the measurement of the solubility. The diameter of the main solubility vessel at the levels of hairlines a and a' is about 9 cm and, therefore, for this overall accuracy, the level of the meniscus in the side arm must be coincident with the meniscus to $\pm$ 0.008 mm. It was not felt that this accuracy could be achieved.

In a trial solubility run using NF_3 as solute, the water volume was measured five times by bringing its meniscus to hairline a' and measuring the vertical length between hairline b and the mercury meniscus in tube C (Figure 2). The adjustment of the pressure in the manometer compensating arm in order to bring the water meniscus coincident with the hairline was found to be very difficult. After each measurement, the position of the

water meniscus was moved and then readjusted to again bring it coincident. The spread, or standard deviation of these results, is, therefore, a measure of the accuracy of making the water meniscus and hairline coincident. The accuracy found (twice the standard deviation of the mean)[120] was $\pm$ 0.12 cm^3, indicating that this method of measuring the solvent volume was not sufficiently accurate.

The total volume of the main solubility vessel was known to within satisfactory limits and therefore the residual gas volume could be calculated, provided that the solvent volume is sufficiently defined. The factor therefore required in order to achieve satisfactory accuracy of the measured solubilities was an accurate method for the delivery of a known volume of solvent (about 300 cm^3) into the main solubility vessel. A solvent calibration vessel was built for this purpose and incorporated in the solubility apparatus between the solvent storage vessel and the solvent inlet to the main solubility vessel. This apparatus is shown in Figure 4. The bulb A was designed such that a volume of about 300 cm^3 could be trapped in between taps T_1, T_2 and T_3. The evacuated bulb A could be filled with solvent through tap T_1 from the storage vessel, and the fixed volume of solvent contained between the three closed taps could then be transferred to the main solubility vessel through tap T_2. Water was forced through the fine (0.5 mm internal diameter) capillary connecting this vessel to the main solubility vessel by the introduction of mercury under pressure through tap T_3 from a reservoir.

FIGURE 4.

Solvent Calibration Vessel.

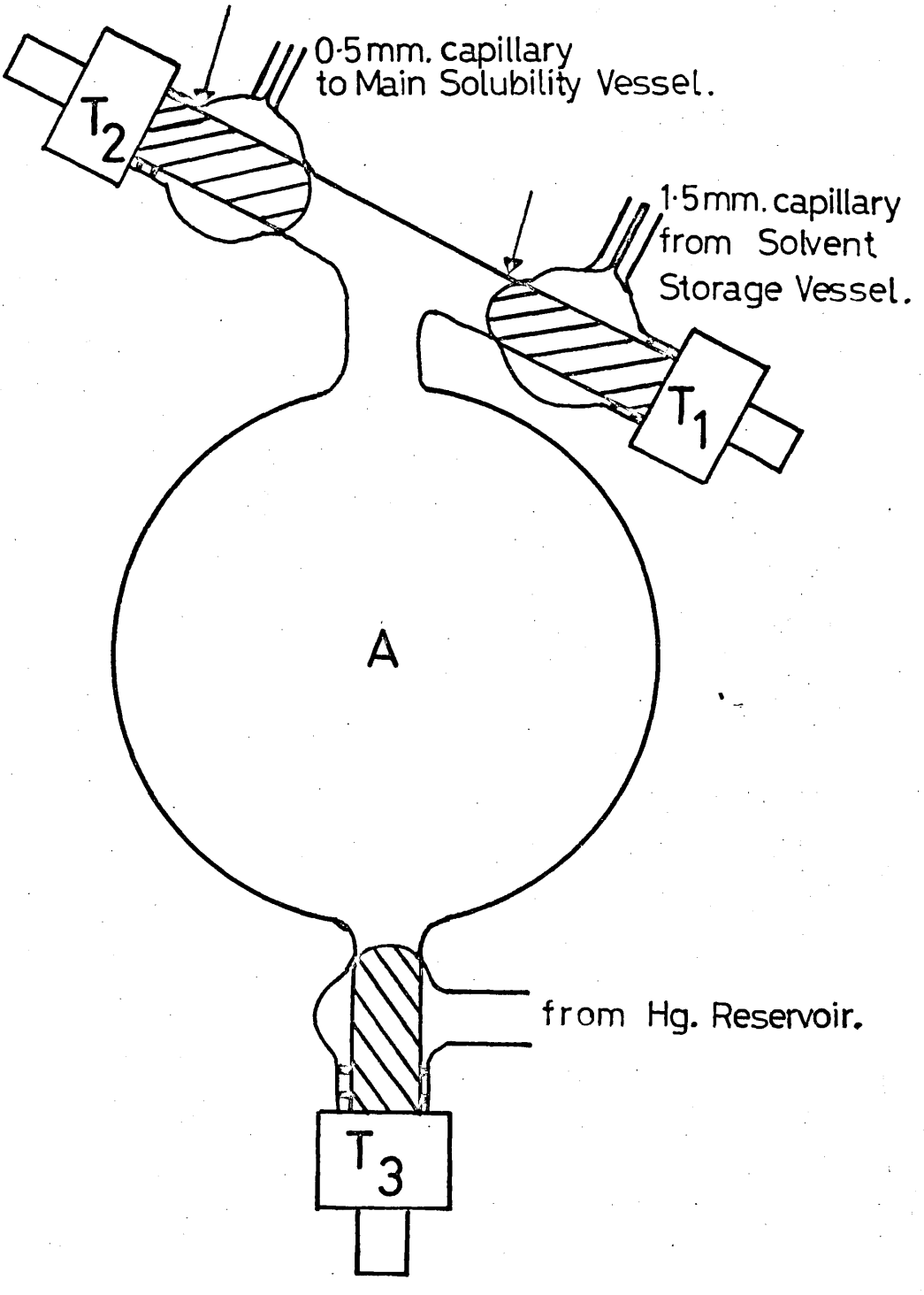

This vessel was calibrated by weighing degassed water delivered from the vessel through the 0.5 mm capillary. The vessel was positioned to be inside the water bath when in use and glass-blown into the solubility apparatus except that the 0.5 mm capillary was not connected to the main solubility vessel. The calibration vessel was filled with degassed water, which was then displaced by mercury and forced out through the capillary tubing and collected in a conical flask. This was cooled in an ice bath to guard against loss of water by evaporation. In order to transfer the water as completely as possible, residual water in the capillary was forced out by allowing mercury to flow through into the conical flask. The small bore of the capillary tubing allowed the mercury thread to act as a piston and force out the water. The flask was then stoppered and weighed before most of the water was decanted. The mercury remaining was washed with methanol, dried, and the flask and mercury then weighed to constant weight, thus allowing the weight of water to be calculated by difference. This process was repeated five times using different flow rates through the capillary to guard against possible systematic errors. The volume of water delivered by this method was calculated from the weight and was 303.121 cm^3 at 25°C, with an accuracy (twice the standard deviation of the mean for six readings) of $\pm$ 0.004 cm^3.

The last calibration required was the measurement of the change in volume of the main solubility vessel with changes in the pressure inside the vessel, or, more precisely, with changes in the difference between the pressures inside and outside the vessel. Smith[84] states that this

was a most important correction for his apparatus. The volume, with negligible pressure difference, had already been calibrated as previously described, but in order to measure the volume with an internal pressure not equal to atmospheric pressure a different method had to be employed. This calibration was achieved by pressure, temperature and apparent volume measurements on gas samples previously determined by addition to the main solubility vessel from the gas burette. Carbon dioxide was chosen, since it was readily obtainable (solid CO_2) and was easily purified by fractionation in the vacuum line. The second virial coefficient is also known,[113] allowing accurate calculations of the amount of gas from pressure, temperature and volume measurements.

Carbon dioxide was measured in the gas burette and the number of moles, n, of gas added to the main solubility vessel was calculated using the equation of state:

$$\frac{PV}{nRT} = 1 + \frac{Bn}{V}$$

(P, pressure; V, volume; T, absolute temperature; R, gas constant; B, second virial coefficient[113])

The main solubility vessel was thermostated and the temperature and pressure were measured, allowing the actual volume of gas to be calculated, again using the equation of state. From the vertical distance from the mercury meniscus to hairline b and from the volume of the main solubility apparatus calibrated with no pressure difference, the apparent volume of the gas was calculated. This progess was repeated

FIGURE 5.

Calibration Graph for Main Solubility Vessel.

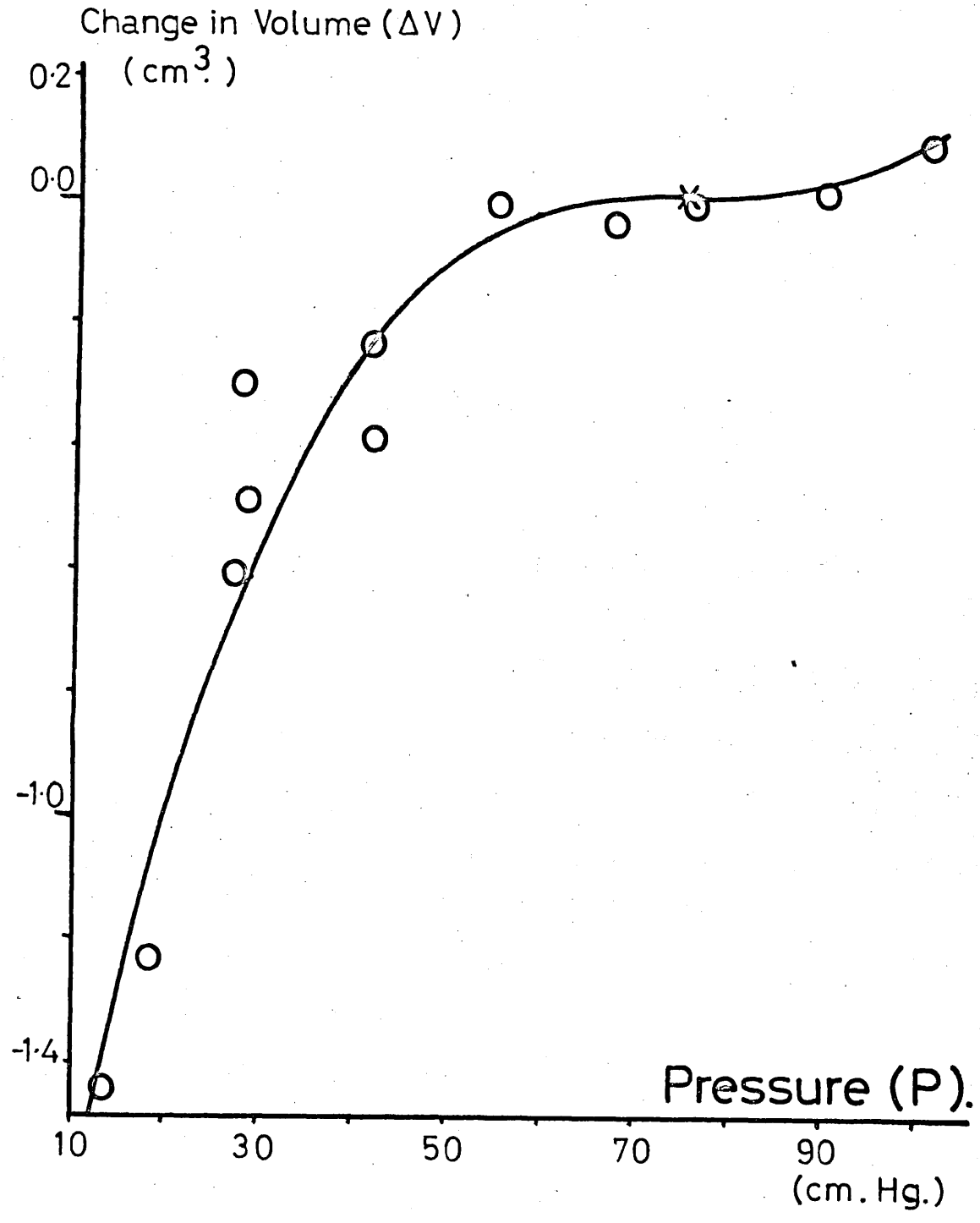

FIGURE 6.

Calibration Graph for Main Solubility Vessel.

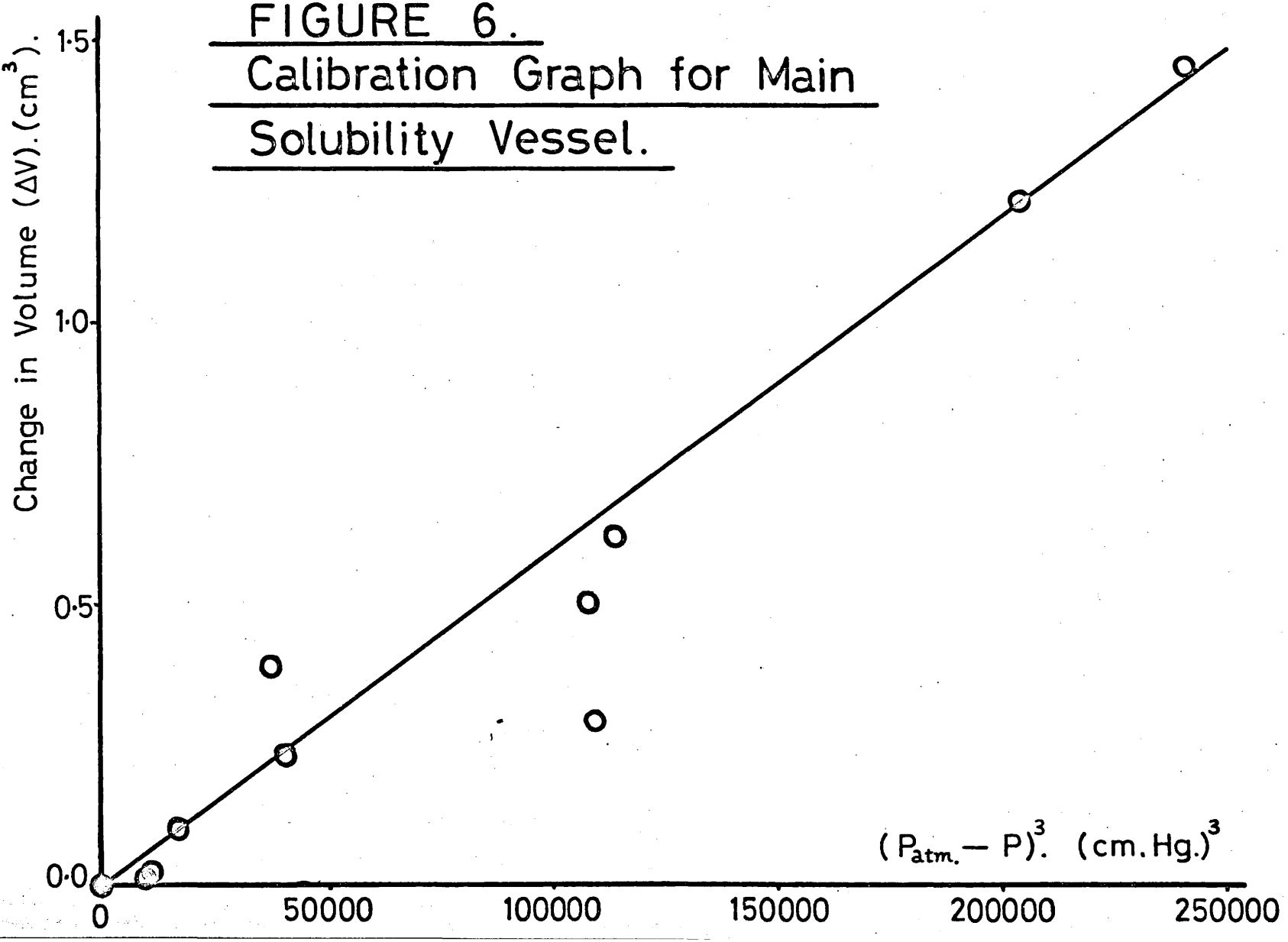

several times using different amounts of gas and thus with different pressures in the main solubility vessel. A graph was plotted of the difference between the actual and apparent volumes of the main solubility vessel, ΔV, against the pressure of gas inside the vessel, and is shown in Figure 5. A graph of ΔV against the cube of the difference (ΔP) between atmospheric pressure (76 cm Hg) and the pressure inside the vessel is linear (Figure 6); $\Delta V = (\Delta P)^3/171,068$ where ΔV is in cm^3 and ΔP is in cm Hg. The accuracy of ΔV was estimated from the linear graph to be $\pm$ 0.02 cm^3.

During this calibration, great care had to be taken to ensure that fluctuations in atmospheric pressure were small. Several readings were discontinued or discarded when these fluctuations became too large (i.e. in excess of $\pm$ 0.02 mm). Because of these difficulties, the intended method of measuring the gas added to the main solubility vessel at the start of solubility runs was discarded. For all solubility runs, the gas was measured only roughly in the gas burette, instead of the intended accurate measurement of the gas introduced using this apparatus. Accurate measurement of the gas, by pressure, volume and temperature measurements in the main solubility vessel before the solvent was added, was found to be far more satisfactory in that fluctuations in atmospheric pressure did not effect the readings.

(g) Readings and Calculations.

The solubility apparatus is shown diagrammatically in Figure 7. The sequence of addition of the solvent and of the gas was found to be

FIGURE 7: The Solubility Apparatus.

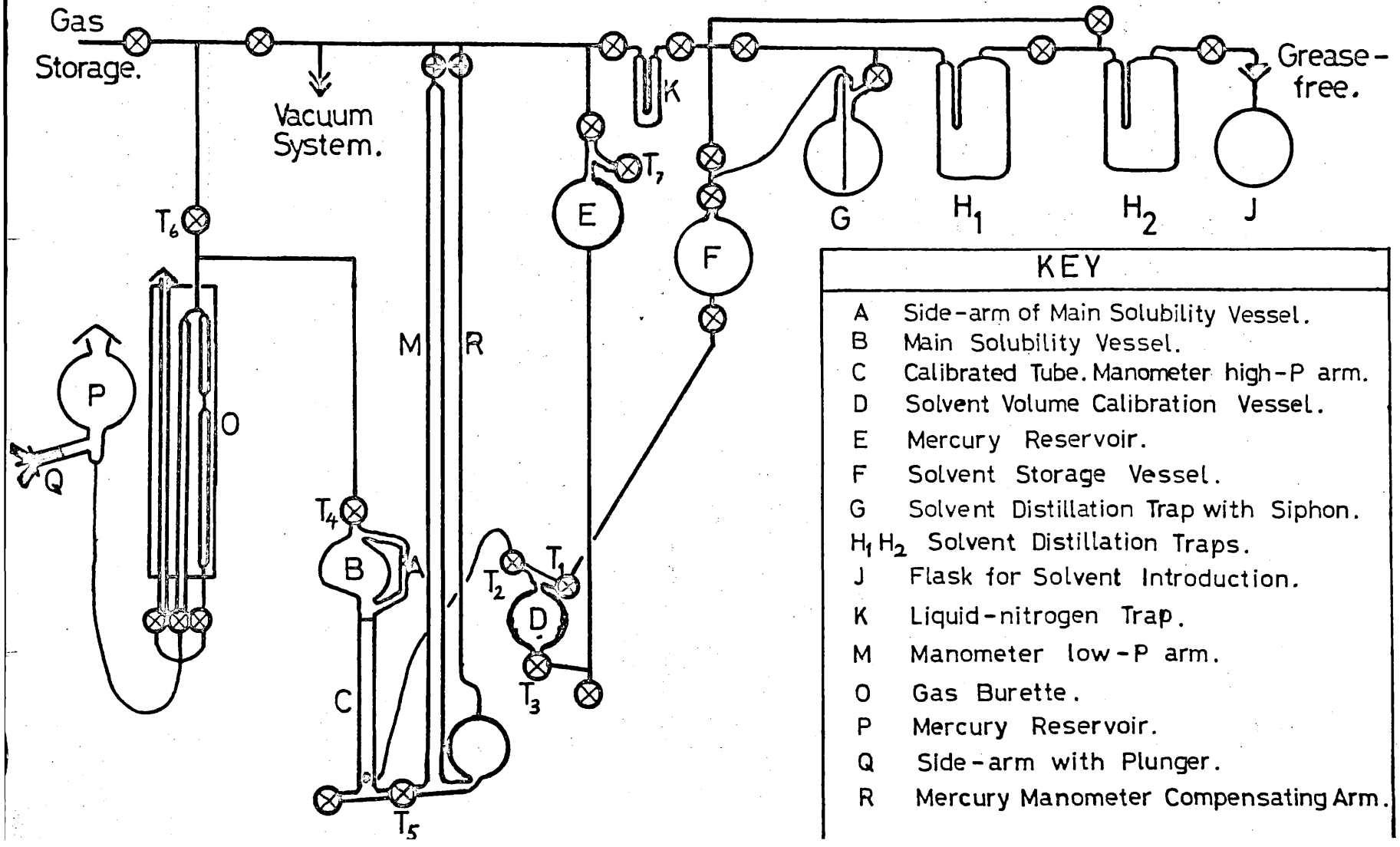

KEY	
A	Side-arm of Main Solubility Vessel.
B	Main Solubility Vessel.
C	Calibrated Tube. Manometer high-P arm.
D	Solvent Volume Calibration Vessel.
E	Mercury Reservoir.
F	Solvent Storage Vessel.
G	Solvent Distillation Trap with Siphon.
H_1 H_2	Solvent Distillation Traps.
J	Flask for Solvent Introduction.
K	Liquid-nitrogen Trap.
M	Manometer low-P arm.
O	Gas Burette.
P	Mercury Reservoir.
Q	Side-arm with Plunger.
R	Mercury Manometer Compensating Arm.

important as mentioned previously and the full method and sequence of operations and readings for a solubility run are given below.

With the degassed water in the solvent storage vessel and with the purified gas stored at -196°C in the main vacuum line, the gas solubility apparatus (gas burette C and main solubility vessel B) was evacuated to better than 10^{-5} torr. By adjustment of the pressure in the manometer compensating arm R, the mercury level in the main solubility vessel was raised to bring the mercury meniscus to between the two hairlines on the side arm A. This prevented too great an addition of gas from the gas burette to the main solubility vessel, ensuring that, after addition of gas, the pressure in the gas burette could be adjusted back to atmospheric pressure. With taps T_4 and T_5 (Figure 7) closed, the gas burette was filled through tap T_6 with gas to a pressure of one atmosphere. The gas burette pressure, volume and temperature were recorded before tap T_4 was opened admitting gas from the burette to the main solubility vessel. The mercury levels in the gas burette were adjusted, such that with tap T_4 closed, the pressure in the gas burette could be readjusted to atmospheric pressure with the correct volume of gas added to the solubility vessel. This process could be repeated if a greater amount of gas was required in the main solubility vessel. These gas burette measurements were used only as a guide, and not as the basis for accurate calculation of the number of moles of gas added. With the required amount of gas in the main solubility vessel, tap T_5 was opened, taking care that the mercury level in the main solubility vessel was kept above the solvent inlet at the bottom of tube C. The evacuated solvent volume calibrating vessel D was filled with the

degassed water from the storage vessel F, but tap T_1 was left open. The bulb D was filled completely and no bubbles of gas could be observed, a further indication that the water was completely degassed. A similar criterion involving the cushioning of the solvent between mercury[89] has been mentioned in Section 1(d).

The thermostat tank was raised, filled and thermostated to 25°C. Mercury was added slowly to reservoir E through tap T_7 and degassed by continuous pumping on the reservoir. About one hour was allowed for thermal equilibration before tap T_1 was closed, calibrating the solvent volume in vessel D. The amount of gas in the main solubility vessel was determined by measurement of the positions of both mercury menisci in the manometer, and of the position of hairline b. This allowed the pressure and volume of the gas sample to be determined and thus the number of moles of gas from the relevant equation of state. For NF_3 and N_2F_4, the equations of state used were those given by Pankratov et al.[115, 116] These were in the form of a van der Waals equation: $(P + n^2A/TV^2)(V - nB) = nRT$ with $A = 7.4300 \times 10^{-6}$ atm. cm^6 and $B = 86.712$ cm^3 for N_2F_4, and with $A = 3.4777 \times 10^{-6}$ atm.cm^6 and $B = 53.674$ cm^3 for NF_3. Pressure, volume and temperature measurements for the gas in the main solubility vessel were repeated as a check on the amount of gas. The accuracy of this method of measuring the gas was estimated to be $\pm 1.0 \times 10^{-6}$ moles (twice the standard deviation of the mean) for an addition of 5×10^{-3} moles of gas ($\pm 0.02\%$).

The thermostat tank was emptied and lowered and the mercury level in the main solubility vessel was lowered to just below the solvent inlet, care being taken, however, to keep the mercury meniscus in the tube C. Tap T_5 was closed and taps T_2, T_3 and T_7 (Figure 7) were opened. Mercury from the reservoir E, entering the solvent volume calibrating vessel (D), was allowed to force the water slowly through the capillary tube into the main solubility vessel. When all the water was expelled, mercury was allowed to flow through the capillary tube until the mercury meniscus in tube C rose to above the solvent inlet. Tap T_2 was closed, and, by admission of air into the manometer compensating arm (R), the level of mercury in the manometer arm M was raised such that on slight opening of tap T_5, the mercury meniscus in tube C rose slowly until just below hairline b. It was observed that if this meniscus rose too fast, some solvent was trapped between the mercury column and the glass below the mercury meniscus. The flow of mercury from the manometer arm M into tube C was therefore controlled by tap T_5 until it could be fully opened without movement of the meniscus.

With known amounts of gas and solvent trapped in the main solubility vessel, the submersible motor driving the magnetic follower was started and the thermostat tank was raised, filled and thermostated. Three hours of fast stirring were found to be sufficient for equilibration between solute in the solution and gas phases, but an extra half-hour or

TABLE 4.

DATA USED IN CALCULATIONS

Acceleration due to gravity. $g = 981.17261 (\pm 0.00064)$ cm.sec^{-2}

(Standard $g = 980.665$ cm.sec^{-2})

Density of Mercury. Ref.[117] p.F5.

Density of Water. Ref.[117] pp F4, F5.

Vapour Pressure of Water. Ref.[113,118]

Isothermal Compressibility of Water.[117,119]

Bulk Modulus (K_B) = $(p_2-p_1)/((V_1-V_2)/V_1)$

p;V = pressure; volume. 1;2 = initial; final.

Isothermal Compressibility (x_t) = $1/K_B$

T(°C)	x_T(cm^{2}dyne^{-1} x 10^{-11})
0	5.02
10	4.78
20	4.58
25	4.57
35	4.48
45	4.44
55	4.44

(76.0 standard cm.Hg. = 1 standard Atmosphere = 1.0133×10^6 dyne cm^{-2})

hour had to be allowed before taking readings for the dispersal of bubbles of gas on the surface of the solvent. After this time, the room and thermostat bath temperatures were recorded and the cathetometer was used to measure the levels of the two mercury menisci, the solvent meniscus, and hairline b and also the relative positions of the two steel rules. These measurements were sufficient for the calculation of the solubility (vide infra). This procedure was repeated several times for each temperature of the thermostat bath, using different pressures of gas above the solvent, thus allowing a check that the system was equilibrated.

An example of the calculations is shown below in order to illustrate the corrections involved. Data used in the calculations, but not previously listed, is given in Table 4.

Example of Calculations

(i) Calculation of the Initial Quantity of Gas (before addition of solvent).

Gas N_2F_4

Bath Thermometer: Reading = 24.81C ; Temperature = 24.97C
= 298.12K.

Level		Cathetometer Reading	Position on Rules
Hg. Meniscus in Tube C		34.827	29.5505 on 60 cm rule
29.5)	60 cm rule	(34.777	
29.6)		(34.876	

Level	Cathetometer Reading	Position on Rules

[Position of Hg meniscus in Tube C = $\frac{(34.827 - 34.777)}{(34.876 - 34.777)} + 29.5$

= 29.5505 on 60 cm rule]

Hairline b	36.235	30.9485 on 60 cm rule
30.9) 60 cm rule 31.0)	(36.187 (36.286	
Hg meniscus in Manometer M,	14.105	52.1677 on 60 cm rule
52.1) 60 cm rule 52.2)	(14.128 (14.227	

Difference between mercury menisci = (52.1677 - 29.5505)

= (22.6172) cm uncorrected for thermal expansionoof rule

= $22.6172\ (1 + 10.9 \times 10^{-6}\ (24.97 - 20.00))$ cm (corrected)

∴ Pressure = 22.6134 cm Hg. at 24.97°C

= 22.6134 (13.5240/13.5955) cm Hg at 0°C

(correcting for change in density of Hg with temperature - all pressures are referred to mercury at 0°C)

= 22.5161 (981.17261/980.665) cm Hg at standard g.

= 22.5277(5) standard cm Hg.

Length of Tube C below hairline b and above Hg meniscus

= 1.3930 cm (uncorrected for thermal expansion of rule)

= $1.3930\ (1 + 10.9 \times 10^{-6}(24.97 - 20.00))$ = 1.3931 cm (corrected).

Volume of Solubility Vessel above Hg meniscus in Tube C (i.e. volume of gas)

= $378.0136\ (1 + (0.99 \times 10^{-5})(-0.03))$

$+ 1.3931(2.0006)(1+(2 \times 0.33 \times 10^{-5})(-0.03))$

= 378.0135 + 1.3931 x 2.000572 = 379.9165 cm^3

Using Van der Waals' equation

$(P + n^2A/TV^2)(V - nB) = nRT$

$P = 22.5277(5)$ cm. Hg. (n = number of moles of gas)

$V = 379.9165$ cm^3

$T = 293.1°$ K

$R = 6236.37$ cm^3 cm.Hg.K.$^{-1}$mol.$^{-1}$

$A = 7.4300 \times 10^{-6}$ atm.cm^6 $= 5.6469 \times 10^{-4}$ cm.Hg.cm.^{6}

$B = 86.712$ cm^3

Rearranging Van der Waals' equation

$PV + n^2A/TV - PnB - n^3AB/TV^2 = nRT$

or $PV = nRT - n^2A/TV + n^3AB/TV^2 + PnB$.

Using the approximation $n \sim 5 \times 10^{-3}$ moles.

$PV \sim 10^4$; $nRT \sim 10^4$; $PnB \sim 10$; $n^2A/TV \sim 10^{-13}$

and $n^3AB/TV^2 \sim 10^{-16}$

Thus the terms n^2A/TV and n^3AB/TV^2 can be neglected.

$\therefore$ $PV = nRT + PnB$

or $n = PV/(RT + PB)$

$= 0.00459061$ moles of N_2F_4 gas.

Average of 3 readings $= 0.00459051$ moles of N_2F_4 gas.

(ii) Calculation of Amount of Gas dissolved.

Gas N_2F_4.

Bath Thermometer: Reading = 24.85°C : Temperature = 25.01°C = 298.16°K.

Thermometer for 100 cm rule: Reading = 21.00°C : Temperature = 21.96°C.

Level	Cathetometer Reading	Position on Rule
Hg meniscus in Tube C	32.661	27.3830 on 60 cm rule
27.4, 27.3 } 60 cm rule	32.673, 32.573	
Hairline b	36.229	30.9367 on 60 cm rule
30.9, 31.0 } 60 cm rule	36.193, 36.291	
Solvent meniscus	43.867	38.5793 on 60 cm rule
38.5, 38.6 } 60 cm rule	43.783, 43.887	
58.0 on 60 cm rule	19.961	3.4162 on 100 cm rule
3.4, 3.5 } 100 cm rule	19.945, 20.044	
Hg meniscus in Manometer H	30.560	79.3901 on 100 cm rule
79.3, 79.4 } 100 cm rule	30.469, 30.570	

Difference between Hg menisci = (58.0 - 27.3830)+(79.3901-3.4162)

= (30.6170)+(75.9739) cm. uncorrected for thermal expansion of the steel rules.

= $30.6170(1+10.9 \times 10^{-6}(5.01)) + 75.9739(1 + 11.1 \times 10^{-6}(1.96))$

= 30.6137 + 75.9756 = 106.5943 cm.Hg at 25.01°C.

$\therefore$ Pressure = 106.5943 (13.5340/13.5955) cm.Hg at 0°C.

= 106.1121 cm.Hg at 0°C.

= 106.1121 (981.17861/980.665)

= 106.1670 standard cm.Hg (corrected for g.).

Solvent column (solvent meniscus to Hg. meniscus in tube C)

= (38.5798 - 27.3830)(1 + 10.9 x 10^{-6}(5.01))

= 11.1974 cm. of water.

Pressure due to solvent column = 11.1974 (0.997041/13.5955)

= 0.8212 cm.Hg at 0°C = 0.8216 standard cm.Hg (corrected for g.).

Length of tube C between hairline b and Hg meniscus.

= (30.9367-27.3830)(1 + 10.9 x 10^{-6}(5.01))

= 3.5539 cm.

$\therefore$ Volume of Main Solubility Vessel above Hg meniscus

= 378.0136(1 + 0.99 x 10^{-5}(0.01))+ 2.0006(1 + 0.66 x 10^{-5})(0.01))(3.5539)

= 385.1234 cm^3.

Volume of Solvent = 308.1206 (0.997044/0.997041)

= 308.1215 cm^3 (without correction applied for Isothermal Compression or for solvent in vapour phase).

ΔV (Isothermal compressibility) = $V(\Delta P)\chi_T$

$\chi_{25°C}$ = 4.57 x 10^{-11} $cm.^2 dyne^{-1}$

ΔP = (76.0 - 105.756) = (-29.756) cm.Hg = -0.39673 x 10^6 dyne cm^{-2}

V = 308.1215 cm^3.

$\therefore$ ΔV (Isothermal compressibility) = 308.1215(-0.39673 x 10^{-6})(4.57x10^{-11})

= - 0.0056 cm^3

Volume of gases above the solvent $\approx$ (385.123 - 308.121)cm^3

= 77.002 cm^3.

Vapour Pressure of water at 25.01C = 2.37435 cm.Hg.

$\therefore$ Water Vapour = $\frac{(2.37435)(77.002)(273.15)(18)}{(298.16)(76)(22.4 \times 10^3)}$ g H_2O.

= 1.771×10^{-3}g of H_2O.

$\therefore$ $\Delta V_{H_2O\ vapour}$ = 1.776×10^{-3} cm^3 of liquid H_2O at 25.01C

$\therefore$ Volume of Water = 308.1215 - 0.0056 - 1.776×10^{-3}

= 308.1141 cm^3.

Volume of gas (N_2F_4) = (385.1234 - 308.1141)

= 77.0093cm^3.

Total Pressure of gases above solvent

= (Difference between Hg menisci)-(Pressure due to solvent column)

= (106.1670 - 0.8216) = 105.3454 cm. Hg.

$\therefore$ Partial pressure of N_2F_4 gas = (Total pressure of gases)-(H_2O vapour pressure)

= 105.3454 - 2.3743(5)

= 102.9710(5) cm.Hg.

Using Van der Waals' Equation : n = PV/(RT + PB)

(n^2A/TV and n^3AB/TV^2 terms are again negligible)

n = (102.97105)(77.0093)/(6236.37 x 298.16 + 102.97105 x 86.712)

= 4.24421×10^{-3} moles N_2F_4.

$\therefore$ Gas dissolved = $4.59851 \times 10^{-3} - 4.24421 \times 10^{-3}$

$= 3.5430 \times 10^{-4}$ moles N_2F_4.

Gas solubilities have been expressed in a great many ways, and those most frequently used are listed and defined below. Most of these require the conversion of the solubility data from the experimental partial pressure of the gas to a standard partial pressure of 760 mm Hg. This correction is made using Henry's Law which states that the amount of gas that dissolves in a given mass of a liquid at a given temperature is very nearly directly proportional to the partial pressure of the gas above the solution. This proportionality becomes more exact with decreasing concentration of the gas dissolved in the solvent and is exact in the limiting case. The exact proportionality is usually used for the conversion to a partial gas pressure of 760 mm Hg and this usually introduces only a negligible error provided that the pressure range is reasonably small.[77] In the present case, the conversion of measurements for NF_3 and N_2F_4, both of which have very low solubilities, can reasonably be expected to produce an error very small when compared with the accuracy of the solubility measurements reported in this thesis.

The Dunsen coefficient (α) is defined as the volume of gas, reduced to 0°C and 760 mm Hg pressure, which is absorbed by the unit volume of solvent (at the temperature of measurement) under a gas partial pressure of 760 mm Hg. This is also known as the absorption coefficient or the

coefficient of absorption and is proportional to gas molarity.

The Kuenen coefficient (S) is defined as the volume of gas in cm^3, corrected to 0^oC and 760 mm.Hg pressure, which, at a partial pressure of 760 mm. Hg, will dissolve in 1g of solvent. This coefficient is proportional to gas molality. The solubility of NF_3 in water, as determined by Smith et al,[84] was expressed by these authors in terms of this coefficient, and, therefore for ease of comparison, the results in this thesis are also reported in terms of the Kuenen coefficients.

The Ostwald coefficient (L) is the ratio of the volume of gas absorbed to the volume of the absorbing liquid, all measured at the same temperature. This is equivalent to the ratio of the concentration of the gas in the liquid phase to that in the gas phase and thus the Ostwald coefficient is an equilibrium constant, and is independent of partial pressure for assumed gas ideality. However, the temperature and total pressure must be designated.

Henry's Law constants (K) can also be used to express solubilities ($Pg = KC_1$ where Pg is the partial pressure of gas and C_1 is the concentration of the dissolved gas). The concentration (C_1) is often expressed as a mole fraction.

Cook[112] has recommended the weight solubility (C_w) as a more logical unit than the Bunsen or Ostwald coefficients. This is defined as the number of moles of gas, with a partial pressure of gas of 760 mm.Hg, absorbed per gram of solvent.

Because of this variety of ways of expressing gas solubilities, it was suggested[73,77] that all publication reporting solubilities should contain a careful exposition of the manner in which the solubilities have been calculated, and should also include sample calculations. This practice has been adopted in this thesis, and sample calculations are given below in order to illustrate the method used in the calculation of both Kuenen coefficients (S) and also mole fraction solubilities.

Gas (N_2F_4) dissolved = 3.5430×10^{-4} mole.

Partial Pressure of gas above solution = 102.9710(5) cm.Hg.

Weight of Solvent (H_2O) = (308.121)(0.997044)g

= 307.2098 g.

Weight of Solvent in vapour phase = 0.00177 g.

∴ Weight of Solvent in liquid phase = 307.2098 − 0.0018

= 307.2080 g.

From Van der Waals' Equation : $n = PV/(RT + Pb)$

1 cm^3 of N_2F_4 gas at N.T.P. (0°C, 760 mm.Hg) = 76/(273.15(6236.37) + 76(96.712))

$= 4.4443 \times 10^{-5}$ mole

∴ 3.5430×10^{-4} mole N_2F_4 = 7.97201 cm^3 N_2F_4 at N.T.P.

∴ Kuenen coefficient (S) = $\frac{\text{Gas dissolved } (cm^3 \text{ at N.T.P.})}{\text{Weight solvent in liquid phase}} \times \frac{76}{\text{partial pressure of gas}}$

$= \frac{7.97201}{307.2080} \times \frac{76}{102.9710(5)}$

∴ **Kuenen coefficient (S) = $19.1528(5) \times 10^{-3}$**

Mole Fraction Solubility Constant (K_M)

$$= \frac{\text{(moles of gas dissolved)}}{\text{(moles of liquid solvent)}}$$ for a partial pressure of gas above the solution of 760 mm.Hg.

$$\underline{\text{or}} = \frac{\text{(moles of gas dissolved)}}{\text{(moles of liquid solvent)}} \times \frac{76}{\text{partial pressure of gas}}$$

Gas dissolved = 3.5430×10^{-4} mole N_2F_4.

Solvent in liquid phase = 307.2072 g = (307.2072/18.0154 mole)

= 17.05248 mole H_2O.

$\therefore$ Mole fraction solubility constant (K_M) =

$$\frac{3.5430 \times 10^{-4}}{17.05248} \times \frac{76}{102.9710(5)}$$

$\therefore$ $\underline{K_M = 1.53349 \times 10^{-5}}$

In order to calculate the enthalpy and entropy change accompanying solution, the solubility results were fitted by the method of least squares to the equation

$$\log (K_M) = a/T + b \log T + c$$

where a, b and c are constants and T is the absolute temperature. This allows the enthalpy and entropy changes to be directly determined using the relationships:

$$\Delta H = -R \left[\frac{\partial \ln (K_M)}{\partial (1/T)} \right]_{\text{sat, P.}} \qquad \text{(van Hoff's equation)}$$

$$\text{and } \Delta S = R \left[\frac{\partial \ln (K_M)}{(\partial \ln(T))} \right]_{\text{sat, P.}}$$

$$\text{and } \Delta S_1 = \Delta S + R \ln (K_M)$$

The entropy change (ΔS_1) is that for the transfer of one mole of gas to a hypothetical solution of unit mole fraction.

A Fortran IV computer program was written to perform the least-squares fit, and to calculate the values of ΔH and ΔS_1, using the University of London CDC 6600 computer.

(h) Results.

The experimental results for the solubility of NF_3 in water at temperatures between 25°C and 45°C are shown in Table5. The results given in the second column of Kuenen coefficients were calculated by back substitution. The results reported by Smith et al[84] are shown in Table 5 for comparison.

In order to obtain a measure of the accuracy of the least-squares fit, the deviations of the experimental results from the results calculated by back substitution were used to calculate the standard deviation of the fit. By this method, the accuracy (twice the standard deviation[120]) was found to be ± 1.2%. This can be compared with that calculated from the estimated accuracies of the calibrations of the apparatus and from the estimated accuracies of the readings taken.

TABLE 5

SOLUBILITY OF NF_3 IN WATER

T(°C)	Kuenen Coefficient x 10^3			
	This Work		Smith et al[84]	
	Experimental	Calculated	Experimental	Calculated
25.06	16.7159			
25.06	17.0929			
25.06	17.2439			
25.06	17.6328	17.699	17.95	17.78
25.06	18.2472			
25.06	18.5904			
25.06	18.2150			
25.06	18.3532			
25.11	17.2518	17.681	17.93	17.76
25.41	17.6007	17.576	17.80	17.66
35.14	14.6620			
35.14	14.8041			
35.14	14.7225	14.816	14.76	14.73
35.14	15.0677			
35.14	14.8273			
45.13	12.7568			
45.13	13.0726	12.946	12.83	12.84
45.13	12.9858			
45.13	12.9703			

Least-squares fit for experimental results:-

$\text{Log}(K_H) = 4596.4/T + 29.558\ \text{Log}(T) - 93.404$

From this consideration, an accuracy of about ± 1% was expected.

Table 6 compares the values of the solubility of NF_3 and of ΔH and ΔS_1 with those reported by Smith et al,[84] (shown in brackets). The agreement of the solubilities reported in this thesis with those of Smith et al was considered to be very satisfactory over the temperature range 25°C to 45°C. Extrapolation of the least-squares fit to below the temperature range of the measurements taken, however, produced a less satisfactory agreement with a difference of 2.7% at 15°C and of 6% at 5°C. The agreement with the values of ΔH and ΔS_1 given by Smith et al was also considered to be satisfactory, especially in view of the small temperature range of the readings reported in this thesis.

The above comparison showed that solubilities measured with the apparatus described in this thesis were accurate to about ± 1%.

The experimental results for the solubility of N_2F_4 in water at temperatures between 15°C and 45°C are shown in Table 7, together with the results from back substitution into the least-squares fit equation. The accuracy of this fit was calculated as above to be ± 0.2%.

It was felt that these results indicated that reaction had taken place during the measurements, as shown by the slow rise in solubility with time at a constant temperature. The first four and last three results were therefore corrected to 25°C in order to allow direct comparison of the mean solubility at 25°C for the first four results with that for the last three results. These mean values were 19.4826×10^{-3}

TABLE 6

NF_3 SOLUTION IN H_2O

T(°C)	Kuenen ($\times 10^3$)	$-\Delta H$ ($Kcal.mol^{-1}$)	ΔS_1 ($cal.\ K^{-1}mol^{-1}$)
5	29.21 (31.06)	4.7 (5.3)	38 (40)
15	22.16 (22.76)	4.1 (4.6)	36 (38)
25	17.72 (17.20)	3.5 (3.8)	34 (35)
35	14.84 (14.76)	2.9 (3.1)	32 (32)
45	12.97 (12.86)	2.3 (2.3)	30 (30)

Values shown in brackets from Smith *et al.*[84]

TABLE 7

SOLUBILITY OF H_2F_4 IN WATER. RESULTS NOT CORRECTED FOR REACTION.

T(°C)	Kuenen Coefficient x 10^3	
	Experimental	Calculated
25.01	19.1528	19.697
25.11	19.1535	19.643
25.01	19.4172	19.697
25.01	19.6686	19.697
45.03	12.8834	13.013
45.03	12.9515	
45.03	13.1417	
34.94	15.4596	15.513
34.94	15.7933	
16.82	25.4334	25.347
16.00	26.2600	26.073
16.00	25.5860	26.073
15.00	27.3218	27.007
24.96	20.1420	19.724
24.96	19.9632	
24.96	20.1884	

Least-squares fit for experimental results:-

$\log (K_H) = 7557.2/T + 50.128 \log (T) - 154.19$

and 20.053 x 10^{-3} (Kuenen coefficients at 25°C) with standard deviations of the mean of 0.124 x 10^{-3} and 0.068 x 10^{-3} respectively. The difference between the two mean values (0.57 x 10^{-3}) was larger than twice the sum of the standard deviations (0.38 x 10^{-3}) and was taken as indicating that a slow reaction had occurred. Calculations showed that this difference between the two means was equivalent to the removal during the solubility run of about 1.8 x 10^{-5} moles of N_2F_4 about 0.4% of the N_2F_4 originally added.

In order to compensate for this reaction, the exponential increase in reaction rate with time found by Hurst and Khayat[38] was assumed, and it was also assumed that the rate was increased by a factor of two for every ten degree rise in temperature. On the further assumption that the products of the reaction were completely dissolved and did not interfere with the solubility of the N_2F_4 remaining intact, the amount of N_2F_4 that had reacted at any given time could be calculated from the initial and terminal (at the time of the last reading) extents of reaction (zero and 1.8 x 10^{-5} moles of N_2F_4 respectively).

Although several assumptions were involved in the above calculation, the magnitude of this correction was very small and thus even a fairly large error in the calculation of the extent of the reaction would only have a small effect on the value of the calculated solubility. Further, using the above assumptions, the rate of reaction of N_2F_4 with water at 60°C can be calculated, and is compatible with the experimental rate measured by Hurst and Khayat.[38] At the end of the solubility run, the

liquid phase was removed from the apparatus and immediately purged of N_2F_4 by pouring onto solid CO_2. Although this process cools the liquid phase, thus increasing the solubility of the N_2F_4, the constant flow of bubbles of CO_2 gas through the liquid was found to be a very effective method of purging. Simultaneously this creates an atmosphere of CO_2 above the liquid, thus preventing oxygen from the air being dissolved and catalysing the reaction of N_2F_4 with the water. A sample was then analysed for fluoride ion using a fluoride electrode (Model 96 - 09, Orion Research Incorporated, Cambridge, Massachusetts, U.S.A.), in conjunction with a specific-ion meter (Model 401, Orion Research Incorporated). Standard fluoride solutions were prepared from 'Analar' sodium fluoride (The British Drug Houses Ltd., Poole). The sample was found to contain 2.55×10^{-4} moles fluoride ion per litre, equivalent to 0.785×10^{-4} moles of fluoride ion in the volume of water used for the solubility run. On the assumption that one mole of N_2F_4 reacts with water to give four moles of fluoride ions ($N_2F_4 + 4OH^- \longrightarrow 2\,NO + 4F^- + 2H_2O$) as was found by Hurst and Khayat,[38] this fluoride ion is equivalent to the reaction of 1.96×10^{-5} moles of N_2F_4. This agrees very well with the calculated extent of reaction of 2.02×10^{-5} moles at the time of purging the liquid phase.

By the above method the extent of reaction, at the time of each solubility measurement, was calculated and subtracted from the amount of N_2F_4 originally added to the main solubility vessel. The results, modified in this way, are shown in Table 8. The accuracy of the least-squares fit (twice the standard deviation) for these modified results

TABLE 8

SOLUBILITY OF N_2F_4 IN WATER. RESULTS CORRECTED FOR REACTION

T(°C)	Kuenen Coefficient x 10^3	
	Experimental	Calculated
25.01	19.0988	19.183
25.11	19.0806	19.130
25.01	19.3184	19.183
25.01	19.5545	19.183
45.03	12.5529	12.555
45.03	12.5501	
45.03	12.6065	
34.94	14.8760	15.074
34.94	15.1077	
16.82	24.6940	24.635
16.00	25.5300	25.329
16.00	24.7068	25.329
15.00	26.4170	26.221
24.96	19.2132	19.210
24.96	19.0683	
24.96	19.2107	

Least-squares fit for experimental results:-

$\log (K_N) = 6936.9/T + 45.345 \log(T) - 140.28$

TABLE 9

SOLUTION OF H_2F_4 IN WATER

(a) NOT CORRECTED FOR REACTION

T (°C)	Kuenen Coefficient (S x 10^3)	$-\Delta H$ (Kcal.mol^{-1})	$-\Delta S_1$ (cal.deg.$^{-1}$mol^{-1})
5	40.31	6.9	45
15	27.01	5.9	42
25	19.70	4.9	38
35	15.49	3.9	35
45	13.02	2.9	32

(b) CORRECTED FOR REACTION

T (°C)	Kuenen Coefficient (S x 10^3)	$-\Delta H$ (Kcal.mol^{-1})	$-\Delta S_1$ (cal.deg.$^{-1}$mol^{-1})
5	38.73	6.7	45
15	26.22	5.8	41
25	19.19	4.9	38
35	15.06	4.0	35
45	12.56	3.1	33

FIGURE 8.

The Solubilities of NF_3 and N_2F_4 in Water.

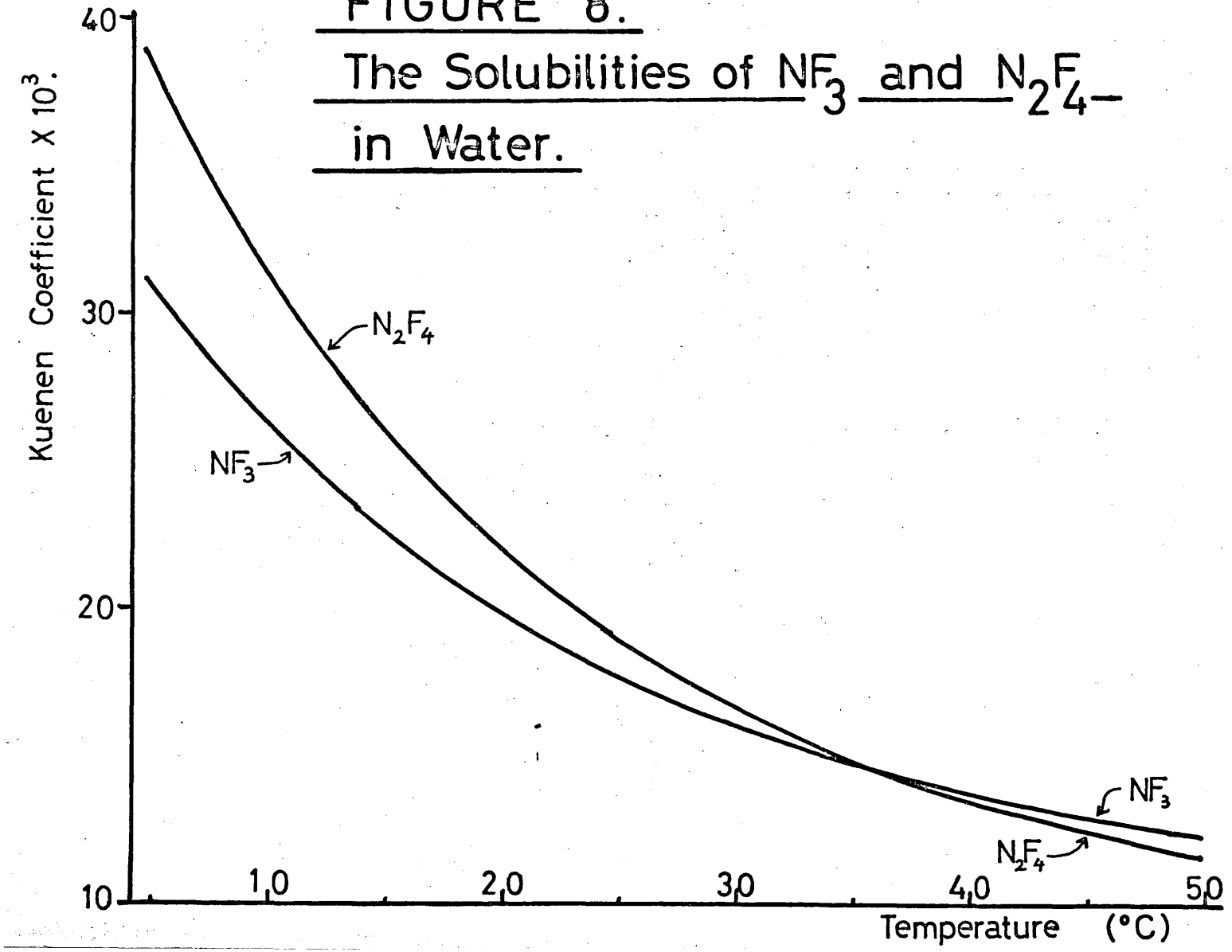

was ± 0.5%. The values of ΔH and ΔS_1 for solution are shown in Table 9 for the readings, both corrected and uncorrected for reaction. This table shows that the small correction applied to the data has made a correction of about 4% in the Knonen coefficients and in the values of ΔH, but that the values of ΔS_1 have been changed very little.

The solubilities of NF_3 and N_2F_4 are shown graphically in Figure 8.

(i) Discussion

Regular solution theory has been widely applied to solutions of gases in non-polar solvents, most consistently by Hildebrand and co-workers.[75,76,79] However, there is a marked difference between the thermodynamic properties of gases dissolved in aqueous solution and those of gases dissolved in non-polar solvents. In particular, the low partial molar volumes and large, negative entropies of solution of gases in water have proved difficult to explain. The failure of regular solution theory when applied to aqueous solutions has led to investigation of other theoretical models of the dissolution process and two fundamentally different models have been invoked.

Frank and Evans[121] postulated the formation of a layer of ordered water molecules around the solute molecules. This so-called iceberg or frozen-layer effect gives a direct explanation of the anomalous entropies of solution of inert gases in water, and the marked temperature dependence of these entropies was explained by the 'icebergs melting' as the temperature rose. The physical basis of this model remains obscure,

but the ordering of the water molecules must depend on increased hydrogen-bonding in the layer around the solute molecule, giving partial hydrogen-bonded cages around each solute molecule.[122] However, nuclear magnetic resonance studies[123] have been unable to substantiate the existence of these iceberg structures, and have not indicated any significant increase or decrease in the degree of hydrogen bonding in water as a result of the solution process.

The second model was proposed by Uhlig.[124] This was a cavity model in which the solubility process was considered to take place in two steps: first, doing work on the solvent against the solvent surface tension to create a cavity, and, second, placing the gas molecule in this cavity and calculating the energy of interaction between the gas and solvent molecules. Eley[125] also considered a two-step process similar to that above, but by more careful thermodynamic analysis, was able to estimate the separate contributions of each step to the energy and the entropy changes involved. This approach gave reasonable success with both water and organic solvents, but it was shown that the case of water was complicated by the possibility of structural modifications.

Pierotti[126] extended the above model using an expression found by Reiss *et al*[127] for the work done in creating a spherical cavity in a fluid, derived from extension of statistical-mechanical theory of hard-sphere fluids. By the introduction of a solvent dipole term, Pierotti[128] developed a theory of gas solubility and obtained good agreement, even for polar solvents, between the experimental and

calculated heats, entropies, and molar heat capacities of solution and also for the partial molar volumes of the solutes. For aqueous solutions this model has been particularly successful, giving accurate estimates of the entropy and enthalpy of solution for a wide range of non-polar gases. For example, the results obtained by Pierotti[128] for CF_4, for which no experimental data were then available, can be compared with the experimental results of Smith et al.[84] This shows that for CF_4, Pierotti's calculated value for the molar enthalpy of solution (ΔH) was only about 8% too high, and that the calculated molar entropy of solution agrees with the experimental value to within experimental accuracy. Unfortunately this theory has not yet been extended to solutions of NF_3, N_2F_4 and other gaseous fluorine compounds, and it has also been criticised[129] for failing to be consistent with surface tension data.

It is not, therefore, possible to compare the experimental results for NF_3 and N_2F_4 with theoretical results obtained from the above theory. However, certain rules have been obtained, empirically interrelating the thermodynamic properties of solution or relating them to other properties of the solutes. Calculations by Dell,[130] using the solubility results of Horiuti,[97] were used by Barclay and Butler to show that the relationship between the enthalpy and entropy of vaporisation of a pure liquid ($\Delta S = A + B\Delta H$) could be extended to cover dilute solutions of a solute in a solvent. In this relationship, A and B are constants

for a given group of substances, such as non-polar liquids, and when extended to cover solubilities, are constants for gases dissolved in a given solvent.

Figure 9 shows a Barclay-Butler plot for gases dissolved in water. The standard states used are, as before, a partial pressure of the gas above the solution of 760 mm Hg and a hypothetical solution of unit mole fraction. Data for the most of the points plotted are those given by Frank and Evans[121] and Horington.[131] Points for NF_3, CF_4 and SF_6 were plotted using the data of Smith et al[84] and for N_2F_4 and NF_3 using the data obtained in this work.

Although the values given by Friedman[83] for the solubility of SF_6 in water were not sufficiently accurate to allow a careful investigation of its temperature coefficient, his data led to an estimate of the enthalpy of solution of -7 kcal.mol^{-1} and of the entropy of solution (ΔS_1) of -30 cal.deg.$^{-1}$mole^{-1} at 25°C. Friedman noted that these values were not compatible with a Barklay-Butler plot for aqueous solutions of gases as given by Frank and Evans[121] and Horington,[131] which showed that the value of ΔS_1 was about 10 cal.deg.$^{-1}$mole^{-1} more negative than that expected for the experimental value of the enthalpy of solution (ΔH). The more accurate study by Smith et al[84] of the solubility of SF_6 in water gave the value of ΔH as -4.9 kcal.mole^{-1}, with a value of ΔS_1 of -41 cal.deg.$^{-1}$mole^{-1} at 25°C. Smith et al

FIGURE 9.

Barclay-Butler Plot.

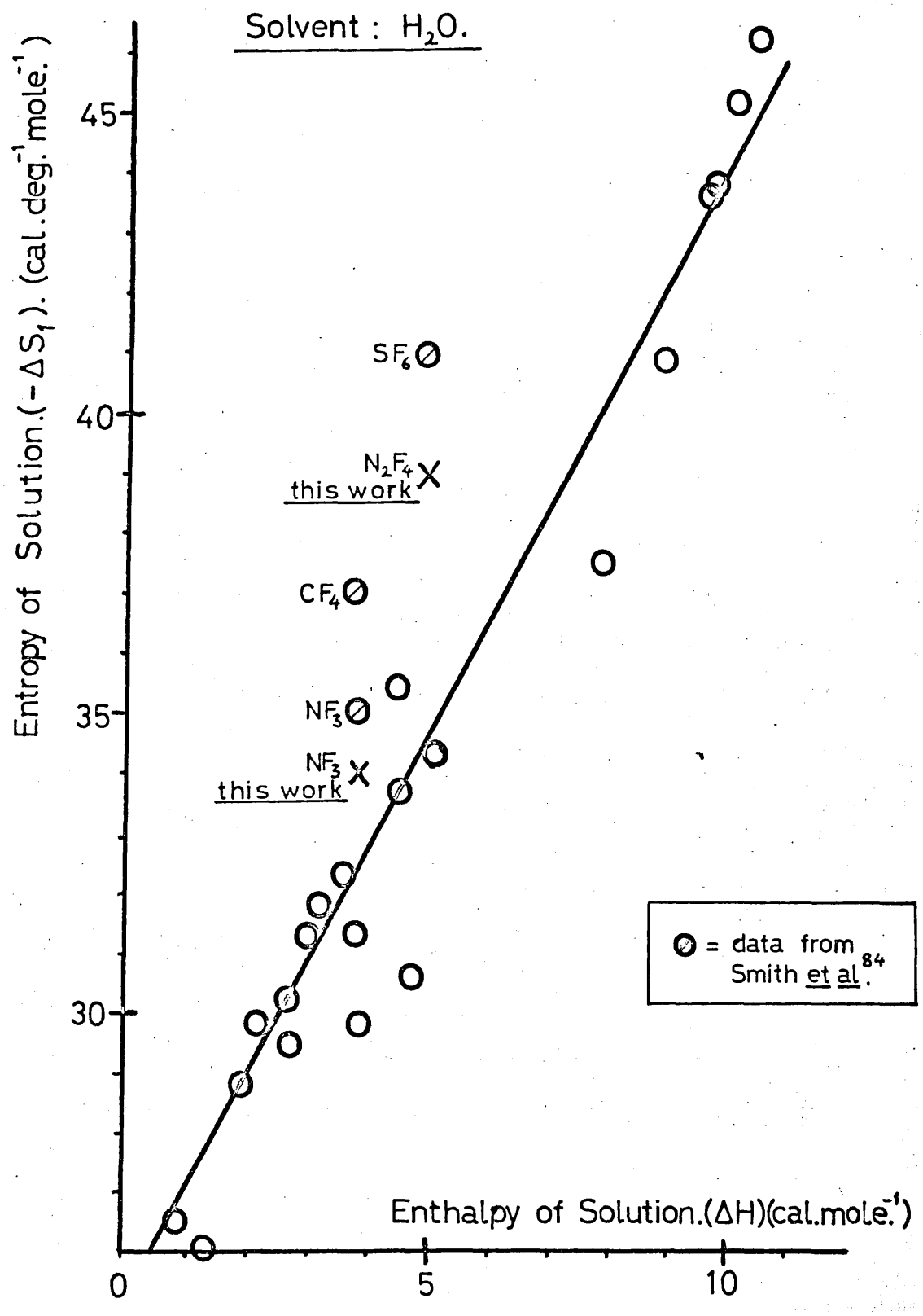

commented that the version of the Barclay-Butler plot given by Frank and Evans[121] predicted an entropy of solution of only -35 cal.deg.$^{-1}$mole^{-1}, but questioned the extent to which this disagreement could be regarded as indicating anomalous behaviour.

Smith et al did not compare their experimental entropies of solution of CF_4 and NF_3 with those predicted by the Barclay-Butler rule from their values of ΔH. In Figure 9, this comparison is made graphically both for these two gases and for N_2F_4.

The Barclay-Butler predicted entropies are in good agreement (to within 1.5 cal.deg.$^{-1}$mole^{-1}) with the experimental values for all the gases for which data were given by Frank and Evans[121] and by Herington.[131] The only exception is benzene, with a difference between the predicted and experimental entropies of 2.5 cal.deg.$^{-1}$mole^{-1}. However, for NF_3, CF_4, N_2F_4 and SF_6, the differences are considerably greater, and it seems probable that this disagreement is not due to experimental error, but is indicative of anamalous behaviour of these gases with regard to the Barclay-Butler rule. It has been shown[132] that the theoretical requirements for conforming solutions which satisfy this rule are stringent, and thus this rule is probably not a good criterion of abnormality.

Powell and Latimer[133] proposed an empirical equation relating the entropy of solution (ΔS_1) of non-polar substances in water at 25°C to the molar volume of the liquid solute at its boiling point (V_l).

This relationship may be written as:-

$$-\Delta S_1 = C + 0.22\, V_1$$

where V_1 is in cm^3 and ΔS_1 is in $cal.deg.^{-1}mole^{-1}$. They found that this relationship accounted most successfully for the entropies of solution of many solute gases of approximately spherical symmetry. Smith *et al*[84] also found that their experimental entropies of solution of CF_4, NF_3 and SF_6 were in excellent agreement with the values predicted by the relationship.

A graph of ΔS_1 against V_1 is shown in Figure 10, using data taken from the graph of Smith *et al*[84] and from Miller and Hildebrand.[135] Points for N_2F_4 and NF_3 were plotted using the values of ΔS_1 obtained in this work, and the value of V_1 for N_2F_4 was calculated using the literature value for the density of liquid N_2F_4 at its boiling point ($1.397\ g.cm^{-3}$)[27,134].

The agreement between the experimental and predicted values for ΔS_1 for N_2F_4 is not as good as for NF_3, SF_6 and CF_4, but the overall agreement is very much better than that obtained using the Barclay-Butler rule. The difference between the experimental ΔS_1 for N_2F_4 (38.4 cal. $deg.^{-1}mole^{-1}$) and the predicted value (40.5 $cal.deg.^{-1}mole^{-1}$) is small, and may, in part, be due to the non-spherical symmetry of the N_2F_4 molecule. The paraffins C_2H_6, $n\text{-}C_3H_8$ and $n\text{-}C_4H_{10}$ also show deviations from this plot in the same direction as for N_2F_4. The points for CF_4 and SF_6, which are marked with asterisks in Figure 10, have been plotted using the values given by Morrison and Johnson,[85, 136] and Parmelee.[137]

FIGURE 10.

Plot of ΔS_1 against V_l.

Solvent : H_2O.

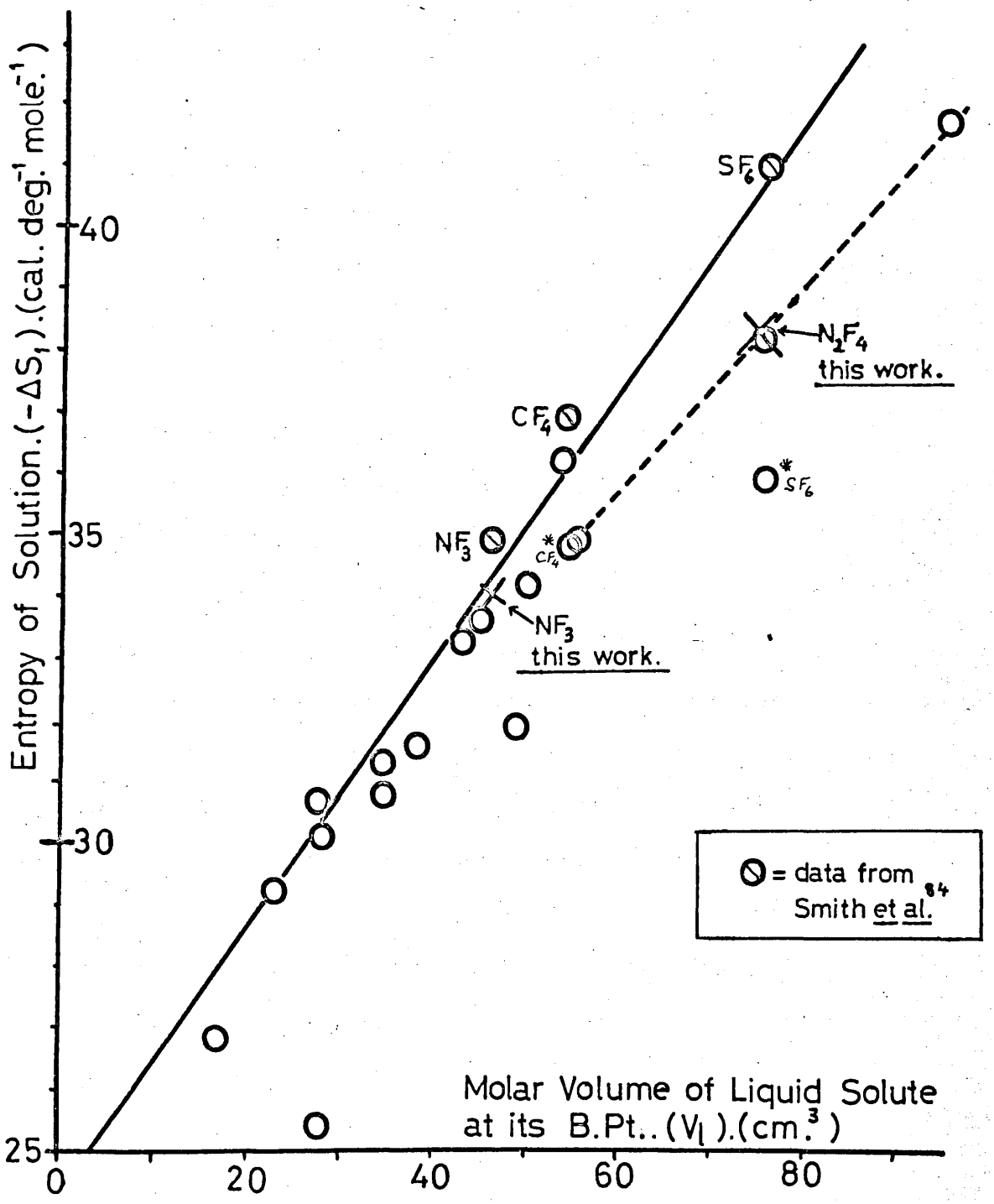

A recent analysis of the thermodynamics of solution of gases in water by Miller and Hildebrand[135] has suggested that the entropies of solution can equally well be related to $V_1^{2/3}$. Using the model of water proposed by Lennard-Jones and Pople,[138] Miller and Hildebrand proposed a model for the loss of entropy upon solution of gases in water that did not postulate the formation of rigid structures of any sort. This model was based on the bending, rather than the breaking, of the hydrogen bonds in ice on melting. Thus the extraordinarily large heat capacity of water can be explained by the ability of these hydrogen bonds to absorb the thermal energy, and this must necessarily decrease when the water molecules are in contact with a nonwetting surface (e.g. P.T.F.E. or paraffin). They proposed that the molecules of an inert gas act similarly, and thus related the loss of entropy to the surface area of the gas molecules, and further to $V_1^{2/3}$.

A graph of ΔS_1 against $V_1^{2/3}$ is shown in Figure 11, using the same data as for Figure 10. In Figure 11, the agreement between the predicted and experimental entropies of solution is excellent for the Inert gases(He, Ar, Kr, Xe) and for the straight chain paraffins (CH_4, C_2H_6, n-C_3H_8, n-C_4H_{10}). This agreement is also excellent for N_2F_4. However, the agreement is not so good for the points plotted using the data from Smith et al for NF_3, CF_4 and SF_6, and these points appear to fall on a separate line (shown as a broken line in Figure 11).

FIGURE 11.

Plot of ΔS_1 against $(V_l)^{2/3}$.

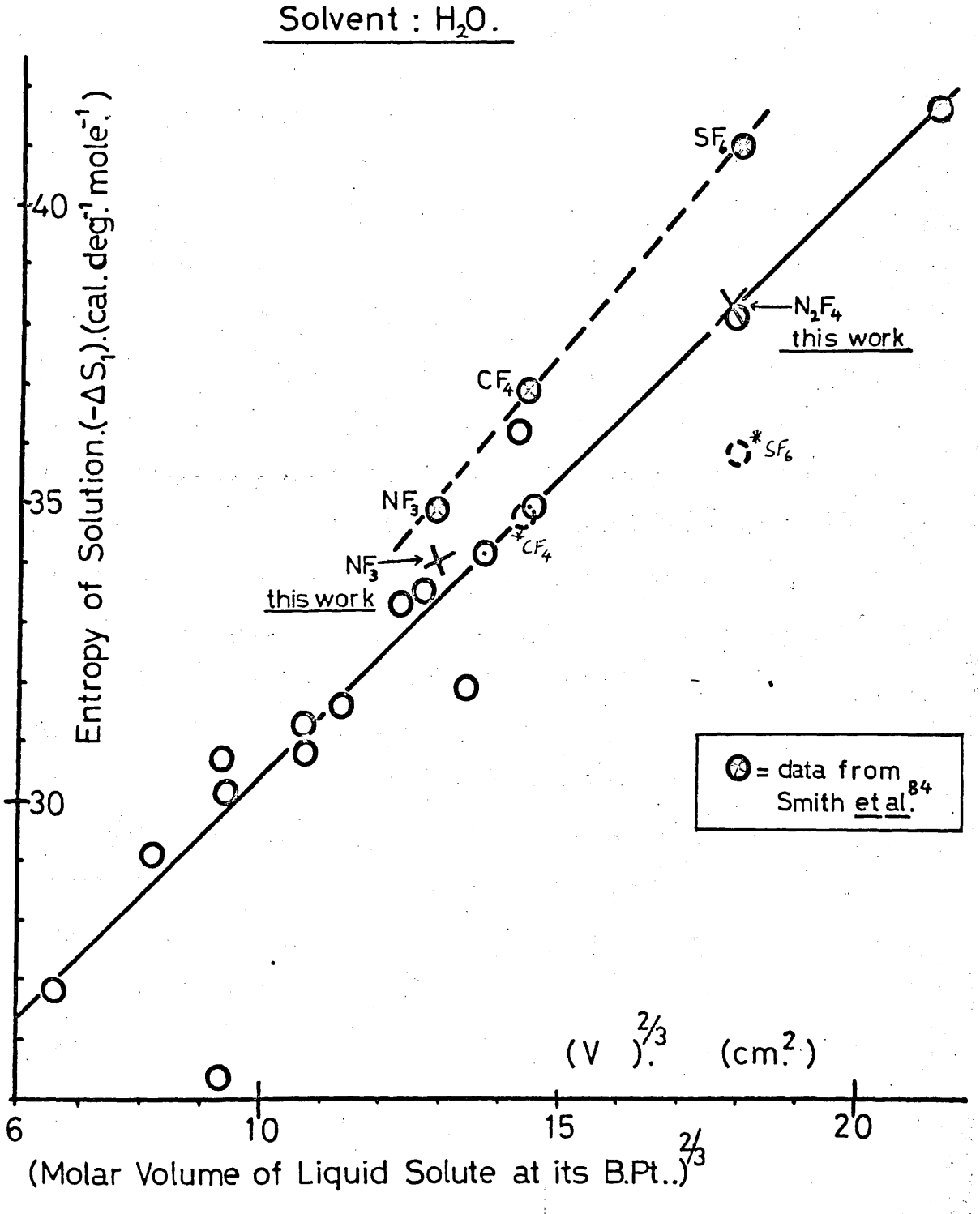

Comparison of Figures 10 and 11 appears to indicate that the entropy of solution may be related to either or both of V_1 and $V_1^{2/3}$, but that different plots are required for the gaseous fluorine compounds of spherical symmetry and for the straight chain paraffins. The excellent agreement of the entropy of solution of N_2F_4 with the plots for the straight chain paraffins (broken line in Figure 10; continuous line in Figure 11) may be fortuitous, but appears to indicate some dependence on the shapes of the gaseous solute molecules.

The above observations lead to the conclusion that the low solubilities of gaseous fluorine compounds are not due to abnormalities giving rise to their large negative entropies of solution, but that these entropies are related to the size of the solute molecules. Thus the frequent comparison of these molecules to the smaller inert gases must be modified in view of the differences in size. Also, with the excellent agreement obtained between the experimental entropies of solution and those predicted using purely thermodynamic theories of gas solution, Smith *et al*[84] concluded that the concept of 'iceberg' formation was not necessary for an adequate explanation of the solubility of non-polar gases in water and the thermodynamic properties thereof.

The relevance of these results for the solubilities of NF_3 and N_2F_4 in water, to an understanding of the toxicology of these compounds is discussed in the introduction to the next section.

PART 1 : SECTION 2

REACTIONS OF NITROGEN-FLUORINE COMPOUNDS WITH AQUEOUS MEDIA

INTRODUCTION

The moderate to high toxicity of NF_3 and N_2F_4[69,142] is somewhat surprising considering the very low aqueous solubilities of these gases. At 37°C, the mammalian body temperature, both of these gases have solubilities of only about 1.1×10^{-5} moles of gas per mole of water for a partial pressure of 760 mm Hg of gas above the solvent.

Studies of the toxicology of these gases have shown that exposure to 10,000 ppm (1%) N_2F_4 for 25 minutes or longer was lethal to rats,[142] and that exposure to the same concentration of NF_3 was almost always lethal after 60 to 70 minutes.[69] This concentration of gas above water would give an equilibrium concentration of dissolved gas of only 1.1×10^{-9} mole fraction or 6.4×10^{-6} moles of gas per litre. If it is assumed that other respiratory gases do not affect the solubility of NF_3 and N_2F_4, and that there is no interaction of these gases, when dissolved, with other substances in mammalian blood, then the equilibrium concentration of these gases in blood, for a concentration of 10,000 ppm in the respiratory gases, would be 6.4×10^{-6} molar (the same as for pure water).

Two main types of interaction between dissolved gas and substances in solution in blood can be envisaged and these are chemical interaction (such as complex formation) and physical interaction, where the dissolved

substances modify the properties of the solvent causing a change in the solubility. In blood, dissolved salts will interact physically with dissolved gases and will affect the solubility of gases by the process known as 'salting-out',[139] and thus reduce the equilibrium concentration of dissolved gases. Thus, if it is assumed that there is no chemical interaction of these gases with the constituents of blood, 6.4×10^{-6} molar may be taken as an upper limit for the equilibrium concentration of either NF_3 or N_2F_4 for a concentration of 10,000 ppm of these gases in the respiratory gases.

The extent of methemoglobin formation by lethal exposure to these gases is characteristically 60% to 70% of the total hemoglobin. In order to compare the rate of reaction between N_2F_4 or NF_3 and blood with data for the rates of reaction with pure water,[38] it is necessary to estimate the amount of N_2F_4 or NF_3 that has reacted to cause these methemoglobin concentrations. The standard 100% hemoglobin concentration in blood is usually taken as 14.8 g hemoglobin per 100 cm^3,[140] and using a typical hemoglobin molecular weight of 64,500,[141] this is equivalent to 2.3×10^{-3} moles of hemoglobin per litre of blood, or to 9×10^{-3} molar Fe in the +2 state. A 60% to 70% conversion of hemoglobin to methemoglobin is, therefore, equivalent to the oxidation of 5.4 to 6.3 millimoles of Fe^{+2} per litre. On the basis of the assumed overall equation for the reaction of N_2F_4 ($10Fe^{2+} + 8H^+ + N_2F_4 \longrightarrow 10Fe^{3+} + 2NH_4^+ + 4F^-$), this oxidation is equivalent to reaction of 0.54 to 0.63 millimoles of N_2F_4 per litre of blood. For NF_3, on the basis

of the overall equation for the reaction[71] ($6Fe^{2+} + 4H^+ + NF_3 \longrightarrow 6Fe^{3+} + NH_4^+ + 3F^-$), the oxidation is equivalent to reaction of 0.9 to 1.0 millimoles of NF_3. Thus the rate of reaction of N_2F_4 with blood is estimated as 0.54 to 0.63 millimoles per litre of blood in 25 minutes or as 1.3 to 1.5 millimoles of N_2F_4 per litre of blood per hour. The rate of reaction of NF_3 with blood is similarly estimated as 0.9 to 1.0 millimoles per litre of blood in 60 to 70 minutes, or as 0.8 to 1.0 millimoles of NF_3 per litre of blood per hour. These rates refer to a temperature of 37°C and an estimated equilibrium concentration of the gases in the blood of $\leq 6.4 \times 10^{-6}$ molar.

These rates may be compared with the data for the reactions of NF_3 and N_2F_4 with aqueous systems as given by Hurst and Khayat.[38] For the hydrolysis of N_2F_4 by pure water at 60°C, they found that about 0.02 millimole of N_2F_4 was hydrolysed by a 5 cm^3 sample of water after 6 days with a pressure of N_2F_4 above the water of about 775 mm Hg. Assuming that the extent of hydrolysis is proportional to the volume of water, this is equivalent to an average rate of hydrolysis of 4.0 millimoles of N_2F_4 per litre of water in 6 days, or of 0.03 millimoles of N_2F_4 per litre of water per hour. This rate refers to a temperature of 60°C and a partial pressure of N_2F_4 above the water of 775 mm Hg. For these conditions, the equilibrium concentration of dissolved N_2F_4 was calculated, from the solubility results given in this thesis, to be about 8.7×10^{-6} mole fraction or 4.8×10^{-4} molar.

If the effects of temperature and concentration of dissolved N_2F_4 are neglected, the above estimates indicate that the rate of reaction of N_2F_4 with blood is about 50 times faster than that for reaction with pure water. If it is assumed that the rate of reaction is directly proportional to the concentration of dissolved N_2F_4 and that the equilibrium concentrations estimated above may be used as approximations to the concentrations of dissolved N_2F_4 during the reactions, then the reaction with blood is about 3700 times faster than that with water. This still neglects a probable increase in reaction rate with increasing temperature, which would further increase this factor.

This comparison indicates that the reaction of N_2F_4 with blood cannot be explained in terms of a mechanism involving simple hydrolysis of N_2F_4, followed by oxidation of hemoglobin by an hydrolysis product. In order to be compatible with the above estimates, this type of two-stage mechanism would require an increase, by a factor of at least 1,000, in the rate of initial hydrolysis of N_2F_4 by blood, above that found for pure water. This would have to be caused by catalysis by some substance dissolved in mammalian blood. This is further emphasised by comparison of the rates of reaction of NF_3 with pure water and with blood. Hurst and Khayat[38] found that NF_3 could be recovered quantitatively after seven days in contact with pure water at 133°C. The hydrolysis of NF_3 by blood, however, proceeds at a rate as estimated above, of 0.8 to 1.0 millimoles of NF_3 per litre of blood per hour.

It therefore seems to be significant that Hurst and Khayat[38] found that NF_3 was readily converted to ammonium ion by acidic or neutral ferrous sulphate solution at 60°C ($6Fe^{+2} + 4H^+ + NF_3 \longrightarrow 6Fe^{+3} + NH_4^+ + 3F^-$). They also found that ferric chloride solutions reacted very slowly with NF_3 at 100°C, yielding nitric oxide and nitrate. This catalysis of the hydrolysis was not found to be a general property of transition metal ions, as shown by the total inertness of NF_3 to solutions of $CoCl_2$, $MnSO_4$, $CuSO_4$ and $NiSO_4$ at 100°C over periods of up to seven days.

Hurst and Khayat found that for a typical reaction of NF_3 with aqueous (0.5N) ferrous sulphate, 44% of the original 3.18 millimoles of NF_3 had reacted with 20 cm^3 of the aqueous solution after 12 days at 60°C with a partial pressure of the NF_3 above the solution of 0.69 atmospheres. This is equivalent to a reaction rate of 0.24 millimoles of NF_3 per litre of solution per hour at 60°C. The equilibrium concentration of dissolved NF_3 in ferrous sulphate solution was estimated to be 3.25×10^{-4} molar; using the same assumptions as used above in the estimation of the concentration in blood. Neglecting the effects of both the difference in temperature and the difference in the estimated concentrations of NF_3 dissolved in the aqueous solutions, the rate of reaction of NF_3 with blood is only three times greater than that for the reaction of NF_3 with aqueous ferrous sulphate. If however the effect of the difference in the concentrations is estimated as above, then the reaction with blood is estimated to be 170 times as fast as the reaction with the aqueous ferrous sulphate.

The presence of ferrous and, to a lesser extent, ferric ions in solution, therefore, markedly effects the rate of reaction of NF_3 with aqueous media and there are considerable similarities between the results obtained by Hurst and Khayat for reaction of NF_3 with aqueous ferrous sulphate solutions the the results for the reaction of NF_3 with blood. It therefore seems likely that the toxicity of NF_3 is a result of direct reaction of NF_3 with hemoglobin, or that hemoglobin acts as a catalyst in the hydrolysis of NF_3, before reacting with one of the hydrolysis products.

No data have been recorded in the literature for reaction of N_2F_4 with aqueous ferrous ion solutions. However, the possibility that ferrous ions might catalyse the hydrolysis of N_2F_4, or react with this gas at a rate in excess of that found for the reaction with pure water, is of interest in relation to the toxicology of N_2F_4. For this reason, this reaction has been studied in this thesis.

(a) Apparatus

This apparatus was designed to allow the monitoring of a reaction of a gas at constant pressure with an aqueous medium. The design of the reaction cell used is shown in Figure 12.

The main body of this cell, B, was fabricated from rigid polypropylene in order to be inert to acidic fluoride solutions. The internal diameter of this polypropylene cup was 5.5 cm with a wall thickness of about 0.75 cm. This large diameter gave a large surface area of contact between the aqueous and gas phases. In order to increase further the rate of solution of the gas into the liquid phase, the effective surface area of contact was

FIGURE 12.

Gas-liquid Reaction Cell.

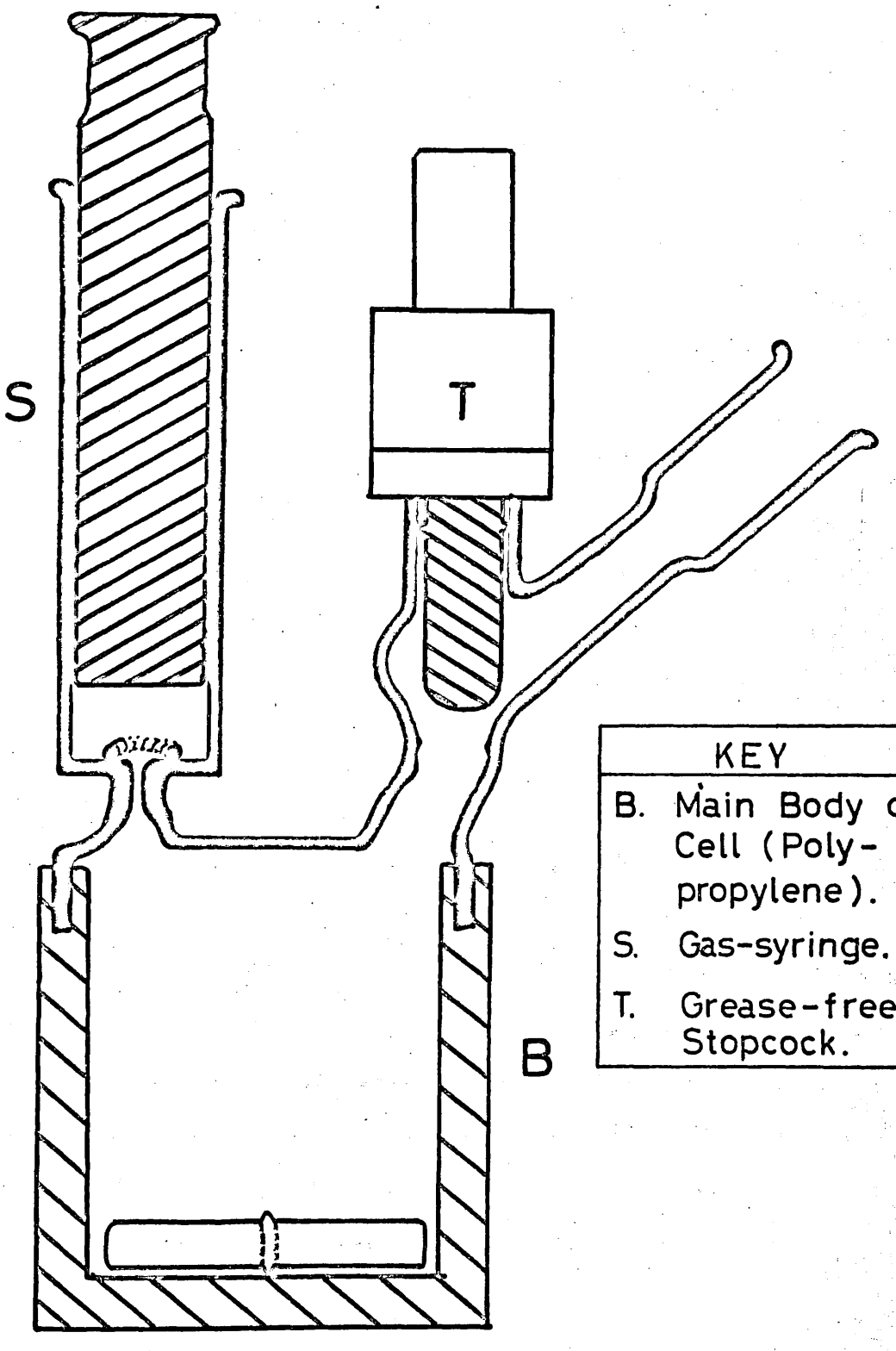

KEY	
B.	Main Body of Cell (Poly-propylene).
S.	Gas-syringe.
T.	Grease-free Stopcock.

increased by continuous fast stirring using a two inch (5 cm.) polypropylene-encapsulated magnetic follower. The internal depth of the cup was about 6.5 cm, allowing the use of a liquid phase volume of about 110 cm^3.

A constant pressure of gases inside the reaction cell was maintained by the use of a vertical all-glass 20 cm^3 gas-syringe, S (Chance Brothers Ltd., Malvern Link, Worcestershire). The freely-moving syringe piston compensated for the constant removal of reactant gas from the gas phase, caused by solution and reaction in the aqueous phase, thus maintaining a constant pressure of gases slightly in excess of atmospheric pressure. A grease-free high-vacuum stopcock, T, ('Uniform', Glass Precision Engineering Ltd., Hemel Hempstead, Hertfordshire) was incorporated for the admission of the reactants into the reaction cell, and was modified in order to allow a hypodermic needle to be inserted into the reaction cell through the opened tap.

The gas syringe and stopcock were glass-blown onto a pyrex-glass lid which fitted into a machined groove, 1 cm deep, in the top of the polypropylene cup. A vacuum-tight seal was obtained by external application of Torr Seal, a commercial low vapour pressure resin, (Varian Associates, Vacuum Division, California, U.S.A.) to the glass-polypropylene boundary. It was found that this seal was maintained for longer periods if the resin was applied while the reaction cell was being evacuated by continuous pumping.

Previous studies of the reactions of N_2F_4 with water[33,66] have indicated that oxygen promotes, the hydrolysis, thus necessitating the complete exclusion

of oxygen from the reaction cell. Hurst and Khayat[38] postulated that the large variations in the rates that they observed for the reaction of N_2F_4 with water were caused by minute amounts of oxygen remaining in the starting materials, even after careful purification, including boiling and vacuum degassing of the water. The ground-glass fit of the plunger in the gas-syringe was sufficiently good to allow only negligible diffusion of gas out of the reaction cell during normal operation, and water applied to the top of the syringe, as well as acting as a lubricant, ensuring free movement of the plunger, was also effective in further sealing the gas syringe against diffusion of gas. Thus under normal operating conditions there was no possibility of entry of air through the gas syringe. However, the extreme sensitivity of reactions of N_2F_4 with water to the presence of minute amounts of oxygen necessitated a design of the apparatus to allow the introduction of all reactants without the introduction of oxygen. This necessitated the evacuation of the reaction cell, with degassing of all the non-volatile starting materials, before the volatile starting materials could be introduced directly from a vacuum line. Although the fit of the piston in the gas-syringe was adequate for normal use, this seal was not sufficient for the evacuation of the reaction cell and a method for temporarily obtaining a vacuum-tight seal had to be found. The application of vacuum grease to the ground-glass surfaces was found to provide an adequate seal for short periods of time. However this prevented free-movement of the piston when in operation and was therefore not acceptable. This problem was overcome by

the use of a 15 mm (outside diameter) 'Viton A' rubber 'O' ring placed between the bottom surface of the syringe piston and the bottom of the syringe barrel (See Figure 12). A clamp was fabricated and used to apply pressure on the piston forcing it onto the 'O' ring to obtain a vacuum-tight seal. This 'O' ring had to be left in position during normal operation, but did not affect the operation of the gas-syringe. In this way, the reaction cell could be evacuated to a pressure of less than 10^{-5} torr and, on closing the tap T, maintained this pressure for several hours. A grease-free high-vacuum joint (J. Young Scientific Glassware Ltd., Acton) was used for connection to the vacuum line in order to prevent contamination of the starting materials with vacuum grease.

A 2' x 1' by 7" high water bath, fabricated from 1/4" thick perspex, was used for thermostatic control in conjunction with a 'tempunit' (heater, thermostat, stirrer and centrifugal pump combination, Techne Ltd., Cambridge). The centrifugal water pump was connected by large-bore polythene tubing to the opposite end of the bath, increasing the effective stirring and allowing the set temperature of 25°C to be maintained to better than $\pm$ 0.1°C.

In order to power the magnetic follower in the reaction cell, the tank was placed on top of an aluminium framework to allow horse-shoe magnets to be rotated under the tank. These were powered by a plastic belt drive from a variable speed motor. The stirring speed could be varied from about 30 revolutions per minute to about 1000 r.p.m.. Eight magnets were incorporated to allow the use of up to eight reactions cells simultaneously for the study of slow reactions, but this facility was not used.

(b) Choice of Reaction, Sampling and Analysis

The above apparatus was used for the study of the reaction of N_2F_4 with an aqueous solution of ferrous ions. Ideally, for direct comparison with the reaction of N_2F_4 with blood, this reaction should be carried out for an aqueous solution of ferrous ions buffered to a pH of about 7.5, the pH of blood. However, at this pH, uncomplexed ferrous and ferric ions are precipitated as hydroxides, thus necessitating the use of solutions of lower pH. In addition, the sensitivity of ferrous sulphate to oxidation by atmospheric oxygen necessitated the use of a more stable source of ferrous ions. Thus a solution of ferrous sulphate made using deoxygenated water was found to give a deep red coloration when salicylic acid was added, indicating a substantial concentration of ferric ions in the original solution (vide infra). Solutions of ferrous ammonium sulphate were, therefore, used in all further work.

Even a pH 5 (sodium acetate/acetic acid buffer solution) solutions of ferrous ammonium sulphate in deoxygenated water were found to be deep brown in colour and eventually precipitated a black-brown solid, even when stoppered. For this reason a much lower pH was used (about pH 0.4) for the reaction. At this pH, solutions of ferrous ammonium sulphate were found to be less sensitive to oxidation by atmospheric oxygen and this facilitated accurate sampling and analysis of the ferric ion concentration in the reaction cell.

In order to monitor the reaction between N_2F_4 and the aqueous ferrous ion solution, a 2 cm^3 syringe was used to remove a 1 cm^3 sample of the solution from the reaction cell through a seven inch hypodermic needle. Contamination of the reaction system with oxygen was avoided by the use of a Suba-Seal inserted in the greaseless joint of the reaction cell. The interspace between the Suba-Seal and the tap was flushed free of oxygen by alternate partial evacuation and flushing with N_2F_4 from a reservoir through a hypodermic needle inserted through the Suba-Seal. The hypodermic needle and syringe used in extracting the 1 cm^3 sample were flushed with nitrogen from a cylinder, to prevent the introduction of oxygen when sampling. The hypodermic needle was inserted through the Suba-Seal, the tap T was then opened and the hypodermic needle was pushed through the tap into the aqueous phase.

The scale on the syringe used was calibrated by weighing the water delivered through the seven inch hypodermic needle. In this way, it was found that a sample of 1 cm^3 could be obtained accurate to $\pm$ 0.006 cm^3 (twice the standard deviation of the mean). This 1 cm^3 sample was found to be sufficient for the determinations of both the fluoride ion and the ferric ion concentrations by the methods described below.

In order to stop the reaction between dissolved N_2F_4 and the aqueous ferrous ions, each 1 cm^3 sample was injected into a capped polythene sample tube (3" x 1") through a 1/16" hole drilled through the cap. Solid CO_2 was placed in these sample tubes at least ten minutes before sampling

in order to flush out oxygen. The injection of the 1 cm^3 samples onto solid CO_2, remaining in the sample tubes, was found to be a very effective method of stopping the reaction, both by lowering the temperature and by removal of dissolved N_2F_4 by gaseous CO_2 bubbling through the aqueous sample. In order to prevent entry of atmospheric oxygen into these sample tubes, they were placed in a glove-box, under an atmosphere of nitrogen, as soon as the initial evolution of CO_2 was complete.

A fluoride electrode (Model 96-09, Orion Research Incorporated, U.S.A.) in conjunction with a specific ion meter (Model 401, Orion Research Inc.) was used for the analysis of fluoride ion concentration. For these measurements, it was necessary to raise the pH of the samples to above pH 5, since, below this pH, hydrogen ions complex with fluoride ions to form significant concentrations of HF and HF_2^-, and these cannot be detected by the electrode. However, the pH could not be raised above about pH 8, since the electrode responds to hydroxide ions as well as fluoride ions. Below pH 8, the hydroxide ion concentration is less than 10^{-6} molar, and this concentration is negligible compared to the fluoride concentrations to be measured ($> 10^{-4}$ molar). In order to avoid further complications due to precipitation of ferrous and ferric ions as hydroxides, all fluoride measurements were made on samples buffered to about pH 6.

The ferric ion concentration was estimated by a method based on the complex formation between salicylic acid and ferric ions. This complex

absorbs strongly in the blue-green region of the visible spectrum with a maximum absorption at about 510 mμ, and has been used as an indicator for the titration of ferric ions against standard solutions of the di-sodium salt of ethylenediamine-tetra-acetic acid.[143] In this work, the ferric ion concentration was estimated colorimetrically by measurement of the transmittance at 510 mμ of solutions of this complex prepared from the 1 cm^3 samples taken from the reaction cell. It was found to be preferable to measure this transmittance for solutions at low pH (about pH 2). At higher pH values, the maximum absorption was shifted to a lower wavelength, and, at pH 5, this maximum was below 500 mμ. This difference was easily detected by eye, the colour of the solution being mauve at pH 5, instead of a blood-red colour at about pH 2. Also the transmittance of solutions had to be measured outside the glove-box making the use of low pH values advantageous due to increased stability of ferrous ions towards oxidation by atmospheric oxygen.

Since changes in pH, with consequent dilution of the 1 cm^3 samples, were required from the reaction sample pH of about 0.4 to about pH 2 for the ferric ion analysis and to about pH 6 for the fluoride analysis, the sequence of these two analyses was determined by their sensitivities. For this reason the fluoride ion analysis always preceeded the ferric ion analysis. Also, ferric and ferrous ions complex with fluoride ions, necessitating the addition of a ligand to complex with both ferrous and ferric ions to the exclusion of the fluoride ions. It was found that sodium salicylate (Na Sal.) would decomplex fluoride ions when added to

solutions containing fluoride, ferrous and ferric ions if added in excess of six moles of salicylate ions per mole of iron (ferrous plus ferric).

A fluoride-analysis-buffering solution was prepared to be 0.25M NaOH, 0.32M Na Sal. and 15% NaAc (Ac = acetate) in deoxygenated water. For the determination of the fluoride ion concentration, 10 cm^3 of this solution were added to the 1 cm^3 sample held in the polythene sample tube. This gave a pH of about 6 on stirring, allowing the fluoride concentration to be measured using the fluoride electrode.

In order to analyse for ferric ions, a pH of 2 was required. Aqueous H_2SO_4 could not be used to lower the pH to this value since salicylic acid was precipitated. The addition of glacial acetic acid, however, was found to lower the pH without this precipitation. 10 cm^3 of deoxygenated glacial acetic acid were added to the solution used in the fluoride analysis, and this solution was then diluted to 100 cm^3 in a volumetric flask using deoxygenated water and repeated rinsing of both the sample-tube and the fluoride electrode. The transmittance at 510 $m\mu$ of this solution in a 1 cm silica cell was measured using SP500 series 2 Ultraviolet and Visible Spectrophotometer (Unicam Instruments Ltd., Cambridge).

Calibrations were required for the analysis of both fluoride and ferric ions by the above methods. For this purpose standard solutions were prepared corresponding to the initial and final solutions in the

reaction cell. These were based on initial concentrations of 0.5M $(NH_4)_2\ SO_4\ Fe^{II}SO_4$, about 15% NaAc and about 1.5M H_2SO_4, and also on the assumed equation for the reaction with N_2F_4:

$$10\ (NH_4)_2SO_4Fe^{II}SO_4 + 8H^+ + N_2F_4 \longrightarrow 10\ NH_4Fe^{III}(SO_4)_2 + 8NH_4^+ + 4NH_4F.$$

The standard final solution was, therefore, prepared as 0.5M $NH_4Fe^{III}(SO_4)_2$, 0.2M NH_4F, about 0.2M $(NH_4)_2SO_4$, about 15% NaAc and about 1.3M H_2SO_4.

By appropriate dilution of the standard final solution with the standard initial solution, a dilution series was prepared, each solution corresponding to the solution in the reaction cell at some time during the reaction. For the analysis of fluoride ion concentrations, it was necessary to calibrate the electrode prior to the measurement of each unknown fluoride solution, and it was therefore essential that the calibrating solutions should be stable over long periods of time. This stipulation was not met by the dilution series, prepared as above, since the effect of oxidation of ferrous to ferric ions by atmospheric oxygen on the activity, and thus the measured concentration, of the fluoride solution was not known. Separate solutions of sodium fluoride in a 15% aqueous solution of NaAc were prepared, and their fluoride activities were adjusted to the same activities as for 1 cm^3 of each of the dilution series diluted with 10 cm^3 of the fluoride-analysis-buffering solution. The fluoride electrode was used for this comparison.

The ferric analysis was calibrated using the same dilution series, a 1 cm^3 sample of each of these standard solutions being prepared for ferric ion analysis as above. The results of this calibration are shown in

Figure 13 and can be represented by the equation: $\log_{10}(I/Io) = 18.0995$ X (molar ferric ion concentration) where I_o is the incident and I the transmitted intensities of light at wavelength 510 mM. For solutions with a ferric ion concentration greater than about 7×10^{-2} molar, the solution as used above had to be diluted by a factor of 10 (10 cm^3 of solution diluted to 100 cm^3) with deoxygenated water. A separate calibration was made as shown in Figure 14 and may be represented by the equation: $Log_{10}(I/I_o) = 1.6863X$(molar ferric ion concentration). All transmittances were measured relative to a blank solution prepared as above, but using a 1 cm^3 sample of an aqueous solution, 15% NaAc and 1.5MH_2SO_4. The accuracy of measurements of ferric ion concentrations by this method, and using the above calibrations, was estimated to be better than $\pm$ 3% at all ferric ion concentrations.

Deoxygenated distilled water and glacial acetic acid ('Analar', British Drug Houses Ltd., Poole) were prepared by boiling these solvents with a stream of nitrogen (oxygen-free) passing through. This steam of nitrogen was continued during cooling, after which these solvents were stored inside the glove box under an atmosphere of nitrogen. All the operations involved in the analysis of the 1 cm^3 samples could therefore be performed inside this glove box, except that the stoppered silica cells had to be removed in order to measure the ferric ion concentration using the spectrophotometer.

The above method for the analysis of both fluoride and ferric ions could be performed in a very short time, allowing the reaction to be sampled at frequent intervals during the first stages of the reaction.

FIGURE 13.

Calibration of Ferric Ion Analysis.

1 cm^3 sample diluted to 100 cm^3.

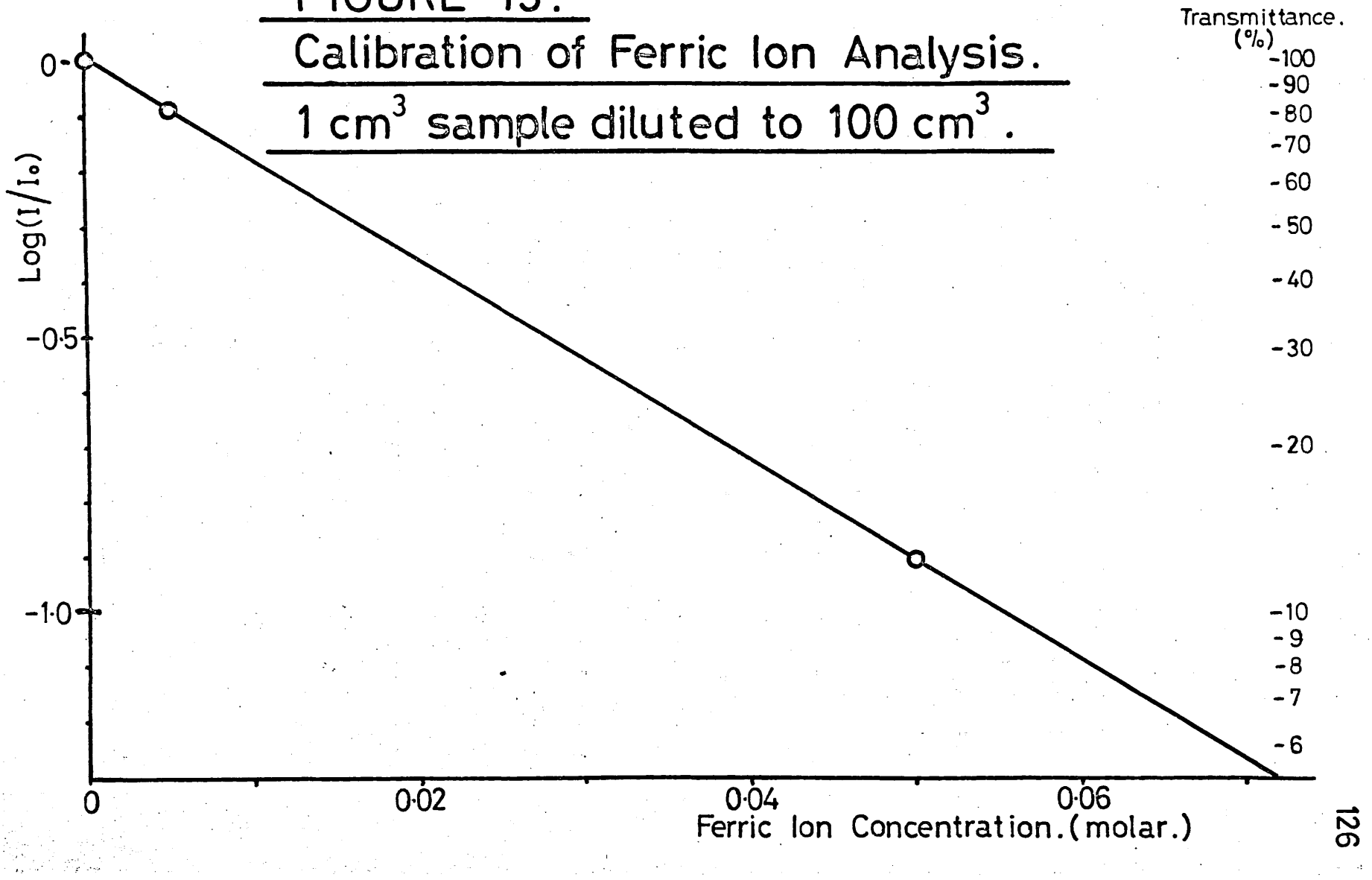

FIGURE 14.

Calibration of Ferric Ion Analysis.

1 cm^3 sample diluted to 1000 cm^3.

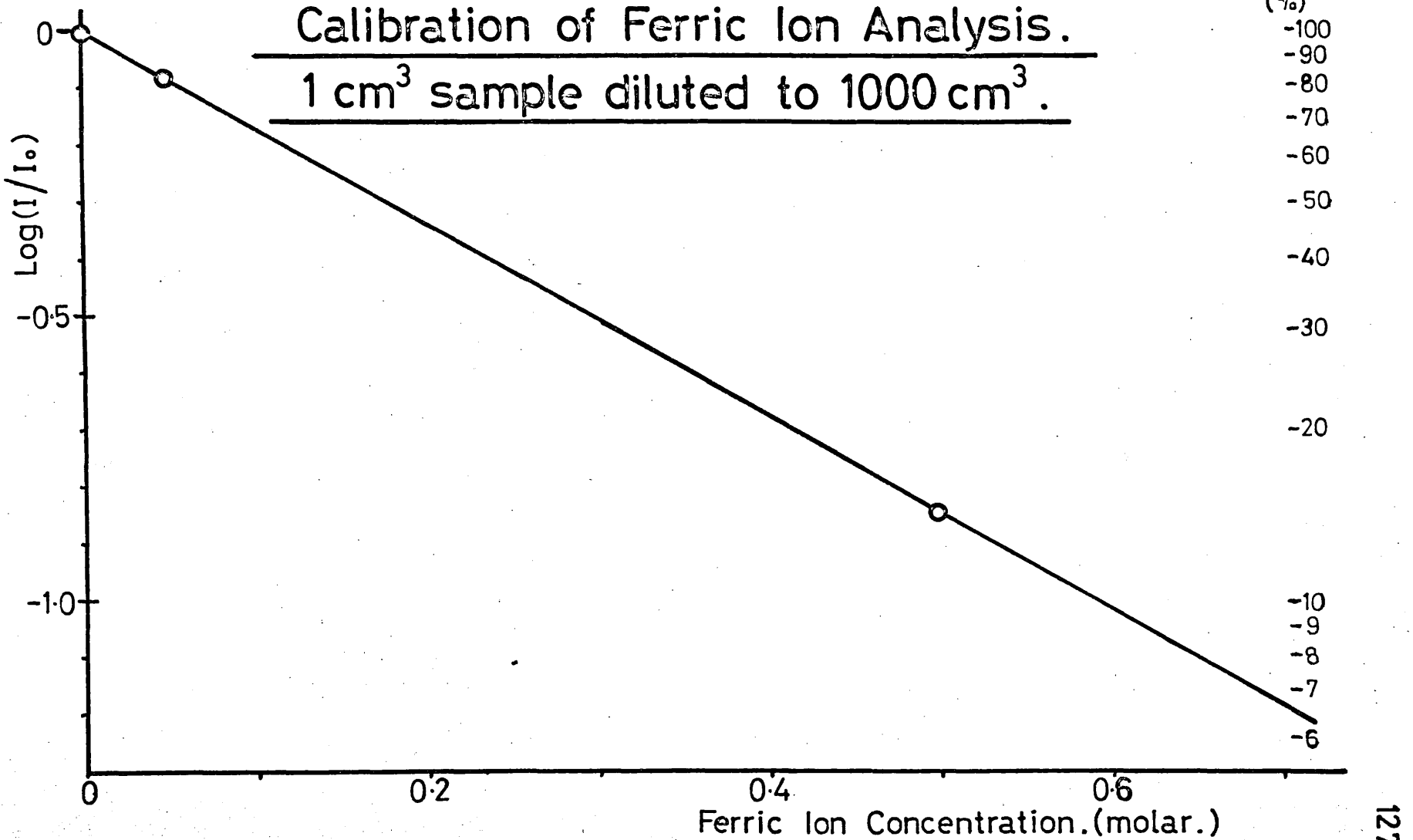

(c) Procedure for the setting-up of the Reaction and Results

In order to estimate the partial pressure of N_2F_4 above the liquid phase in the reaction system, the weight (39.65 g) and diameter (0.824 in = 1.05 cm) of the gas-syringe piston were measured, and, from these, the total pressure of gases in the reaction cell was calculated to be 0.35 cm Hg greater than atmospheric pressure. It was assumed that the sum of the vapour pressures of the components of the aqueous phase (vapour pressure mainly from solution of acetic acid in water) was approximately the same as for pure water, giving a partial pressure of the N_2F_4 gas above the aqueous phase of about 1.5 cm Hg less than atmospheric pressure.

In order to fill the reaction cell without the introduction of oxygen, the cell, with the syringe piston clamped down onto the viton ring, was evacuated and then transferred to the nitrogen-filled glove box. The tap was opened and 21.57 g $(NH_4)_2SO_4Fe^{II}SO_4.6H_2O$ ('Analar', British Drug Houses Ltd., Poole) and 8.61 g Na_2SO_4 ('Analar', B.D.H. Ltd.) were added through a glass funnel inserted through the tap of the reaction cell. The reaction cell was returned to the vacuum line, and evacuated carefully to avoid loss of the powdered solids. The cell was pumped for 24 hours to remove all traces of oxygen, before 5.57 cm^3 concentrated sulphuric acid (Specific Gravity 1.840, May and Baker Ltd., Dagenham) were added to the cell in the glove box. The cell was re-evacuated and pumped overnight.

Meanwhile a solution of 7.1 cm^3 glacial acetic acid ('Analar', B.D.H. Ltd.) in 90 cm^3 distilled water was degassed by vacuum trap-to-trap

distillation, using the apparatus previously described for the degassing of water (Section 1, (d)). About 80 cm^3 of this degassed acetic acid solution was then added to the cell, after it had been evacuated overnight, and the cell contents were stirred by activation of the magnetic follower to obtain about 110 cm^3 of solution approximately equivalent to 0.5M $(NH_4)_2\ SO_4Fe^{II}SO_4$, 1.5M H_2SO_4 and 15% HAc. (0.5M $(NH_4)_2\ SO_4Fe^{II}SO_4$ + 0.55M Na_2SO_4 + 0.95M H_2SO_4 + 1.1M HAc ≡ 0.5M $(NH_4)_2\ SO_4Fe^{II}SO_4$ + 1.1M (15%) HAc + 1.5M H_2SO_4).

When the solids in the reaction cell had been dissolved, N_2F_4, purified as previously described (Section 1, (d)), was added to the reaction cell to give a total pressure of about 107 cm Hg. With the tap firmly closed, the cell was disconnected from the vacuum line, the Suba-Seal was fitted to the greaseless joint and the clamp holding the syringe piston was released, allowing the piston to rise. The pressure of N_2F_4 added to the cell of 107 cm Hg was calculated such that, on release of this piston clamp, the cell would contain a pressure of 76 cm Hg (atmospheric pressure) with the gas syringe full of N_2F_4.

The cell was placed in the thermostat bath at 25°C, and stirring was started. Zero time for the reaction was taken as the time of filling the cell with N_2F_4 gas. The aqueous reaction phase was sampled at frequent intervals for 96 hours, and the samples analysed for fluoride and ferric ions. The results are shown in Figures 15, 16 and 17.

FIGURE 15: Reaction of N_2F_4 with Ferrous Ions.

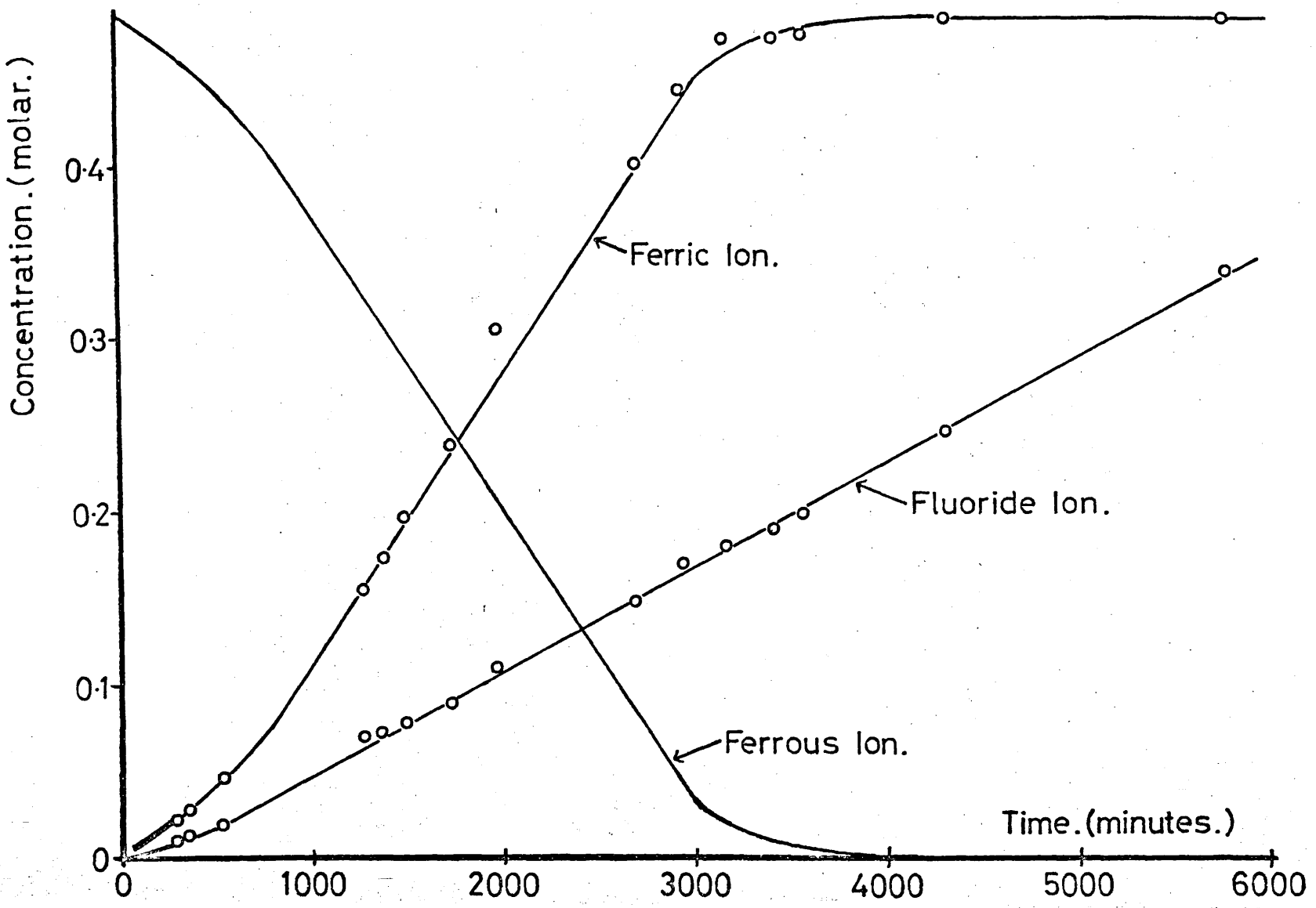

FIGURE 16: First 2000 minutes of Reaction.

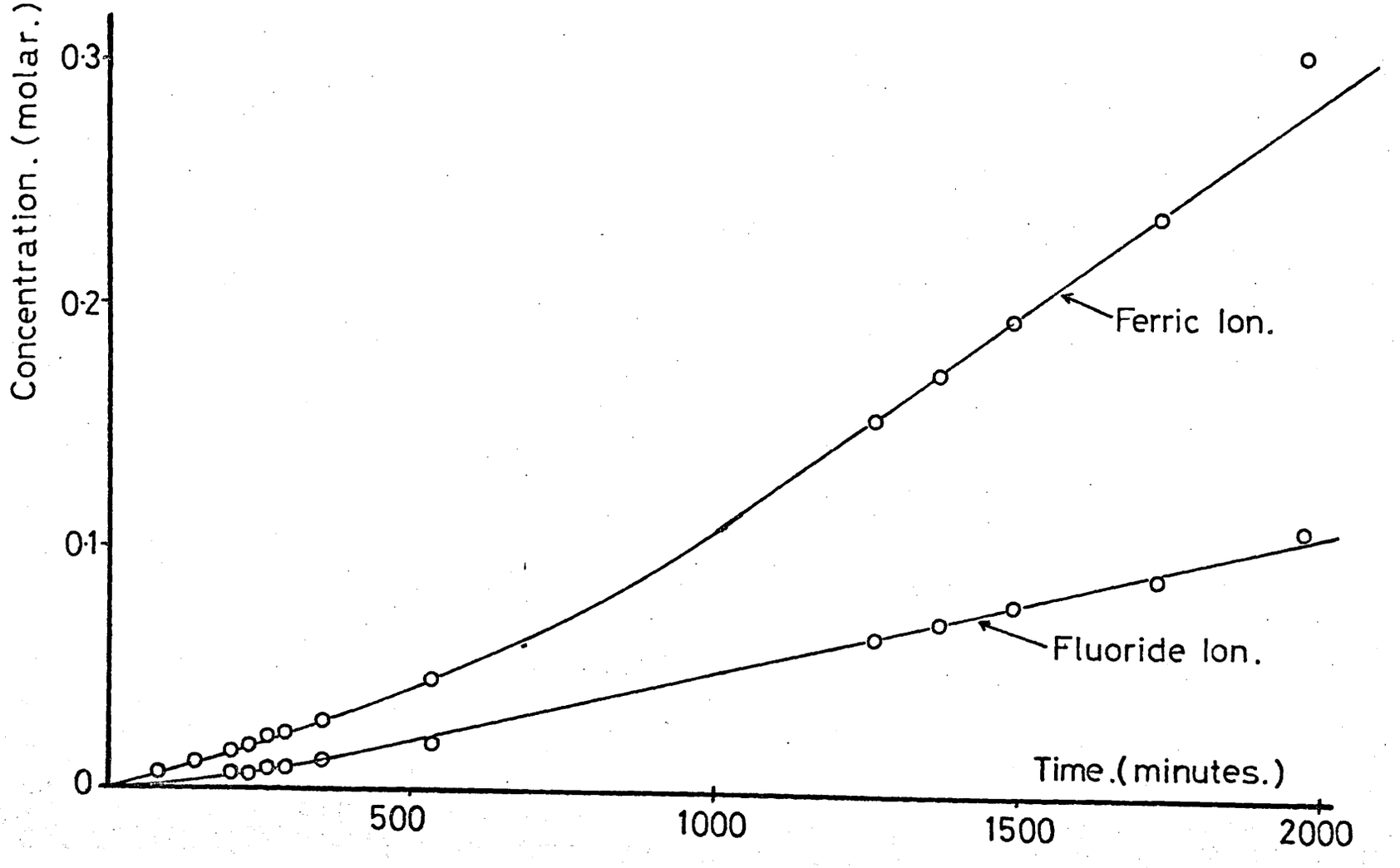

FIGURE 17: First 600 minutes of Reaction.

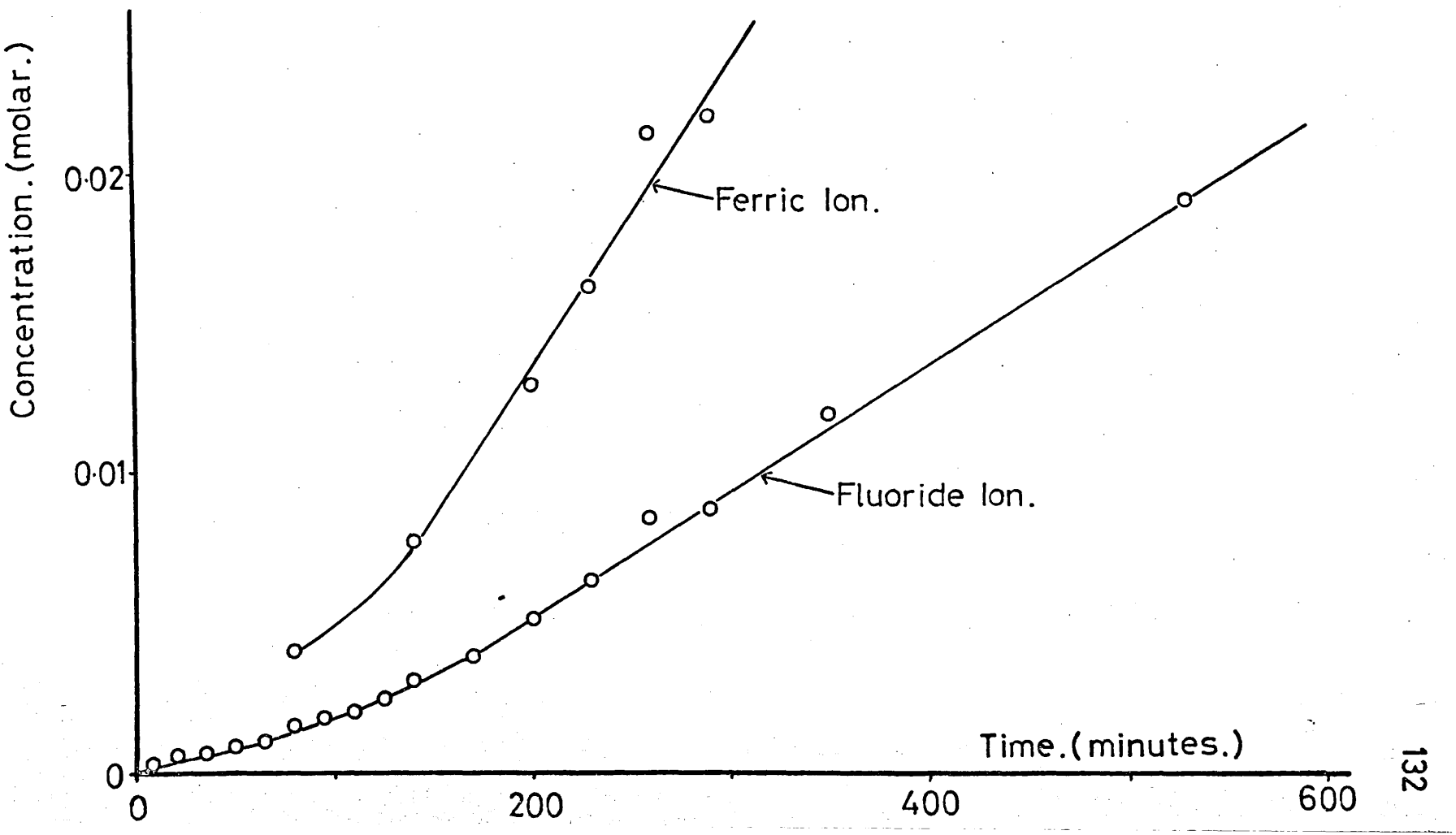

(d) Analysis of Reaction Products

At the end of 96 hours of reaction, a portion of the gases from the reaction cell was transferred to an infrared gas cell, and the infrared spectrum of this phase was recorded over the range 4000 cm^{-1} to 400 cm^{-1} (Model 337 Grating Infrared Spectrophotometer, Perkin-Elmer Ltd., Beaconsfield). Several spectra were recorded, each using a lower pressure of gas in the gas cell. The remainder of the gases in the reaction cell was stored and later analysed by mass spectrometry (Model MS902, Associated Electrical Industries Ltd., London). The liquid phase, remaining in the reaction cell, was kept under a stream of oxygen-free nitrogen for 24 hours in order to purge it of dissolved N_2F_4, and was then analysed for nitrite ions.

The infrared spectra were complicated by apparent reaction of the gaseous sample with the KBr plates. No precautions were taken to remove water vapour from this sample, since this might lead to the removal of other gaseous products, and therefore the reaction of the sample with the KBr plates was probably due to attack by the water vapour followed by solution of some of the gaseous products. Infrared absorptions caused by this interaction with the KBr plates were still fairly intense even after evacuation followed by pumping on the cell for 12 hours. These residual peaks were therefore neglected in the interpretation of the gas-phase infrared spectra.

The major component of the gaseous sample was unreacted N_2F_4, with characteristic absorptions centred on about 735 cm^{-1} and about 960 cm^{-1}.

Strong absorptions at about 1320 cm^{-1} and 1300 cm^{-1}, together with weaker absorptions at about 2600 cm^{-1}, 2350 cm^{-1}, 1290 cm^{-1} and 520 cm^{-1}, were assigned to NOF by comparison of these frequencies, relative intensities and band shapes with literature data.[144,145] Bands centred on 766 cm^{-1} and 1037 cm^{-1} should also be observed for NOF, but were not resolved from the very intense absorptions assigned to N_2F_4 in these regions of the spectra. A medium strength band centred at about 1900 cm^{-1} was assigned to NO by comparison with literature data.[146]

Bands at 1613 cm^{-1}, 1313 cm^{-1} and 750 cm^{-1} would be expected if NO_2 was present in the gaseous sample.[147,148] The very intense absorption by N_2F_4 centred on 735 cm^{-1} did not allow the possibility of resolving any absorption due to NO_2 at 750 cm^{-1}, and thus the complete absence of any absorption at either 1613 cm^{-1} or 1313 cm^{-1} was taken as indicating that NO_2 was not present in the gaseous sample.

The mass spectrum of the stored portion of gaseous sample mainly confirmed the above interpretation of the infrared spectra. The ions, together with their relative abundances and probable assignments, are listed in Table 10. The ions at $^{m}/_{e}$ values of 104, 87, 86, 85, 66, 53, 52, 47 and 33 have been assigned to a mixture of N_2F_4 and SiF_4. N_2F_4 must be present since SiF_4 does not give rise to any ion of $^{m}/_{e}$ 52 or 53 (assigned to NF_2^+). However, the relative abundances of the ions assigned in Table 10 to the mixture of SiF_4 and N_2F_4 are not in agreement with literature data for pure N_2F_4[149, 150, 151] but are consistent with the

TABLE 10

MASS SPECTRUM OF GAS PHASE SAMPLE AFTER REACTION OF N_2F_4 WITH AQUEOUS FERROUS IONS.

m/e	Relative Abundances (%)	Probable Assignment
104	3.5	$N_2F_4^+/SiF_4^+$
87	4.0	SiF_3^+
86	6.5	$N_2F_3^+/SiF_3^+$
85	100.0	$N_2F_3^+/SiF_3^+$
66	0.7	$N_2F_2^+/SiF_2^+$
53	1.4	NF_2^+
52	69.0	NF_2^+
49	1.2	NOF^+
47	1.4	N_2F^+/SiF^+
45	1.4	CO_2H ?
33	33.0	NF^+/SiF_2^{++}
30	100.0	NO^+
20	1.0	HF^+
19	0.6	F^+
14	0.3	N^+

relative intensities expected for a mixture of SiF_4 and N_2F_4 using literature data for SiF_4.[151] The presence of NO and NOF in the sample was confirmed by ions at $^m/_e$ 30 and $^m/_e$ 49. The presence of SiF_4 in the sample was probably caused by reaction of NOF with the 'Pyrex' glass storage ampule.

The aqueous solution from the reaction cell was tested for the presence of nitrite ions by the method of Shinn[152] as modified by Kershaw and Chamberlin.[153] However, it was found that sulphanilamide formed a yellow complex with ferric ions which turned red on the addition of N-(1-naphthyl)-ethylene diamine dihydrochloride, thus masking the red coloration expected from solutions of nitrite ions. This was overcome by complexing the ferric ions with the disodium salt of ethylene-diamine tetra-acetic acid before addition of the sulphanilamide.
A 1 cm^3 sample of the solution from the reaction cell was added to 5 cm^3 of saturated solution of the disodium salt of ethylene-diamine tetra-acetic acid. 5 cm^3 of a 1% solution of sulphanilamide (B.D.H. Ltd., Poole) in 1:4 HCl was added, followed by 5 cm^3 of a 0.02% aqueous solution of N-1-Naphthyl-ethylene diamine dihydrochloride (B.D.H. Ltd.,Poole). As a blank solution, 1 cm^3 of the previously prepared standard solution, corresponding to the complete oxidation of ferrous to ferric ions, was treated in exactly the same way as the 1 cm^3 sample of the solution from the reaction cell. The blank remained yellow after addition of all the reagents, but the reaction-solution sample turned bright red indicating the presence of nitrite ions.

(e) Discussion

Figure 18 shows a plot of the ferric ion concentration at any given time versus 2.5 times the fluoride ion concentration at the same time. The solid line is of unit gradient, and the agreement of the plotted points with this line indicates that 5 moles of fluoride ions were liberated during the oxidation of 2 moles of ferrous ions to the ferric state. This supports the equation that was proposed for the reaction ($5(NH_4)_2\,SO_4Fe^{II}SO_4+4H^++\frac{1}{2}N_2F_4 \longrightarrow 5\,NH_4Fe^{III}(SO_4)_2+6NH_4^++2F^-$).

However, from Figure 15, it was apparent that the recorded rate of the reaction producing fluoride ions was not affected by the ferrous ion concentration. Even after 4,300 minutes of reaction, when the ferrous ions had been completely oxidised, the rate of increase of the fluoride ion concentration was unaffected. Further, the rate of oxidation of ferrous to ferric ions was not affected by the ferrous ion concentration, with a possible exception at very low ferrous ion concentrations when it appeared that there was a slight tailing of the almost linear increase of the ferric ion concentration just before the maximum concentration was reached. The non-linear increase in both the ferric and fluoride ion concentrations during the first 150 minutes (Figure 17) was attributed to the slow increase in the concentration of dissolved N_2F_4 with time, reaching a dynamic equilibrium concentration after about 140 minutes.

There are two possible interpretations of this apparent zero order dependence of the reaction on the ferrous ion concentration. The first is that the rate of the reaction was controlled by the rate of solution of

FIGURE 18: Graph of Ferric Ion Concentration versus 2·5(Fluoride Ion Concentration).

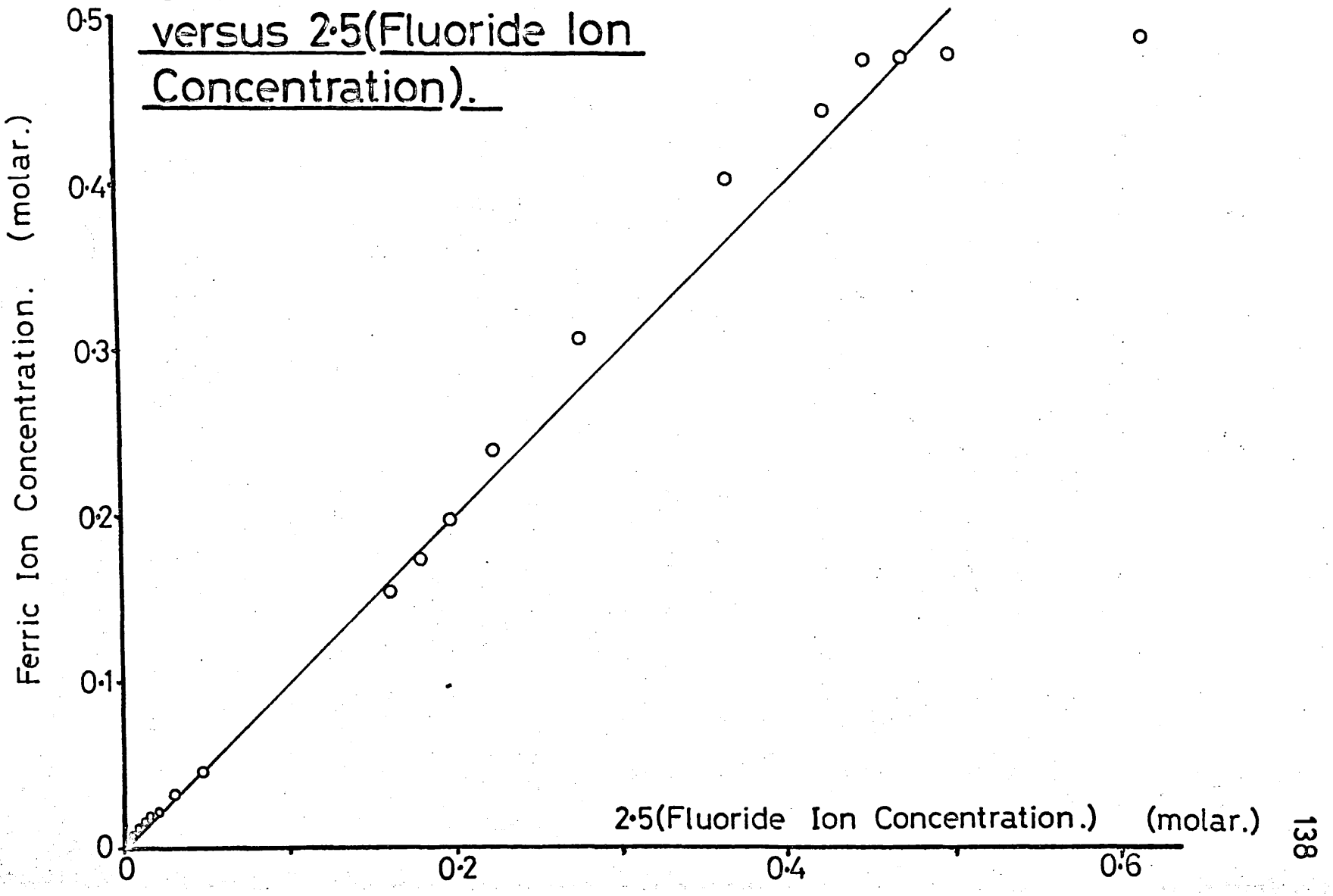

N_2F_4 into the aqueous medium, this rate being slow when compared with the rate of reaction of N_2F_4 with the aqueous medium. The other possibility is that the rate of reaction is, in fact, independent of ferrous ion concentration (zero order dependence on Fe^{2+} concentration).

Some insight into the factors controlling the rate of this reaction may be gained from the experimental data. The reaction may be considered as progressing in two stages; solution of N_2F_4 into the aqueous phase, followed by reaction of dissolved N_2F_4 to produce fluoride ions:-

$$N_2F_4(g) \underset{K_G}{\overset{K_S}{\rightleftharpoons}} N_2F_4(aq.) \xrightarrow{K_R} F^- + \text{other products.}$$

K_S, K_G and K_R, in the above representation, are the rates of solution, desorption and reaction of N_2F_4 respectively. If an equilibrium concentration of N_2F_4 is maintained during reaction in the aqueous phase, then $K_S = K_G + K_R$.

K_S, the rate of solution of N_2F_4 is independent of the aqueous N_2F_4 concentration ($[N_2F_4(aq.)]$), but K_G, the rate of desorption of N_2F_4 is directly proportional to $[N_2F_4(aq.)]$. Both of these rates are independent of the volume of the aqueous phase, provided that the effective surface area of contact between the gas and aqueous phases remains constant with changes in volume. This is a good approximation to the present case, where the withdrawal of 1 cm^3 samples lowers the aqueous meniscus, but does not appreciably effect the surface area of this meniscus. K_R, the rate of reaction of N_2F_4 to produce fluoride ions, however, is dependent on

both $[N_2F_{4(aq.)}]$ and the volume of the aqueous phase (V).

$\therefore$ K_S = constant, with varying $[N_2F_{4(aq.)}]$ and V.

and $K_G = k_g[N_2F_{4(aq.)}]$ and is independent of V.

and $K_R = k_r[N_2F_{4(aq.)}]$ V. (assuming 1st order dependence of rate on $[N_2F_{4(aq.)}]$).

When an equilibrium concentration of N_2F_4 in the aqueous phase has been set up, then:

$K_S = K_G + K_R = (k_g + k_rV)[N_2F_{4(aq.)}]$.

or $[N_2F_{4(aq.)}] = K_S/(k_g + k_rV)$

If $K_S \gg k_r[N_2F_{4(aq.)}]V$, then the equilibrium $[N_2F_{4(aq.)}]$ maintained in solution is approximately equal to the equilibrium concentration expected if no reaction was occurring in the aqueous phase. Thus:-

$$K_S \simeq K_G = k_g[N_2F_{4(aq.)}]$$

and $K_S \gg k_rV[N_2F_{4(aq.)}]$ and therefore $k_g \gg k_rV$. Thus the equilibrium $[N_2F_{4(aq.)}] = K_S/(k_g + k_rV)$ is virtually independent of the volume of the aqueous phase (V). Further, the rate of reaction of N_2F_4 is $(k_r[N_2F_{4(aq.)}]V)$ and is almost directly proportional to the volume V, but the rate of increase in fluoride ion concentration $(4\ k_r[N_2F_{4(aq.)}])$ is virtually independent of the volume.

If, however, $K_S \ll k_r[N_2F_{4(aq.)}]V$, then the equilibrium $[N_2F_{4(aq.)}] = K_S/(k_g + k_rV)$ is much less than the equilibrium $[N_2F_{4(aq.)}]$ expected if no

reaction was occurring, and $K_G \ll K_S$ and also $K_G \ll K_R$. Thus $k_g \ll k_r V$, and the equilibrium $[N_2F_{4(aq.)}] = K_S/(k_g + k_rV)$ is very nearly inversely proportional to the volume, V. Thus, for this case corresponding to the rate of reaction being controlled by the rate of solution of N_2F_4, the rate of reaction of N_2F_4 is nearly independent of V, since this rate is $(k_r[N_2F_{4(aq.)}]V)$ and $[N_2F_{4(aq.)}] \simeq C/V$, where C is a constant. The rate of increase in the fluoride ion concentration is $4k_r[N_2F_{4(aq.)}]$, and is, therefore, virtually inversely proportional to the volume of the aqueous phase, V.

In the present experiment, the rate of increase in the fluoride ion concentration showed a marked dependence on the volume of the aqueous phase. Thus, after 200 minutes of reaction, the volume of the solution was 98 cm^3 and the rate of increase in the fluoride ion concentration was (Figure 17) 4.24×10^{-5} moles $litre^{-1} minute^{-1}$; after 1490 minutes, the volume was 90 cm^3 and the rate was 5.89×10^{-5} moles $litre^{-1} minute^{-1}$; and after 5040 minutes, the volume was 82 cm^3, and the rate was 6.39×10^{-5} moles $litre^{-1}$ $minute^{-1}$. If the reaction rate was strictly controlled by the rate of solution of N_2F_4, then the rate of increase in the fluoride ion concentration should be inversely proportional to the volume of the aqueous solution:

$d[F^-]/dt = C/V$ where C is a constant, equal to the rate of formation of fluoride ions in the aqueous phase. Thus the product of the rate of increase of the fluoride ion concentration and the volume should be constant. This product was 5.2×10^{-6} moles/minute after 5040 minutes;

5.3×10^{-6} moles/minute after 1490 minutes; and 4.3×10^{-6} moles/minute after 200 minutes. The excellent agreement between the values for 1490 and 5040 minutes of reaction, indicates that the rate of reaction of N_2F_4 with aqueous ferrous ions was controlled by the rate of solution of N_2F_4 into the aqueous phase ($K_S \ll K_R$). The product, $V(d[F^-]/dt)$, after 200 minutes of reaction is not in such good agreement, but this may indicate that the equilibrium $[N_2F_{4\ aq.}]$ had not been attained at this stage in the reaction.

Because the rate of the reaction was controlled by the rate of solution of N_2F_4, the information, that could be obtained from the results for the reaction, was limited, and in particular it was not possible to determine the effect of ferrous ions on the rate of reaction. Thus no further reactions were studied.

However, the results do show that the experimental rate of increase of the fluoride ion concentration was not affected even when the ferrous ions had been completely oxidised. The almost constant rate of increase of the fluoride ion concentration before exhaustion of ferrous ions has been explained as due to the rate of reaction being controlled by the rate of solution of N_2F_4. However, if ferrous ions are involved in increasing the rate of reaction, the continued constant rate of increase of the fluoride ion concentration after the oxidation of all the ferrous ions is surprising.

Two possible explanations can be given, the first of which is that the reaction of dissolved N_2F_4 with aqueous ferrous ions proceeds in two stages. The first stage is the reaction of N_2F_4 with the aqueous medium at a rate unaffected by ferrous ions. The reaction products expected from this hydrolysis are fluoride ions, NO[38] and NOF.[66] All these products were definitely formed in the later stages of the reaction observed, as shown by the increase in the fluoride ion concentration in the aqueous phase, and by the presence of NO and NOF(infrared and mass spectra) in the gas phase after termination of the reaction. Ferrous ions would then be oxidised in the second stage by NO or NOF, or by nitrite ions, presumably formed by the interaction of NO or NOF with the aqueous solution, which were identified in the reaction solution at the end of the reaction. Zero order dependence on ferrous ions, however, would be surprising in view of the effect of ferrous ions on the hydrolysis of NF_3.

An alternative explanation is that the rate of hydrolysis of N_2F_4 is catalysed by ferric ions to such an extent that this hydrolysis is much faster than the rate of solution of N_2F_4. This would explain the continued and almost constant rate of increase of the fluoride ion concentration, since both the rate of oxidation of ferrous ions and the rate of hydrolysis of N_2F_4 would be controlled by the rate of solution. In view of the catalysis of the hydrolysis of NF_3 by ferric ions observed by Hurst and Khayat,[38] this explanation does not appear implausible.

The rate of the observed reaction of N_2F_4 with aqueous ferrous ions at about pH 0.4 was about 0.9 millimoles N_2F_4/litre/hour, and this is far faster than the rate of hydrolysis of N_2F_4 by pure water of about 0.03 millimoles N_2F_4/litre/hour. However, Hurst and Khayat[38] observed that hydrogen ion concentration had a marked effect on the rate of hydrolysis of N_2F_4, and from their data for 1M H_2SO_4, the rate of hydrolysis at pH 0 was estimated to be about 0.5 millimoles N_2F_4/litre/hour, for a partial pressure of N_2F_4 gas of about 0.7 atmosphere. Direct comparison of these two rates, however, cannot be justified since the rate of reaction of N_2F_4 with aqueous ferrous ions at pH 0.4 was controlled by the rate of solution of N_2F_4. It is, therefore, possible that such a comparison would merely compare the rates of solution in the two experiments. However, this marked increase in the rate of hydrolysis of N_2F_4 with increased hydrogen ion concentration might well account for the fast rate of the observed reaction with aqueous ferrous ions at pH 0.4, without the need to postulate acceleration of the reaction by ferrous ions.

In summary, the results for the reaction of N_2F_4 with aqueous ferrous ions at pH 0.4 confirmed the postulated equation for the reaction: $10(NH_4)_2SO_4Fe^{II}SO_4+2H^++N_2F_4 \rightarrow 10NH_4Fe^{III}(SO_4)_2+12NH_4+4F^-$ and the rate of this reaction was found to be controlled by the rate of solution of N_2F_4 into the aqueous phase. The continued steady increase in the fluoride ion concentration, after complete oxidation of the ferrous ions, strongly suggested that the presence of ferrous ions did not affect the rate of reaction. This would indicate that ferrous ions were oxidised by

an hydrolysis product and not by direct reaction with dissolved N_2F_4. However, it has not been possible to reject an alternative explanation in which this continued steady increase in the fluoride ion concentration would result from a rate of hydrolysis of N_2F_4, possibly catalysed by ferric ions, that was also controlled by the rate of solution of N_2F_4.

PART 2. PHOSPHORUS-FLUORINE COMPOUNDS.

INTRODUCTION

The trivalent halides of phosphorus and their trivalent derivatives can, in many cases, be considered as model compounds in the study of the equivalent nitrogen compounds (Part 1: Introduction). However, the chemistry of phosphorus compounds is of interest in its own right, and much insight into phosphorus-halide and phosphorus-phosphorus bonding has been gained recently.

Phosphorus trifluoride has received much attention since it was first prepared in 1884,[154] but the study of the phosphorus (trivalent)-fluorine bond has recently been expanded by the preparation of difluoroiodophosphine.[155,156,157] This compound has proved a valuable intermediate in the preparation of compounds containing $-PF_2$ groups, including difluorophosphine,[158] μ-oxo-bisdifluorophosphine ($F_2P-O-PF_2$),[159] cyanodifluorophosphine[159] and tetrafluorodiphosphine.[159,160]

Although both silicon and sulphur, situated respectively to the left and right of phosphorus in the Periodic Table, form numerous chain and cyclic compounds, interest in phosphorus-phosphorus bonding has only developed fairly recently.[161,162,163,164,165,166] Tetraiododiphosphine (diphosphorus tetraiodide, P_2I_4) was first prepared in 1813[167,168] by Gay-Lussac, but other, more convenient, preparative methods have since been found.[169,170,171] Chemical methods of preparation of tetrachlorodiphosphine have met with little success, but milligram quantities have been

prepared by physical means[172,173] and improved physical preparations have been found.[174] Thus with the preparation of tetrafluorodiphosphine, only tetrabromodiphosphine has yet to be prepared to complete the halogen series (neglecting At). Despite several attempts at its preparation, tetrabromodiphosphine has never been isolated, although its presence has been postulated[175] in neutron irradiated phosphorus tribromide.

The preparation of difluoroiodophosphine completed the series of difluorohalophosphines (excepting At), the chloro-[176] and bromo-[177] difluorophosphines being well known.

The properties of PF_3 have been studied extensively. Raman spectra of PF_3 in the liquid and gaseous phases were recorded by Yost and Anderson in 1934[178], and the infrared spectrum has been studied.[179,180,181,182] The geometry of PF_3 has received much attention as it is considered of basic importance in the study of the stereochemistry of inorganic molecules.[183,184,185,186,187] Early studies[188,189] indicated a large $\hat{FPF}$ of 104° with a P-F bond length of 1.52Å, indicating that the geometry of PF_3 was anomalous in the series of phosphorus trihalides[183] ($\hat{ClPCl}$ = 100°, $\hat{BrPBr}$ = 101.5° and $\hat{IPI}$ = 102°). However, this structure was not consistent with the rotational constant, B_o, obtained from studies of its microwave spectrum.[190,191] These microwave investigations were not able to characterise completely the geometry, since both phosphorus and fluorine have only single stable isotopes, and the assumption of various $\hat{FPF}$ led to differing P-F bond lengths.[191,192,193,194] Mirri[194] estimated the $\hat{FPF}$ from the Coriolis coupling constant and the force

constants and obtained an upper limit for this angle of 98°, in agreement with a later electron diffraction study,[195] which gave the $\hat{FPF}$ to be 98.2 ± 0.6°. The P-F bond length obtained from this study,[195] however, was not consistent with the microwave data. A recent electron diffraction study of PF_3[196] has confirmed the $\hat{FPF}$ as 97.8 ± 0.2°, and the P-F bond length, 1.57Å (± 0.0012Å) was in agreement with the microwave rotational constant, B_o.

In this work, this geometry[196] has been used to update the statistical thermodynamic functions for PF_3. The gas-phase infrared spectrum was also studied as a result of disagreement in the literature[178,180,181] over the fundamental frequencies.

In a previous report[156] of the gas-phase infrared spectrum of PF_2I above 200 cm^{-1}, assignments were made for four of the six expected fundamental frequencies. Although estimates of the remaining two vibrational frequencies have been made in order to compute the statistical thermodynamic functions,[197] force constants[198] and mean amplitudes of vibration,[199] no further study of the spectrum has been recorded in the literature. In this work, the liquid- and solid-state Raman and gas-phase infrared spectra over the range 20-1200 cm^{-1}, and the solid-phase infrared spectrum over the range 375-1200 cm^{-1}, were recorded. Assignments have been made for all six fundamental frequencies, and these frequencies have been used to compute statistical thermodynamic functions.

Two studies of the gas-phase infrared spectrum of P_2F_4[159,160] have been reported, together with one report of the Raman spectrum of liquid

P_2F_4 at -20°C.[159] The relative simplicity of the spectra, and the small number of bands, suggested that P_2F_4 is of higher symmetry than the possible cis (C_{2v}), gauche (C_2) or semi-eclipsed (C_2) configurations. Barring an unusual number of degeneracies, nine (C_{2v}) or twelve (C_2) infrared active and twelve Raman active fundamentals should be observed for these lower symmetry configurations. Parry et al.[159] also found that the mutual exclusion rule, indicative of a centre of symmetry, was probably operative, but were unable to show this conclusively since the Raman and infrared spectra were recorded for P_2F_4 in different physical states. The polarization properties of the Raman bands supported the interpretation of the spectra in terms of a trans (C_{2h}), rather than the far less probable planar (D_{2h}), configuration.

The geometries around both P-P (trivalent) and N-N bonding have been the subject of much research. The spectra of P_2H_4 have been interpreted in terms of a gauche configuration,[200,201] while P_2Cl_4[202] and P_2I_4[203,204] both appear to have trans symmetries. Vibrational spectra of $P_2(CH_3)_4$ indicate a gauche-trans rotameric mixture in the liquid phase, but only the trans form in the solid.[205] The situation has been complicated in many cases, where two or more different physical properties have been measured, indicating two or more different configurations. X-ray and neutron diffraction studies have shown that N_2H_4 is probably eclipsed (cis, C_{2v}),[206,207] but microwave, electron diffraction and vibrational

spectra indicate a gauche structure.[208,209,210,211] Microwave and electron diffraction studies on N_2F_4 have been interpreted in terms of a gauche structure,[212,213] but vibrational and nuclear magnetic resonance spectra indicate a trans-gauche equilibrium.[214,215]

In the absence of gas electron diffraction or microwave data for the P_2F_4 molecule, the inference of a trans configuration from vibrational spectroscopy[159] has influenced the interpretation of nuclear magnetic resonance studies. Thus the ^{19}F and ^{31}P spectra[159,160] have been interpreted[216,217] in terms of an assumed trans structure (XX'AA'X''X''' spin system). A study of the temperature dependence of the spectra[217] showed that, although the directly-bonded P-P coupling, other one-bond couplings, and the geminal F-F coupling were insensitive to temperature changes, the vicinal F-F coupling showed relatively large changes over the temperature range -101°C to -1°C. This suggested that more than one rotamer might have been contributing to the spectrum. The sign of the directly-bonded P-P coupling constant was found to be negative,[217] opposite in sign to that predicted by published theoretical studies.[218,219]

The inference of a trans configuration for P_2F_4 from vibrational spectra[159] is contrary to the results of semi-empirical self-consistent field and extended Hückel molecular orbital calculations for P_2H_4 and P_2F_4.[219] This study predicted that the stability of the various rotamers should decrease in the order gauche > cis > trans. This, however, was in contrast both with the ab initio theoretical order[220,221,222] and with the order predicted from simple electrostatic considerations[103,223,224] which

predict the order trans > gauche > cis. This difference was related[219] to a combination of σ- and π-bonding factors.

The molecule $H_2P\text{-}PF_2$ has recently been prepared[225,226] and the structure was determined, from its microwave spectrum and dipole moment data, to be trans.[227]

One of the most interesting and characteristic properties of N_2F_4 is its reversible dissociation at the N-N bond to give stable NF_2 radicals. This equilibrium has received much attention.[11] The possibility that P_2F_4 might exhibit a similar reversible dissociation prompted an electron spin resonance study.[159] A single resonance line was observed for liquefied P_2F_4, while more complex spectra were obtained for gaseous P_2F_4 and CCl_4 solutions, both of which appeared to give the same spectrum. Although these signals were weak, they were interpreted as indicating the presence of PF_2 radicals. PF_2 radicals have also been postulated as reaction intermediates.[228] A study of the thermal decomposition of P_2F_4 with temperature by mass spectrometry[229] revealed decreasing $P_2F_4^+$ intensity and increasing PF_2^+ intensity with increasing temperature. At 350°C, the intensity of the PF_2^+ ion was reduced to zero by reduction of the exciting potential to 13 eV, but increased temperature increased the PF_2^+ intensity, indicating the formation of PF_2 radicals by dissociation of P_2F_4 above 350°C.

A further study[230] has produced the electron spin resonance spectrum of PF_2 radicals isolated in rare gas matrices at 20.4°K. The radicals were formed by either ultra-violet irradiation or by thermal decomposition

of P_2F_4 and PF_2H, the same spectrum being recorded in all cases, but with the addition of the H radical spectrum from PF_2H. The intense twelve-line spectra were analysed to show that the PF_2 radical was stationary (not free-rotating) in the matrix, as found for NF_2 radicals in rare-gas matrices.[231] However, significant dissociation of P_2F_4 into PF_2 radicals was not observed at room temperature, and the gaseous mixture of inert gas and P_2F_4 had to be heated to 200°C before deposition in order to observe the spectrum.

Thus, P_2F_4 only dissociates to give PF_2 radicals at temperatures well in excess of those at which NF_2 radicals may be observed from N_2F_4. This indicates that the P-P bond is considerably stronger than the N-N bond ($D(N-N) \sim 20$ kcal.mol^{-1} [11]). Also, further interest in diphosphine derivatives has arisen from the essentially constant length of the P-P bond (~ 2.21Å)[232] in many compounds, even though the dissociation energies of these bonds vary with constituents. The bond dissociation energies, that have been measured, vary from 86 kcal.mol^{-1} for $P_2(C_2H_5)_4$[233] to 58 kcal.mol^{-1} for P_2Cl_4,[234] with 74 kcal.mol^{-1} for P_2H_4[235] and 65 kcal.mol^{-1} for P_2I_4.[236]

An estimate of the P-P bond dissociation energy for P_2F_4 is, therefore, of value towards the understanding both of P-P bonding and also of PF_2 radical formation. In this work this has been achieved by mass spectrometric measurements on P_2F_4 and some other P-F compounds (Part 2: Section 2).

Burg et al.[237,238] have attributed the intense ultraviolet absorption

of some diphosphines to the π-acceptor bonding power of the P 3d orbitals, and thus to the P-P bond. Further work[226,239] has demonstrated that this absorption is probably general for compounds containing the P-P bond and should, therefore, prove to be of value in structure elucidation of these compounds. However, these absorption properties are not exclusively characteristic of P-P bonding, as shown by the similar ultra-violet spectrum of the monophosphine, PTH_2.[240]

Burg *et al*[238] qualitatively attributed the changes in the wavelength of maximum absorption ($\lambda_{max.}$) for three diphosphines to the changes in the electronegativities of the substituent groups. Huheey[239] showed that there was a reasonable relationship between $\lambda_{max.}$ and the electro-negativity of the substituents, provided that a consistent set of electronegativities was used. The linear relationship between Taft's σ^* parameter[241] and electronegativity, as measured by the effect of the constituent group on the infrared frequency of an adjacent carbonyl group,[242] allowed the electronegativities to be assigned from σ^* values.

In this work, the ultra-violet spectrum of P_2F_4 has been recorded, and the decrease in intensity with time of the absorption has been followed.

SECTION 1

Vibrational and Ultraviolet Spectra and Related Properties

a. Vibrational Spectra and Thermodynamic Functions of PF_2I

For an assumed C_s symmetry for PF_2I, six fundamental vibrations ($4a' + 2a''$) are expected, both species being active both in the infrared and Raman. The gas-phase infrared spectrum, observed in this work, is shown in Figure 19, with the bands listed in Table 11. For the region above 250 cm^{-1}, the frequencies are in good agreement with those of Rudolph *et al.*[156] Two fundamental modes (a' and a'') are expected below this, but only one region of absorption, centred at about 203 cm^{-1}, could be detected in the infrared spectrum.

The liquid-phase Raman spectrum (Table 11) was considerably complicated by fast decomposition of PF_2I to give PF_3 and PI_3.[156] Strong bands at 330 cm^{-1}, 306 cm^{-1}, and 113 cm^{-1} were attributed to PI_3,[203,243] this assignment being further enforced by comparison with the solid-phase Raman spectrum of PI_3, recorded in this work using the same spectrometer, which showed bands at 315 cm^{-1}(m), 284 cm^{-1}(s), 108 cm^{-1}(s), and 81 cm^{-1}(s) (where s, strong; m, medium). No previous reference was found in the literature for the Raman spectrum of solid PI_3, but these frequencies are in good agreement with the previously determined solid-phase infrared[203] and solution Raman[243] spectra. No bands attributable to PF_3 were found in the liquid-phase Raman spectrum of PF_2I. Polarisation data for the PF_2I bands could not be obtained due to the fast decomposition of PF_2I in the laser beam.

TABLE 11

INFRARED AND RAMAN SPECTRA OF DIFLUOROIODOPHOSPHINE

Infrared (cm^{-1})		Raman (cm^{-1})	
(Gas)	(Solid)	(Solid)	(Liquid)[a]
851 (s)	821.5 (s)	862 (m)	873 (w)
846 (s)	806 (vs)	807 (m)	
418 (m)			
413 (m)	397.5 (w)	398 (m)	408 (m)
408 (m)			
381 (m)			
375 (m)		378 (s)	372 (m)
369 (m)			
208 (w)			
		207 (vs)	
202.5 (w)			204.5 (m)
		201 (m)	
197.5 (w)			
		83 (w)	
		66 (w)	
		56 (w)	

[a] After removal of PI_3 bands.[203]

s, strong; m, medium; w, weak; v, very.

FIGURE 19: Gas-phase Infrared Spectrum of PF_2I.

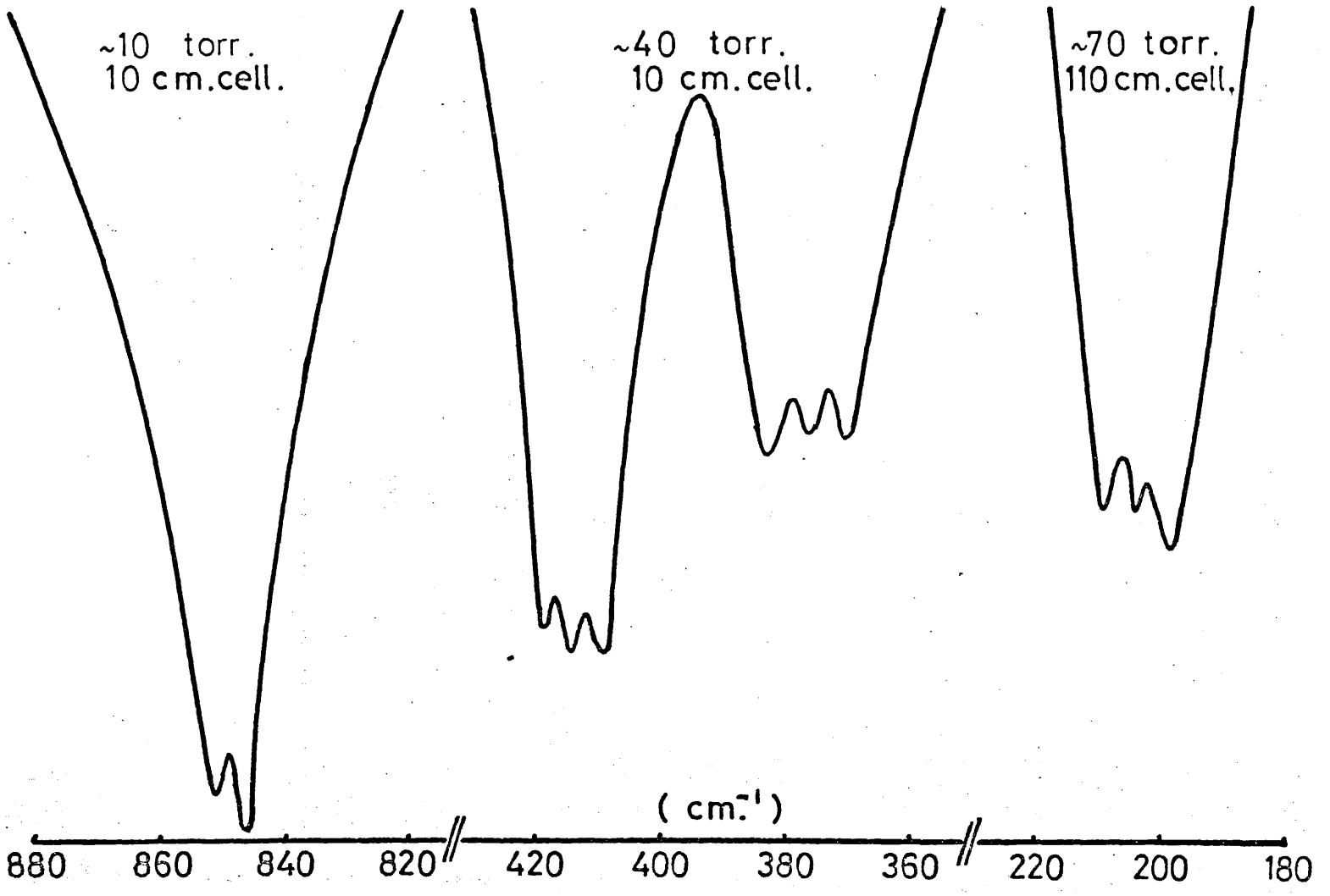

The Raman spectrum of PF_2I in the solid-phase (Figure 20; Table 11) showed no sign of any decomposition of the PF_2I, and showed only one region of Raman emission below 250 cm^{-1} attributable to fundamental vibrations of the PF_2I molecule. This appeared as a strong asymmetric band centred at 207 cm^{-1}. A strong, sharp band at 114 cm^{-1} and a broad, weak band at 229 cm^{-1} (overtone of 114 cm^{-1}?) appeared in one spectrum, but were not observed in a later spectrum obtained using a different sample. Since all other bands in the two spectra were in agreement, these two bands (114 cm^{-1} and 229 cm^{-1}) must be assigned to an impurity in the PF_2I sample used for the first spectrum, or to a lattice band, that failed to appear in the second spectrum due to different deposition conditions. Under higher resolution, the strong asymmetric band, centred at 207 cm^{-1} in the solid-state Raman spectrum, was split to show clearly two bands at 207 cm^{-1} and 201 cm^{-1} (Figure 20).

Normal coordinate calculations were employed in order to calculate an approximate set of vibrational frequencies and normal coordinates. The object of these calculations was not to attempt to evaluate a force-field, but rather to employ a "reasonable" set of constants transferred from the parent PF_3 and PI_3 [244] molecules in order to assist in the assignment of the observed frequencies. Hence no great effort was made to force a fit between experimental and observed frequencies, although several small adjustments were made from the preliminary choice in order to produce a reasonable match. In the absence of published structural data for PF_2I, an assumed molecular geometry was used. This geometry was

FIGURE 20.

Solid-phase Raman Spectrum of PF_2I.

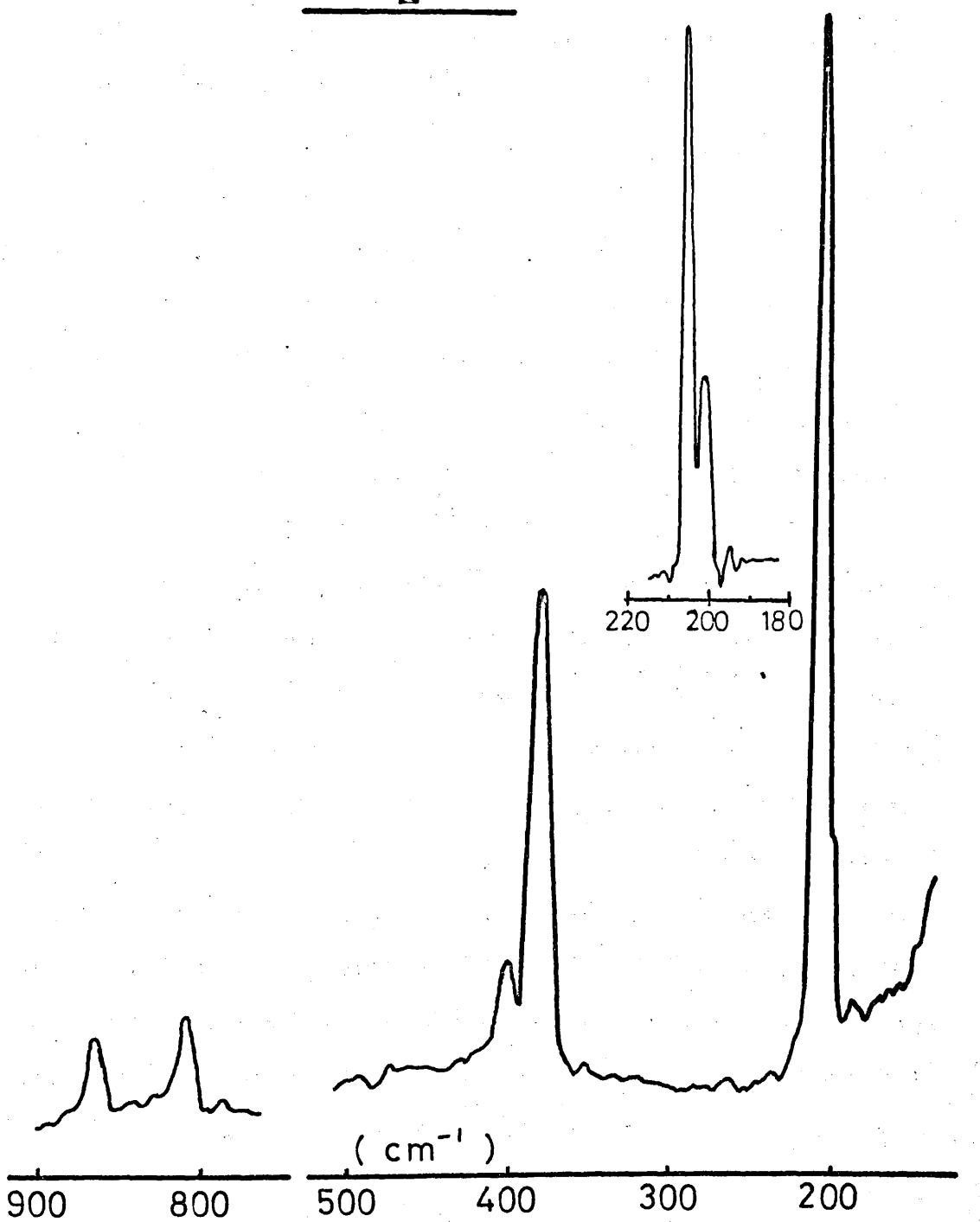

also used for the calculation of the thermodynamic functions of PF_2I and is discussed later in this section. The force constants finally adopted are listed in Table 12. These values are similar to those used by Müller et al,[198] with the exception of the P-I stretching force constant (f_{P-I}). For this a value of 130 Nm^{-1} was used in the present calculations compared to 250 Nm^{-1} employed by Müller et al.

The B matrix elements were computed directly from a set of cartesian coordinates for the molecule. Subsequently solution for the eigenvalues and eigenvectors of $(M^{-\frac{1}{2}}B)F(M^{-\frac{1}{2}})$ was obtained (where F is the force constant matrix for the internal coordinates and $M^{-\frac{1}{2}}$ is the diagonal matrix with the non-zero entries equal to the square roots of the reciprocals of the atomic masses). The set of frequencies calculated using the above force field is shown in Table 13, together with the approximate potential energy distribution among the internal coordinates for each mode. Observed gas-phase frequencies are also shown for comparison.

On the basis of these approximate normal coordinate calculations, the two lowest frequency fundamentals were predicted to lie at about 181 cm^{-1}(a') and at 209 cm^{-1}(a"). In the absence of infrared absorption or Raman shifts below 200 cm^{-1}, it seemed likely that these fundamental must be located in the region of 200 cm^{-1}. The infrared absorption was complex (Figure 19) and could easily have consisted of two overlapping bands. That this was the case was supported by the splitting of the strong, asymmetric band centred at 207 cm^{-1} in the

TABLE 12

FORCE CONSTANTS FOR PF_2I UTILISED IN NORMAL COORDINATE CALCULATIONS

Stretching[a]		Bending[a]	
PI	130	FPI	49
PF	490	FPF	65
PI/PF	10	FPI/FPI	3
PF/PF	30	FPI/FPF	3

[a] Units of Nm^{-1}.

TABLE 13

OBSERVED AND CALCULATED GAS-PHASE INFRARED FREQUENCIES (cm^{-1})

Observed	Calculated	Species	Potential Energy Distribution
851	859	a'	93% PF str.
846	833	a"	99% PF str.
413	401	a'	9?% FPF def.
375	382	a'	46% PI str.,53% FPI def.
204	209	a"	99% FPI def.
198	181	a'	55% PI str., 43% FPI def.

solid-state Raman spectrum. The more intense Raman band (?07 cm^{-1}) has accordingly been assigned to the symmetric (a') mode, and the weaker band (?01 cm^{-1}) to the a" mode.

The strong infrared bands, centred at 413 cm^{-1} and 375 cm^{-1}, both had the same overall shape and were assigned by Rudolph *et al*[156] as FPF symmetric deformation and PI stretching modes respectively. The solid-state Raman spectrum had bands at 395 cm^{-1}(w) and 377 cm^{-1}(s), and the liquid-phase Raman had bands at 408 cm^{-1}(m) and 372 cm^{-1}(m), which were identified with these modes. The normal coordinate calculations yielded a' bands at 401 cm^{-1} and 38? cm^{-1} in agreement with this assignment, the 38? cm^{-1} mode being considerably mixed in character, and the large contribution from the P-I stretch in this mode may qualitatively account for the greater intensity relative to the higher frequency mode.

The bands at 851 cm^{-1} and 846 cm^{-1} were strong in the infrared and weak in the Raman and are certainly the P-F stretching modes in agreement with previous assignments for these modes for both PF_2I[156] and other P-F molecules.[197] The higher frequency band at 862 cm^{-1} in the solid-state Raman spectrum was the more intense of the two, suggesting that it was the symmetric (a') mode, in agreement with the assignment of Rudolph *et al*.[156] This assignment was supported by the calculationswhich also indicated that these modes were almost pure P-F stretches (Table 13).

While the Raman bands at 862 cm^{-1} for the solid-phase and at 873 cm^{-1} for the liquid-phase presumably correlated with one of these infrared bands, the solid-phase Raman band at 807 cm^{-1} (no equivalent Raman band observed for PF?I in the liquid-phase) was approximately 40 cm^{-1}

removed from the nearest infrared band at 846 cm^{-1} and correlation between these infrared and Raman bands thus appeared tenuous, even though the PF_2I was in different physical states. However both PF_2Cl and PF_2Br[197] show fairly large shifts of about 24 cm^{-1} in the assigned P-F asymmetric stretch between the gas-phase infrared and liquid-phase Raman bands, indicating the possibility of such a large shift as apparently observed for PF_2I. The infrared spectrum of PF_2I in the solid-phase, was, therefore, recorded (Table 11) in an attempt to confirm this correlation. This showed a strong band split to give maxima at 821.5 cm^{-1} and 806 cm^{-1}, with a shoulder on the high frequency side at about 835 cm^{-1}, and thus confirmed the correlation between the infrared and Raman spectra. A band at 397.5 cm^{-1}, observed in the infrared spectrum of PF_2I in the solid phase also correlates very well with the band at 398 cm^{-1} in the solid-state Raman spectrum of PF_2I. No other bands were observed in the range 375 cm^{-1} to 1000 cm^{-1}.

The bands at 83 cm^{-1}, 66 cm^{-1}, and 56 cm^{-1} observed in the solid-phase Raman spectrum were presumed to be associated with lattice vibrations.

In the absence of published structural data for PF_2I, it was necessary to make certain assumptions about the molecular geometry in order to carry out both the normal coordinate analysis and the computation of the statistical thermodynamic functions. The structural parameters for PF_2I were estimated by comparison with PF_3,[196] PI_3[245a] and P_2I_4,[245b] taking P-I = 2.47Å and $\hat{IPI}$ = 100.0°. The values used in the calculations were obtained by using the P-F bond length = 1.570Å and $\hat{FPF}$ = 97.8° from PF_3

and the P-I bond length above. $\hat{IPF}$ (99°) was taken as the mean of $\hat{FPF}$ in PF_3 and $\hat{IPI}$ in PI_3. The estimated limits of error in these bond lengths were ±0.05Å and in the angles ± 2°.

Using the ideal gas, harmonic oscillator approximation and the above geometrical assumptions together with the observed gas-phase infrared fundamental frequencies (Table 13), the rotational and vibrational contributions, and thus the total statistical thermodynamic functions for PF_2I were calculated. These are presented in Table 14. By varying the bond lengths and bond angles within the experimental limits given above, and by varying the vibrational frequencies within the estimated experimental limits (± 2 cm^{-1}) and repeating the calculations with the adjusted data, the maximum percentage errors over the temperature range considered were found to be ± 0.3% for C_p°, ± 0.2% for $(H_T^\circ - H_o^\circ)/T$, ± 0.4% for $-(G_T^\circ - H_o^\circ)/T$ and ± 0.4% for S°.

These results may be compared with those of Müller *et al*[197] which were computed using estimated values (190 cm^{-1} and 170 cm^{-1}) for the two lowest frequency fundamentals, and on the basis of P-F = 1.55Å. The maximum percentage deviations of their results from the present work, caused mainly by differences in the fundamental frequencies employed, are ± 0.815% in C_p°, ± 1.622% in $(H_T^\circ - H_o^\circ)/T$, ± 0.452% in $-(G_T^\circ - H_o^\circ)/T$ and ± 0.524% in S°.

TABLE 14

COMPUTED THERMODYNAMIC FUNCTIONS FOR DIFLUOROIODOPHOSPHINE - PERFECT GAS AT 101.325 kNm^{-2} (1 Atm)

PRODUCT OF THE 3 PRINCIPAL MOMENTS OF INERTIA = $3.884805 \times 10^{-113} g.^3 cm.^6$

	$cal.mole^{-1}deg^{-1}$	$cal.mole^{-1}deg.^{-1}$	$cal.mole^{-1}deg.^{-1}$	$cal.mole^{-1}deg.^{-1}$
$T^\circ K$	C_p°	$(H_T^\circ - H_0^\circ)/T$	$-(G_T^\circ - H_0^\circ)/T$	S°
100.00	10.468	8.704	52.779	61.483
179.60[a]	13.212	10.138	58.258	68.396
200.00	13.748	10.480	59.367	69.846
273.15	15.311	11.576	62.800	74.376
298.15	15.739	11.907	63.828	75.735
299.85[b]	15.766	11.929	63.896	75.825
300.00	15.769	11.931	63.902	75.833
400.00	17.052	13.063	67.496	80.559
500.00	17.861	13.948	70.510	84.458
600.00	18.334	14.647	73.117	87.764
700.00	18.734	15.207	75.419	90.626
800.00	18.977	15.664	77.480	93.144
900.00	19.151	16.042	79.348	95.390
1000.00	19.280	16.360	81.055	97.415

[a] M.pt.[156] [b] B.pt. [156]

(1 cal = 4.1868 J)

b. Infrared Spectrum and Thermodynamic Functions of PF_3

Some confusion has been caused in the literature following the almost simultaneous publication of two papers concerning the infrared spectrum of PF_3. Gutowsky and Liehr[181] listed the gas-phase fundamental frequencies as 892 cm^{-1}, 848 cm^{-1}, 532 cm^{-1} and 487 cm^{-1}, in good agreement with the gas- and liquid-phase Raman spectra previously reported.[178] Wilson and Polo,[180] however, listed the gas-phase fundamental frequencies as 892 cm^{-1}, 860 cm^{-1}, 487 cm^{-1} and 344 cm^{-1}, having assigned eight other bands (not including any absorption in the region near 532 cm^{-1}) as overtone and combination bands. No further publications could be found in the literature resolving the difference between those two sets of fundamental frequencies, even though a recent paper[182] has reported the high resolution spectra of the 892 cm^{-1} and 487 cm^{-1} bands.

In this work, high pressure (about 30 torr) spectra of PF_3 in the gas-phase failed to locate any absorption at or around 532 cm^{-1}, and the frequencies for the three fundamental vibrations above 400 cm^{-1}, as given by Wilson and Polo,[180] were confirmed. Therefore, the statistical thermodynamic functions for PF_3 have been calculated in this work using the fundamental frequencies recorded by Wilson and Polo and using the ideal gas, harmonic oscillator approximation. The geometry used was that recently reported by Morino et al[196] (P-F = 1.57 ($\pm$ 0.0012)Å and $\hat{FPF}$ = 97.8 ($\pm$ 0.2)°). The probable errors in these functions were not estimated by repeating the calculations using adjusted data (as for PF_2I) as it is certain that the error caused by inaccuracies in the geometry and

TABLE 15

COMPUTED THERMODYNAMIC FUNCTIONS FOR PHOSPHORUS TRIFLUORIDE - PERFECT GAS AT 101.325 kNm^{-2} (1 Atm).

PRODUCT OF THE 3 PRINCIPAL MOMENTS OF INERTIA = $2.069909 \times 10^{-114} g.^3 cm.^6$

	$cal.mole^{-1}deg.^{-1}$	$cal.mole^{-1}deg.^{-1}$	$cal.mole^{-1}deg.^{-1}$	$cal.mole^{-1}deg.^{-1}$
$T^\circ K$	C_p°	$(H_T^\circ - H_o^\circ)/T$	$-(G_T^\circ - H_o^\circ)/T$	S°
100.00	8.741	8.102	45.085	53.187
121.65[a]	9.344	8.268	46.688	54.956
171.65[b]	10.817	8.797	49.616	58.413
200.00	11.620	9.140	50.986	60.126
273.15	13.479	10.061	53.971	64.032
298.15	14.027	10.371	54.866	65.237
300.00	14.066	10.394	54.930	65.324
400.00	15.791	11.542	58.081	69.623
500.00	16.928	12.513	60.764	73.278
600.00	17.678	13.316	63.119	76.435
700.00	18.187	13.978	65.223	79.201
800.00	18.543	14.527	67.127	81.654
900.00	18.799	14.988	68.865	83.853
1000.00	18.990	15.380	70.465	85.844

[a] M.pt.[117] [b] B.pt.[117]

(1 cal = 4.1868J).

fundamental frequencies is small when compared with the error inherent in the ideal gas, harmonic oscillator approximation. The results are presented in Table 15.

These results were compared with those given by Nagarajan[126] over the temperature range 100°K to 1000°K. This showed some marked differences, and the maximum percentage deviations of the results given by Nagarajan from those recorded in this work were ± 6.9% in C_p°, ± 6.9% in $(H_T^\circ - H_o^\circ)/T$, ± 2.6% in $-(G_T^\circ - H_o^\circ)/T$ and ± 2.6% in S°. These were well outside the probable errors in the functions given in this work. Nagarajan had used the fundamental frequencies as given by Gutowsky and Liehr[131] and the geometry given by Sheridan et al[246] (P-F = 1.535Å and $\hat{FPF}$ = 100°).

However, the results given in Table 15 differ only insignificantly (± 0.1%) from those given by Müller et al.[197] Although Müller et al used the same fundamental frequencies as used in this work, this good agreement is somewhat surprising since they used a substantially different geometry (P-F = 1.55Å, $\hat{FPF}$ = 104°).

c. The Decomposition of PF_2I

Rudolph et al[156] have shown that PF_2I disproportionates according to the equation:

$$3PF_2I(g) \longrightarrow 2PF_3(g) + PI_3(c)$$

Using available thermodynamic data, the standard free energy change for this decomposition reaction has been calculated taking the bond energies

in $PF_2I_{(g)}$ as equal to the mean bond dissociation energies in $PF_{3(g)}$ and $PI_{3(g)}$.

$$\bar{D}(P\text{-}I_{(PI_3)}) = 1/3\ (\Delta H^\circ_f(P_{(g)}) + 3\Delta H^\circ_f(I_{(g)}) - \Delta H^\circ_f(PI_{3(g)})$$

$$\bar{D}\ (P\text{-}F_{(PF_3)}) = 1/3(\Delta H^\circ_f(P_{(g)}) + 3\Delta H^\circ_f(F_{(g)}) - \Delta H^\circ_f(PF_{3(g)})$$

Using the above assumption for the bond energies in $PF_2I_{(g)}$:

$$\Delta H^\circ_f(PF_2I_{(g)}) = \Delta H^\circ_f(P_{(g)}) + 2\Delta H^\circ_f(F_{(g)}) + \Delta\ H^\circ_f(I_{(g)}) - \bar{D}(P\text{-}I) - 2\bar{D}(P\text{-}F)$$

$$\therefore \Delta H^\circ_f(PF_2I_{(g)}) = 2/3\Delta H^\circ_f(PF_{3(g)}) + 1/3\Delta H^\circ_f(PI_{3(g)}).\quad \underline{\text{Eqn. 1}}$$

It is necessary to estimate $S^\circ(PI_{3(c)})$:

The vapour pressure of PI_3 [236] at 298.15°K = 0.003891 mm Hg. and

$$S^\circ_{p=0.003891\ mm}(PI_{3(g)}) = S^\circ_{p=760\ mm}(PI_{3(g)}) + R\ln\left(\frac{760}{0.003891}\right)$$

where R is the gas constant (Perfect Gas Assumption).

For the equilibrium: $PI_{3(c)} \xrightleftharpoons{298.15^\circ K} PI_{3(g)}$ ($p = 0.003891$ mm Hg)

$\Delta G^\circ = 0$ and $\Delta S^\circ = \Delta H_{subl.}/T$ where $\Delta H_{subl.}$ is the enthalpy of sublimation of PI_3 at 298.15°K.

$$\therefore S^\circ(PI_{3(c)}) = S^\circ_{p=0.003891\ mm}(PI_{3(g)}) - \Delta H_{subl.}/T$$

$$= S^\circ_{p=760\ mm}(PI_{3(g)}) - \Delta H_{subl.}/T + R\ln\left(\frac{760}{0.003891}\right)$$

The entropy of $PI_{3(g)}$ at 298.15°K [247] ($S^\circ(PI_{3(g)}) = 89.45$ cal.mole^{-1}deg.$^{-1}$

$$\therefore\ S^\circ(PI_{3(c)}) = 113.66 - \Delta H_{subl.}/T$$

For the disproportionation of PF_2I (as written above)

$$\Delta S_{disprop.} = 2\,S^{\circ}(PF_{3(g)}) + S^{\circ}(PI_{3(c)}) - 3\,S^{\circ}(PF_2I_{(g)})$$

Using the values of $S^{\circ}(PF_{3(g)})$ and $S^{\circ}(PF_2I_{(g)})$ from Tables 14 and 15.

$$\Delta S_{disprop.} = 2(65.237) + 113.66 - \Delta H_{subl.}/T - 3(75.735)$$

$$= (16.93 - \Delta H_{subl.}/T) \text{ cal. mole}^{-1}\text{deg.}^{-1}$$

Also: $\Delta H_{disprop.} = 2\Delta H_f^{\circ}(PF_{3(g)}) + \Delta H_f^{\circ}(PI_{3(c)}) - 3\Delta H_f^{\circ}(PF_2I_{(g)})$

but $\Delta H_f^{\circ}(PI_{3(c)}) = \Delta H_f^{\circ}(PI_{3(g)}) - \Delta H_{subl.}$

and using Equation 1:

$$\Delta H_{disprop.} = -\Delta H_{subl.}$$

$$\therefore \Delta G_{disprop.} = \Delta H_{disprop.} - T\Delta S_{disprop.}$$

$$= -\Delta H_{subl.} - T(16.93 - \Delta H_{subl.}/T) \text{ cal.}$$

$$\therefore \Delta G_{disprop.} = -5.0 \text{ kcal.}$$

Thus for the reaction: $3PF_2I_{(g)} \longrightarrow 2PF_{3(g)} + PI_{3(c)}$. $\underline{\Delta G = -5.0 \text{ kcal.}}$

The enthalpy of formation of $PF_2I_{(g)}$ can be estimated using the above assumption for the bond energies and literature values:

$\Delta H_f^{\circ}(PF_{3(g)})^{248} = -226.03 \text{ kcal.mole}^{-1}$

$\Delta H_f^{\circ}(PI_{3(g)})^{236} = 1.3 \text{ kcal.mole}^{-1}$

giving: $\underline{\Delta H_f^{\circ}(PF_2I_{(g)}) = -150.2 \text{ kcalmole}^{-1}}$

Also using: $S^{\circ}(P_{(c)})^{247} = 9.89$ cal.mole^{-1}deg.$^{-1}$

$S^{\circ}(F_{2(g)})^{247} = 48.44$ cal.mole^{-1}deg.$^{-1}$

and $S^{\circ}(I_{2(c)}) = 27.757$ cal.mole^{-1}deg.$^{-1}$

$\Delta S_f^{\circ}(PF_2I_{(g)}) = 3.5965$ cal.deg.$^{-1}$mole^{-1}

and $\Delta G_f^{\circ}(PF_2I_{(g)}) = -151.3$ kcal.mole^{-1}

However, the decomposition of PF_2I may also be considered in terms of an equilibrium between PF_2I, and PF_3 and PI_3 in the gas phase

$$3PF_2I_{(g)} \underset{}{\overset{K}{\rightleftharpoons}} 2PF_{3(g)} + PI_{3(g)}$$

Using the assumption for the bond energies for PF_2I and the literature thermodynamic values given above.

ΔH (left to right of equilibrium as written above) = 0

and ΔS (left to right of equilibrium as written above) = -7.28 cal.mole^{-1}deg.$^{-1}$

$\therefore$ $\Delta G = 2.2$ kcal.

and K, the equilibrium constant is given by:

$\Delta G = -RT\ln K$ giving $K = 0.006$

$$= \frac{(pp PF_3)^2 (pp PI_3)}{(pp\ PF_2I)}$$

(pp = partial pressure)

Thus for unit pressure of pure PF_2I originally, the PF_2I equilibrates to give partial pressures of PI_3 of x units, and of PF_3 of 2x units, leaving a partial pressure of PF_2I of (1-3x) units.

$$\therefore \quad 0.026 = \frac{x\,(2x)^2}{(1-3x)} \qquad \text{for } 0.33 \geqslant x \geqslant 0$$

which solves to give $x = 0.15$

Thus for an original pressure of pure PF_2I of 1 atmosphere (760 mm Hg.), the partial pressure of PI_3 at equilibrium at 293.15°K would be 115 mm. However, this partial pressure of PI_3 cannot be reached since it is higher than the vapour pressure of PI_3 at 293.15°K. Thus the disproportionation of PF_2I may be considered as due to the equilibrium of PF_2I with PF_3 and PI_3, all in the gas phase, this equilibrium being displaced by condensation of PI_3.

d. Vibrational and Nuclear Magnetic Resonance Spectra of P_2F_4.

Parry *et al*[159] have recorded the gas-phase infrared and the liquid-phase Raman spectra of P_2F_4. On the basis of the small number of bands observed and of apparent non-coincidence of bands in the two spectra, they interpreted their results in terms of a trans conformation (C_{2h} point group) for the P_2F_4 molecule, tentatively assigning four infrared-active bands and six Raman-active bands as fundamentals.

For this proposed[159] trans conformation, twelve fundamental vibrations would be expected, six being active in the infrared ($3a_u + 3b_u$) and six in the Raman ($4a_g + 2b_g$). On this basis, only two infrared active fundamentals remained unobserved by Parry *et al*.

In the present work, the gas-phase and solid-phase infrared spectra over the range 300 cm^{-1} to 4000 cm^{-1}, and the solid-phase Raman spectrum

over the range 100 cm^{-1} to 1100 cm^{-1} have been recorded. The gas-phase infrared spectrum (10 cm cell, pressure ~10 torr) showed only one region of absorption, and this was originally resolved to give three maxima at 822 cm^{-1}, 835.5 cm^{-1} and 846.5 cm^{-1}. Under higher resolution, a fourth maximum was observed at 827 cm^{-1}. This region of absorption is shown in Figure 21, and the frequencies are compared with those of Parry et al[159] and of Colburn et al[160] in Table 16.

The agreement of the two highest frequency maxima with those reported by Parry et al is reasonable, especially as the maximum at 835.5 cm^{-1} was broad. However the agreement of the two lowest frequency maxima is less good, there being a difference of about 6 cm^{-1} between the frequencies reported by Parry et al and those determined in this work. These two frequencies are, however, in better agreement ($\pm$ 3 cm^{-1}) with those reported by Colburn et al.

Although no other absorptions were observed between 300 cm^{-1} and 4000 cm^{-1} in the above spectrum, on increasing the pressure in the gas cell to about 80 torr, a very weak region of absorption, centred at about 400 cm^{-1}, was observed. The shape of this absorption was similar to that observed for PF_2I (Figure 19), two maxima being resolved at about 410 cm^{-1} and 390 cm^{-1}. Parry et al[159] also observed a very weak absorption in this region of the spectrum and were able to resolve maxima at 417.8 cm^{-1}, 412.2 cm^{-1}, 406.8 cm^{-1} and 378.7 cm^{-1}, tentatively assigning this region of absorption to a PF_2I impurity. The weak absorption, observed in this work, at about 400 cm^{-1} was therefore similarly assigned.

TABLE 16

VIBRATIONAL SPECTRA OF P_2F_4.

GAS			LIQUID	SOLID	
Infrared[a]			Raman[a]	Raman[a]	Infrared[a]
Ref. 159.	Ref. 160.	This Work	Ref. 159.	This Work	This Work
846.9 (vvs)	842 (s)	846.5 (vs)			
839 (vvs)		835.5 (vs)			
833.9 (vvs)	830 (vs)	827 (vs)			
827.8 (vvs)	820 (s)	822 (vs)			
			825 (m,p?)	812 (s)	815 (m,sh)
			803 (w, dp?)	797 (m)	797 (s)
			541 (vs, p)	546 (vs)	
			453 (w, dp?)		
[417.3 (vw)]					
[412.2 (vw)]	408 (vw)	[410 (vw)]			
[406.8 (vw)]					
			403 (vw, p)		
[373.7 (vw)]		[380 (vw)]			
			377 (s,p)	385 (vs)	
365 (m)					
361 (m)	356 (w)				
				274 (m)	
			214 (m,p)	217 (vs)	

a; Units of cm^{-1}

s, strong; m, medium; w, weak; v, very; sh, shoulder; p, polarised; dp, depolarised.

(Frequencies given in square brackets have been assigned to PF_2I impurity).

FIGURE 21: Gas-phase Infrared Spectrum of P_2F_4.

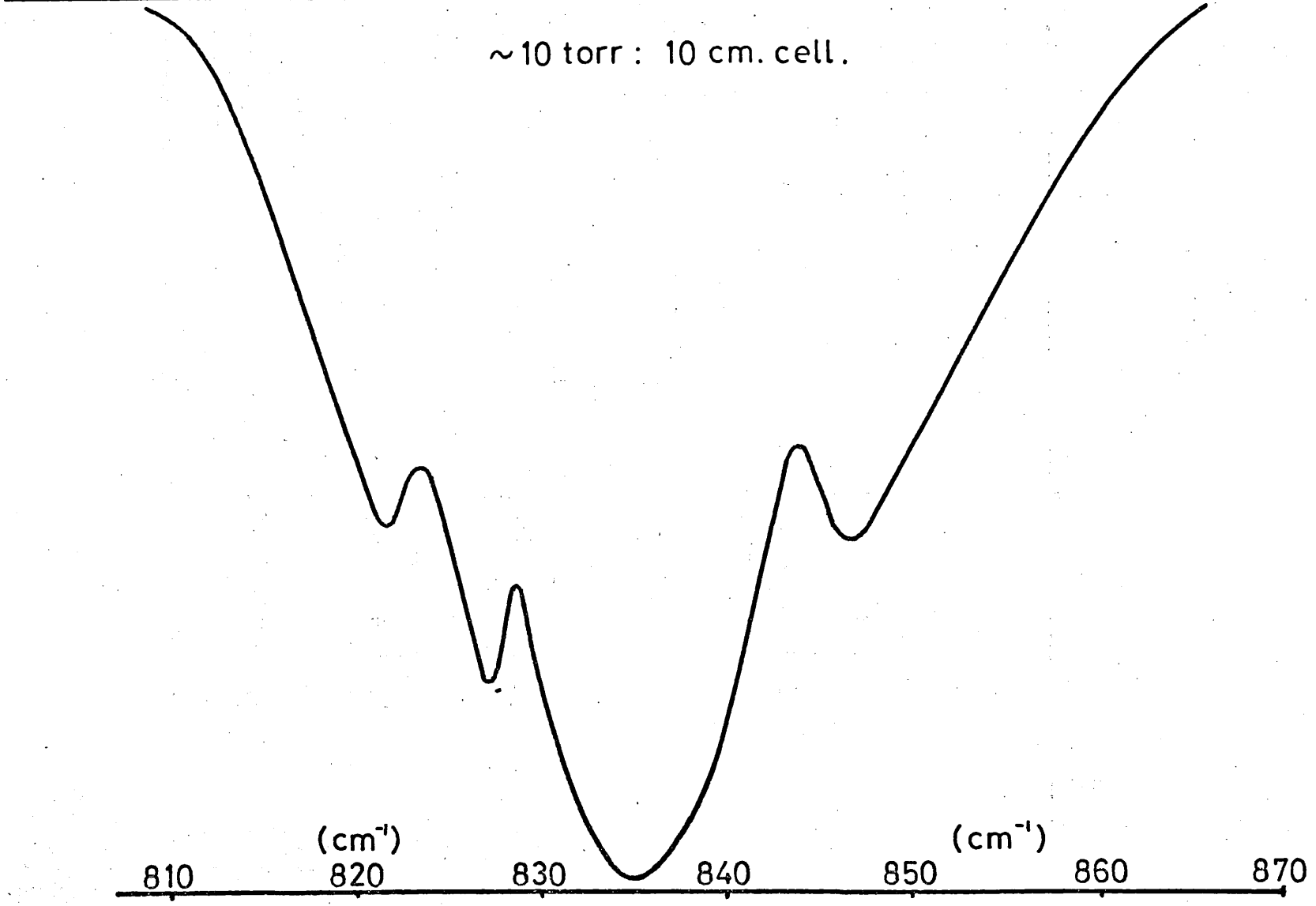

With this higher pressure (~80 torr) of P_2F_4 in the cell, three other very weak maxima were recorded, which had not been previously observed, at about 935 cm^{-1}, 970 cm^{-1} and 1025 cm^{-1}. These, however, increased in intensity with time, indicating slow decomposition of P_2F_4. A small shoulder at about 892 cm^{-1} also appeared on the side of the absorption due to P_2F_4 (well off scale), and this was attributed to the Q branch of the P-Q-R band structure for PF_3 centred on 892 cm^{-1}. The maxima at 935 cm^{-1} and 1025 cm^{-1} were not assigned.

An attempt was also made to record the gas-phase infrared spectrum of P_2F_4 over the range 30 cm^{-1} to 400 cm^{-1} using a far-infrared interferometric spectrometer equipped with a 110 cm gas cell (vide infra). However, while attempting to record the spectrum with a pressure of P_2F_4 in this cell of only 20 torr, the gas decomposed so extensively that the inside of the cell was coated with an orange-yellow deposit and no absorptions were recorded. The mid-infrared spectrum (400 cm^{-1} to 4000 cm^{-1}) was recorded for a gaseous sample removed from the interferometer cell on completion of the run. Absorptions centred at 487 cm^{-1} (P-Q-R triplet; medium intensity), about 860 cm^{-1} (very strong and broad), 892 cm^{-1} (very strong and very sharp), about 905 cm^{-1} (medium) and 672 cm^{-1} (very weak) were all assigned to PF_3 indicating extensive decomposition of P_2F_4 to PF_3 and phosphorus-fluorine polymer.[229] It was not possible to determine from this spectrum if the decomposition of P_2F_4 had gone to completion, since the very intense absorption by PF_3

centred at 860 cm^{-1} did not allow the resolution of possible absorption by P_2F_4 in this region of the spectrum. The only other absorptions observed were bands at 970 cm^{-1} and 1025 cm^{-1} (as observed in the gas-phase infrared spectrum of P_2F_4 with a pressure of about 80 torr) and these were presumed to be due to a decomposition product of P_2F_4 (possibly phosphorus-fluorine polymer). Using lower pressures ($\sim$ 10 torr) of P_2F_4 in the interferometer gas-cell, decomposition of the gas appeared to be less extensive, but no absorptions were observed.

The Raman spectrum of P_2F_4 in the solid-phase (Figure 22; Table 16) showed no sign of any decomposition of the P_2F_4, and a mid-infrared (400 cm^{-1} to 4000 cm^{-1}) spectrum (gas-phase) of the sample, after the solid-phase Raman spectrum had been recorded, showed only absorptions attributable to P_2F_4. The frequencies of five of the Raman emissions were in good agreement with those observed by Parry et al[159] for P_2F_4 in the liquid phase, and the small differences (up to 13 cm^{-1}) presumably reflect the different physical states of the P_2F_4 for the two spectra. A band at 403 cm^{-1} was tentatively assigned by Parry et al as an overtone of the fundamental at 214 cm^{-1}, but no equivalent band was found in the solid-phase Raman spectrum (this work). More seriously, Parry et al tentatively assigned a weak emission at 453 cm^{-1} in their liquid-phase Raman to a fundamental vibration (ω_{PF_2}, symmetric, in-phase). In this work, no corresponding emission from P_2F_4 in the solid-phase could be located, suggesting that the band observed by Parry et al might have been caused by an impurity in their sample. However an emission at 274 cm^{-1}

FIGURE 22 : Solid-phase Raman Spectrum of P_2F_4 .

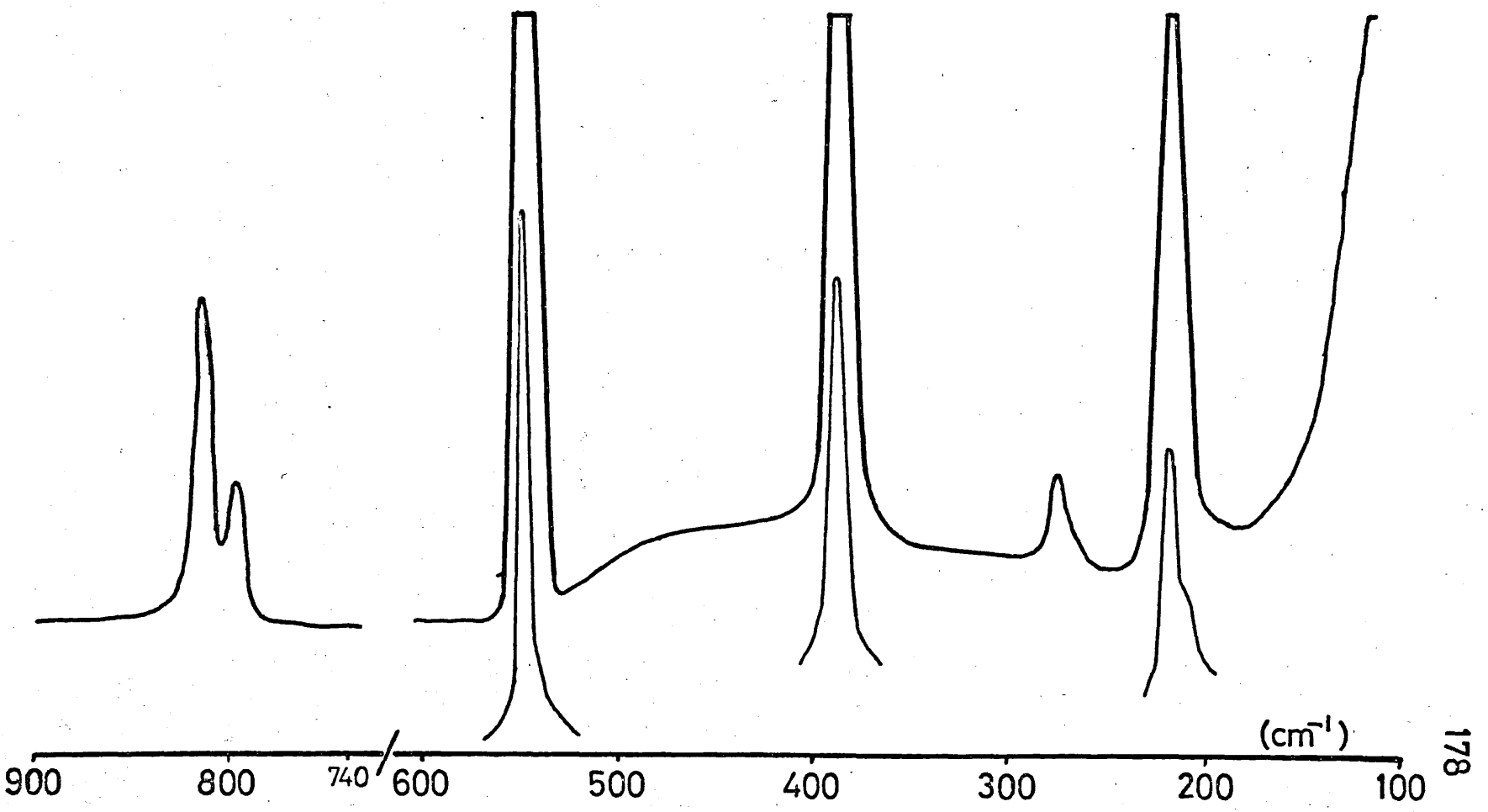

(medium) was observed for P_2F_4 in the solid-phase, and therefore this has been assigned as the sixth Raman-active fundamental frequency.

This change in the Raman-active fundamental frequencies, from those listed by Parry et al,[159] necessitated rearrangement of their tentative assignments. The two highest frequency Raman fundamentals must be the two P-F stretches in agreement with the assignment of Parry et al. The band associated with the P-P stretch is expected to be polarised and to be the most intense feature in the Raman spectrum.[226] The bands at 546 cm^{-1} and 385 cm^{-1} were both very strong and polarised,[159] but by analogy with P_2Cl_4,[202] $(CF_3)_2$ P-PF_2[226] and H_2P-PF_2,[226] the P-P stretching frequency is expected to be much higher than the latter band. Thus the band at 546 cm^{-1} has been assigned as the P-P stretching frequency in agreement with Parry et al. The rest of the Raman active bands have been tentatively assigned on this basis in Table 17.

The infrared spectrum of P_2F_4 in the solid phase was also recorded in this work over the range 380 cm^{-1} to 4000 cm^{-1}. Although the small number (6) of bands observed in the solid-phase Raman spectrum strongly indicates that P_2F_4 has a trans (C_{2h}) configuration, the other criterion used by Parry et al[159] to support the interpretation of their spectra on the basis of this configuration was the apparent operation of the mutual exclusion rule, indicative of a centre of symmetry. However, since their spectra were recorded with the sample in different physical states, they could not be completely certain that this latter criterion was satisfied. Indeed, the large shifts observed for PF_2X (X=I, Br or Cl) in the P-F

TABLE 17

TENTATIVE ASSIGNMENTS FOR THE FUNDAMENTAL VIBRATIONS OF P_2F_4.

Infrared (gas) (cm^{-1})	Raman (solid) (cm^{-1})	Assignment[b]
846.5)		ν_{PF}, asym., out-of-phase.
835.5)		
827)		ν_{PF}, sym., out-of-phase.
822)		
	812	ν_{PF}, sym., in-phase
	797	ν_{PF}, asym., in-phase
	546	ν_{PP}, sym.
	385	ω_{PF_2}, sym., in-phase.
365[a]		δ_{PF_2}, sym., out-of-phase.
361[a]		ρ_{PF_2}, asym.
	274	δ_{PF_2}, sym., in-phase.
	217	ρ_{PF_2}, sym.

[a] Reference 159.

[b] ν, stretch; ω, wag; δ, scissors; ρ, twist.

stretching frequencies with changes in phase (see Part 2; Section 1a) indicate that it is possible that the two highest frequency bands in the gas-phase infrared may correspond to those in the liquid-phase Raman.

The solid-phase infrared spectrum showed only one region of absorption in the range 380 cm^{-1} to 4000 cm^{-1}, and this appeared as a strong asymmetric band centred at 797 cm^{-1}. Under higher resolution, two shoulders were resolved on the high frequency side of this band at about 803 cm^{-1} and at about 815 cm^{-1}. The shoulder at 803 cm^{-1} was much weaker than that at 815 cm^{-1}, and it therefore seems probable that the two highest frequency gas-phase infrared bands correspond to bands at 797 cm^{-1} and at about 815 cm^{-1} in the solid-phase infrared spectrum.

The coincidence of these frequencies in the solid-phase infrared with those in the solid-phase Raman spectrum (Table 16) is probably fortuitous, but does illustrate the possibility that there may be coincidences in the infrared and Raman spectra due to the P_2F_4 molecule having a lower symmetry than the trans (C_{2h}) conformation. This, however, seems unlikely since for either a cis (C_{2v}) or gauche (C_2) symmetry, all twelve fundamental vibrations should be active in the Raman, and of these twelve Raman bands, nine (C_{2v}) or all twelve (C_2) should be coincident with bands in the infrared.

The nuclear magnetic resonance spectrum of liquid P_2F_4[159] has been interpreted[216,217] in terms of an assumed trans configuration ($XX'AA'X''X'''$ spin system). No attempt was reported[216,217] to try to interpret the data on the basis of either a gauche or semi-eclipsed configuration. The possible rotameric structures of P_2F_4 are shown in

FIGURE 23.

Possible Rotameric Structures of P_2F_4.

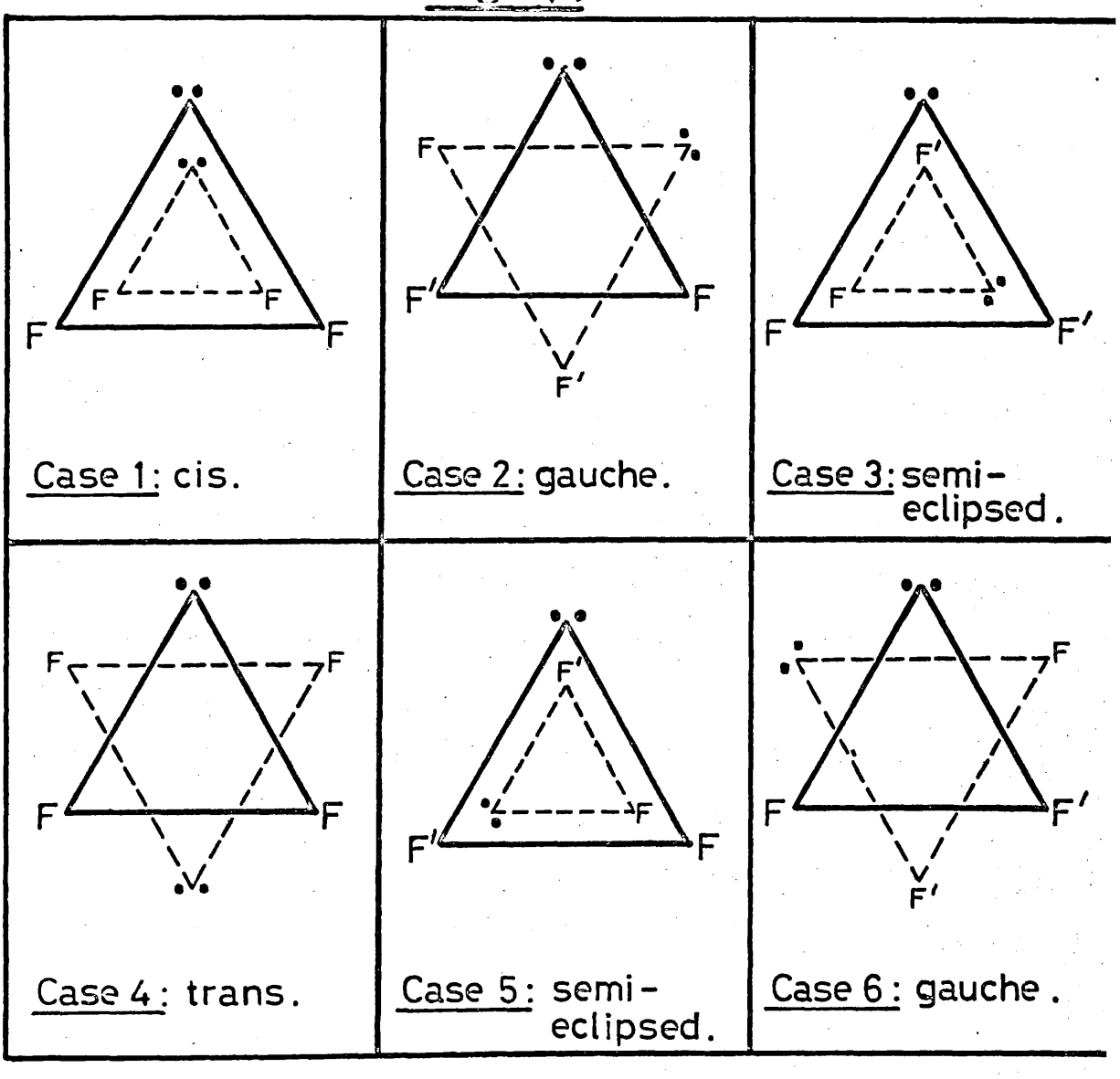

Case 7: Fast restricted rotation between semi-eclipsed rotamers (cases 3 and 5).

Case 8 : Fast restricted rotation between gauche rotamers (cases 2 and 6).

Figure 23, together with the two additional possibilities of fast restricted rotation between either the two gauche rotamers, as is probably the case for P_2H_4,[249] or the two semi-eclipsed rotamers. These possibilities can be broadly classified into two groups. The first is those cases where all four fluorine nuclei are chemically equivalent (cases 1, 4, 7 and 8) and the second is where there are two non-equivalent pairs of equivalent fluorine nuclei (cases 2, 3, 5 and 6). This second group corresponds to an XYAA'X'Y' spin system, whereas the first group corresponds to an XX'AA'X"X"' spin system.

In this work the UMA NMR BASIC Computer program (Science Research Council, Atlas Computer Laboratory, Chilton) was used to determine whether the experimental n.m.r. spectra[217] could be analysed on the basis of an XYAA'X'Y' spin system. The coupling constants given by Rudolph and Newmark[217] for liquid P_2F_4 at $-1^{\circ}C$ were used throughout. Figure 24 shows the calculated spectrum obtained using these values for an XX'AA'X"X"' spin system, and this is in good agreement with the experimental spectrum with an rms error of only 0.03 Hz.[217] Figure 25 shows the spectrum obtained using the same coupling constants and the same chemical shifts for all fluorine nuclei as for Figure 24, but for an XYAA'X'Y' spin system. This spectrum is not dissimilar from that observed experimentally (Figure 24). However, if the chemical shifts of the two non-equivalent pairs of equivalent fluorine nuclei are made different, then the spectrum immediately becomes far more complex. This is shown in Figure 26, where the same coupling constants, as above, have been used,

FIGURE 24 : N.M.R. Spectrum of P_2F_4 : Computed Spectrum for Trans Rotamer.

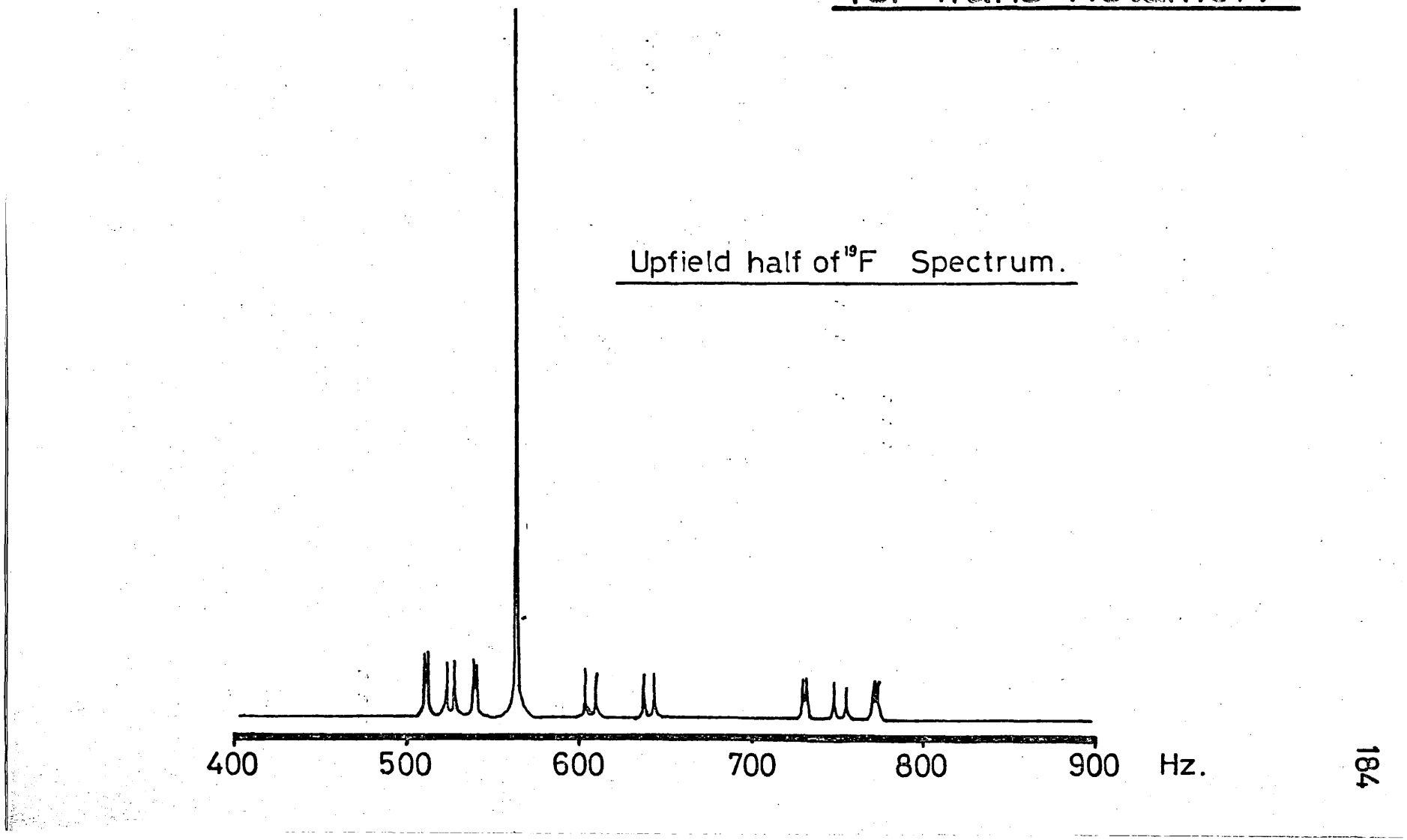

FIGURE 25: Computed N.M.R.Spectrum for XYAA'X'Y' Spin System;

All 4 F Chemical Shifts Equal.

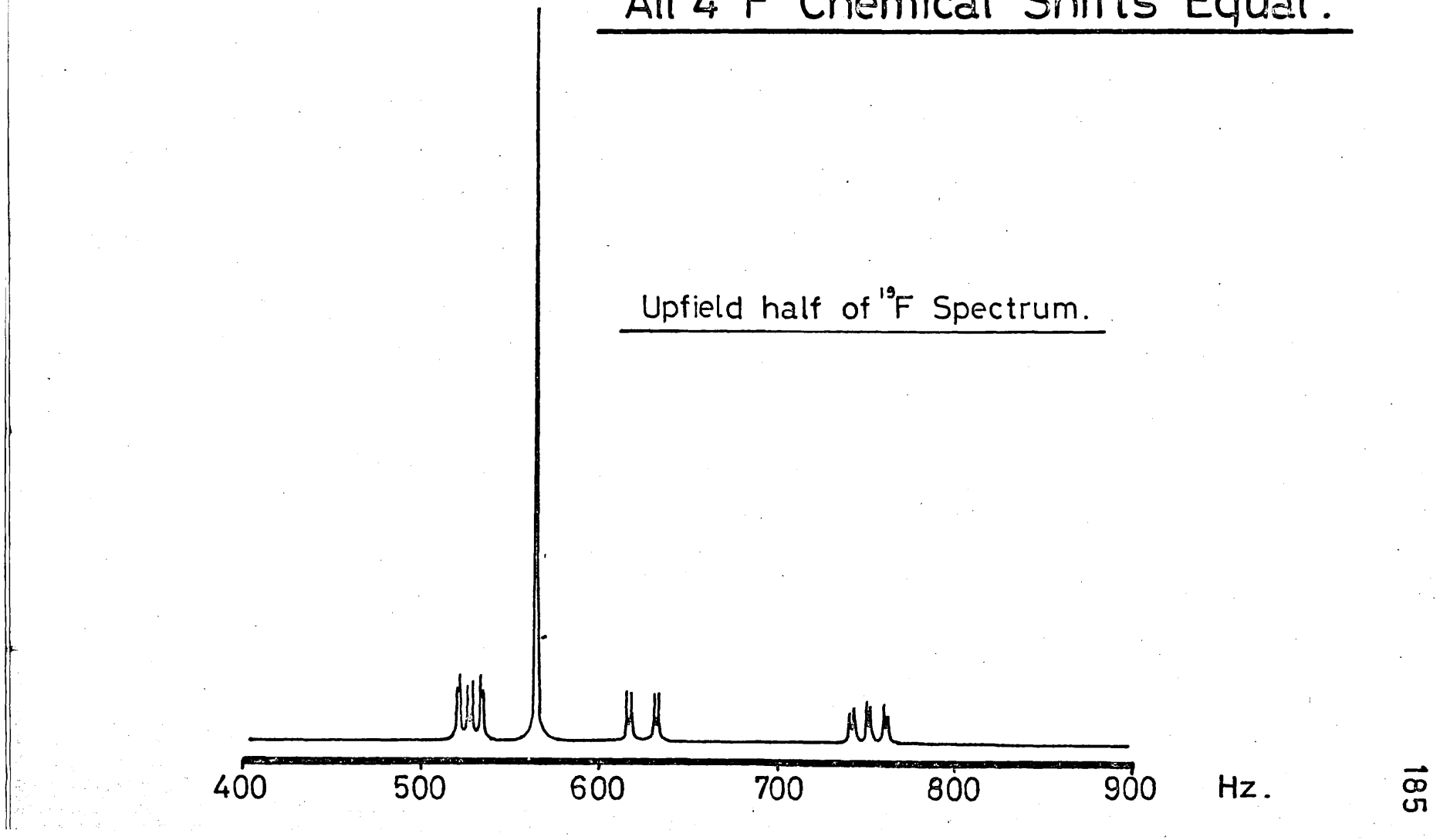

FIGURE 26: Computed N.M.R. Spectrum for XYAA'X'Y' Spin System;

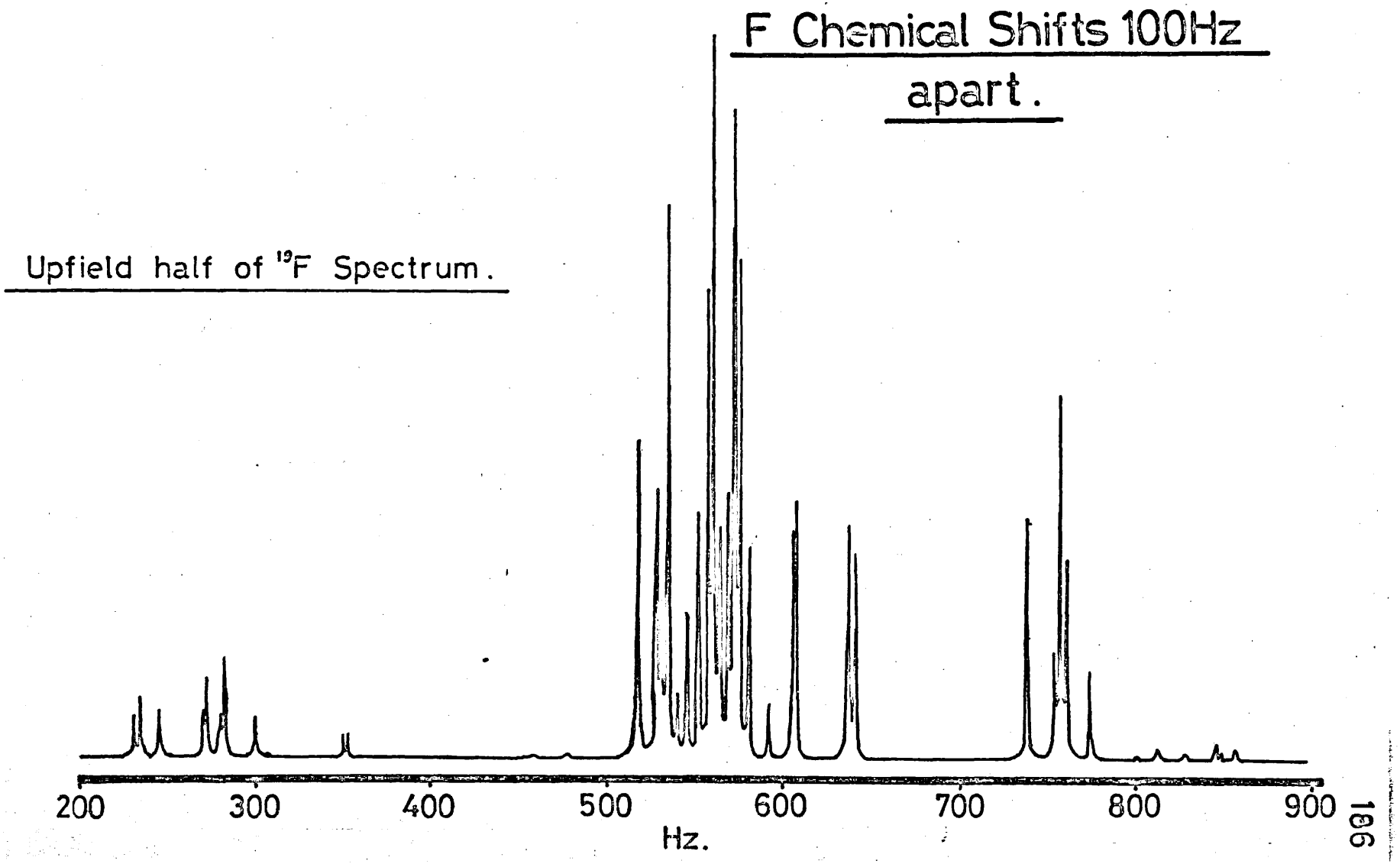

but the chemical shift of one pair of equivalent fluorine nuclei was set 100 Hz greater than that of the other non-equivalent pair. It was apparent from the complexity of the spectrum in Figure 26, that the experimental spectrum for P_2F_4 could not be interpreted on the basis of an XYAA'X'Y' spin system since an appreciable difference is expected between the chemical shifts for the non-equivalent pairs of equivalent fluorine nuclei. Thus the observed spectrum can only be interpreted on the basis of the first group of possible structures (Cases 1, 4, 7 and 8 in Figure 23) as an XX'AA'X"X"' spin system.

Theoretical studies[219] have indicated that the magnitude of the directly bonded P-P coupling constant should show a marked dependence on the rotameric form. However Rudolph and Newmark[217] have shown that the observed spectrum is relatively unaffected by temperature (from $-1^{\circ}C$ to $-101^{\circ}C$), strongly indicating that the observed spectrum is not due to fast rotation of the PF_2 groups about the P-P bond or to fast restricted rotation between either the two gauche (cases 2 and 6 in Figure 23) or the two semi-eclipsed (cases 3 and 5 in Figure 23) rotamers. This in turn strongly indicates that P_2F_4 exists, at these temperatures, in either a cis or a trans configuration. However, without data for similar molecules of known configuration for comparison with the data for P_2F_4, it is not possible, on the basis of the nuclear magnetic spectrum, to differentiate between these two rotamers.

Therefore, the evidence of the vibrational spectra, and in particular the small number of bands observed in the infrared and Raman spectra, must

be interpreted as strongly favouring a trans configuration for the P_2F_4 molecule. However, the possibility that the P_2F_4 molecule might have a different configuration (possibly cis) cannot be discarded, especially in view of the coincidence of the two highest frequency bands in the solid-phase infrared and Raman spectra, since this coincidence would have to be fortuitous for interpretation of these spectra in terms of a trans configuration.

e. The Ultraviolet spectrum and decomposition of P_2F_4

Previous studies of the ultraviolet spectra of diphosphine derivatives[236,237,238,239] have attributed the intense absorptions observed to the π-acceptor bonding power of the P3d orbitals, and thus to the P-P bond. In this work, the ultraviolet spectrum of P_2F_4 has been recorded over the range 2000Å to 7000Å (Model SP.200, Ultraviolet Spectrophotometer, Unicam, Cambridge) and a typical spectrum is shown in Figure 27 (10 cm silica cell; pressure of $P_2F_4 \sim 1$ torr). Three maxima were observed at 3000Å, 2605Å and 2050Å, of which the absorption at 2605Å was by far the most intense. This value of $\lambda_{max.}$ (2605Å) is in good agreement with the value obtained by Solan,[230] which has recently been reported in the literature.[226]

For three different samples of P_2F_4 (pressures ranging from about 4 torr to about 12 torr), ultraviolet spectra were recorded at frequent intervals following introduction of the sample to the silica cell.

FIGURE 27: Ultraviolet Spectrum of P_2F_4.

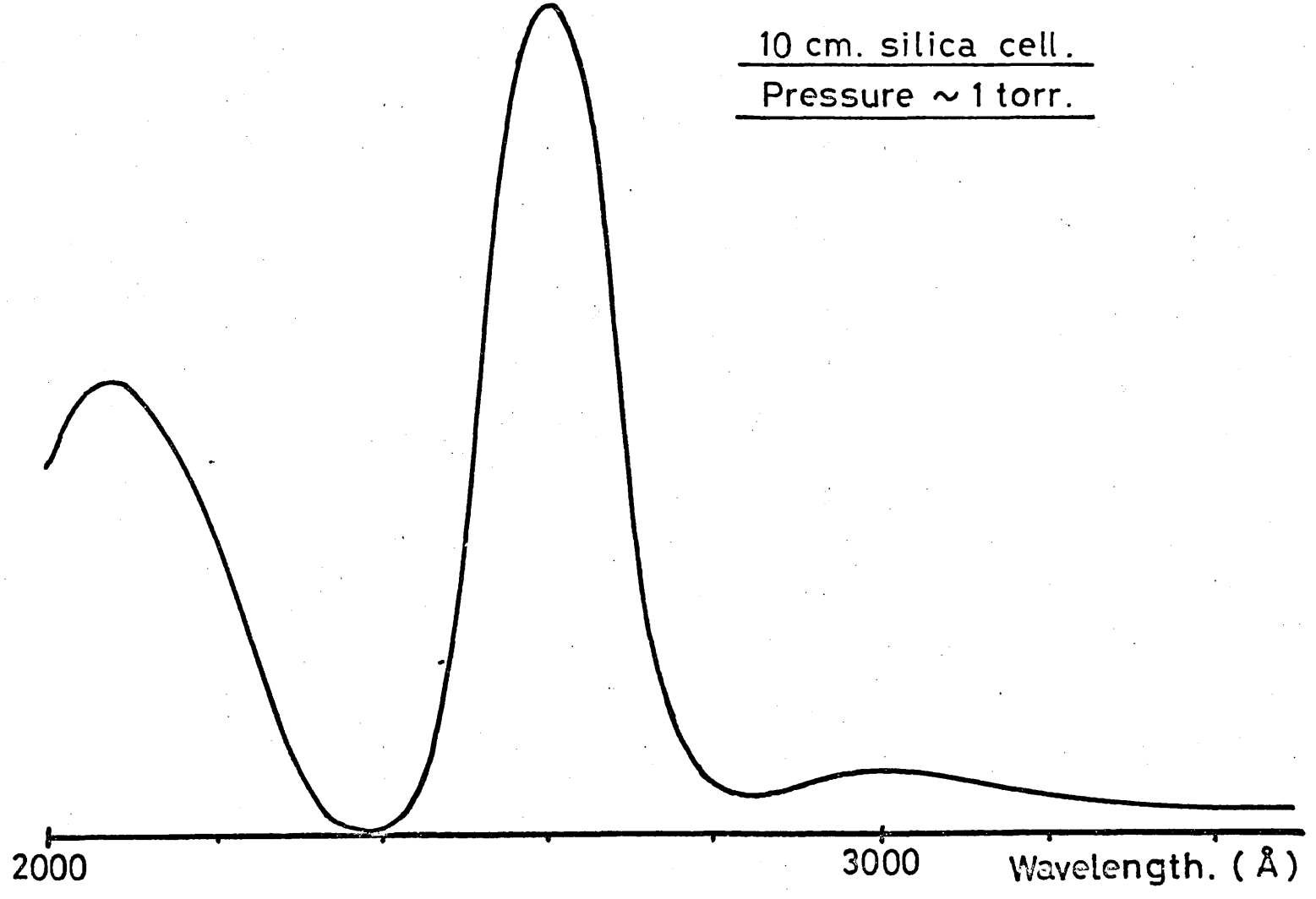

The spectra for all three samples showed a steady decrease with time in the intensities of the absorptions at 3000Å and at 2605Å, without change in the wavelengths of these absorptions. The absorption at 2050Å also showed a steady, but relatively much smaller, decrease in intensity with time, but this was accompanied by an increase in the wavelength of maximum absorption, eventually reaching a value of 2140Å. This decrease in the intensities of all three absorptions was attributed to decomposition of the P_2F_4 samples, and strongly indicated that all three maxima were due to absorptions by P_2F_4, and not by some impurity in the samples. However, the behaviour of the absorption originally centred on 2050Å indicated that some product, from the decomposition of P_2F_4, was absorbing in the ultraviolet at about 2140Å, thus lowering the apparent rate of decrease in the P_2F_4 absorption at 2050Å and also moving the position of maximum absorption to higher wavelength with time.

A previous study[229] of the decomposition of P_2F_4 had investigated the thermal dissociation of P_2F_4 at elevated temperatures (up to 900°C) and had shown that under these conditions P_2F_4 decomposes to give PF_3. The other products were phosphorus-fluorine polymers and some P_4F_6 was also detected. In the present work, it has been confirmed that PF_3 was a major product of the decomposition of P_2F_4 at room temperature. Two samples of P_2F_4 were allowed to decompose at room temperature, one of which was irradiated with ultraviolet light, and the gaseous products of the decomposition were analysed by recording their mass spectra. In both cases the spectra showed that PF_3 was the only major gaseous component of the

decomposition products. It therefore appeared that the orange-yellow solid, deposited during decomposition of the P_2F_4, was the only other product, and that this solid was not sufficiently volatile to be recorded in the mass spectra.

PF_3 does not absorb in the ultraviolet spectrum in the range 2000Å to 7000Å (this work: 10 cm silica cell; pressure of PF_3 of about 30 torr). Thus it seems likely that the absorption at about 2140Å, which increased in intensity with time in the ultraviolet spectra of decomposing P_2F_4, was caused by deposition of the orange-yellow solid on the sides of the silica cell.

Huheey[239] plotted values of $\lambda_{max.}$ against the electronegativities of the substituent groups for several diphosphines and he interpreted the result as indicating that a relationship did exist, but the correlation was not high. In order to obtain a consistent set of group electronegativities, Huheey used values based on those given by Magnrise,[242] who had correlated the effect of several organic groups on the infrared stretching frequency of an adjacent carbonyl group with electronegativities given by Gordy.[251] Gordy gives the value of 3.95 for the substituent electronegativity of fluorine, and using this value, $\lambda_{max.}$ for P_2F_4 does not appear to correlate with the relationship proposed by Huheey[239] (Figure 28).

Rudolph and Schiller[226] have, however, recently questioned the validity of an intense ultraviolet absorption as evidence for $p\pi$-$d\pi$ bonding in diphosphines. The absorption features are not exclusively characteristic of P-P bonded diphosphines since the monophosphine PHF_2

FIGURE 28.

Plot of $\lambda_{max.}$ against Electronegativity of Substituents for Diphosphines.

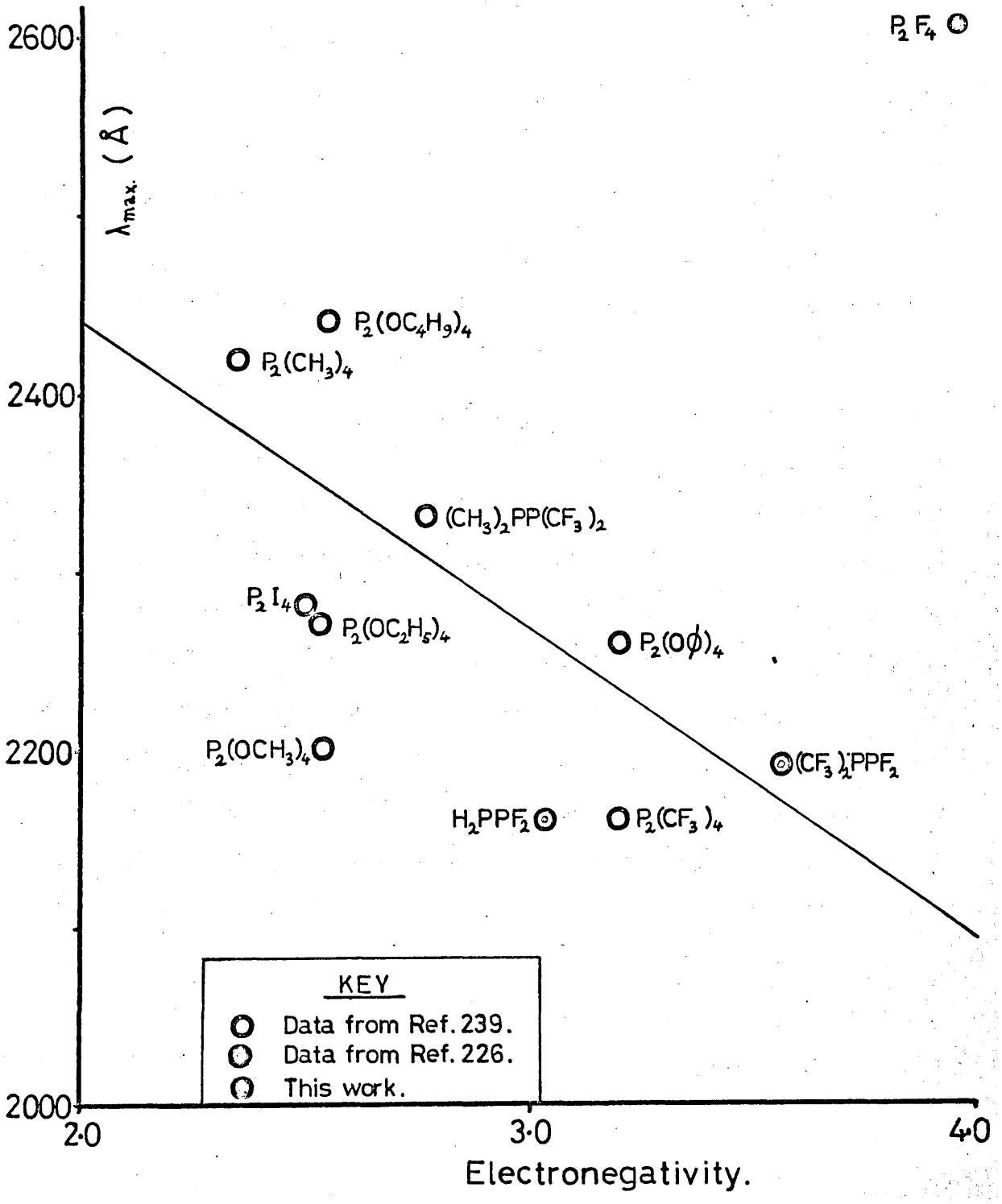

gives ultraviolet spectra similar to those observed for diphosphines. Rudolph and Schiller also noted two opposite trends in the value of $\lambda_{max.}$ as a function of substituent group electronegativity. Thus in the triad $(CF_3)_2PP(CF_3)_2$ - $(CF_3)_2PP(CH_3)_2$ - $(CH_3)_2PP(CH_3)_2$, $\lambda_{max.}$ shifts to longer wavelength with decreasing substituent electronegativity, but in the triad $(CF_3)_2PP(CF_3)_2$ - $(CF_3)_2PPF_2$ - F_2PPF_2, $\lambda_{max.}$ shifts to longer wavelength with increasing substituent electronegativity.

Although the main purpose of following the decrease with time of the absorption intensities in the ultraviolet spectrum of P_2F_4 was to demonstrate that the absorptions observed were due to P_2F_4, they also allow the rate of the decomposition reaction to be monitored. However, from comparison of the absorbances at 2605Å for samples of P_2F_4 at pressures of about 12 torr and at about 4 torr, it was apparent that the linear absorption scale of the spectrophotometer used was not maintained at high absorbances. However, from the series of spectra obtained using the lowest initial pressure of P_2F_4, it was possible to use the smaller absorption at 3000Å (Absorbances < 0.55) in order to monitor the rate of the decomposition reaction.

On the assumption that the absorption centred at 2605Å is symmetric either side of this maximum, this absorption should not interfere perceptibly with that at 3000Å, and thus the absorbance at 3000Å should be proportional to the concentration of P_2F_4. Figure 29 shows the decrease in the absorbance (a) at 3000Å during the first 100 minutes of

FIGURE 29.

Decrease of P_2F_4 Absorbance (a) at 3000Å with Time (t).

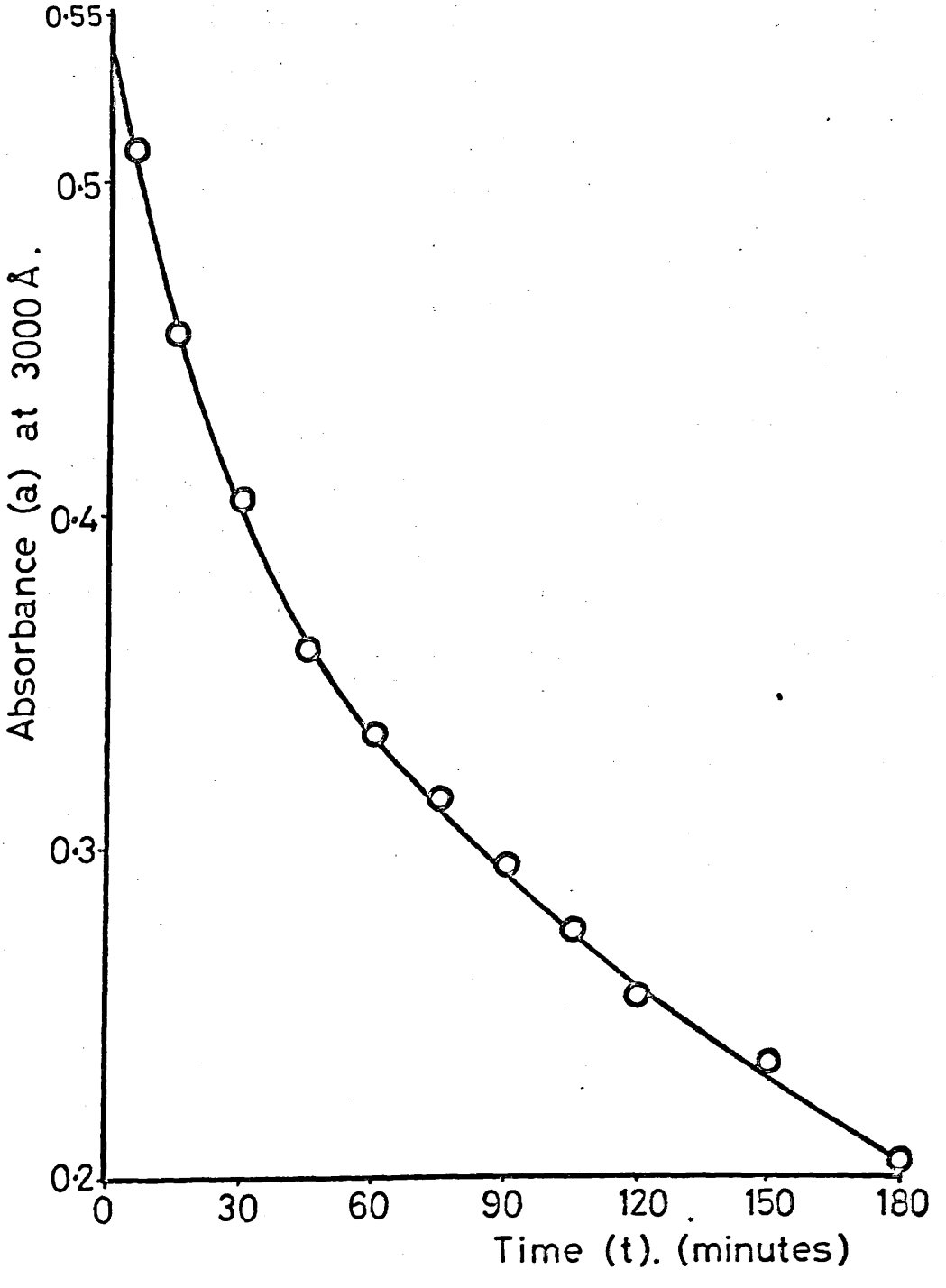

FIGURE 30.

Graph of $Log_{10}(-da/dt)$ versus $Log_{10}(a)$.

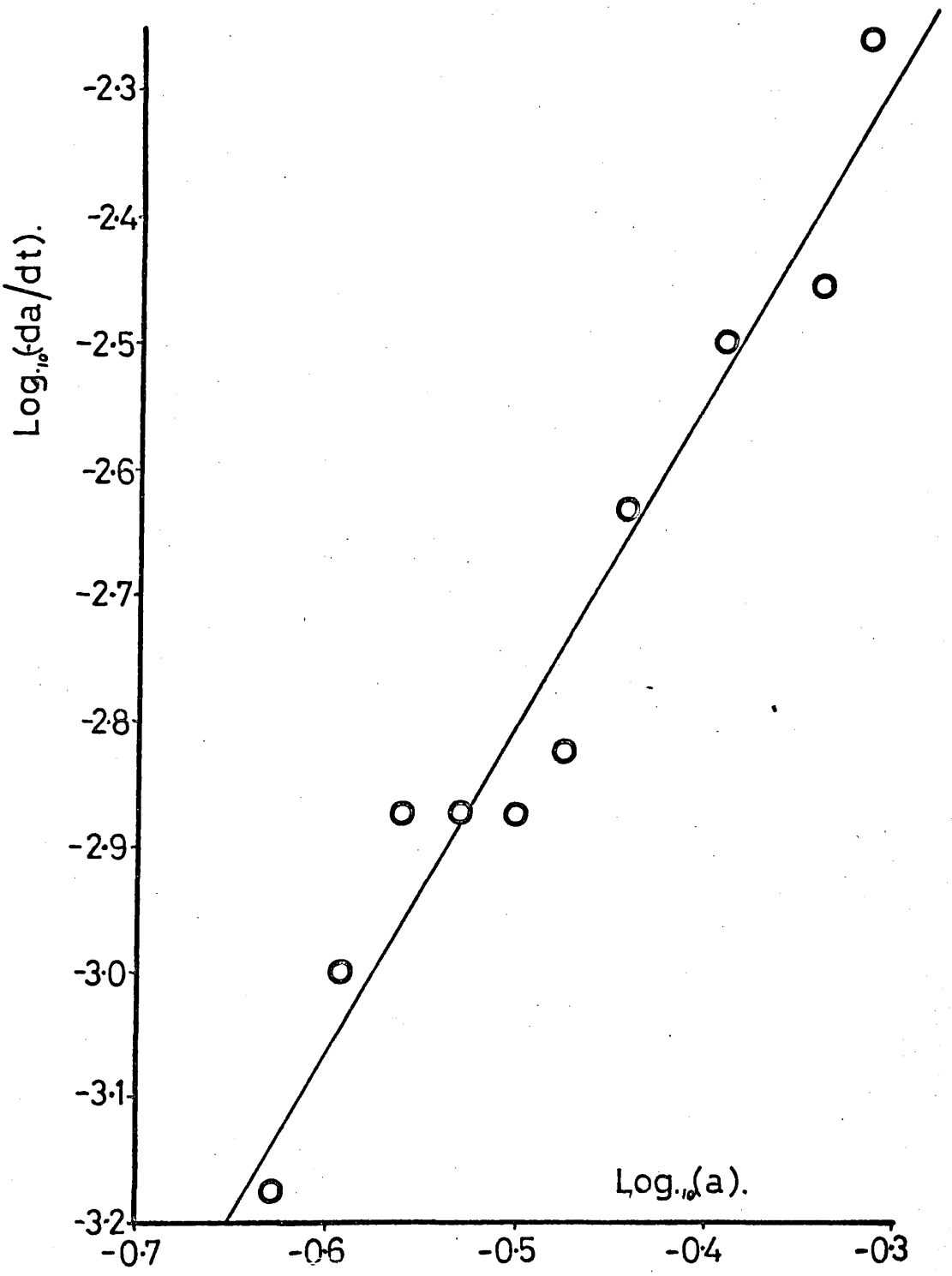

decomposition. After 130 minutes, the absorbance became too small to allow its accurate estimation. Figure 30 shows a graph of $\log_{10}(-\frac{dp}{dt})$ versus log (a) [where a is the absorbance at 3000Å and t is the time in minutes from the introduction of P_2F_4 into the ultraviolet gas cell]. A straight line was fitted to the experimental points by the method of least squares [$(4 + \log_{10}(-\frac{da}{dt})) = 2.5935\ (1 + \log_{10}(a)) - 0.0999$], and, from this, the order of the decomposition reaction with respect to P_2F_4 (the gradient of the straight line) was estimated to be 2.5935 with an accuracy (twice the standard deviation of the fit) of $\pm$ 3%.

PART 2: SECTION 2.

MASS SPECTROMETRIC APPEARANCE POTENTIAL MEASUREMENTS ON SOME PHOSPHORUS-FLUORINE COMPOUNDS - THE P-P BOND DISSOCIATION ENERGY IN P_2F_4.

INTRODUCTION

The reversible dissociation of N_2F_4 at the N-N bond to give stable NF_2 radicals has been studied by ultraviolet spectroscopy,[252,253,254] pressure-temperature measurements,[253] electron paramagnetic resonance spectroscopy,[255,256,257] and mass spectrometric analysis.[258] These results have been reviewed and evaluated by Colburn.[11] All the results were in good agreement ($\pm$ 1.1 kcal.mole^{-1}) and give an average value for the N-N bond dissociation energy in N_2F_4 ($D_{(N-N)}$) of 20.3 kcal.mole^{-1}.[27] Studies of the electron paramagnetic resonance spectrum of P_2F_4,[159,230] however, have shown that the P-P bond in P_2F_4 is considerably stronger than the N-N bond in N_2F_4. Thus the P-P bond dissociation energy in P_2F_4 cannot be estimated similarly from studies of its dissociation to give PF_2 radicals by ultraviolet spectroscopy, pressure-temperature measurements or electron paramagnetic resonance spectroscopy. At room temperature the concentration of PF_2 radicals is too small to allow accurate measurements, and also, even at this temperature, the equilibrium concentration of PF_2 radicals cannot be maintained due to decomposition of the P_2F_4. This bond dissociation energy can, however, be estimated from mass spectrometric appearance potential measurements.

Mass spectrometric measurements have been previously used for estimating the P-P bond dissociation energies in the diphosphines $P_2(C_2H_5)_4$,[233] P_2Cl_4,[234] P_2H_4[235,259] and P_2I_4.[236,260] In the present work, the first ionization potentials and appearance potentials of the fragment ion PF_2^+ have been measured for the molecules P_2F_4, PF_2I, PF_3 and PF_2H. Using these results, the P-P bond dissociation energy in P_2F_4 has been estimated.

In a mass spectrometer, ions are formed from neutral molecules by electron impact. In order to observe a given ion in the mass spectrum of a molecule, the energy of the exciting electrons must be equal to or greater than the appearance potential of the given ion (Ionization potential in the case of the parent ion).

Electron impact techniques, however, suffer from lack of an absolute energy scale. Although the magnitude of the electron beam energy can be estimated as the potential through which the electrons have been accelerated, there is in practice a distribution of electron energies within this beam. This is generally attributed to the Maxwellian energy distribution of electrons emitted thermoionically from a heated filament.[261] Attempts to remove the effect of this energy spread by analytical methods[262] have been only partially successful due to lack of knowledge of the exact form of the electron energy distribution and also to the inherent inaccuracy of the experimentally-measured ion current used to construct the ionization-efficiency curves. Other studies have attempted to reduce this energy spread either analytically[263] or experimentally.[264,265,266] Alternatively, a calibrating gas (usually argon) can be used to fix the energy scale and

this has been used in the majority of the methods employing electron impact to measure ionization or appearance potentials. This latter method has been used in the present work, employing either argon or acetone as the calibrating compound. Throughout this thesis each of these calibrating compounds is referred to as "calibrant", and each of the phosphorus-fluorine compounds, for which appearance and ionization potentials have been determined, is referred to as "unknown".

The determination of energy thresholds for fragmentation processes by electron impact methods, however, suffers the disadvantage that these processes can sometimes involve production of fragment ions with kinetic energy or electronic excitation. For only a few examples (e.g. O^+ from O_2 and N^+ from N_2[267]) have such phenomena been clearly identified and studied. However, comparison with threshold data from other methods has indicated that these factors may not be very significant and that reasonable thermochemical quantities may be derived from electron impact threshold data.

a. Experimental

Appearance and ionization potentials were measured using a Model MS 902 spectrometer (Associated Electrical Industries Ltd., London) with an electron impact source (200°C) and either an electron multiplier or a scintillator/photomultiplier[268] collector. All measurements were carried out with the instrument set to resolving power 1000 (10% valley definition) with a trap current of 10 μA and the ion repeller set at the potential of the ion chamber. The electron beam energy adjustment was not automated, but was monitored by a digital voltmeter giving an accurac

of $\pm$ 0.01 eV in the range 0-50 eV.

Owing to the great reactivity of the gases to be measured, it was found necessary to take extra precautions in conditioning the instrument surfaces before each determination. The inlet reservoir system and ion source were baked and purged with acetic acid vapour for 36 hours. The system was then conditioned further with successive aliquots of the compound (unknown) to be measured.

For appearance and ionization potential determinations, a fresh sample of the (unknown) gas was admitted to the reservoir from a break-seal glass ampoule, and sufficient calibrant gas (argon or acetone) was added to provide equal ion currents of the calibrant and unknown peaks at a reference electron beam energy setting. This reference setting was usually chosen as 50 eV,[269] but for some measurements the setting used was much lower (20 eV to 30 eV) and only about 15 eV above the onset of the ion being monitored. The collector meter reading was then normalised to 100% (Collector reading of 10,000 at the reference electron beam energy setting) and ionization efficiency curves were obtained by a method similar to that of Lossing et al.[269] For normalisation at 50 eV, the collector meter readings were recorded at 0.2 eV intervals from a relative peak height of about 40% down to onset (collector reading $< 0.05\%$ of the original abundance), and this procedure was then repeated at the same voltage intervals from onset back up to about 40% abundance. The mean values of the collector readings for the "down" and "up" curves

were then used to plot ionisation efficiency curves. The determination of each curve required 15 to 20 minutes. The above procedure was adopted for both the calibrant and the unknown ions, the two curves being recorded consecutively.

For normalisation at between 20 eV and 30 eV, the same procedure was adopted as for normalisation at 50 eV, but readings were taken at 0.2 eV intervals between the reference electron beam energy setting and onset. (From a relative peak height of 100% to < 0.05% and from < 0.05% back to 100%).

The purity of samples was confirmed by low resolution mass scans prior to measurement of ionisation efficiency curves. These spectra were similar to those reported in the literature.[156,158,159,160]

b. Estimation of Appearance Potentials from Ionization Efficiency curves

Figure 31 shows a typical ionisation efficiency curve (PF_2^+ from P_2F_4. Normalised at 50 eV). The portion AB of this curve is approximately exponential as a result of the Maxwellian distribution of electron energies in the electron beam. Above this "exponential" region, there is an approximately linear region (BC), and this tails off at higher electron beam energies (CD).

A number of methods have been used for obtaining ionization and appearance potentials from ionisation efficiency curves.[270,271,272] These methods may be broadly classified into two groups. In the first of these, each of the ionization efficiency curves (calibrant and unknown) is extrapolated individually back to the voltage axis. The simplest

FIGURE 31.

Typical Ionization Efficiency Curve.

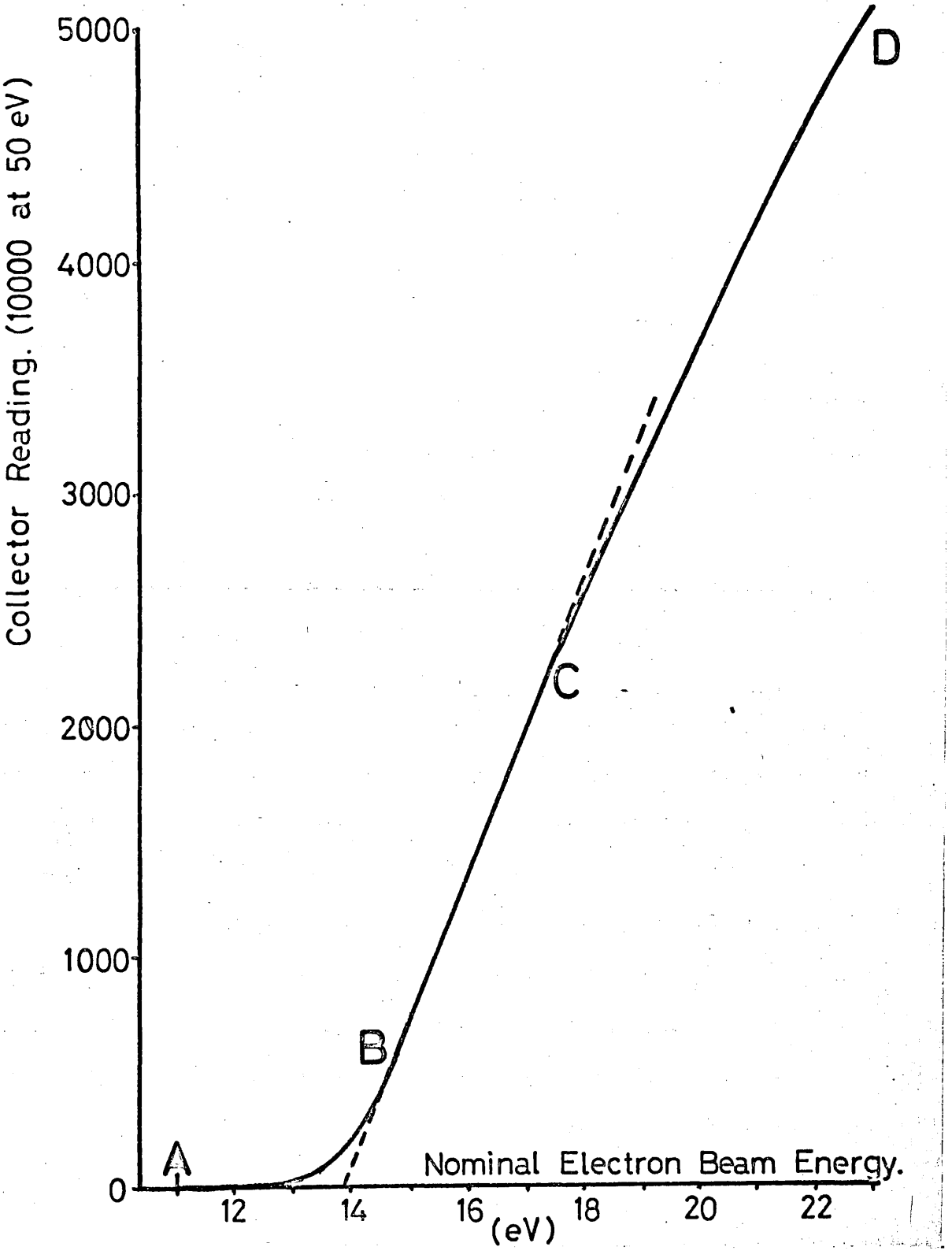

extrapolation is where the appearance potential is taken as the "initial break" in the ionisation efficiency curve, that is, the voltage at which the ion current is "first detected" (A in Figure 31). This, however, involves the tacit assumption that the ionization efficiency curve intercepts the voltage axis at a finite angle, whereas the "exponential" lower portion of the curve (AB in Figure 31), is, in fact, asymptotic to this axis. This method was used by Stevenson and Hipple[273] who found that it was not completely satisfactory since considerable personal judgement was involved in the choice of the initial break, and also since greatest weight was given to measurements of least accuracy (i.e. near the appearance potential). The alternative in this group of methods is to extrapolate the "linear" portion (BC in Figure 31) of the ionization efficiency curve back to the voltage axis. This method has been used with some success by Vought[274] and by Kaffeland and Lad,[275] but has been criticised.[269] Also it cannot be expected to give results as precise[276] as those given by the initial break method or by the methods, given below, in the second group.

The second group of methods involves the extrapolation to the voltage axis of the difference between the unknown and calibrant ionization efficiency curves. Lossing et al[269] plotted ionisation efficiency curves (normalised at 50 eV) for a number of gases in semi-logarithmic form (log. (collector reading) against nominal electron beam energy). In the region below the 5% level (below 5% of the original peak height at 50 eV), these semi-logarithmic plots are approximately linear, corresponding to the "exponential" portion of the ionisation

efficiency curves (AB in Figure 31). At and below the 1% level, Lossing *et al*[169] found that the curves were parallel to within the error of measurement, with the exception of the curves for N_2 and CO_2. Thus the difference (on the voltage scale) between the unknown and calibrant curves at or below the 1% level could be taken as the difference between the appearance potentials for the calibrant and the unknown for those cases where the curves were parallel. This method has been frequently used for the interpretation of ionisation efficiency curves in order to evaluate appearance potentials (e.g. Ref. 277, 278), and, in particular, was used for the estimation of the P-P bond dissociation energy in P_2I_4.[260] However, the use of this method is limited to cases where the ionization efficiency curves of the calibrant and unknown are parallel.

Warren[279] has proposed a method by which the voltage difference between the unknown and calibrant curves can be extrapolated to the voltage axis without requiring that the two curves should be parallel at and below the 1% level. In this method, the ionization efficiency curves for the unknown and calibrant ions are plotted (collector reading against nominal electron beam energy) so as to make parallel the approximately linear portions of the curves (region DC in Figure 31). This may be achieved by scaling-up the collector readings for the curve with the lower gradient by a factor equal to the ratio of the gradients of the two (calibrant and unknown) approximately linear regions.

Differences of voltage between the two curves (δV), for various collector readings (I), are then determined, and a graph of δV against I is then plotted. This graph is then extrapolated to zero collector reading, and the extrapolated value of δV is taken as the difference between the appearance potentials of the two ions.

Warren found that this method gave very good results for the ionisation potentials of several gases (Kr, Ne, O_2, CO_2 [279]) and for the appearance potentials of parent and fragment ions from CH_4, provided that the ions were of high or moderate relative abundance.[267] However, considerable difficulty was found in applying this method to ions of low relative abundance (e.g. CH^+ and C^+ from CH_4 [267]). In the estimation of the P-P bond dissociation energy for P_2Cl_4,[234] this method was also found successful for the interpretation of the ionization efficiency curves for ions from PCl_3 and P_2Cl_4.

In the present work, Lossing's method[169] was not found to be adequate for the interpretation of the ionisation efficiency curves (normalised at 50 eV) for ions from the phosphorus-fluorine compounds studied. Comparison of the curves for the calibrant and unknown showed that they were not parallel at or below the 1% level. Some curves were, therefore, normalised at lower potentials (20 to 30 eV) in an attempt to obtain parallel curves for the calibrant and unknown at and below the 1% level. However this attempt was not successful, although the curves

obtained deviated from parallelism to a lesser extent.

Due to the inapplicability of Lossing's method,[169] all appearance and ionization potentials reported in this work have been estimated from the ionization efficiency curves by a method similar to that of Warren.[267,279] However, Warren's method requires measurements of the "tail" of the ionization efficiency curves ("exponential" region AB in Figure 31) and this must inevitably lead to inaccuracies. These may arise from three main factors, of which the first is the poor signal-to-noise ratio at very low ion currents (collector readings < 10, or below the 0.1% level). Secondly, any zero error in the collector readings will markedly effect these readings near onset. In the present work, the zero setting was made immediately prior to the measurement of each ionization efficiency curve, but fluctuations in the "dark current" during measurements may still lead to inaccuracies. Lastly, inaccuracies may be caused by processes, other than that being considered, giving rise to the ion being measured (or an ion of the same m/e value) and with a lower appearance potential. Such processes elongate the "tails" of the ionization efficiency curves, as has been observed for some halogen compounds of C[279] and Si,[274] where the "tails" were attributed to a small number of ions being produced by thermal dissociation and not to an impurity.

The method used in the present work was adopted in an attempt to minimise these inaccuracies. The experimental ionization efficiency curves were plotted (as in Figure 31) for both the unknown and calibrant

ions. The ratio of the gradients of the "linear" portions of these two curves (BC in Figure 31) was then taken as the "Warren factor".[279] The value of this factor was characteristically between 1.0 and 3.0. The experimental collector readings for the curve with the lower slope were then multiplied by the "Warren factor" to make the linear portions of the two curves parallel.

The errors due to the poor signal-to-noise ratio at low ion currents should be random, and can therefore be minimised by fitting the experimental points to a smooth curve. For this purpose the approximately linear semi-logarithmic plots (log. (collector reading) against nominal electron beam energy) are more amenable than the approximately exponential tails of the ionization efficiency curves. Thus the experimental points for each of the ionization efficiency curves from just above the 10% level down to onset (typically 15 to 20 points from about 4 eV above onset down to onset) were fitted by the method of least squares to a power series polynominal of the form:

$$(\text{nominal electron beam energy}) = \sum_{n=0}^{n=n} (a_n[\log.(\text{collector reading})^n]).$$

It was found that 5 terms ($n = 4$ in above equation) were sufficient to give a good fit, the fifth coefficient (a_4) being typically very small. The standard deviation of these fits (calculated as $\sqrt{(\sum_{m=1}^{m=k} \Delta_m^2)/k(k-1)}$, where Δ_m is the deviation of the m'th point from the smooth curve measured parallel to the voltage axis and k is the number of points fitted) was typically about 2.5×10^{-3} eV.

The method used for the comparison of the curves for the calibrant and unknown was the same as that used by Warren,[267,279] and the differences in voltage (δV) between the smooth fitted curves for the calibrant and unknown for various collector readings(I) were determined. For this comparison, only the lower portions of the curves are of interest, and thus the differences (δV) were calculated from the equations for the two smooth fitted curves for 30 values of I equally spaced from a collector reading of 4 to one of 120 (from 0.04% level to 1.2% level). The values of δV were then plotted against I and also fitted to a 3 term polynomial of the form:

$$\delta V = \sum_{n=0}^{n=2} [a_n \text{ (collector reading)}^n].$$ The standard deviation of these fits (calculated as above) was typically of the order of 2×10^{-3} eV. Most of the curves deviated very little from linearity (third coefficient, a_2, very small) and showed little change in δV with changing I. In these cases, the extrapolated value of δV for a collector reading of zero was taken as the difference between the appearance potentials of the unknown and calibrant ions.

A Fortran IV computer program was written allowing the appearance potentials to be computed, (using the University of London C.D.C. 6600 computer), from the ionization efficiency curves for the calibrant and the unknown by the above procedure. The "Warren factors", however, were estimated manually.

In some cases the plots of δV against I showed marked deviations from linearity, some plots showing definite tailing of the curves at low collector readings (low I). While the extrapolation to zero collector reading of near linear plots of δV against I is reasonable, the extrapolation of curves deviating more markedly from linearity is liable to objection.[279] Three different causes may be distinguished, as shown in Figure 32. For the first pair of curves (1a, b), a poor choice of "Warren factor" has failed to make the "linear" portions of the ionization efficiency curves (calibrant and unknown) parallel. A few of the ionization efficiency curves showed no definite "linear" region, and personal judgement was required in order to obtain a reasonable estimate of the "Warren factor". The effect on the plots of δV against I of a poor choice of "Warren factor" is shown in Figure 32, case 1b.

In the second case, a zero error in the collector readings for one of the ionisation efficiency curves causes a near linear plot of δV against I to tail sharply at low I. The last pair of curves in Figure 32 (3a, b) show the effect of an ion, of the same m/e value, being formed by some process having a lower appearance potential than that being studied. This type of behaviour is expected if there are impurities in the sample (either originally or caused by reaction at the instrument surfaces) or if thermal dissociation of the sample is not negligible. The form of the plots of δV against I is similar to that caused by a zero error (case 2), but these two cases can usually be distinguished.

FIGURE 32.

Causes of Non-linear δV versus I Plots.

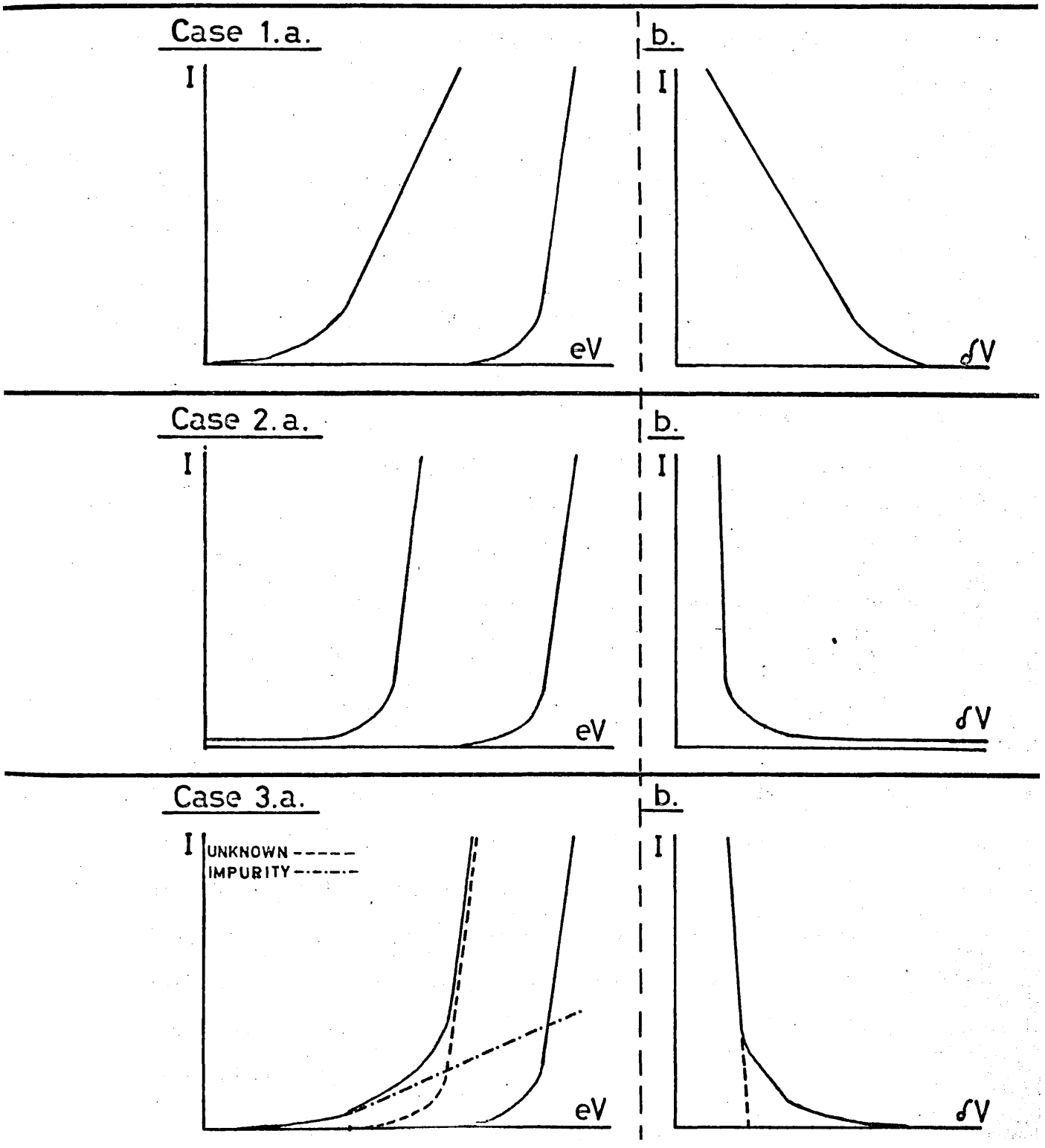

For curves of the type shown in Case 1, Figure 32, suitable adjustment of the "Warren factor" and recalculation gives a δV versus I plot that is linear and which shows little change in δV with changing I. Trial calculations showed that similar changes in the "Warren factor" would not give "near linear" δV versus I plots for pairs of ionization efficiency curves into one of which a deliberate zero error had been introduced. In the present work, small adjustments in the "Warren factors" employed in the calculations were only required in two cases.

For curves of the type shown in Case 2 (Figure 32), suitable adjustment of the experimental points for one of the ionization efficiency curves by addition (or subtraction) of a constant (zero error constant) to the collector reading will produce a δV versus I plot of the type required. For these cases, the relative zero error between the calibrant and unknown curves is much more important than the absolute zero error for each curve. Thus if the zero error is the same (in magnitude and sign) for both curves, the plot of δV versus I will still be linear, and the error in the difference between the appearance potentials (taken as δV at $I = 0$) will be negligible if δV is almost constant with changing I. The absolute value of the zero error for each ionization efficiency curve may only be estimated by assuming that the "tails" of the ionization efficiency curves should be strictly exponential. Thus comparison, near onset, of the experimental ionization efficiency curves with a strictly exponential curve (or for semi-logarithmic plots, comparison with a straight line) will give an indication of the absolute value of the zero error. Using a separate computer program, the ionization efficiency semi-logarithmic plots for the

unknown were compared with a straight line developed from the fitted curve for the calibrant by making the 3rd, 4th and 5th coefficients of this polynomial equal to zero. Successive calculations using zero factors from +3 to -3 in unit steps applied to the unknown curve allowed the δV versus I plots for each of these zero factors to be computed and compared. These calculations were repeated, comparing the calibrant semi-logarithmic plots with straight lines developed from the unknown fitted polynomials. From observations of the changes in the δV versus I plots with changes in zero factor, and in particular of the way in which the curves tailed at low I, it was possible to estimate the probable zero error for each curve. Zero error constants found in this way were in the range +1 to -2 (zero error constant added to experimental collector readings for correction).

Plots of δV versus I, of the type shown in Case 3, Figure 32, are caused by an "impurity" ion (either the same ion as being observed, but formed by a different process such as thermal dissociation, or an ion of the same m/e formed from an impurity). Where this effect is very small, the resulting δV versus I plots may not be distinguishable from curves of the type shown in Case 2 (due to zero error). However, for such small "impurity" ion currents, the application of a zero error constant (negative in sense defined above) equal to the ion current of the "impurity" ion at the appearance potential of the unknown (or calibrant) ion, provides exactly the correction required. It was felt that some of the curves, that were made linear by application of a zero error constant, had been corrected in this way for very small "impurity" ion currents (Maximum

contribution from "impurity" ion, at appearance potential of ion being studied would be in these cases $\leq$ 2 collector units). In cases where the contribution from the "impurity" ion is greater than that above, but still small (up to about 20 collector units), extrapolation of the straight portion of the δV versus I curve (as shown by broken line in Case 3.b, Figure 32) will give a value of δV at zero I which can be taken as the difference in the appearance potentials. This introduces only a very small, and probably insignificant error, and this extrapolation was only employed for one pair of ionization efficiency curves for which the δV versus I plot tailed at $I < 16$ (This result is marked in Table 18 with an asterisk).

c. Results and Calculations

The experimental results for the appearance and ionization potentials measured are given in Table 18, and the proposed mechanisms for the formation of the fragment ions are given in Figure 33. In order to estimate the ionization potential of the PF_2 • radical, it was necessary to make certain assumptions concerning the PF_2-X bond dissociation energies (X = F, I and H). For PF_3 and PF_2H, there are no experimental data for the bond dissociation energies, and the mean bond energies for PF_3 (calculated from literature values for $\Delta H_f^o(PF_{3(g)})$,[248] $\Delta H_f^o(P_{(g)})$[247] and $\Delta H_f^o(F_{(g)})$[247]; see Part 2, Section 1c of this thesis) and for PH_3 [230] have been used. Although the mean bond energy in PI_3 could be used as an approximation for $D(PF_2\text{-}I)$, the first P-I bond dissociation energy for

TABLE 13

RESULTS FOR APPEARANCE AND IONIZATION POTENTIALS

Run No.	Ion	Parent Molecule	Calibrant[a]	Normalised at (eV)[d]	δV at I=0 (eV)[d]	Appearance Potential[b] (eV)[d]	[Mean][c]
1	PF_2^+	P_2F_4	Ar	50	-4.911	10.849	[10.90(±0.07)]
2	PF_2^+	P_2F_4	Ar	21	-4.858	10.902	
3*	PF_2^+	P_2F_4	Ar	50	-4.785	10.975	
4	PF_2^+	P_2F_4	Ar	20	-4.866	10.894	
5	$P_2F_4^+$	P_2F_4	Ar	50	-6.522	9.238	[9.31(±0.07)]
6	$P_2F_4^+$	P_2F_4	Ar	27	-6.385	9.375	
7	PF_2^+	PF_3	Acetone	50	+3.773	13.453	[13.52(±0.06)]
8	PF_2^+	PF_3	Ar	50	-2.230	13.530	
9	PF_2^+	PF_3	Ar	50	-2.196	13.564	
10	PF_3^+	PF_3	Acetone	50	+1.795	11.475	[11.64(±0.13)]
11	PF_3^+	PF_3	Ar	50	-4.122	11.638	
12	PF_3^+	PF_3	Ar	50	-4.060	11.710	
13	PF_3^+	PF_3	Ar	50	-4.038	11.722	
14	PF_2^+	PF_2I	Ar	50	-4.977	10.783	
15	PF_2I^+	PF_2I	Ar	50	-6.155	9.605	
16	PF_2^+	PF_2H	Acetone	50	+2.075	11.755	[11.68(± 0.09)]
17	PF_2^+	PF_2H	Ar	50	-4.156	11.604	

/continued

TABLE 13 (continued)

Run No.	Ion	Parent Molecule	Calibrant[a]	Normalised at (eV)[d]	δV at I=0 (eV)[d]	Appearance Potential[b] (eV)[d]	[Mean][c]
18	PF_2H^+	PF_2H	Acetone	50	+0.700	10.470	[10.46(±0.01)]
19	PF_2H^+ ,	PF_2H	Ar	50	-5.309	10.451	
20	$(CH_3)_2CO^+$	$(CH_3)_2CO$	Ar	50	-5.783	9.977	[10.00(±0.02)]
21	$(CH_3)_2CO^+$	$(CH_3)_2CO$	Ar	25	-5.734	10.020	
22	$C_6H_6^+$	C_6H_6	Ar	26	-6.242	9.518	
23	$C_6H_6^+$	C_6H_6	Ar	26	-6.200	9.560	[9.52 (±0.04)]
24	$C_6H_6^+$	C_6H_6	Ar	26	-6.280	9.480	

a. Calibrant curves for: (Ar) $Ar \longrightarrow Ar^+$

(Acetone) $CH_3.CO.CH_3 \longrightarrow CH_3.CO.CH_3^+$

b. Calculated using literature values for ionization potentials of Ar[276] and Acetone.[276]

c. Limits, given in brackets after the mean values for the Appearance Potentials are the spread of the experimental results.

d. 1eV = 23.0609 kcal. = 96.4870 kJ.[276]

FIGURE 33.

Proposed Mechanisms and Thermodynamic Cycles for Formation of Fragment Ions.

$P_2F_4 \xrightarrow{A_1} PF_2^+ + PF_2^\bullet + e$ $D(F_2P\text{-}PF_2)$ ↓ $2\,PF_2^\bullet \xrightarrow{I} PF_2^+ + PF_2^\bullet + e$	$A_1 = 10{\cdot}90$ eV $= 251{\cdot}5$ kcal.mole^{-1}
$PF_3 \xrightarrow{A_2} PF_2^+ + F^\bullet + e$ $D(F_2P\text{-}F)$ ↓ $PF_2^\bullet + F^\bullet \xrightarrow{I} PF_2^+ + F^\bullet + e$	$A_2 = 13{\cdot}52$ eV $= 311{\cdot}7$ kcal.mole^{-1} $D(F_2P\text{-}F) = 119{\cdot}39$ kcal.mole^{-1} $\therefore I = 192{\cdot}3$ kcal.mole^{-1}
$PF_2I \xrightarrow{A_3} PF_2^+ + I^\bullet + e$ $D(F_2P\text{-}I)$ ↓ $PF_2^\bullet + I^\bullet \xrightarrow{I} PF_2^+ + I^\bullet + e$	$A_3 = 10{\cdot}78$ eV $= 248{\cdot}7$ kcal.mole^{-1} $D(F_2P\text{-}I) = 52$ kcal.mole^{-1} $\therefore I = 196{\cdot}7$ kcal.mole^{-1}
$PF_2H \xrightarrow{A_4} PF_2^+ + H^\bullet + e$ $D(F_2P\text{-}H)$ ↓ $PF_2^\bullet + H^\bullet \xrightarrow{I} PF_2^+ + H^\bullet + e$	$A_4 = 11{\cdot}68$ eV $= 269{\cdot}3$ kcal.mole^{-1} $D(F_2P\text{-}H) = 77$ kcal.mole^{-1} $\therefore I = 192{\cdot}3$ kcal.mole^{-1}

Weighted (according to number of readings per parent molecule) Mean Value of I ($I.P._{PF_2^\bullet}$) = 193 kcal.mole^{-1}

$\therefore D(F_2P\text{-}PF_2) = 58$ kcal. mole^{-1}

TABLE 19

SUMMARY OF RESULTS FROM ELECTRON IMPACT STUDIES

Ionization Potential of PF_2· radical (using results from PF_3)[a] = 198.4 kcal.mole^{-1}

(using results for PF_2I)[b] = 196.7 kcal.mole^{-1}

(using results for PF_2H)[c] = 192.4 kcal.mole^{-1}

Ionization Potential of PF_2· radical (weighted mean)[d] = 193 kcal.mole^{-1}

$D(P_2F-PF_2)$[f] = 53 kcal.mole^{-1}

Ionization Potential[e] of: P_2F_4 = 9.31 eV = 215 kcal.mole^{-1}

PF_3 = 11.64 eV = 268 kcal.mole^{-1}

PF_2I = 9.60 eV = 221 kcal.mole^{-1}

PF_2H = 10.46 eV = 241 kcal.mole^{-1}

Ionization Potential[e] of: $(CH_3)_2CO$ = 10.00 eV = 231 kcal.mole^{-1} [9.69 ± 0.01 eV][g]

C_6H_6 = 9.52 eV = 220 kcal.mole^{-1} [9.247 ± 0.005 eV][g]

a. Using $D(PF_2-F)$ = 119.4 kcal.mole^{-1}

b. Using $D(PF_2-I)$ = 52 kcal.mole^{-1} [260]

c. Using $D(PF_2-H)$ = 77 kcal.mole^{-1} [230]

d. Estimated error limits (+7, -12) kcal.mole^{-1}

e. Estimated error limits (+0.1, -0.3)eV; (+2,-7)kcal.mole^{-1}

f. Estimated error limits (± 9) kcal.mole^{-1}

g. Values given in brackets are best literature values.[276]

1 eV = 23.0609 kcal.mole^{-1}

PI_3[$D(PI_2-I)$ = 52 kcal.mole^{-1}] has been estimated from experimental electron impact studies,[260] and this was considered to be a better approximation for $D(PF_2-I)$. Using these values in the thermodynamic cycles shown in Figure 33, together with the results for the appearance potentials for the PF_2^+ ion from PF_3, PF_2I and PF_2H, the ionization potential of the PF_2•radical has been estimated as 193 kcal.mole^{-1} (see Figure 33). Using this value in the thermodynamic cycle for P_2F_4 (Cycle 1: Figure 33), the P-P bond dissociation energy in P_2F_4 was estimated as 58 kcal.mole^{-1}.

These results together with the results for the ionization potentials of the phosphorus-fluorine molecules studied, are given in Table 19. The results obtained for the ionization potentials of acetone and benzene (measured as a check on the experimental and calculational methods used in the present work) are also given in Tables 18 and 19.

Discussion

The estimated value of 58 kcal.mole^{-1} for the P-P bond dissociation energy in P_2F_4 is, as expected, much greater than the N-N bond dissociation energy in N_2F_4 (20.3 kcal.mole^{-1}) [11,27] (see Part 2: Section 2; Introduction). This value may also be compared with previous estimates of P-P bond dissociation energies for the diphosphines $P_2(C_2H_5)_4$ [233] (86 kcal.mole^{-1}), P_2H_4 [235] (74 kcal.mole^{-1}), P_2I_4 [260] (65 to 73 kcal.mole^{-1}) and P_2Cl_4 [234] (52 to 63 kcal.mole^{-1}). These literature values show a general decrease in D(P-P) with increasing electronegativity of the substituent groups, and thus the value of $D(F_2P-PF_2)$ is expected to be less than $D(Cl_2P-PCl_2)$. Sandoval *et al* [234] estimated the value of $D(Cl_2P-PCl_2)$ as 73 kcal.mole^{-1} from appearance potential measurements on the PCl_2^+ ion from PCl_3 and P_2Cl_4, and by assuming that the literature value [231] [E(P-Cl) = 78 kcal.mole^{-1}] might be taken as equal to $D(PCl_2-Cl)$. This method is exactly analogous to that by which $D(F_2P-PF_2)$ has been estimated in the present work indicating that the value of $D(F_2P-PF_2)$ should be compared with a value of $D(Cl_2P-PCl_2)$ of 73 kcal.mole^{-1}. Thus the value of $D(F_2P-PF_2)$ is, as was expected, less than $D(Cl_2P-PCl_2)$. Sandoral *et al* [234] also estimated $D(Cl_2P-PCl_2)$ as 52 kcal.mole^{-1} from appearance potential measurements on the PCl^+ ion from PCl_3 and P_2Cl_4 (using same approximation as above for $D(PCl_2-Cl)$. In view of the greater uncertainty in assigning the dissociation processes for the production of the PCl^+ ions from PCl_3 and P_2Cl_4, and since there is a greater possibility of excess kinetic energy being associated with the fragments produced (greater number of fragments that for PCl_2^+ from PCl_3 and P_2Cl_4), the

present author considers that the former estimate of 73 kcal.mole^{-1} for $D(Cl_2P-PCl_2)$ is the more reliable.

It is difficult to make reliable estimates for the probable error limits associated with the appearance potential measurements. Electron impact techniques cannot be expected to give results as accurate as those from spectroscopy (identification of a molecular Rydberg series) or from photoionization. Thus fragmentation threshold energies from electron impact studies may sometimes be up to 0.5 eV higher than those obtained from photoionization studies. For this reason, error limits estimated from the reproducibility of electron impact measurements (e.g. twice the standard deviation of the mean of the results) are not satisfactory, since systematic errors are then neglected.

The spread of the results, shown in Table 18, indicates that these results were reproducible to within about $\pm$ 0.1 eV. However, the results for the ionization potentials of acetone and benzene (both obtained using Ar as calibrant) are higher than literature values obtained by photoionization (and spectroscopy in the case of benzene). Thus for the ionization potential of acetone, the value of 10.00 eV obtained in the present work is about 0.3 eV greater than the best literature values (9.69 $\pm$ 0.01 eV)[276] and the results obtained for benzene in the present work (9.52 eV) are also about 0.3 eV higher than the best literature values (9.247 $\pm$ 0.005 eV).[276] However, the results obtained in this work are compatible with literature values for the ionization potentials for both of these molecules obtained by electron impact

measurements.[276] Thus, although the probable random error limits for the ionization and appearance potentials given in Tables 18 and 19 are ± 0.1 eV, there is also a probable systematic error of up to 0.3 eV.

The value given in Table 19 for the ionization potential of the $PF_2^{\bullet}$ radical was calculated from the measured appearance potentials for the PF_2^+ ion from PF_2X(X = F, I and H) using assumed values for $D(PF_2-X)$, and these assumptions must introduce a further error. The three results obtained from measurements on PF_3, PF_2I and PF_2H are, however, in good agreement, indicating that the values chosen for $D(PF_2-X)$ are mutually consistent. No literature data was found for dissociation energies for any of these compounds. Some indication of the error involved in this assumption for PF_3 may, however, be obtained by comparison with data for NF_3,[282] for which $D(NF_2-F) < \bar{E}(N-F)_{NF_3}$ by 8 kcal.mole^{-1}. For PF_2H, it was also assumed that $D(PF_2-H) = \bar{E}(PH)_{PH_3}$. It has been shown that $D(P-H)_{PH\ radical} = \bar{E}(PH)_{PH_3}$,[283] but that $D(PH_2-H) > \bar{E}(PH)_{PH_3}$ by about 7 kcal.mole^{-1}.[284] Finally for PF_2I, it was assumed that $D(PF_2-I) = D(PI_2-I)$, and data for the PI_3 molecule shows that $D(PI_2-I) > \bar{E}(PI)_{PI_3}$ by about 2 kcal.mole^{-1}.[280]

In view of the close approximation of the mean bond energies ($\bar{E}$) to the first dissociation energies for the above Group V trihalides, the assumptions made in the calculations of the ionization potential of the $PF_2^{\bullet}$ radical appear reasonable, and the error introduced in these assumption has been estimated as ± 5 kcal.mole^{-1}.

Two main methods have been used for the determination of bond dissociation energies from electron impact data. These have been called

the direct and indirect methods.[285] The direct method involves taking the difference between an appearance potential and an ionization potential:

(A = appearance potential)

(ΔE = minimum energy for process)

$R'-B \longrightarrow R'^{+} + B + e$; $A_1 \geqslant \Delta E_1$ (1)

$R' \longrightarrow R'^{+} + e$; $A_2 \geqslant I(R')$ (2)

$D(R'-B) = \Delta E_1 - I(R') \leqslant A_1 - A_2$

Process (2) involves the removal of a non-bonding electron from the radical R', and thus it is reasonable to assume that $A_2 = I(R')$. However, it is not reasonable to assume that $A_1 = \Delta E_1$. Thus $D(R'-B)$ estimated as $(A_1 - A_2)$ will only be an upper limit for this bond dissociation energy.

The indirect method involves taking the difference between two appearance potentials for similar processes:

$R'-C \longrightarrow R'^{+} + C + e$: $A_3 \geqslant \Delta E_3$ (3)

$R'-B \longrightarrow R'^{+} + B + e$: $A_4 \geqslant \Delta E_4$ (4)

$D(R'-C) \longrightarrow R' + C$; ΔE_5 (5)

Eqn (6). $D(R'-B) = \Delta E_4 - \Delta E_3 + \Delta E_5 \leqslant A_3 - A_4 + \Delta E_5$

The equality sign in equation (6) holds for either of two conditions: (1) that $A_3 = \Delta E_3$ and $A_4 = \Delta E_4$, or (2) that the appearance potentials (A_3 and A_4) exceed the minimum energies for the processes (ΔE_3 and ΔE_4) by the same amount. Hipple and Stevenson[285] showed that appearance potentials for similar processes were likely to conform with the second of the above conditions ($A_3 - \Delta E_3 = A_4 - \Delta E_4$).

In the present work, the indirect method has been used for the estimation of $D(F_2P-PF_2)$ using the appearance potentials of the PF_2^+ ion from P_2F_4 and from PF_2X (X=F, I, and H). It therefore seems reasonable to expect that the systematic errors in the appearance potentials (from P_2F_4 and from PF_2X) were equal. On this basis, the error in the estimated value for $D(F_2P-PF_2)$ is only due to the random errors in the appearance potentials [$\pm$? kcal.mole^{-1} for each appearance potential] and to the error introduced in the approximation made for $D(PF_2-X)$ [$\pm$ 5 kcal.mole^{-1}]. The probable error limits for $D(F_2P-PF_2)$ have therefore been estimated as $\pm$ 9 kcal.mole^{-1}.

No results have been reported in the literature for the ionization potentials of P_2F_4, PF_2I, and PF_2H, but there have been three reports concerning the ionization potential of PF_3. Price et al[276,286] estimated this ionization potential from photon impact measurements as 9.71 eV, about 2 eV lower than the electron impact result obtained in the present work (11.64 eV). More recently Dugger et al[287] have reported the value of 11.5 ($\pm$ 0.1) eV, in excellent agreement (to well within experimental error) with the result obtained in the present work. Green et al[288] have reported the value of 12.3 eV obtained from photoelectron spectroscopy (this value is almost 0.7 eV higher than that reported in the present work). While the agreement of the result reported in this work (11.64 eV) is in excellent agreement with the value of Dugger et al[287] (11.5 eV) also obtained from electron impact studies, the disagreement with the two divergent photon impact measurements[286,288]

(which should theoretically be capable of more accurate results than electron impact measurements) cannot be explained by the present author.

PART 2: SECTION 3.

EXPERIMENTAL

a. Preparations of Phosphorus-Fluorine Compounds

The synthesis of PF_2I was in three stages:

1. $2Et_2NH + PCl_3 \longrightarrow Et_2NPCl_2 + Et_2NH.HCl$.

2. $Et_2NPCl_2 + 2NaF \longrightarrow Et_2NPF_2 + 2NaCl$.

3. $Et_2NPF_2 + 2HI \longrightarrow PF_2I + Et_2NH.HI$.

Diethylaminodichlorophosphine was prepared as outlined by Kosolapoff[289] and by Burg and Slota[290] by slow addition of phosphorus trichloride (Reagent grade; B.D.H. Ltd., Poole) to an etherial solution of diethylamine (Reagent grade; B.D.H. Ltd.). Diethylaminodichlorophosphine was separated from the solid $Et_2NH.HCl$ by ether extraction. The ether was distilled off and the crude product purified by distillation under reduced pressure [Fraction collected: B. Pt. 65°C-68°C at 8 torr; Yield (based on PCl_3) = 80%].

In the second stage, diethylaminodichlorophosphine was fluorinated by the method given by Schmutzler[291] by slow addition to a suspension of dried NaF ('Analar'; B.D.H. Ltd.) in sulpholane (tetramethylene sulphone; Koch-Light Laboratories Ltd., Colnbrook). The yield of this reaction (20%) was initially lower than that obtained by Schmutzler (72%). However, a greatly improved yield (75%) was obtained by continuous removal of product by distillation at a pressure of 100 torr. The product was purified by further distillation under reduced pressure [Fraction collected: B. Pt. 46°C - 48°C at 100 torr (literature:[291] B. Pt. = 47°C at 100 torr). Yield = 75%]. The identity of the

product was confirmed by comparison of the infrared spectrum (600 cm^{-1} to 4000 cm^{-1}, Model 337 Grating Infrared Spectrophotometer, Perkin-Elmer Ltd., Beaconsfield) with that reported in the literature.[291]

PF_2I was prepared as outlined by Parry et al.[156,157] The use of diethyl - rather than dimethylaminodifluorophosphine facilitated separation of PF_2I from unreacted starting material. Anhydrous HI was prepared as described by Hoffman and Heintz[292] by reaction of iodine with tetrahydronaphthalene (Reagent grade; B.D.H. Ltd.). PF_2I was purified by high vacuum trap-to-trap distillation, being retained at -126°C, while PF_3 passed through to a trap at -196°C. Impurities less volatile than PF_2I (Et_2NPF_2 and possibly PI_3) were retained in a trap at -30°C. Although PF_2I only momentarily came into contact with vacuum grease on removing the gas from the reaction vessel, it was found that initial use of Silicone High Vacuum Grease (Edwards High Vacuum Ltd., Crawley) caused an unexplained infrared band to appear at 1140 cm^{-1}. In all subsequent preparations this was avoided by using Kel-F Grease (Minnesota Mining and Manufacturing Company).

The above method of purification of PF_2I was not able to separate PF_2I from unreacted HI. Use of excess Et_2NPF_2 in the preparation of PF_2I reduced the amount of HI left unreacted, but traces of this impurity still remained. PF_2I, free of HI, was therefore obtained by mixing impure PF_2I with P_2F_4 (vide infra) followed by high-vacuum trap-to-trap distillation to remove PF_2H and residual P_2F_4 (vide infra).

The PF_3, formed as a secondary product in the preparation of PF_2I was retained, and required no further purification.

P_2F_4 was prepared by the method given by Rudolph *et al*[159] from the reaction of PF_2I with Hg.

$$2PF_2I + 2\ Hg \longrightarrow F_2P\text{-}PF_2 + Hg_2I_2.$$

Purification of P_2F_4 was hampered by small amounts of PF_2I and of other impurities. These were PF_3 (from the decomposition of PF_2I and P_2F_4) and PF_2H (probably from reaction of HI with P_2F_4[158,159]) and, to a much smaller extent, $F_2P\text{-}O\text{-}PF_2$ (source unknown). These impurities were separated from P_2F_4 and the small amount of PF_2I, and each obtained pure by high-vacuum distillation through traps held at -126°C, -136°C, -160°C and -196°C. Only P_2F_4 and PF_2I were retained at -126°C. $F_2P\text{-}O\text{-}PF_2$ was retained at -136°C, PF_2H at -160°C and PF_3 at -196°C. The identity and purity of the fractions retained at -136°C, -160°C and -196°C was confirmed by infra-red spectra (400 cm^{-1} to 4000 cm^{-1}. Model 337, Perkin-Elmer Ltd.) by comparison with literature data (References 159, 158 and see Part 2: Section 1b of this thesis). The purity of the PF_3 and PF_2H was also confirmed by their mass spectra (Part 2: Section ?).

No completely satisfactory method was found for the separation of P_2F_4 from the small PF_2I impurity. Repeated fractionation of the -196°C fraction of the impure P_2F_4 through a trap at -112°C to one at -196°C, however, retained most of the PF_2I impurity at -112°C as shown by the infra-red and mass spectra of the P_2F_4 obtained by this method (Part 2: Section 1d and 2a). Some P_2F_4 was, however, lost by this method, being retained at

-112°C. Alternatively, following deliberate mixing of P_2F_4 with PF_2I to remove the HI impurity from the latter, repeated fractionation of the -112°C fraction through a trap at -112°C to one at -196°C produced virtually pure PF_2I as the -112°C fraction, but some PF_2I was lost, passing through the -112°C trap to the one at -196°C.

PF_2I, P_2F_4 and PF_2H were stored separately in previously evacuated vessels at -196°C.

b. Vibrational Spectra.

(i) Infrared

The mid infrared region (4000 cm^{-1} to 375 cm^{-1}) was covered using a Model SP 100 Spectrophotometer (Unicam Instruments, Cambridge). This instrument was calibrated using liquid indene containingsmall amounts of camphor and cyclohexane.[293,294] This region of the spectrum of P_2F_4 was also recorded using a Model SP1200 Spectrophotometer (Unicam Instruments, Cambridge) fitted with a chart expansion accessory, and calibrated using a polystyrene film. Where accurate frequencies were not required, a Model 337 Spectrophotometer (Perkin-Elmer Ltd., Beaconsfield) was used allowing spectra to be recorded in a very short time. This speed was advantageous when studying unstable gases (PF_2I and P_2F_4). This instrument was also used for adjustment of the pressures of gases in the cell before use with the former two instruments (SP 100 and SP 1200).

A 10 cm. path-length cell was used throughout for gas-phase spectra in this region. KBr plates were originally sealed onto the glass body of the cell using Cold-Cure Silastomer 9161 (Hopkin and Williams Ltd., Chadwell

Heath, Essex). This white silicone-rubber, however, turned brown on exposure to PF_2I, and for this compound spectra were also recorded with the plates sealed using Picien Wax (Edwards High Vacuum Ltd., Crawley). Spectra of PF_2I and P_2F_4 in the solid-state were obtained by spraying these gases on to a liquid-nitrogen-cooled CsI plate in vacuo. The main features of the low temperature cell used are shown in Figure 34.

The region 420 cm^{-1} to 190 cm^{-1} of the gas-phase infrared spectrum of PF_2I was examined using a far infrared grating spectrometer constructed in the Department. A 10 cm. path-length cell was used with polyethylene windows sealed to the glass body of the cell using Picien Wax.

The region 420 cm^{-1} to 190 cm^{-1} of the gas-phase infrared spectrum of PF_2I was covered using a far-infrared interferometric spectrometer ("Cube" Interferometer, Grubb-Parsons/N.P.L.)[100 Gauge Beam-Splitter]. This instrument was adapted to take a 110 cm. path-length gas cell with polyethylene windows, and was also used in the attempt to record the gas-phase infrared spectrum of P_2F_4 over the range 400 cm^{-1} to 30 cm^{-1} (using a 2) Gauge Beam-Splitter; see Part 2;; Section 1d).

(ii) Raman

All Raman spectra were recorded using a Cary 81 Raman Spectrometer (Cary Instruments, Subsidiary of Varian, California) detecting 180° scattered radiation. A He-Ne laser[6328Å][50 mw] (Spectra-Physics) was used for excitation.

Solid-state Raman spectra of PF_2I and P_2F_4 were obtained using an evacuated low-temperature cell designed by the present author, and

FIGURE 34.

Low-temperature Infrared Cell.

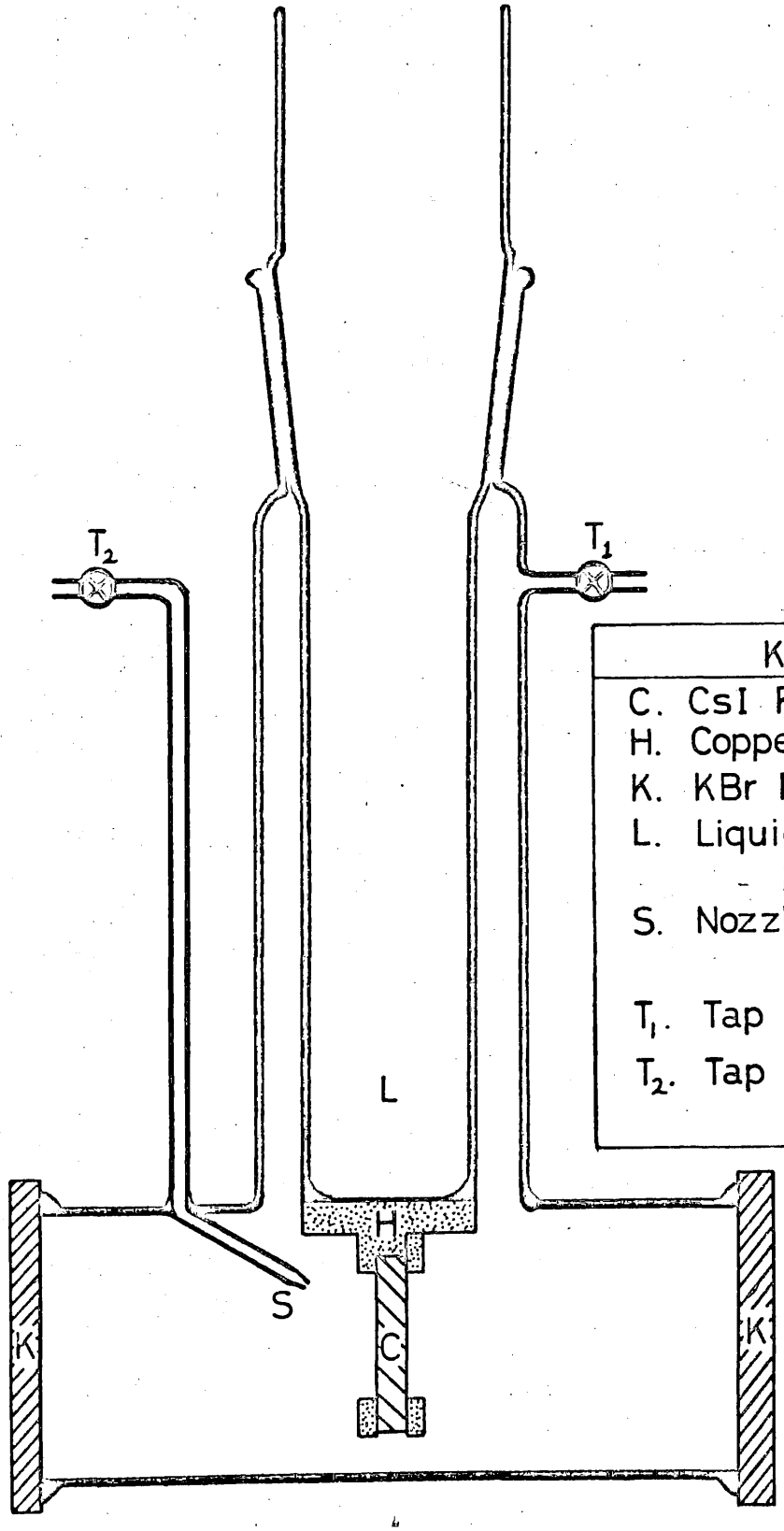

KEY

C. CsI Plate.
H. Copper Holder for 'C'.
K. KBr Plates.
L. Liquid-Nitrogen Reservoir.
S. Nozzle for Spraying Gases.
T_1. Tap for Evacuation.
T_2. Tap for Introduction of Gas.

FIGURE 35.

Low-temperature Raman Cell.

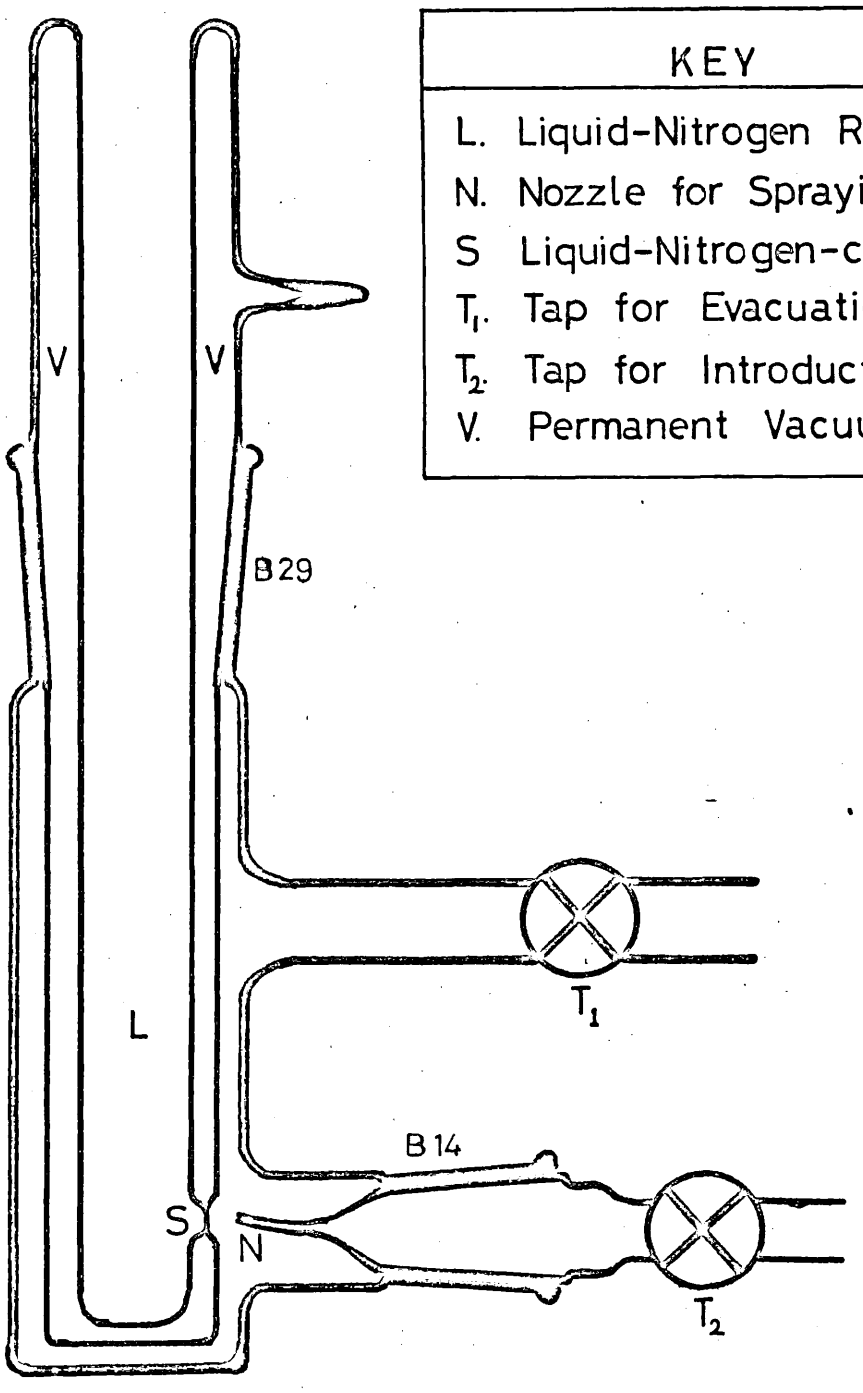

KEY
L. Liquid-Nitrogen Reservoir.
N. Nozzle for Spraying Gases.
S Liquid-Nitrogen-cooled Spot.
T_1. Tap for Evacuation.
T_2. Tap for Introduction of Gas.
V. Permanent Vacuum.

constructed in the Department. The main features of this cell are shown in Figure 35. A jet of the gaseous compound was allowed to impinge on a spot cooled by liquid-nitrogen: the spot was then rotated before placing the cell in the sample compartment of the Raman Spectrometer.

The liquid-phase Raman spectrum of PF_2I was obtained by allowing PF_2I to melt while sealed in a capillary tube.

APPENDIX

VACUUM LINE

A vacuum line was designed and fabricated from 'Pyrex' glass to allow the preparation, purification, manipulation and storage of the phosphorus-fluorine and nitrogen-fluorine gases. This apparatus is shown in Figure 36.

The principal feature of this vacuum line was the use of grease-free high-vacuum stopcocks for the sections of the line used for purification and storage. This allowed the gases to be manipulated while contacting only 'Pyrex' glass and P.T.F.E.. Initially, grease-free stopcocks made commercially by J. Young (Scientific) Glassware Ltd., Acton, were used, but were found inadequate, despite several small design modifications by the manufacturers. The glass-pistons, fitted with P.T.F.E. 'O' rings (in a later modification a Viton A 'O' ring was used to back the vacuum-to-atmosphere P.T.F.E. 'O' ring seal), were found to be vulnerable to fracture, especially at the constrictions incorporated for the seating of the 'O' rings. The above stopcocks were therefore replaced by 'Uniform' No-grease High-vacuum stopcocks (Glass Precision Engineering Ltd., Hemel Hempstead). These stopcocks had a solid P.T.F.E. piston, using two P.T.F.E. rings to maintain the vacuum-to-atmosphere seal, and were found very satisfactory under normal operating conditions. However, at lower temperatures (less than about 20°C), it was found that the vacuum-to-atmosphere seal was not maintained. It was, therefore, necessary to modify a few of these stopcocks in order to maintain this seal at lower temperatures. This was especially important for the stopcocks that were

FIGURE 36: The Vacuum Line.

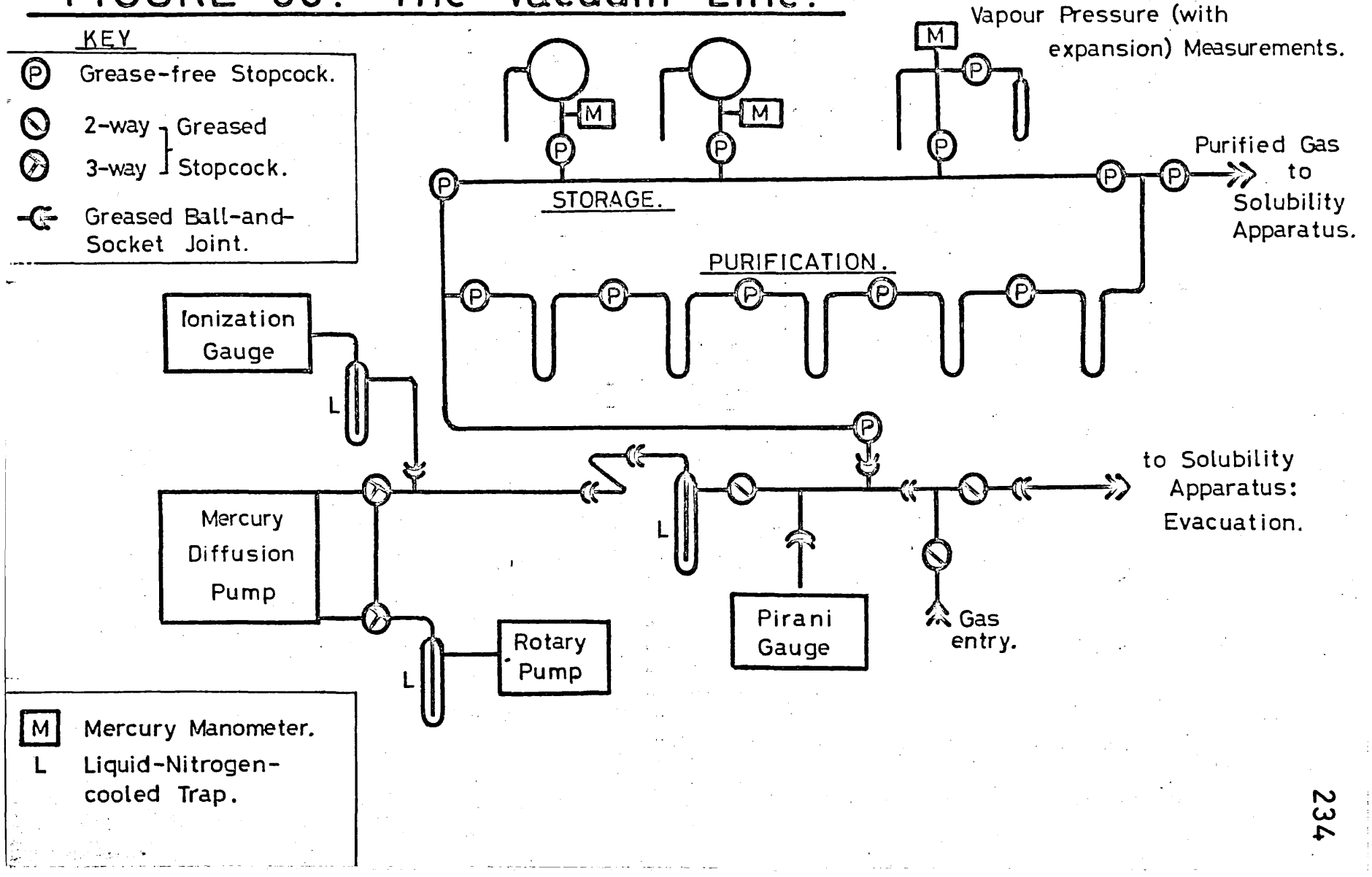

FIGURE 37.
Modified 'Uniform' Stopcock.

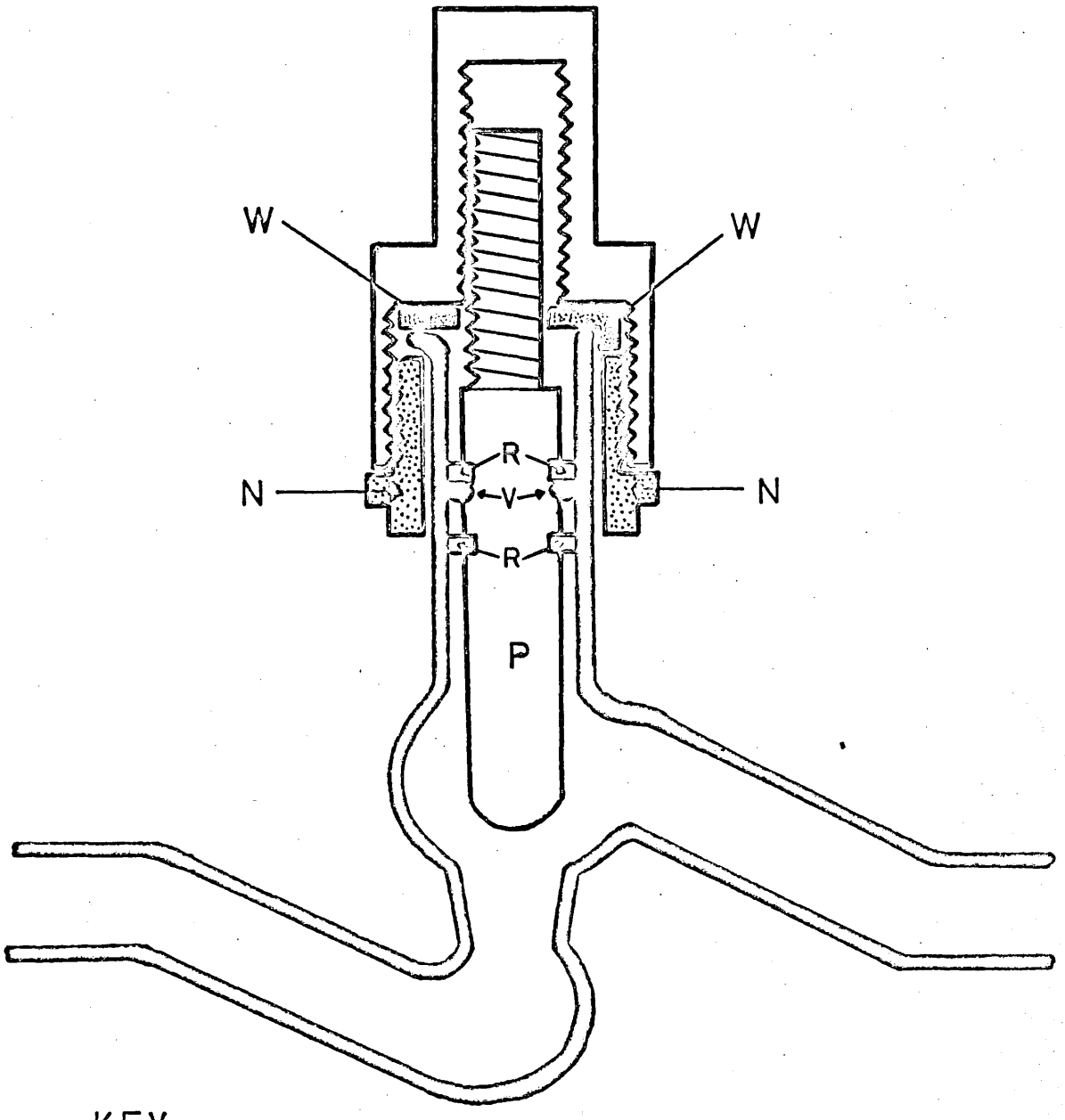

KEY

N.	Retaining Nut.
P.	P.T.F.E. Piston.
R.	P.T.F.E. 'O' Ring.
V.	Viton 'O' Ring.
W.	Location Washer.

used inside the thermostating tank in the gas-solubility apparatus (Part 1; Section 1e). This modification involved the incorporation of a Viton A ring to back the P.T.F.E. rings, and is shown in Figure 37.

A Pirani Vacuum Gauge (Edwards High Vacuum Ltd., Crawley) was used for general monitoring of the pressure in the vacuum line, but the low pressure range (linear from 0 to 5×10^{-3} torr) was not sufficiently sensitive or accurate for precise pressure determinations. An ionization gauge (Ionivac 1M30 with gauge head 1R32C, Leybold-Heraeus GmbH and Co., Cologne) was therefore used when precise pressure estimations or greater sensitivity were required (e.g. Part 1; Section 1d). Pressures down to 10^{-6} torr (the lower limit of the gauge head) could be maintained.

With the exceptions of traps at -80°C (solid CO_2/acetone) and at -196°C (liquid-nitrogen), traps were refrigerated using standard slush baths,[295] prepared from common solvents cooled using liquid-nitrogen. All trap temperatures quoted in this thesis are therefore nominal values, being the literature[295] temperatures for the slushes used.

REFERENCES

REFERENCES

1. Moissan, H., "Le Fluor et ses composés", p.245, Steinheil, Paris (1900).

2. Sidgwick, N.V., "The Chemical Elements and their Compounds", Vol. 1, p.704, Clarendon Press, Oxford (1950).

3. Ruff, O., and Geisel, E., Ber., 36, 2677 (1903).

4. Ruff, O., Fischer, J., and Luft, L., Z. Anorg. Allgem. Chem., 172, 417 (1928).

5. Haller, J.F., Ph. D. Thesis, Cornell University (1942).

6. Bauer, S.H., J. Amer. Chem. Soc., 69, 3104 (1947).

7. Gervasi, J.A., Brown, H., and Bigelow, L.A., J. Amer. Chem. Soc., 78, 1679 (1956).

8. Holzmann, R.T., "Advanced Propellant Chemistry", Advances in Chemistry Series, No.54, p.1, American Chemical Society, Washington D.C. (1966).

9. Barrère, M., Office Nationale d'Etudes et de Recherche Aerospatiales, Missiles Rockets, 15, 32 (1964).

10. Colburn, C.B., and Kennedy, A., J. Amer. Chem. Soc., 80, 5004 (1958).

11. Colburn, C.B., in "Advances in Fluorine Chemistry", Vol. III, ed. Stacey, M., Tatlow, J.C., and Sharpe, A.G., Butterworths, Washington D.C. (1962).

12. Ruff, O., and Staub, L., Z. Anorg. Allgem. Chem., 198, 32 (1931).

13. Kennedy, A., and Colburn, C.B., J. Amer. Chem. Soc., 81, 2906 (1959).

14. Freeman, J.P., Kennedy, A., and Colburn, C.B., J. Amer. Chem. Soc., 82, 5304 (1960).

15. Petry, R.C., J. Amer. Chem. Soc., 82, 2400 (1960).

16. Callery Chemical Company, Results on Contract No. NOa(s) 58-454-d, January 31, 1961 - September 30, 1961.

17. Marshall, M.D., and Bernauer, W.H., United States Patent 3,238,013 (1966).

18. Hoffman, C.J., and Neville, R.G., Chem. Rev., 62, 1 (1962).

19. Colburn, C.B., Parker, C.O., and Stevenson, K., p.30N, Abs. 138th A.C.S. Meeting, New York, September 1960.

20. Rohm and Haas Company, Unpublished Results on Contract No. DA-01-021-ORD-5135, January 25, 1957 - September 1, 1960.

21. Gould, J.R., and Smith, R.A., Chem. Eng. News, 38, 85, (1960).

22. E.I. du Pont de Nemours and Company, British Patent No. 895,943, May 9, 1962.

23. Martin, K.J., J. Amer. Chem. Soc., 87, 394 (1965).

24. Hoffman, C.J., and Neville, R.G., Chem. Rev., 62, 1 (1962).

25. Pankratov, A.V., Russ. Chem. Rev., 32, 157 (1963).

26. Ruff, J.K., Chem. Rev., 67, 665 (1967).

27. Lawless, E.W., and Smith, I.C., "Inorganic High-energy Oxidizers", Edward Arnold Ltd., London (1968).

28. Armstrong, G.T., Marantz, S., and Coyle, C.F., J. Amer. Chem. Soc., 81, 3798 (1959).

29. Jarry, R.L., and Miller, H.C., J. Phys. Chem., 60, 1412 (1956).

30. Emeleus, H.J., and Sharpe, A.G., ed., "Advances in Inorganic and Radio Chemistry", Vol. 3, Academic Press, Inc., New York (1961).

31. Rogers, M.T., Speirs, J.L., and Panish, M.B., J. Phys. Chem., 61, 366 (1957).

32. American Oil Company, First Annual Report, Contract No. DA-31-124-ARO(D)-78, Feb. 1964.

33. Ruff, O., Z. Anorg. Allgem. Chem., 197, 273 (1931).

34. Torkelson, T.R., Oyen, F., Sadek, S.E., and Rowe, V.K., Toxicol. App. Pharmacol., 4, 770 (1962).

35. Clayton, J.W., J. Occupational Med., 5, 271 (1962).

36. Carson, T.R., and Wilinski, F.T., Toxicol. App. Pharmacol., 6, 447 (1964).

37. Lester, D., J. Pharmacol. Exptl. Therap., 77, 154 (1943).

38. Hurst, G.L., and Khayat, S.I., "Advances in Chemistry Series", No. 54, "Advanced Propellant Chemistry," p.245, American Chemical Society, Washington D.C. (1966).

39. Comly, H.H., J. Amer. Med. Ass., 129, 112 (1945).

40. Sattelmacher, P.G., "MethÄmoglobinÄmie durch Nitrate im Trinkwasser", Schriftenreihe d. Vereins f. Wasser-, Boden-, und Lufthygiene, No. 20, Fischer, Stuttgart (1962).

41. Subbotin, F.N., Materialy Resp. Itog. Nauchn. Konf. po Gigiene, Leningrad, Sb. 1963; Chem. Abstr., 62, 12359 (1965).

42. Schwartz, A.S., and Rector, E.J., Amer. J. Dis. Child., 60, 652 (1940).

43. Bergh, A.A.H. Van Den, Dtsch. Arch. Klin. Med., 83, 86 (1905).

44. Hölscher, P.M., and Matzschka, J., Dtsch. Med. Wschr., 89, 1751 (1964).

45. Sinios, A., Münch. Med. Wschr., 106, 1100 (1964).

46. Sinios, A., and Wodsak, W., Dtsch. Med. Wschr., 90, 1856 (1965).

47. Singley, T.L., Ann. Intern. Med., 57, 800 (1962).

48. Becker, E., Dtsch. Med. Rundschau, 3, 900 (1949).

49. Büch, O., Sammlung V. Vergiftungsfällen, 14, 53 (1952).

50. Tepperman, J., Marquardt, R., Reifenstein, G.H., and Lozner, E.L., J. Amer. Med. Ass., 146, 983 (1951).

51. Austin, J.H., and Drabkin, D.L., J. Biol. Chem., 112, 67 (1935).

52. Marshall, W., and Marshall, C.R., J. Biol. Chem., 158, 137 (1945).

53. Kakizaki, T., Sato, M., and Hasegawa, H., Ind. Health (Japan), 2, 124 (1964); Chem. Abstr., 62, 12063 (1965).

54. Jung, F., and Remmer, H., Arch. Exp. Path. Pharmak., 206, 459 (1949).

55. Remmer, H., Diss. Berlin, 1944 "Über die Reaktion des Nitritis mit Blutvarbstoff".

56. Kiese, M., Pharmacol. Rev., 18, 1091 (1966).

57. Botke, K., Creinacher, I., and Tietze, C., Arch. Exp. Path. Pharmak., 229, 220 (1956).

58. Jung, F., and Stoytchev, T., Acta. Biol. Med. Germ., 14, 482 (1965).

59. Kiese, M., and Rauscher, E., Arch. Exptl. Pathol. Pharmakol., 251, 201 (1965).

60. Cohen, C., Martinez, M., and Hochstein, P., Biochemistry, 3, 901 (1964).

61. Rein, H., Ristau, O., and Jung, F., Folia Haemat., Lpz., 82, 191 (1964).

62. Kiese, M., and Soetbeer, H., Arch. Exp. Path. Pharmak., 207, 437 (1949).

63. Kiese, M., and Weger, N., Arch. Toxikol., 21, 89 (1965).

64. Spicer, S.S., and Neal, P.A., J. Pharmacol., 95, 438 (1949).

65. Barton, G.M.G., Lancet, 1, 190 (1954).

66. Dost, F.N., Finch, A., Reed, D.J., and Wang, C.H., J. Inorg. Nucl. Chem., 31, 3765 (1969).

67. Beach, L.K., J. Inorg. Nucl. Chem., 26, 2033 (1964).

68. Dost, F.N., Reed, D.J., Cooper, T.D., and Wang, C.H., Toxicol. App. Pharmacol., 17, 573 (1970).

69. Dost, F.N., Reed, D.J., and Wang, C.H., Toxicol. App. Pharmacol., 17, 585 (1970).

70. Greenberg, L.A., and Lester, D., J. Pharmacol. Exp. Ther., 81, 182 (1944).

71. Dost, F.N., Reed, D.J., Johnson, D.E., and Wang, C.H., J. Pharmacol. Exp. Ther., 176, 448 (1971).

72. Kotani, M., Ann. N.Y. Acad. Sci., 158, 20 (1969).

73. Markham, A.E., and Kobe, K.A., Chem.Rev., 28, 519 (1941).

74. Croxton, F.E., U.S. Department of Commerce, Office of Technical Service, AECU-100 (1949).

75. Hildebrand, J.H., and Scott, R.L., "The Solubility of Nonelectrolytes", Reinhold Publishing Corp., New York, 3rd Ed. (1950).

76. Hildebrand, J.H., and Scott, R.L., "Regular Solutions," Prentice-Hall, Inc., Englewood Cliffs, N.J. (1962).

77. Battino, R., and Clever, H.L., Chem. Rev., 66, 395 (1966).

78. Scott, R.L., J. Phys. Chem., 62, 136 (1958).

79. Hildebrand, J.H., Prausnitz, J.M., and Scott, R.L., "Regular and Related Solutions - The Solubility of Gases, Liquids and Solids", Van Nostrand Reinhold Co., New York (1970).

80. Dymond, J.H., J. Phys. Chem., 71, 1829 (1967).

81. Hildebrand, J.H., Proc. Nat. Acad. Sci. U.S., 57, 542 (1967).

82. Miller, K.W., J. Phys. Chem., 72, 2243 (1968).

83. Friedman, H.L., J. Amer. Chem. Soc., 76, 3294 (1954).

84. Ashton, J.T., Dawe, R.A., Miller, K.W., Smith, E.B., and Stickings, E.J., J. Chem. Soc., 1968A, 1793 (1968).

85. Morrison, T.J., and Johnstone, N.B.B., J. Chem. Soc., 1955, 3655 (1955).

86. Winkler, L.W., Ber., 22, 1764 (1889).

87. Pierce, L., and Pace, E.L., J. Chem. Phys., 23, 551 (1955).

88. Dymond, J., and Hildebrand, J.H., Ind. Eng. Chem. Fundamentals, 6, 130 (1967).

89. Cook, M.W., and Hanson, D.N., Rev. Sci. Instr., 28, 370 (1957).

90. Mader, W.J., Vold, R.D., and Vold, M.J., "Physical Methods of Organic Chemistry", 3rd Ed., Pt. I, Vol. 1, Interscience Publishers, Inc., New York (1959) p.677.

91. Cook, M.W., Hanson, D.N., and Alder, B.J., J. Chem. Phys., 20, 748 (1957).

92. Ben-Naim, A., and Baer, S., Trans. Faraday Soc., 59, 2735 (1963).

93. Burrows, G., and Preece, F.H., J. Appl. Chem. (London), 3, 451 (1953).

94. Dombacher, W.C., Johnson, D.P., and Cross, J.L., "Mercury Barometers and Manometers", Nat. Bur. Stand. Monograph 8, U.S. Dept. of Commerce, Washington D.C. (1960).

95. Sears, J.E., and Clark, J.S., Proc. Roy. Soc., 139A, 130 (1933).

96. Beattie, J.A., Jacobus, D.D., Gaines, J.M., Jr., Benedict, M., and Blaisdell, B.E., Proc. Am. Acad. Arts Sci., 74, 327 (1941).

97. Horiuti, J., Sci. Papers Inst. Phys. Chem. Res. Tokyo, 17, 125 (1931).

98. Clever, H.L., Battino, R., Saylor, J.H., and Gross, P.M., J. Phys. Chem., 61, 1078 (1957).

99. Baldwin, R.R., and Daniel, S.G., J. Appl. Chem. (London), 2, 161 (1952).

100. Colburn, C.B., and Johnson, F.A., Inorg. Chem., 1, 715 (1962).

101. Johnson, F.A., and Colburn, C.B., J. Amer. Chem. Soc., 83, 3043 (1961).

102. Schoenfelder, C.W., J. Chromatog., 7, 281 (1962).

103. Kuznetsova, T.V., Egorova, L.F., Rips, S.M., Zorchenkov, A.N., and Pankratov, A.V., Izvest. Sibirsk. Otdel. Akad. Nauk SSSR, Ser. Khim. Nauk, 1, 68 (1968). English Translation UDC 546.16'17:541.12.03.

104. Harmony, M.D., and Myers, R.J., J. Chem. Phys., 37, 636 (1962).

105. Durig, J.R., and Lord, R.C. Spectrochim. Acta, 19, 1377 (1963).

106. Kotov, Y.I., and Tatevski, V.M., Opt. i Spektroskopiya, 14, 443 (1963) [p. 237 in English Translation].

107. Moskvitina, E.N., Kuzyakov, Y.Y., Knyazeva, N.A., and Tatevskii, V.M., Opt. i Spektroskopiya, 16, 768 (1964). [p. 418 in English Translation].

108. Durig, J.R., and Clark, J.W., J. Chem. Phys., 48, 3216 (1968).

109. Koster, D.F., and Miller, F.A., Spectrochim. Acta., 24A, 1487 (1968).

110. Marshall, M.D., and Dermuer, W.H., U.S. Patent No. 3,238,013, March 1, 1966.

111. Marshall, M.D., Private Communication, Callery Chemical Company (1969).

112. Cook, M.W., Ph. D. Thesis, U.S. Atomic Energy Commission, UCRL-2459, Jan. 14 (1954).

113. Kaye, G.W.C., and Laby, T.H., "Tables of Physical and Chemical Constants and Some Mathematical Functions", 13th Ed. (1966), New Impression (1969), Longmans, Green and Co. Ltd., London.

114. Kine, J., "Physical Organic Chemistry", p. 137, McGraw-Hill, New York (1956).

115. Kunnetsova, T.V., Egorova, L.F. Kips, S.N. Zercheninov, A.N., and Pankratov, A.V., Izvest. Sibirsk, Otdel. Akad. Nauk SSSR, Ser. Khim. Nauk, 1, 68 (1969). English Translation UDC 546.16'17: 541.12.03, p.59.

116. Pankratov, A.V., Rips, S.M., Zercheninov, A.N., and Kuznetsova, T.V., Russian J. Phys. Chem., 43, 205 (1969).

117. "Handbook of Chemistry and Physics," 45th edition, Ed. R.C. Weast, Chemical Rubber Co. Ltd., Ohio. (1964-1965).

118. Osborne, N.S., and Meyers, C.H., J. Res. Nat. Bur. Stand., 13, 1 (1934).

119. Tyrer, D., J. Chem. Soc., 105, 2534 (1914).
Philip, N.M., Proc. Indian Acad. Sci., 9A, 109 (1939).
Gibson, R.E., and Leffler, O.H., J. Amer. Chem. Soc., 63, 898 (1941).
Marshall, J.G., Staveley, L.A.K., and Hart, K.R., Trans. Faraday Soc., 52, 23 (1956).

120. Rossini, F.D., and Deming, W.E., J. Washington Acad. Sci., 29, 416 (1939).

121. Frank, H.S., and Evans, M.W., J. Chem. Phys., 13, 507 (1945).

122. Némethy, G., and Scheraga, H.A., J. Chem. Phys., 36, 3382, 3401, (1962).

123. Balazs, E.A., Bothner-By, A.A., and Gergely, J., J. Mol. Biol. 1, 147 (1959).

124. Uhlig, H.H., J. Phys. Chem., 41, 1215 (1937).

125. Illey, D.D., Trans. Faraday Soc., 35, 1201, 1421 (1939).

126. Pierotti, R.A., J. Phys. Chem., 67, 1840 (1963).

127. Reiss, H., Frisch, H.L., Helfand, E., and Lebowitz, J.L., J. Chem. Phys., 32, 119 (1960).

128. Pierotti, R.A., J. Chem. Phys., 69, 281 (1965).

129. BenNaim, A., and Friedman, H.L., J. Phys. Chem., 71, 448 (1967).

130. Dell, R.F., Trans. Faraday Soc., 33, 496 (1937).

131. Herington, E.F.G., J. Amer. Chem. Soc., 73, 5803 (1951).

132. Longuet-Higgins, H.C., Proc. Roy. Soc., 205A, 247 (1951).

133. Powell, R.E., and Latimer, W.M., J. Chem. Phys., 19, 1139 (1951).

134. Stauffer Chemical Company, Technical Bulletin, "Nitrogen Trifluoride and Tetrafluorohydrazine," Market Development Department (Feb. 1960).

135. Miller, K.W., and Hildebrand, J.H., J. Amer. Chem. Soc., 90, 3001 (1968).

136. Morrison, T.J., and Johnson, N.B., J. Chem. Soc., 1954, 3441 (1954).

137. Parmelee, H.M., Refrig. Eng., 61, 1341 (1953).

138. Lennard-Jones, J., and Pople, J.A., Proc. Roy. Soc., 205A, 155 (1951). Pople, J.A., Proc. Roy. Soc., 205A, 163 (1951).

139. Morrison, T.J., and Johnson, N.B., J. Chem. Soc., 1955, 3655 (1955).

140. Long, C., Ed., "Biochemists' Handbook", E. and F.N. Spon Ltd., London (1961).

141. Braunitzer, G., Hilse, K., Rudloff, V., and Hilschmann, N., Adv. Protein Chem., 19, 1 (1964).

142. Dost, F.N., Reed, D.J., Finch, A., and Wang, C.H., Toxicol. App. Pharmacol., 19, 766 (1971).

143. Vogel, A.I., "A Textbook of Quantitative Inorganic Analysis including Elementary Instrumental Analysis", Longmans, Green and Co. Ltd., London, 3rd Ed. (1961).

144. Jones, E.A. and Woltz, P.J.H., J. Chem. Phys., 19, 1516 (1950).

145. Woltz, P.J.H., Jones, E.A., and Nielsen, A.H., J. Chem Phys., 20, 378 (1952).

146. Penner, S.S., and Weber, D., J. Chem. Phys., 21, 649 (1953).

147. Nakamoto, K., "Infrared Spectra of Inorganic and Coordination Compounds", J. Wiley and Sons, Inc., New York (1963).

148. Arakawa, E.T., and Nielsen, A.H., J. Mol. Spectroscopy, 2, 413, (1958).

149. Colburn, C.B., and Kennedy, A., J. Amer. Chem. Soc., 80, 5004 (1958).

150. Longhram, E.D., and Nader, C.L., J. Chem. Phys., 32, 1578 (1960).

151. Herron, J.T., and Dibeler, V.H., J. Chem. Phys., 33, 1595 (1960).

152. Shinn, M.D., Ind. Eng. Chem. Analyt., 13, 33 (1941).

153. Kershaw, W.F., and Chamberlin, N.S., Ind. Eng. Chem. Analyt., 14, 312 (1942).

154. Moissan, H., Compt. Rend., 99, 655 (1884).

155. Cavell, R.G., J. Chem. Soc., 1964, 1992 (1964).

156. Rudolph, R.W., Morse, J.G., and Parry, R.W., Inorg. Chem., 5, 1464 (1966).

157. Morse, J.G., Cohn, K., Rudolph, R.W., and Parry, R.W., Inorg. Synth., 10, 147 (1967).

158. Rudolph, R.W., and Parry, R.W., Inorg. Chem., 4, 1339 (1965).

159. Rudolph, R.W., Taylor, R.C., and Parry, R.W., J. Amer. Chem. Soc., 88, 3729 (1966).

160. Lustig, M., Ruff, J.K., and Colburn, C.B., J. Amer. Chem. Soc., 88, 3875 (1966).

161. Cowley, A.H., Chem. Rev., 65, 617 (1965).

162. Huheey, J.E., J. Chem. Educ., 40, 153 (1963).

163. Maier, L., Progr. Inorg. Chem., 5, 27 (1963).

164. Paddock, N.L., Roy. Inst. Chem. Lectures, Monographs, Reports, No.2 (1962).

165. Sasse, K., "Methoden der organischen Chemie", Vol. 12, Pt. 1, p.182, Verlag, Stuttgart (1963).

166. Banks, R.E., and Haszeldine, R.N., Advan. Inorg. Chem. Radiochem., 1, 337 (1961).

167. Gay-Lussac, J.L., Ann. Chim. Phys., (1), 88, 311 (1813).

168. Gay-Lussac, J.L., Ann. Chim. Phys., (1), 91, 5 (1814).

169. Germann, F.E.E., and Traxler, R.N., J. Amer. Chem. Soc., 49, 307 (1927).

170. Baudler, E., Z. Naturforsch., 13b, 266 (1958).

171. Levchenko, E.S., Sheinkman, I.E., and Kirsanov, A.V., Zh. Obshch. Khim., 29, 1474 (1959); Chem. Abs., 54, 7395 (1960).

172. Jolly, W.L., Lindahl, C.B., and Kopp, R.N., Inorg. Chem., 1, 958 (1962).

173. Finch, A., Canad. J. Chem., 37, 1793 (1959).

174. Sandoval, A.A., and Moser, H.C., Inorg. Chem., 2, 27 (1963).

175. Teague, J.L., and Sandoval, A.A., Radiochim. Acta, 11, 57 (1969).

176. Booth, H.S., and Bozarth, A.R., J. Amer. Chem. Soc., 55, 3390, (1933).

177. Booth, H.S., and Frary, S.G., J. Amer. Chem. Soc., 61, 2934 (1939).

178. Yost, D.M., and Anderson, T.F., J. Chem. Phys., 2, 624 (1934).

179. Dausch, L.W., and Smith, D.C., Analyt. Chem., 23, 853 (1951).

180. Wilson, M.K., and Polo, S.R., J. Chem. Phys., 20, 1716 (1952).

181. Gutowsky, H.S., and Liehr, A.D., J. Chem. Phys., 20, 1652 (1952).

182. Reichman, S., and Overend, J., Spectrochim. Acta, 26A, 379 (1970).

183. Gillespie, R.J., J. Chem. Educ., 40, 295 (1963).

184. Gillespie, R.J., Angew. Chem., 79, 885 (1967); Angew. Chem. Intern. Ed. Engl., 6, 819 (1967).

185. Gillespie, R.J., J. Amer. Chem. Soc., 82, 5978 (1960).

186. Hansen, K.W., and Bartell, L.S., Inorg. Chem., 4, 1775 (1965).

187. Bartell, L.S., and Hansen, K.W., Inorg. Chem., 4, 1777 (1965).

188. Brockway, L.O., and Hall, F.T., J. Amer. Chem. Soc., 56, 2373 (1934).

189. Pauling, L., and Brockway, L.O., J. Amer. Chem. Soc., 57, 2684 (1935).

190. Mirri, A.M., Scappini, F., and Favero, P.G., Spectrochim. Acta., 21, 965 (1965).

191. Gillian, O.R., Edwards, H.D., and Gordy, W., Phys. Rev., 75, 1014 (1949).

192. Kisliuk, P., J. Chem. Phys., 22, 86 (1954).

193. Williams, Q., Sheridan, J., and Gordy, W., J. Chem. Phys., 20, 164 (1952).

194. Mirri, A.M., J. Chem. Phys., 47, 2823 (1967).

195. Horch, O.L., University Microfilms, Ann Arbor, Mich., Order No. 64-827; Diss. Abs., 24, 2286 (1963).

196. Morino, Y., Uchitsu, K., and Moritani, T., Inorg. Chem., 8, 867 (1969).

197. Müller, A., Diemann, E., Krebs, B., and Glemser, O., Z. Naturforsch., 23b, 599 (1968).

198. Müller, A., Krebs, B., Ulvebrell, I., Vini, B., and Cyvin, S.J., J. Mol. Structure, 2, 149 (1968).

199. Ulvebrell, I., Vini, B., Cyvin, S.J., Müller, A., and Krebs, B., J. Mol. Structure, 2, 158 (1968).

200. Ehren, E.R., J. Chem. Phys., 23, 1954 (1956).

201. Mahler, H., and Schmidt, L., Z. Anorg. Chem., 292, 249 (1957).

202. Frankiss, S.G., and Miller, F.A., Spectrochim. Acta., 21, 1235 (1965).

203. Frankiss, S.G., Miller, F.A., Starmovich, H., and Sans, T.T., Spectrochim. Acta, 23A, 543 (1967).

204. Leung, Y.C., and Waser, J., J. Chem. Phys., 60, 539 (1956).

205. Durig, J.R., and Divorio, J.S., Inorg. Chem., 8, 2706 (1969).

206. Collin, R.L., and Lipscomb, W.N., Acta Cryst., 4, 10 (1951).

207. Ewing, W.I., Zocchi, M., and Levy, H.A., Program of the Annual Meeting of the American Crystallographic Association, Paper H3, Aug, 1961.

208. Kasuya, T., and Kojima, T., J. Phys. Soc. Japan, 18, 364 (1963).

209. Cignàre, P.A., and Schomaker, V., J. Amer. Chem. Soc., 65, 2035 (1963).

210. Morino, Y., Iijima, T., and Murata, Y., Bull. Chem. Soc. Japan, 33, 46 (1960).

211. Yamaguchi, A., Ichishima, I., Shimanouchi, T., and Mizushima, S-I, Spectrochim. Acta, 16, 1471 (1960).

212. Lide, D.R., and Mann, D.R., J. Chem. Phys., 31, 1129 (1959).

213. Bohn, R.K., and Bauer, S.H., Inorg. Chem., 6, 304 (1967).

214. Durig, J.R., and Clark, J.W., J. Chem. Phys., 48, 3216 (1968).

215. Colburn, C.B., Johnson, F.A., and Haney, C., J. Chem. Phys., 43, 4506 (1965).

216. Johnson, F.A., and Rudolph, R.W., J. Chem. Phys., 47, 5449 (1967).

217. Rudolph, R.W., and Newmark, R.A., J. Amer. Chem. Soc., 92, 1195 (1970).

218. Finer, D.C., and Harris, R.K., Chem. Comm., 1968, 110 (1968).

219. Couley, A.H., and White, W.D., J. Amer. Chem. Soc., 91, 1913, 1917, 1922 (1969).

220. Veillard, A., Theoret. Chim. Acta. 5, 413 (1966).

221. Pedersen, L., and Morokuma, K., J. Chem. Phys., 46, 3941 (1967).

222. Fink, W.H., Pan, D.C., and Allen, L.C., J. Chem. Phys., 47, 895 (1967).

223. Gillespie, R.J., and Nyholm, R.S., Quart. Rev., 11, 339 (1957).

224. Gillespie, R.J., Canad. J. Chem., 38, 818 (1960).

225. Rudolph, R.W., and Schiller, H.W., J. Amer. Chem. Soc., 90, 3581 (1968).

226. Rudolph, R.W., and Schiller, H.W., Inorg. Chem., 10, 2500 (1971).

227. Kuczowski, R.L., Schiller, H.W., and Rudolph, R.W., Inorg. Chem., 10, 2505 (1971).

228. Morse, K.W., and Parry, R.W., J. Amer. Chem. Soc., 89, 172 (1967).

229. Solan, D., and Timms, P.L., Chem. Comm., 1968, 1540 (1968).

230. Wei, M.S., and Current, J.H., J. Chem. Phys., 52, 1592 (1970).

231. Kasai, P.H., and Whipple, E.B., Mol. Phys., 9, 497 (1965).

232. Cowley, A.H., Chem. Rev., 65, 617 (1965).

233. Grishin, N.N., Bogolybov, G.M., and Petrov, A.A., Zhur. Obshchei Khim., 38, 2603 (1968); Chem. Abs., 70, 96045 (1969).

234. Sandoval, A.A., Moser, H.C., and Kiser, R.W., J. Phys. Chem., 67, 124 (1963).

235. Saalfeld, F.E., and Svec, H.J., Inorg. Chem., 3, 1442 (1964).

236. Finch, A., Gardner, P.J., and Hameed, A., J. Inorg. Nucl. Chem., 32, 2869 (1970).

237. Grant, L.R., and Burg, A.B., J. Amer. Chem. Soc., 84, 1834 (1962).

238. Burg, A.B., et al, WADC Tech. Rept. 57-126, Pt. 3, 82 (1959).

239. Mahoney, J.E., Univ. Microfilms (Ann Arbor, Mich.), Order No. 61-4314; Diss Abs., 22, 1400 (1961).

240. Burdett, J.K., Hodges, L., Dunning, V., and Current, J.H., J. Chem. Phys., 74, 4053 (1970).

241. Taft, R.W. Jr., in Newman, M.S., "Steric Effects in Organic Chemistry", J. Wiley and Sons, New York (1956).

242. Kagarise, R.E., J. Amer. Chem. Soc., 77, 1377 (1955).

243. Stammreich, H., Forneris, R., and Tavares, V., J. Chem. Phys., 25, 580 (1956).

244. Manley, T.R., and Williams, D.A., Spectrochim. Acta, 21, 1773 (1965).

245. Tables of Interatomic Distances and Configuration in Molecules and Ions. The Chemical Society, London.
a. Special Publication No.11 (1958).
b. Special Publication No.18 (1965).

246. Williams, Q., Sheridan, J., and Gordy, W., J. Chem. Phys., 20, 164 (1952).

247. Wagman, D.D., Evans, W.H., Parker, V.B., Halow, I., Bailey, S.M., and Schumm, R.H., "Selected Values of Chemical Thermodynamic Properties", Technical Note 270-3, Nat. Bur. Stand., Washington D.C. (1968).

248. Duus, H.C., and Nykytiuk, D.P., J. Chem. Eng. Data, 9, 585 (1964).

249. Lynden-Bell, R.M., Trans. Faraday Soc., 57, 888 (1961).

250. Solan, D., Ph. D. Thesis, University of California, Berkeley, U.S.A. (1969).

251. Gordy, W., J. Chem. Phys., 14, 305 (1946).

252. Johnson, F.A., "Advances in Chemistry Series", No. 36, pp. 123-127, American Chemical Society, Washington, D.C. (1962).

253. Johnson, F.A., and Colburn, C.B., J. Amer. Chem. Soc., 83, 3043 (1961).

254. Kuznetsova, L.H., Kuzyakov, Y.Y., and Tatevski, V.M., Opt. i Spectroskopiya, 16, 542 (1964).

255. Ettinger, R., and Colburn, C.B., Inorg. Chem., 2, 1311 (1963).

256. Piette, L.H., Johnson, F.A., Booman, K.A., and Colburn, C.B., J. Chem. Phys., 35, 1481 (1961).

257. Doorenbos, H.E., and Loy, B.R., J. Chem. Phys., 32, 2393 (1964).

258. Herron, J.T., and Dibeler, V.H., J. Chem. Phys., 35, 747 (1961).

259. Saalfeld, F.E., and Svec, H.J., Inorg. Chem., 2, 50 (1963).

260. Finch, A., Hameed, A., Gardner, P.J., and Paul, N., Chem. Comm., 1969, 391 (1969).

261. Field, F.H., and Franklin, J.L., "Electron Impact Phenomena and the Properties of Gaseous Ions", p.14, Academic Press Inc., New York (1957).

262. Morrison, J.D., J. Chem. Phys., 19, 1305 (1951); J. Chem. Phys., 39, 200 (1963).

263. Winters, R.E., Collins, J.H., and Courchene, W.L., J. Chem. Phys., 45, 1931 (1966).

264. Clarke, E.M., Canad. J. Phys., 32, 764 (1954).

265. Fox, R.E., Hickam, W.H., Kjeldaas, T., and Grove, D.J., Rev. Sci. Instr., 26, 1101 (1955); Phys. Rev., 84, 859 (1951).

266. Marmet, P., and Kerwin, L., Canad. J. Phys., 38, 787 (1960).

267. McDowell, C.A., and Warren, J.W., Diss Faraday Soc., 10, 53 (1951).

268. Daly, N.R., McCormick, A., and Powell, R.E., Rev. Sci. Instr., 39, 1163 (1968).

269. Lossing, F.P., Tickner, A.W., and Bryce, W.A., J. Chem. Phys., 19, 1254 (1951).

270. Field, F.H. and Franklin, J.L., "Electron Impact Phenomena and the Properties of Gaseous Ions, "Academic Press Inc., New York (1957).

271. Krauss, M., and Dibeler, V.H., "Mass Spectrometry of Organic Ions", ed., McLafferty, F.W., Academic Press Inc., New York (1963).

272. McDowell, C.A., "Mass Spectrometry", ch. XII, McGraw-Hill Book Co., Inc., New York (1963).

273. Stevenson, D.P., and Hipple, J.A., J. Amer. Chem. Soc., 64, 2769, 1588, 2766 (1942); ibid, 65, 209 (1943).

274. Vought, R.H., Phys. Rev., 71, 93 (1947).

275. Koffel, M.E., and Lad, R.A., J. Chem. Phys., 16, 420 (1948).

276. Franklin, J.L., Dillard, J.G., Rosenstock, H.M., Herron, J.T., Draxl, K., and Field, F.H., "Ionization Potentials, Appearance Potentials, and Heats of Formation of Gaseous Positive Ions", Nat. Stand. Ref. Data Ser., NBS 26, Washington (1969).

277. Kiser, R.W., and Gallegos, E.J., J. Phys. Chem., 66, 947 (1962).

278. Lappert, M.F., Litzow, M.R., Pedley, J.B., Riley, P.N.K., and Tweedale, A., J. Chem. Soc. 1968A, 3105 (1968).

279. Warren, J.W., Nature, 165, 810 (1950).

280. Hartley, S.B., Holmes, W.S., Jacques, J.K., Mole, M.F., and McCoubrey, J.C., Quart. Rev., 17, 204 (1963).

281. Cottrell, T.L., "The Strengths of Chemical Bonds", 2nd ed., p.283, Butterworths Scientific Publications, London (1958).

282. Dibeler, V.H., and Walker, J.A., Inorg. Chem., 8, 1728 (1969).

283. Price, W.C., Private Communication reported in: Cade, P.E., and Huo, W.M., J. Chem. Phys., 47, 649 (1967).

284. McAllister, T., and Lossing, F.P., J. Phys. Chem., 73, 2996 (1969).

285. Hipple, J.A., and Stevenson, D.P., Phys. Rev., 63, 121 (1943).

286. Price, W.C., and Passmore, T.R., Disc. Faraday Soc., 35, 232 (1963).

287. Dugger, D., Kiser, R.W., McDowell, M.V., and Saalfeld, F.E., Previously Unpublished Data reported in: Saalfeld, F.E., McDowell, M.V., Gondal, S.K., and MacDiarmid, A.G., J. Amer. Chem., Soc., 90, 3634 (1968).

288. Green, J.C., King, D.I., and Eland, J.H.D., J. Chem. Soc., 1970D, 1121 (1970).

289. Kosolapoff, G.M., "Organophosphorus Compounds", J. Wiley and Sons, Inc., New York (1950).

290. Burg, A.B., and Slota, P.J., J. Amer. Chem. Soc., 80, 1107 (1958).

291. Schmützler, R., Inorg. Chem., 3, 415 (1964).

292. Hoffman, C.J., and Heintz, E.A., Inorg. Synth., 7, 190 (1963).

293. "Tables of Wave numbers for the Calibration of Infrared Spectrometers", Commission of Molecular Structure and Spectroscopy of I.U.P.A.C., Butterworths, London (1961).

294. Jones, R.N., Jonathan, N.B.W., McKenzie, M.A., and Nadeau, A., Spectrochim. Acta., 17, 77 (1961).

295. Rondeau, R.E., J. Chem. Eng. Data, 11, 124 (1966).